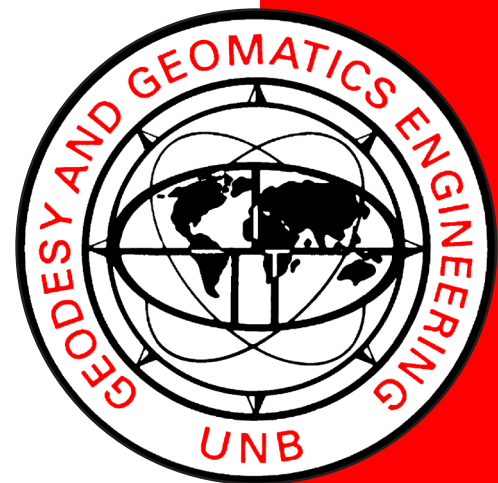


# **MAST TRACKING CAPABILITY OF EM3002D USING WATER COLUMN IMAGING**

**AUKE VAN DER WERF**

**September 2010**



**TECHNICAL REPORT  
NO. 274**

# **MAST TRACKING CAPABILITY OF EM3002D USING WATER COLUMN IMAGING**

Auke van der Werf

Department of Geodesy and Geomatics Engineering  
University of New Brunswick  
P.O. Box 4400  
Fredericton, N.B.  
Canada  
E3B 5A3

September 2010

© Auke van der Werf, 2010



## PREFACE

This technical report is a reproduction of a thesis submitted in partial fulfillment of the requirements for the degree of Master of Science in Engineering in the Department of Geodesy and Geomatics Engineering, September 2010. The research was supervised by J.E. Hughes Clarke, and support was provided by the Dutch Navy and Rijkswaterstaat (Dutch Public Works).

As with any copyrighted material, permission to reprint or quote extensively from this report must be received from the author. The citation to this work should appear as follows:

van der Werf, Auke (2010). *Mast Tracking Capability of EM3002D Using Water Column Imaging*. M.Sc.E. thesis, Department of Geodesy and Geomatics Engineering Technical Report No. 274, University of New Brunswick, Fredericton, New Brunswick, Canada, 162 pp.

## **DEDICATION**

I dedicate this thesis to the memory of my grandparents. I would like to thank my parents and sister for their continuing support and encouragement.

## ABSTRACT

When a wreck or other hazard to navigation is found, it is necessary to determine the least depth above it to ensure safety of navigation. For objects with a high aspect ratio such as masts this is particularly difficult. Single beam, lidar and even conventional multibeam bottom detection routinely fail to detect such objects. In these instances the International Hydrographic Organization (IHO) requires, for objects in water depths less than 40 m, that the position and least depth be determined with an alternative method, for example a mechanical bar sweep or divers.

Previous trials of the Ocean Mapping Group (Hughes Clarke, 2006a) have demonstrated that multibeam Water Column Imaging (WCI) has the potential to reveal mast-like objects in the water column. The difference between WCI and conventional multibeam measurements is that WCI records the signal for each physical beam throughout the whole water column. WCI was originally designed for fish finding, not for depth measurements. The current output is an image that approximates a vertical plane. The challenge is to convert a specific point in this image data into a robust depth detection. Two steps are involved: (1) we have to select the most likely echo candidate in the imaging space and (2) we have to transform to a depth and horizontal position in the geographic frame. The first issue can be dealt with using operator selection or image analysis. The problem is that the features can be ambiguous (there are multiple solutions/interpretations possible), otherwise bottom detection would have succeeded in the first instance. For the second issue we need to determine the steering angles and two

way travel time from (1), then we have to recreate the sounding geometry at transmit and receive in order to determine the beam's geographic launch angle, perform a ray trace, and reduce the solution to the vessel reference point. Whereas these transformations are well understood for conventional bottom detections, there is insufficient information to do the same transformations for detections derived from WCI.

Field trials were executed as part of this thesis to collect WCI data for this research. Data were collected with a Dutch Navy survey launch of a wreck in 20 metres of water on the Dutch continental shelf. A "bar-sweep" toolkit was developed in the multibeam processing software package "Swathed" to determine and calculate the least depth of the mast. A significant component of this research was to transform the water column data to depths in the geographic frame, to calculate the depth and position of each sample in the water column image. Analysis of data around mast-like objects was undertaken to calculate the least depth of the mast. This method was applied for 20 passes over a wreck in and the solutions agree within 20 cm vertically ( $2\sigma$ ), and meet IHO Special Order vertical accuracy.

## ACKNOWLEDGEMENTS

There are a number of people without whom this thesis might not have been written, and to whom I am greatly indebted.

- The Dutch Navy for providing funding and support.

Thanks to Jan Appelman, Diederick van der Plas, Ide Nijman and Theo Hamburger.

- Rijkswaterstaat for providing funding.

Thanks to Cees Boogaard, Simon Bicknese and Ben Dierikx.

- Dr. John Hughes Clarke and Dr. Jonathan Beaudoin for supervising this project, from whom I have gained knowledge that will aid me in my future career. Both for help during this research and essential software modifications.

- Everyone within the Ocean Mapping Group for answering any question I had.

- Hydrographic Society Benelux for providing funding.

Thanks to Niels Kinneging and Rob van Ree.

Special thanks to two friends. Pim Kuus for never ending help, support and feedback. Ronald Perluka, who encouraged and helped me to go to UNB. Finally, although their contributions to this thesis might not be directly related, I have to thank my roommates and the friends I made during my stay in Fredericton.

# TABLE OF CONTENTS

DEDICATION.....	ii
ABSTRACT.....	iii
ACKNOWLEDGEMENTS.....	v
TABLE OF CONTENTS.....	vi
LIST OF TABLES.....	xi
LIST OF FIGURES.....	xii
LIST OF ACRONYMS.....	xxiii
1 INTRODUCTION.....	1
1.1 Objectives.....	3
1.2 Contributions.....	6
1.3 Thesis structure.....	8
2 ACOUSTIC BACKGROUND.....	9
2.1 Introduction to Multibeam theory.....	9
2.2 Kongsberg EM3002.....	11
2.3 Dynamic focusing.....	13
2.4 Resolution.....	15
2.5 Dual Head.....	17
2.6 Conventional Bottom Detections.....	19
2.7 High Definition Beam Forming.....	23
2.8 Imaging Geometry.....	25
2.8.1 Receiver side lobes.....	25

2.8.2	Transmit side lobes .....	30
2.8.3	Noise patterns.....	31
2.8.4	Incomplete Occlusion .....	32
3	ACQUISITION.....	34
3.1	Survey Platform.....	35
3.2	Object .....	37
3.3	(SIS) Settings.....	39
3.3.1	Installation parameters .....	39
3.3.2	Runtime parameters .....	40
3.4	Methodology .....	42
4	SOFTWARE DEVELOPMENT .....	44
4.1	Backscatter Time-series .....	45
4.2	Visualization tools.....	48
4.2.1	Polar plot.....	49
4.2.2	Range resolution .....	51
4.3	Angular resolution.....	53
4.4	Vertical Profile.....	54
4.5	Analysis tools .....	56
4.6	Common-range plot.....	57
4.7	Imaging Geometry Quality Factor (IGQF) .....	58

5	WATER COLUMN IMAGE GEO-REFERENCING.....	61
5.1	Kongsberg Data Structures.....	63
5.2	Re-point water column receiver angles.....	65
5.3	Depth Calculation.....	69
5.4	Geographic Launch Vector Determination .....	71
5.5	Ray-tracing.....	73
5.6	Reduction .....	74
5.7	Results .....	75
5.8	Output.....	81
5.9	Tides.....	83
6	ANALYSIS.....	84
6.1	Methodology .....	85
6.1.1	Select lines .....	85
6.1.2	Select swaths.....	86
6.1.3	Analyze .....	87
6.2	Imaging Geometry Quality Factor (IGQF) .....	92
6.3	Julian Day 184, survey 3.....	93
6.3.1	Line 0005 .....	94
6.3.2	Line 0006 .....	97
6.3.3	Line 0007 .....	100



6.3.4	Line 0015 .....	102
6.3.5	Line 0017 .....	104
6.3.6	Line 0019 .....	106
6.3.7	Results.....	108
6.4	Julian Day 184, survey 4.....	109
6.4.1	Line 0003 .....	110
6.4.2	Line 0004 .....	112
6.4.3	Line 0006 .....	114
6.4.4	Line 0007 .....	117
6.4.5	Line 0008 .....	119
6.4.6	Line 0015 .....	121
6.4.7	Line 0017 .....	123
6.4.8	Line 0018 .....	125
6.4.9	Line 0020 .....	127
6.4.10	Results.....	129
6.5	Julian Day 196, survey 1 .....	130
6.5.1	Line 0010 .....	131
6.5.2	Line 0018 .....	133
6.5.3	Line 0020 .....	135

6.5.4	Line 0021 .....	137
6.5.5	Line 0022 .....	139
6.5.6	Results.....	141
6.6	Results .....	142
6.6.1	Vertical.....	142
6.6.2	Horizontal .....	147
7	CONCLUSIONS AND RECOMMENDATIONS .....	151
7.1	Conclusions .....	151
7.2	Recommendations .....	154
	BIBLIOGRAPHY.....	159
	CURRICULUM VITAE	

## LIST OF TABLES

Table 1.1 - IHO – S44 Minimum Standards for Hydrographic Surveying.....	5
Table 2.1 - The bandwidths calculated by $\sim 1/T$ . .....	16
Table 3.1 - Table with the angular offsets from the patch test, note that the difference in heading between both heads is $6^\circ$ . .....	39
Table 3.2 - Locations of the ships reference frame.....	39
Table 3.3 - The sampling frequency versus pulse length used during acquisition. ....	42
Table 3.4 - A summarized survey log of all the surveys. ....	43
Table 4.1 - Correlation between pulse length, sampling frequency and range sampling. 52	
Table 5.1 - Number of solutions for each beam spacing method. ....	64
Table 6.1 – Depth and position results of survey 3 on Julian day 184. ....	108
Table 6.2 – Depth and position results of Julian Day 184 survey 4. ....	129
Table 6.3 – Depth and position results of survey 1 on Julian day 196. ....	141
Table 6.4 – The standard deviation, special order TVU at 95% confidence level and the maximum allowable TVU selected by survey. ....	145
Table 6.5 - The standard deviation, special order TVU at 95% confidence level and the maximum allowable TVU selected by Quality Factor.....	146
Table 6.6 - The standard deviation, special order THU at 95% confidence level and the maximum allowable THU selected by survey. ....	148
Table 6.7 - The standard deviation, special order THU at 95% confidence level and the maximum allowable THU selected by Quality Factor.....	149

## LIST OF FIGURES

Figure 2.1 - Mill Cross configuration. ....	9
Figure 2.2 - A beam pattern in the shape of a fan athwart on the vessel created by the transmit array (left).....	10
Figure 2.3 - Imaging showing the angular resolution (right). The beam widths are not the real beam widths but are exaggerated for illustrative purposes. ....	12
Figure 2.4 - Effect of dynamic focusing for a linear array. ....	14
Figure 2.5 - Top image shows a single headed system with a maximum swath width of approximately 130 degrees. The bottom image shows a dual headed system with a maximum swath width over 200 degrees. ....	18
Figure 2.6 - Phase detection in red and amplitude detection in blue. ....	19
Figure 2.7 - Bottom detection.....	21
Figure 2.8 - For the bottom detection algorithm to not ignore the mast it needs to be picked up in more than one swath. ....	22
Figure 2.9 – High definition equidistant distribution of soundings.....	24
Figure 2.10 – More lines (based on linear or quadratic regression) fitted to a signal with a longer envelope. ....	24
Figure 2.11 – Receiver Side lobes, highlighted selected range and selected angle. ....	27
Figure 2.12 – Receiver side lobes appear in the signal plotted in a common range plot..	27
Figure 2.13 – Receiver side lobes appear in the signal plotted in a fixed angle time-series plot.....	27
Figure 2.14 –Mast inside the minimum slant range.....	29

Figure 2.15 – Common range plot of the selected range of the mast inside the minimum slant range.....	29
Figure 2.16 – Mast outside the minium slant range.....	29
Figure 2.17 – Common range plot of the selected range of the mast outside the minimum slant range.....	29
Figure 2.18 – Transmit side lobes.....	30
Figure 2.19 – Noise patterns. ....	31
Figure 2.20 – Common range plot where the radial noise patterns become apparent. ....	31
Figure 2.21 – Fixed angle time-series plot where the noise patterns becomes apparent. .	32
Figure 2.22 – Mast inside the minimum slant range, in green highlighted the selected angle and selected range.....	33
Figure 2.23 – Incomplete occlusion.....	33
Figure 3.1 - One of the survey launches of the Dutch Navy (left). ....	35
Figure 3.2 - The heads on this survey launch are mounted at an angle of $\pm 25$ degrees.	35
Figure 3.3 - Sound Velocity Profiles were taken before each survey. ....	36
Figure 3.4 - The HD147. Reference: “Visserij Jaarboek 2006”. ....	37
Figure 3.5 - Side scan sonar image of the Hardalion and the HD147. ....	38
Figure 3.6 - Positions of the surveyed objects. ....	38
Figure 3.7 - Showing the user defined maximum range (travel time).....	41
Figure 3.8 - Longitudinal lines over the wreck of the HD147 (left).....	42
Figure 4.1 – On the left is a presentation of a single headed multibeam system, on the right is a representation of the backscatter in a polar plot (after Hughes Clarke [2008]). .....	46

Figure 4.2 – (b) The sample amplitude time-series plotted in decibels.....	47
Figure 4.3 -Backscatter is recorded and represented using several scales.....	47
Figure 4.4 – Representation of the polar plot (across track profile) and the vertical profile (along track profile).....	48
Figure 4.5 – Backscatter intensities are plotted against each beam pointing angle.....	50
Figure 4.6 – Polar plot where the port head overlays the starboard head (top), polar plot where the starboard head overlays the port head (bottom). In the zoomed area the transducer offsets become apparent.....	50
Figure 4.7 - Image resolution with different sampling frequencies, shown in the polar plot frame. In yellow the (scaled) range sampling is represented. ....	51
Figure 4.8 – Table showing the number of samples per range (in meters) for each sampling frequency. ....	52
Figure 4.9 - In this figure two different angular sectors are used, +/- 65° (top), +/- 95° (bottom).....	53
Figure 4.10 – Vertical profile with the corridor placed straight below the ship. ....	54
Figure 4.11 – Representation of the vertical profile moved away from nadir.....	55
Figure 4.12 – Polar plot with selected beam and selected range highlighted.....	56
Figure 4.13 – Fixed angle time-series plot.....	56
Figure 4.14 - Common-range plot .....	57
Figure 4.15 – Top of the mast detected in different beam angles for each head. ....	57
Figure 4.16 - Image describing calculation of the “quality” of each sample.....	60
Figure 4.17 – Representation of the calculated Imaging Geometry Quality Factor for an EM3002D with the highest range resolution.....	60

Figure 5.1 - Due to beam steering the plane takes on a conic form.....	62
Figure 5.2 – Left, the water column time-series as a straight line along the beam pointing angle, represented in a flat plane relatively below the ship. Right, representation of the water column time-series along a ray-refracted path, where the beams take on a conical shape. ....	62
Figure 5.3 – The water column beam pointing angle has to be uncorrected for the roll, to “un-point” it to the equivalent of a receiver-relative steering angle. ....	66
Figure 5.4 – The beam pointing angles for a single low density (i.e. 160 beams). ....	67
Figure 5.5 – The difference between the beam pointing angle from the raw range and beam angle structure and the adjusted angle from the water column structure.....	68
Figure 5.6 - The difference between the one-way travel time to the bottom detection from the raw range and beam angle structure and the one-way travel time to the detected range from the water column structure.....	68
Figure 5.7 - The difference in roll.....	68
Figure 5.8 – Right handed coordinate system (from Hughes Clarke [2008]).....	70
Figure 5.9 - The beam-pointing vector lies on the intersection of the transmitter cone of ensonification and the receiver cone of sensitivity.....	72
Figure 5.10 – The beam pointing vectors for all beams in the geographical coordinate system. In red for the port head and in green for the starboard head. ....	72
Figure 5.11 – Representation of ray-tracing in the vessel coordinate system, i.e. relative to the local level [after Beaudoin, 2004]. ....	73
Figure 5.12 - Internal offsets in typical EM3000D installation.....	74

Figure 5.13 – z (depth) and y (across-track) values from the depth structure, versus z (depth) and y (across-track) calculated according to UNB (newmergeAtt).....	76
Figure 5.14 – The difference between z (depth) values from the depth structure, depth values calculated according to UNB (newmergeAtt).....	76
Figure 5.15 - The x (along-track) and y (across-track) values from the depth structure, versus x (along-track) and y (across-track) calculated according to UNB.....	77
Figure 5.16 – Difference between the across-track values from the depth structure, versus across-track calculated according to UNB. ....	77
Figure 5.17 – Difference between the along-track values from the depth structure, versus along-track calculated according to UNB. There are two lines, one for the starboard head, and one for the port head.....	77
Figure 5.18 – The UNB original solution versus the final output from the Water Column Solution using common two way travel times. ....	79
Figure 5.19 - Difference between the UNB original solution and the final output of the Water Column algorithm.....	79
Figure 5.20 – Top-view, along and across track plotted. The x axis scale is stretched. ...	80
Figure 5.21 – Along track difference.....	80
Figure 5.22 – Across track difference. There are two lines, one for the starboard head, and one for the port head. ....	80
Figure 5.23 – Representation of a single ray-traced path in a vertical plane relative to the transducer. Note that the depths and the across track distances of each ray-traced sample are the same in the cone and the vertical plane 3D. ....	81



Figure 5.24 - Each ray-traced sample is represented in the 2D vertical plane relative below the ship.....	82
Figure 5.25 – The output of the ray-trace with an exaggerated revised sound velocity profile .....	82
Figure 6.1- Reducing the processing time by selecting the survey lines close to the wreck. Preferably the wreck should be located within the MSR. ....	85
Figure 6.2 - Reducing the processing time by selecting swaths. When located within the MSR the wreck usually shows up in the vertical profile as shown in this image. ..	86
Figure 6.3 – Synthetic polar plot image, representing the top of the mast. Due to receiver side lobes the top of the mast is projected onto beams which don't have the mast on their maximum response axis. ....	89
Figure 6.4 – Common-range plot, representing the top of the mast. ....	89
Figure 6.5 – Fixed angle time-series plot, representing the top of the mast. ....	90
Figure 6.6 – Top of the mast picked up by transmit side lobes. ....	91
Figure 6.7 - The IGQF introduced for each line. ....	92
Figure 6.8 – DTM of the data collected in survey 3 on Julian Day 184.....	93
Figure 6.9 – DTM with position and orientation (left), image with IGQF (right) for line number 0005 on Julian day 184, survey 3 (left).....	94
Figure 6.10 – Julian Day 184, survey 3, line 0005 - (a) vertical profile, (b) polar plot with real data, (c) polar plot zoom, (d) common-range plot, (e) fixed angle time-series plot.....	96
Figure 6.11 - DTM with position and orientation (left), image with IGQF (right) for line number 0006, Julian day 184, survey 3.....	97

Figure 6.12 – Julian Day 184, survey 3, line 0006 - (a) vertical profile, (b) polar plot with real data, (c) polar plot zoom, (d) common-range plot, (e) fixed angle time-series plot.....	99
Figure 6.13 - DTM with position and orientation (left), image with IGQF (right) for line number 0007, Julian day 184, survey 3.....	100
Figure 6.14 – Julian day 184, survey 3, line 0007 - (a) vertical profile, (b) polar plot with real data, (c) polar plot zoom, (d) common-range plot, (e) fixed angle time-series plot.....	101
Figure 6.15 - DTM with position and orientation (left), image with IGQF (right) for line number 0015, Julian day 184, survey 3.....	102
Figure 6.16 – Julian day 184, survey 3, line 0015 - (a) vertical profile, (b) polar plot with real data, (c) polar plot zoom, (d) common-range plot, (e) fixed angle time-series plot.....	103
Figure 6.17 - DTM with position and orientation (left), image with IGQF (right) for line number 0017, Julian day 184, survey 3.....	104
Figure 6.18 – Julian day 184, survey 3, line 0017 - (a) vertical profile, (b) polar plot with real data, (c) polar plot zoom, (d) common-range plot, (e) fixed angle time-series plot.....	105
Figure 6.19 - DTM with position and orientation (left), image with IGQF (right) for line number 0019, Julian day 184, survey 3.....	106
Figure 6.20 – Julian day 184, survey 3, line 0019 - (a) vertical profile, (b) polar plot with real data, (c) polar plot zoom, (d) common-range plot, (e) fixed angle time-series plot.....	107

Figure 6.21 - Digital terrain model of the data collected in survey four on Julian Day 184. .....	109
Figure 6.22 - Map with position and orientation (left), image with IGQF (right) for Julian day 184, survey 4, line number 0003. ....	110
Figure 6.23 – Julian Day 184, survey 4, line 0003 - (a) vertical profile, (b) polar plot with real data, (c) polar plot zoom, (d) common-range plot, (e) fixed angle time-series plot.....	111
Figure 6.24 - Map with position and orientation (left), image with IGQF (right) for Julian day 184, survey 4, line number 0004. ....	112
Figure 6.25 – Julian day 184, survey 4, line 0004 - (a) vertical profile, (b) polar plot with real data, (c) polar plot zoom, (d) common-range plot, (e) fixed angle time-series plot.....	113
Figure 6.26 - Map with position and orientation (left), image with IGQF (right) for Julian day 184, survey 4, line number 0006. ....	114
Figure 6.27 – Julian day 184, survey 4, line 0006 - (a) vertical profile, (b) polar plot with real data, (c) polar plot zoom, (d) common-range plot, (e) fixed angle time-series plot.....	116
Figure 6.28 - Map with position and orientation (left), image with IGQF (right) for Julian day 184, survey 4, line number 0007 .....	117
Figure 6.29 – Julian day 184, survey 4, line 0007 - (a) vertical profile, (b) polar plot with real data, (c) polar plot zoom, (d) common-range plot, (e) fixed angle time-series plot.....	118

Figure 6.30 - Map with position and orientation (left), image with IGQF (right) for Julian day 184, survey 4, line number 0008. ....	119
Figure 6.31 – Julian day 184, survey 4, line 0008 - (a) vertical profile, (b) polar plot with real data, (c) polar plot zoom, (d) common-range plot, (e) fixed angle time-series plot. ....	120
Figure 6.32 - Map with position and orientation (left), image with IGQF (right) for Julian day 184, survey 4, line number 0015. ....	121
Figure 6.33 – Julian day 184, survey 4, line 0015 - (a) vertical profile, (b) polar plot with real data, (c) polar plot zoom, (d) common-range plot, (e) fixed angle time-series plot. ....	122
Figure 6.34 - Map with position and orientation (left), image with IGQF (right) for Julian day 184, survey 4, line number 0017. ....	123
Figure 6.35 – Julian day 184, survey 4, line 0017 - (a) vertical profile, (b) polar plot with real data, (c) polar plot zoom, (d) common-range plot, (e) fixed angle time-series plot. ....	124
Figure 6.36 - Map with position and orientation (left), image with IGQF (right) for Julian day 184, survey 4, line number 0018 ....	125
Figure 6.37 – Julian day 184, survey 5, line 0018 - (a) vertical profile, (b) polar plot with real data, (c) polar plot zoom, (d) common-range plot, (e) fixed angle time-series plot. ....	126
Figure 6.38 - Map with position and orientation (left), image with IGQF (right) for Julian day 184, survey 4, line number 0020. ....	127

Figure 6.39 – Julian day 184, survey 4, line 0020 - (a) vertical profile, (b) polar plot with real data, (c) polar plot zoom, (d) common-range plot, (e) fixed angle time-series plot.....	128
Figure 6.40 - Digital terrain model of the data collected in survey 1 on Julian Day 196. .....	130
Figure 6.41 - Map with position and orientation (left), image with IGQF (right) for Julian day 196, survey 1, line number 0010 .....	131
Figure 6.42 – Julian day 196, survey 1, line 0010 - (a) vertical profile, (b) polar plot with real data, (c) polar plot zoom, (d) common-range plot, (e) fixed angle time-series plot.....	132
Figure 6.43 - Map with position and orientation (left), image with IGQF (right) for Julian day 196, survey 1, line number 0018 .....	133
Figure 6.44 – Julian day 196, survey 1, line 0018 - (a) vertical profile, (b) polar plot with real data, (c) polar plot zoom, (d) common-range plot, (e) fixed angle time-series plot.....	134
Figure 6.45 - Map with position and orientation (left), image with IGQF (right) for Julian day 196, survey 1, line number 0020 .....	135
Figure 6.46 – Julian day 196, survey 1, line 0020 - (a) vertical profile, (b) polar plot with real data, (c) polar plot zoom, (d) common-range plot, (e) fixed angle time-series plot.....	136
Figure 6.47 - Map with position and orientation (left), image with IGQF (right) for Julian day 196, survey 1, line number 0021 .....	137

Figure 6.48 – Julian day 196, survey 1, line 0021 - (a) vertical profile, (b) polar plot with real data, (c) polar plot zoom, (d) common-range plot, (e) fixed angle time-series plot.....	138
Figure 6.49 - Map with position and orientation (left), image with IGQF (right) for Julian day 196, survey 1, line number 0022 .....	139
Figure 6.50 – Julian Day 196, survey 1, line 0022 - (a) vertical profile, (b) polar plot with real data, (c) polar plot zoom, (d) common-range plot, (e) fixed angle time-series plot.....	140
Figure 6.51 – Depth results selected by survey (i.e. by angular sector and pulse length). .....	145
Figure 6.52 – Depth results selected by Quality Factor.....	146
Figure 6.53 – Graph of the final positions in Northing and Easting selected by survey.	148
Figure 6.54 - Graph of the final positions in Northing and Easting selected by Quality Factor.....	149
Figure 6.55 – The positions of the final solutions plotted on top of a DTM of the wreck. .....	150
Figure 7.1 – Survey lines towards the wreck, to reveal the position and orientation of the wreck, and ensure safety of navigation for the survey vessel. ....	157
Figure 7.2 – Survey lines to detect the least depth of the wreck with WCI.....	158

## LIST OF ACRONYMS

BTRK	Bottom Tracking solution
CARIS	Computer Aided Resource Information System
CD	Chart Datum
CW	Continuous Wave
DTM	Digital Terrain Model
HD	High Definition
HDBF	High Definition Beam Forming
HOV	Hydrografisch Opnemings Vaarhuig
IHO	International Hydrographic Organization
GPS	Global Positioning System
LAT	Lowest Astronomical Tide
LIDAR	Laser Imaging Detection And Ranging
LRK	Long Range Kinematic
MBES	Multi Beam Echo Sounder
MSL	Mean Sea Level
MSR	Minimum Slant Range
NM	Nautical Mile
OMG	Ocean Mapping Group
OWTT	One Way Travel Time
QINSy	Quality Integrated Navigation System

QPS	Quality Positioning Services
RP	Reference Point
RTK	Real Time Kinematic
RX	Receive
SBES	Single Beam Echo Sounder
SIS	Seafloor Information System
SSS	Side Scan Sonar
THU	Total Horizontal Uncertainty
TVU	Total Vertical Uncertainty
TWTT	Two Way Travel Time
TX	Transmit
UNB	University of New Brunswick
UTM	Universal Transverse Mercator
WCI	Water Column Imaging
ZOC	Zones of Confidence



# 1 INTRODUCTION

The Hydrographic Service of the Dutch Navy is responsible for conducting hydrographic surveys and publishing charts and other nautical information covering the Dutch Continental Shelf and adjacent waters together with the waters surrounding the Netherlands Antilles and Aruba [Netherlands Hydrographic Service, 2009]. A part of the hydrographic operational procedures of the Dutch Navy is the measurement and determination of the least depth above wrecks and other hazards to navigation. The least depth above wrecks and other features has to be determined to ensure safety of navigation. The Dutch Navy uses primarily Multi Beam Echo Sounder (MBES) for depth determination of the seafloor. However, MBES may fail to detect relatively small objects which are located in the water column above the seafloor (for example masts or other small objects on wrecks). For detection of wrecks the Dutch Navy normal uses a Side Scan Sonar (SSS) and a magnetometer. After a wreck or obstruction is detected the least depth of the wreck has to be determined. For determination of the least depth of a wreck a combination of equipment is used, Single Beam Echo Sounder (SBES), MBES and SSS. However, as explained in § 2.2.4.1 of the Manual on Hydrography, IHO (2005), it may be an critical issue to detect small features on wrecks with MBES due to, for example, the beam footprint or “filtering” algorithms (gating and near proximity rules). The Dutch Navy is a member of the International Hydrographic Organization (IHO); therefore, the products that are published have to meet the standards of the IHO. Most of the wrecks on the Dutch Continental Shelf are located in water shallower than 40 meters; therefore, the IHO requires that the position and least depth are determined with the best available

method (IHO, 2008, paragraph 3.4). Even when surveying with a suitable system 100% detection of features can never be guaranteed ( IHO, 2008, paragraph 3.5), the Dutch Navy can therefore consider to use a mechanical bar-sweep to determine the least depth above a wreck, thereby increasing the confidence of safe navigation. A mechanical bar-sweep has some drawbacks; it is time-expensive because multiple passes have to be made, a lot of manpower is needed, it uses fragile equipment, and can only be executed under fair weather and conditions with low swell. Due to those limitations only around 15 mechanical bar-sweeps per year are performed. Therefore, the Dutch Navy is looking to improve the methods for wreck detection. Previous trials of the Ocean Mapping Group (Hughes Clarke, 2006) have demonstrated that multibeam Water Column Imaging (WCI) has the potential to reveal mast-like objects in the water column. If this method could be made robust and easy to use, it would represent an opportunity to cut down on the necessity of mechanical bar-sweeping.

## 1.1 Objectives

### 1) *EM3002D Water Column Imaging mast tracking capability assessment*

An assessment has to be made to see if the least-depth point of a wreck can be precisely and reliably detected and visualized based on WCI. If a least-depth point is detected and can be visualized, it can either be selected by a human operator or by image analysis (software). The question is if a human operator is able to select the most likely echo candidate in the imaging space. The goal of this research is to enable hydrographers of the Dutch Navy (and their partners), with the aid of this report, to select the least depth in a water column image. The problem for image analysis is that the features are ambiguous (otherwise bottom detection would have succeeded in the first instance). The current UNB software is already compatible with dual head EM3002 data. A task is to modify the current UNB software to be able to detect the least depth of a mast-like object. Part of this research is to execute trials together with the Dutch Navy to collect WCI data.

2) *Software modifications extending the UNB software (Swathed) to calculate the least depth in the UNB Water Column Imaging toolkit.*

The problem is that the current output (in SIS) is an image rather than a discrete solution as depths and positions in the 3D geographic frame. The challenge is to transform this image data or at least the most likely echo candidate detected in (1) to depths and positions in the 3D geographic frame. The question is if there is sufficient ancillary information (in the water column structure) to make this transformation. To transform an echo candidate, the angles from (1) need to be properly re-pointed. Then the sounding geometry at transmit and receive has to be recreated in order to determine the beam's geographic launch angle. After that a ray-trace needs to be performed. Finally, the solution needs to be reduced to the vessel reference point. While these transformations are well understood for conventional bottom detections, incomplete information is currently retained with the water column data structure to perform the same calculation.

After a solution is calculated in the geographic frame, the precision and reliability of WCI and eventually the suitability of the method research should be assessed. The goal is to determine the least depth of a wreck from multiple passes and to look at the variance of the results with respect to the IHO-S44 special order. Ultimately comparing the least depth determined with WCI to the least depth determined with a mechanical bar-sweep/divers would provide the highest level of confidence. The Dutch Navy requires that the depth determined with WCI does not exceed the maximum allowable TVU for IHO special order specifications, as described in the IHO standards for Hydrographic Surveys, Special Publication no.44 (S-44), 4th edition (Table 1.1).

<b>IHO STANDARDS FOR HYDROGRAPHIC SURVEYS (S-44)</b>	
<b>Minimum Standards for Hydrographic Surveys</b>	
	<b>Special order</b>
<b>Description of areas</b>	Areas where under-keel clearance is critical
<b>Maximum allowable THU 95% Confidence level</b>	2 metres
<b>Maximum allowable TVU 95% Confidence level</b>	a = 0.25 metre b = 0.0075
<b>Full Sea floor Search</b>	Required
<b>Feature Detection</b>	Cubic features > 1 metre

**Table 1.1 - IHO – S44 Minimum Standards for Hydrographic Surveying**

3) *Recommendations on the operational procedures of wreck detection using Water Column Imaging for the Dutch Navy.*

The final goal of the Dutch Navy is to have WCI implemented in their current acquisition and processing software (QINSy). This leads to another part of the thesis where recommendations will be given on the operational procedures for the Dutch Navy to collect and assess such data.

## 1.2 Contributions

The significant contributions of this research are presented here.

**Calculate depths in the geographic frame:** One of the most significant developments was to implement an algorithm to be able to calculate (and ray-trace) the depth and position of each sample from the water column structure in the geographic frame, for data collected in high definition mode. The angle stored in the water column datagram could not be used for a direct ray-trace, therefore, a significant component of this research was how to re-point the beam angle stored in the water column structure. Water Column Images used before in Swathed were an image approximating the across-track/depth structure rather than true depths in the 3D geographic frame, which were a qualitative tool comparable to side scan sonar wherein an image was produced, but only approximate depth calculation was made. Therefore, it could only be used as an examination tool on bathymetric data (i.e. bottom tracking solutions). The contribution of this research is that each recorded sample can be placed in the geographic frame, which makes WCI a quantitative tool, and makes it suitable for objective least depth determination. With this development WCI can be used for Hydrographic purposes, and will be available in commercial hydrographic software packages in the near future (QINSy, CARIS).

**Development of a bar-sweep toolkit (in Swathed):** The “bar-sweep” toolkit developed in the course of this research is an upgrade of the existing water column toolkit specifically for wreck least depth determination. Existing visualization methods like the polar plot, the vertical profile and the time/angle plot were used and further developed, thereby extending the functionality for the dual head geometry. Those visualization tools are used together with analysis tools which view the backscatter along a fixed angle or common range to determine the top of the mast manually. Manual analysis was performed to determine the least depth of a mast like object.

**WC data acquisition:** There was no EM3002 WCI data collected up to the horizontal (the whole water column from the waterline to the seafloor) over a wreck before; therefore, trials were executed with the Dutch Navy, which uses a Kongsberg EM3002 dual head for data acquisition. Only a dual (or tilted) head multibeam can image out to the horizontal. Conventional single head EM3002 systems use an angular sector of +/- 65 degrees. During acquisition different settings (for example, angular sector and pulse length) were used, to analyze the influence of those settings are on mast tracking, from which the results are given in the recommendations.

### 1.3 Thesis structure

Chapter 2 provides the necessary theoretical background to understand the bottom imaging geometry performance of a multibeam system and reviews previous work on WCI geometry, the effect of side lobes and angular responses, which are required background concepts that are critical to this work. Chapter 3 gives the specifications of the wreck, and explains the methodology and the settings used during the field trials. Chapter 4 explains how WCI is implemented in Swathed and describes the significant modifications and developments; visualization, analysis and processing techniques are discussed. In Chapter 5 special attention is given on how to georeference the water column image, from the raw data structure to depths and positions in the geographic frame. In Chapter 6, analyses of data around a mast-like object is undertaken, to calculate the least depth of the mast. Results for each survey are given and compared to the IHO special order. Conclusions and recommendations are presented in Chapter 7.



## 2 ACOUSTIC BACKGROUND

### 2.1 Introduction to Multibeam theory

There are different designs of multibeam echo sounders. The EM3002 is a so-called “flat” or “linear” configuration, which consists of two linear arrays installed perpendicular to each other, often called a Mills Cross configuration. Arrays are structures made up of many elementary transducers [Figure 2.1].

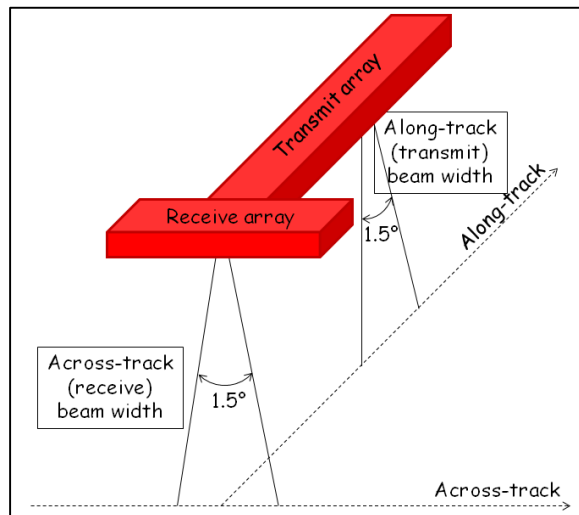


**Figure 2.1 - Mill Cross configuration.**

The array that transmits is installed with its long axis in the along track direction, and is built up from a series of transducers, each of which are excited either simultaneously (unsteered) or sequentially (steered). This creates a beam pattern in the shape of a fan athwart on the vessel [Figure 2.2, left].

The array that receives is installed with its long axis in the across track direction, and is built up from of of a series of hydrophone transducers. By combining the received signal on each transducer either as received (unsteered), or through simultaneous application of different time delays (steered) a series of receive beams are formed which are narrow in the across track direction and successively offset from each other [Figure 2.2, right].

This process of steering both transmitter and receiver beams, generates narrow beams whose array relative angles can be precisely defined.

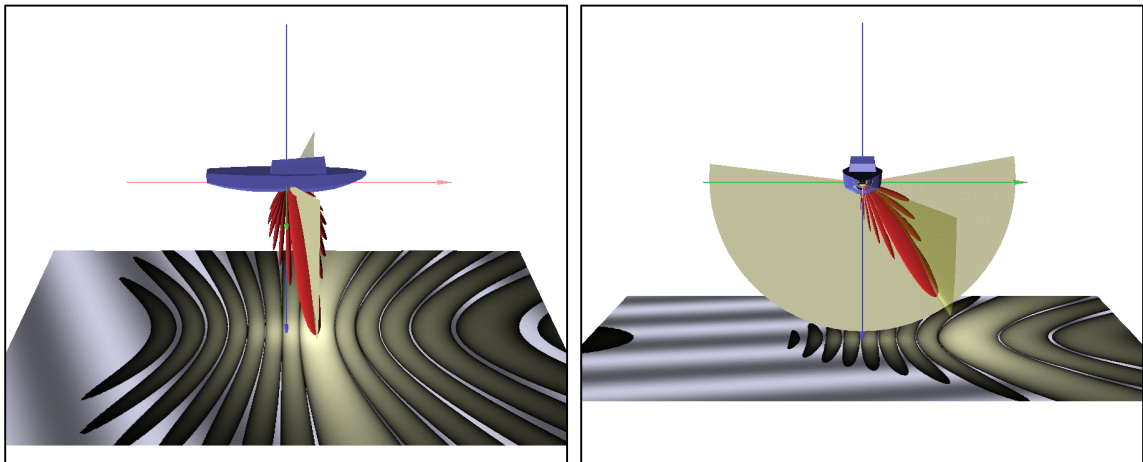


**Figure 2.2 - A beam pattern in the shape of a fan athwart on the vessel created by the transmit array (left). In this example the transmit beam is steered forward. Receive sensitivity of a single receiver beam in across track direction (right).**

## 2.2 Kongsberg EM3002

The Dutch Navy operates a dual head EM3002 ( $1.5^\circ \times 1.5^\circ$ ) from their survey launches and is considering upgrading the dual head EM3000 on their 81 meter hydrographic survey vessels (HOV's). The upgrade to EM3002 should be made because these systems would then be capable of logging water column data. The EM3000 can be upgraded to an EM3002 by using the EM3000 sonar heads in combination with a new processing unit.

The EM3002 is a single sector multibeam. For this sector it uses a frequency of 300 kHz. This makes the EM3002 suitable for shallow water survey for depths 0.5-150 m [Kongsberg, 2009]. The array lengths used in an EM3002 result in  $1.5^\circ$  by  $1.5^\circ$  beams at broadside. For receiver beams, the beam width grows as  $1/\cosine$  of the steering angle. Thus, at 60 degrees steering the receiver beam width is 3 degrees (still  $1.5^\circ$  degrees fore-aft). The importance of narrow beams is achievable accuracy for mast imaging. The small beam widths are able to reveal more details of the wreck or mast, as we can see in Figure 2.3 on the right. In the left image in Figure 2.3 not all the details of the wreck are revealed and only the single point which is selected by the bottom tracking solution will show up. With conventional bottom tracking solutions there would only be one solution per physical beam, so only a single echo per beam can be derived. With high definition beam forming and a certain geometry there are potentially more solutions per physical beam, explained further in § 2.7.

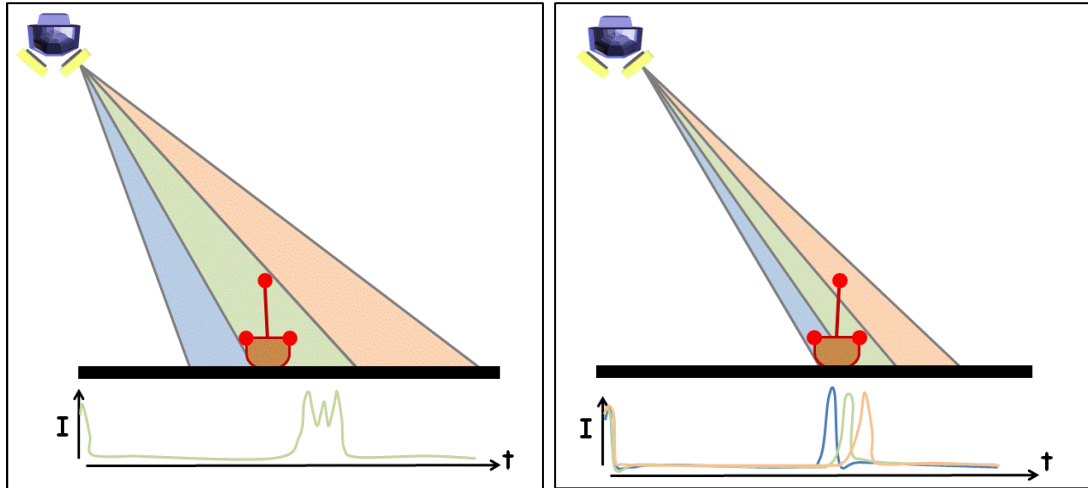


**Figure 2.3 - Imaging showing the angular resolution (right). The beam widths are not the real beam widths but are exaggerated for illustrative purposes.**

The EM3002 is compensated for both roll and pitch due to its electronic pitch compensation system and roll stabilized beams; therefore the system performance is also relatively stable in marginal weather conditions. Stabilization for pitching is obtained by steering the transmit beam electronically forward or aft at the time of transmission, based upon input from the motion sensor. Each receive beam is stabilized for roll by the beam former, using input in real time from the motion sensor. All beam pointing angles are related to the gravity vertical axis [Nilsen, 2007]. It should be noted that, while the roll steering for a receiver beam at time of recorded bottom detection is used for conventional bathymetric derivation, for WCI, there are potentially different receiver steering values for every time slice in the receive cycle.

### 2.3 Dynamic focusing

The EM3002 uses dynamic focusing. This means that it is possible to measure objects in the water column close to the transducer, even in the near field. Without this capability mast-like objects may not appear in the water column image, due to oscillation of the signal in the near field zone.

The acoustic near field distance is also referred to as the Fresnel range and is about 7 meters for the EM3002 [Nilsen, 2007]. In the near field the full directivity of the beam is not yet fully achieved. The acoustic level fluctuates and the projected beam width is fairly constant. Between the near and the far field is a zone with intensity oscillations. In the far field, oscillations no longer occur and the pressure decreases monotonically as the beam pattern is fully formed.

A solution to measure within the acoustic near field is to use dynamic focusing of the receive beams. Dynamic focusing is a technique that works around the near field limitation by creating a virtual receive array that has the same radius of curvature as the incoming energy. This is done by adding phase (or time) offsets to the (receive) array elements. The phase offsets change with time, allowing the radius of the virtual array to change with range. Dynamic focusing is only used on reception. The result is that the position of the focal point follows the distance to the expected target of that point in the receive cycle, as shown in Figure 2.4 [Hughes Clarke, 2003, Lurton, 2002]. In (2.1) the equation to calculate the Fresnel distance is given [Lurton, 2002]. Where  $L$  is the length of a linear or rectangular antenna (or diameter of a disc). And  $\lambda$  is the wavelength of the signal.

$$D_f = \frac{L^2}{4\lambda} \quad (2.1)$$

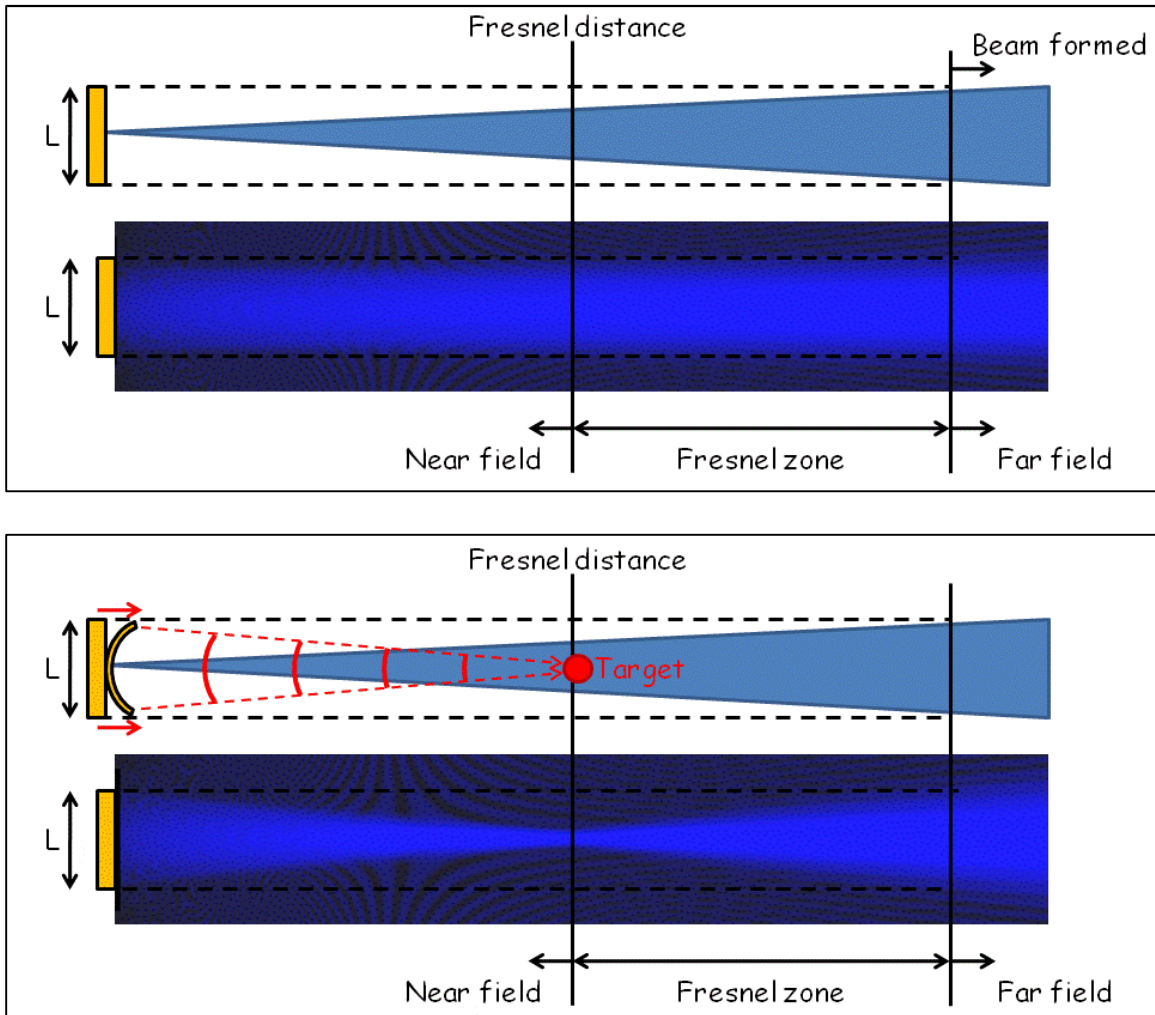


Figure 2.4 - Effect of dynamic focusing for a linear array. Standard beam forming (top), the beam is formed only beyond the near field. Inside the acoustic near field the beam is as wide as the physical size of the transducer ( $L$ ). Beyond the Fresnel distance the field doesn't oscillate any more. Dynamic focusing (bottom); the focus point (target in red) has shifted as a function of time/range. As the target moves away from the array the magnitude of the focusing decays. [Hughes Clarke, 2003, Lurton, 2002].

## 2.4 Resolution

The EM3002 uses operator-controlled transmit pulse length and receiver bandwidth; these characteristics control the achievable range resolution. The EM3002 allows for the following pulse length settings: automatic, 50, 100, 150 or 200 micro seconds. Long pulse lengths allow for better return signal strength (good signal to noise ratio). Short pulse lengths allow for good range resolution. How range resolution influences the water column image will be explained in chapter 4. The benefits of a wide bandwidth are greater potential range resolution (i.e. shorter pulse length) but inversely the detriment of a wide bandwidth is more sensitivity to noise.

**Receiver bandwidth:** The EM3002 has settings for a receiver bandwidth of either 4 or 8 kHz (cutoff frequencies). The receiver bandwidth is the range of frequencies over which the receiver listens. A wide receiver bandwidth allows for more frequency range than a narrow receiver bandwidth.

**Pulse bandwidth:** The bandwidth of the selected pulse length, is not necessarily the same as the receiver bandwidth. For a pulse length of 50 or 100  $\mu$ s the pulse bandwidth exceeds the receiver bandwidth for an EM3002 (Table 2.1). Using the frequency response curve, the pulse bandwidth is conventionally measured at -3dB on each side of the maximum (power) value. The -3dB pulse bandwidth can be calculated by (2.2) (Lurton, 2002), where  $f$  is the central frequency of the sonar head in Hertz and  $T$  the pulse length in seconds:

$$\frac{\sin(2\pi T(f-f_0))}{2\pi T(f-f_0)} = \frac{1}{\sqrt{2}} \quad (2.2)$$

For a continuous wave (CW) pulse, the spectrum would be centered about the central frequency and the bandwidth would be  $\sim 1/T$  (2.3) (where T is the pulse length in seconds).

$$BW \approx \frac{0.886}{T} \approx \frac{1}{T} \quad (2.3)$$

Thus short pulse lengths have a higher bandwidth than long pulse lengths [Table 2.1]. Note that the signal bandwidth is independent of central frequency. A pulse length of 150  $\mu\text{s}$  and a bandwidth of 8 kHz are normally used. A pulse length of 200  $\mu\text{s}$  and a bandwidth 4 kHz can be used to increase range at the expense of resolution. A pulse length of 100  $\mu\text{s}$  and a bandwidth 8 kHz can give a resolution advantage at short range. [Lurton, 2002, Nilsen, 2007]. From Table 2.1 one can see that the signal band width for pulses of 50  $\mu\text{s}$  and 100  $\mu\text{s}$  exceed the maximum receiver band width (8 kHz).

<b>1/Pulse length</b>	<b>Bandwidth</b>
1/50 $\mu\text{s}$	20 kHz
1/100 $\mu\text{s}$	10 kHz
1/150 $\mu\text{s}$	6.7 kHz
1/200 $\mu\text{s}$	5 kHz

**Table 2.1 - The bandwidths calculated by  $\sim 1/T$ .**



## 2.5 Dual Head

The EM3002 can be used in a dual head configuration. A dual head is implemented using two multibeam heads installed at offset angles. Typical dual head systems are mounted between  $\pm 20^\circ$  and  $\pm 40^\circ$ . Depending on the mounting angle the dual head can have an angular coverage more than  $180^\circ$ . That means the dual head system is able to image out to above the horizontal, as drawn in Figure 2.5 (bottom). For a single head EM3002 the maximum angular sector is  $130^\circ$ , drawn in Figure 2.5 (top). However, also (single) cylindrical transducers are capable of much wider swaths, in principle to image above the horizontal as well. The advantage of being able to image above the horizontal, is that it is not necessary to sail directly over a wreck. When the depth of a wreck is unknown it would be safer for the survey vessel not to pass directly over a wreck, which was necessary with a single head.

If the swath width is reduced, the full number of soundings is still produced inside the active swath. The result is a denser pattern of soundings. Because the boresite of a dual head is tilted to the side, the oblique beam widths are smaller as less steering is involved. The advantage of a dual head, over a single head with the same coverage, are narrower physical receive beams which will potentially lead to a higher resolution at oblique angles (however, at nadir they are now slightly worse).

When using a dual head system, the frequency of the second head has to differ from the frequency of the first head so they will not interfere with each other. In the dual head configuration, the TX/RX frequency for the port head is 293 kHz and for the starboard head is 307 kHz [Kongsberg, 2009]. Therefore, a maximum bandwidth for each

pulse of 14 kHz is allowed (which is associated with a pulse length not smaller than 72  $\mu$ s). The bottom tracking swath width can be up to 10 times the water depth for EM3002D depending upon bottom backscatter strength, water salinity and temperature [Nilsen, 2007]. Even though the bottom tracking swath width might be limited to 10 times the water depth, WCI records which reflect a time series, irrespective of successful bottom detection, can potentially log beyond this point.

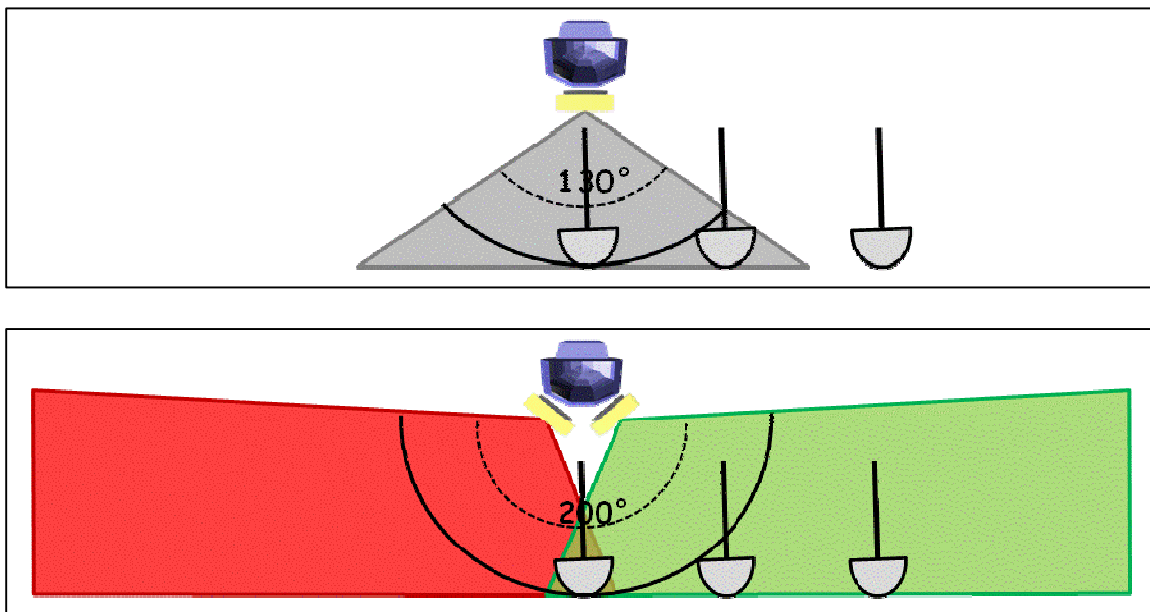


**Figure 2.5 - Top image shows a single headed system with a maximum swath width of approximately 130 degrees. The bottom image shows a dual headed system with a maximum swath width over 200 degrees.**

## 2.6 Conventional Bottom Detections

An EM3002 multibeam system uses different techniques to measure the time/angle combinations which are used to calculate the bathymetry. Each echo is received from a different direction. Those echoes received from high grazing angles (commonly about vertical) have a short echo envelope, whereas echoes received outside the central beams at lower grazing angles most commonly have a longer echo envelope. For echoes with a small envelope, amplitude detection is used whereas for echoes with a longer envelope, phase detection is used. For low relief seafloors typical resulting distribution of amplitude and phase detections is shown in Figure 2.6.

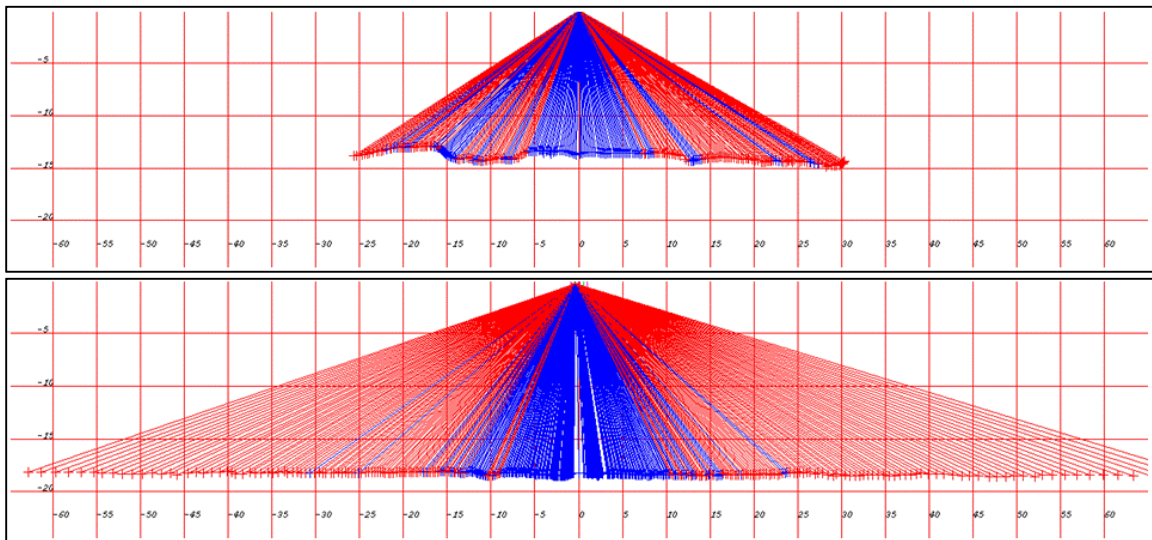


**Figure 2.6 - Phase detection in red and amplitude detection in blue. In the top image a single head multibeam, in the bottom image a dual head multibeam. Data collected in high density mode and thus there are 254 solutions in the top image, and 512 solutions in the bottom image. On the X axis across track and on the Y axis depth. Blue zones outside the central sector generally correspond to inward facing slopes.**

**Amplitude detection;** uses the maximal amplitude instant for the signal time envelope in a given beam. Amplitude detection uses a centre-of-gravity calculation, in which samples within 10 dB (Nilsen, 2007) from the maximum amplitude are used. The travel time is calculated to the centre of gravity, as represented in Figure 2.7. The angle is the central axis (beam pointing angle) of the beam considered.

**Phase detection;** the receive array is divided into two partly overlapping sub arrays. Two half beams are calculated by use of time delay. The two half beams are steered in the same direction using a common reference point. The phase difference between the two received time-series are computed at each instant. The detection is done by fitting a line (based on linear or quadratic regression) to the phase signal. Where this line crosses zero (no phase difference) corresponds to the arrival of a signal from a target exactly at the central beam axis (beam pointing angle), as shown in Figure 2.7. This point is used for the conventional phase detection point (EM3000 or EM3002 low density). Points on the line are used for high definition beam forming (HDBF) as will be explained in § 2.7.

For typical low relief seafloors, most solutions away from nadir use phase detection. For masts, however, the local grazing angle is usually high, and thus amplitude detections dominate.

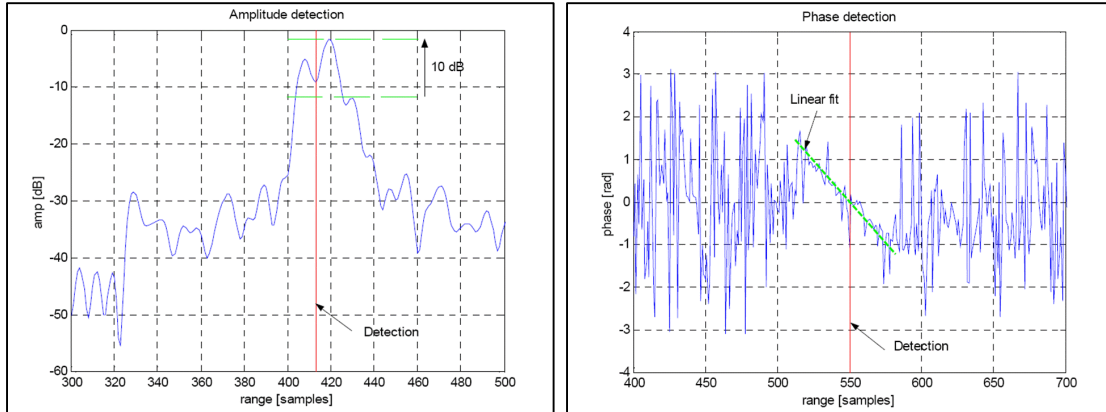


**Figure 2.7 - Bottom detection: For short echoes the bottom detection is made using full beam amplitude (left). For longer echoes the detection is based on the split beam phase. The zero crossing is where the linear fit crosses zero. Graphs from Nilsen, 2007.**

In order not to frequently mistrack on false echoes, the EM3002 bottom detection algorithm uses spike filters and range gating. Those filters and gates, however, tend to reject the discontinuous distribution of scatterers observed around features like masts on wrecks. As will be explained in chapter 6, echoes from small proud objects around and above the wreck such as masts are of great concern.

Gating is a digital signal processing method that provides an expected time window so that a particular event or signal from among many will be selected and others will be eliminated or discarded. The gates are set based on prior ping results. The tightness of gating is user controlled, for example; for a flat bottom the range gate can be set to small (in extent with medium or large) to reduce unwanted detection of echoes in the water column. For most benign sedimented seafloors, the expected change in depth from ping to ping is small, so tight gates allow cleaner bottom tracking in high noise conditions where spurious non-seabed solutions appear.

For another filter (in the bottom detection algorithm) there needs to be a record of (continuous) backscatter from around the mast location in multiple consecutive swaths. Whether the mast is picked up in more than one swath depends on the speed of the survey vessel (since EM3002 uses pitch steering as well), as shown in Figure 2.8.

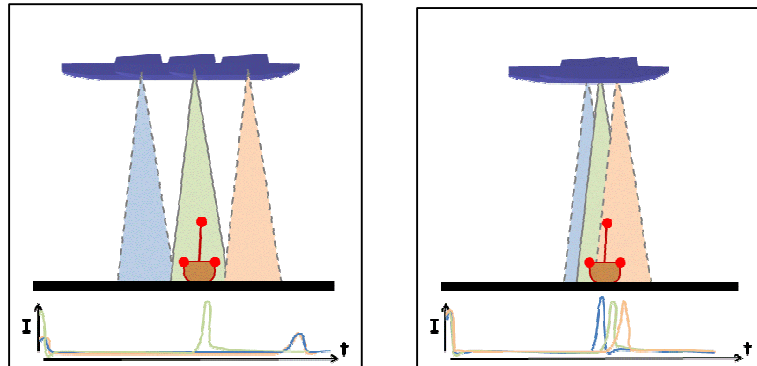


**Figure 2.8 - For the bottom detection algorithm to not ignore the mast it needs to be picked up in more than one swath. Whether the mast is picked up in more than one swath depends on the speed of the survey vessel (since EM3002 uses pitch steering as well). In the left image the mast is only occluded in one swath, in the right image the mast is occluded in all three swaths. In the left image the survey vessel would have a higher speed than in the right image.**

The along-track distribution of soundings depends on the speed of the vessel and the ping rate. A typical survey speed for a wreck would be  $< 5$  knots. With a lower speed there is a higher chance of detecting an object in multiple consecutive swaths. Depending on the bottom tracking algorithm this might influence whether bottom tracking solutions appear on the wreck or not. The ping rate is controlled by the depth and the angular sector used. Especially when using a wide angular sector of  $\pm 95^\circ$ , there is a significant compromise on the ping rate.

## 2.7 High Definition Beam Forming

The EM3002 is able to use three different beam spacing methods.

- (1) Equidistant, which gives a uniform distribution of soundings on the seafloor, uses 160 beams.
- (2) Equiangular, beams which are distributed with an equal angular spacing based on the angular coverage used. This gives many soundings close to the centre of the survey line, and fewer on the edge of the swath, uses 160 beams per head.
- (3) High definition equidistant, which produces 254 soundings. This is achieved by using the equiangular physical beam spacing and also using the high definition beam forming (HDBF) method to generate several soundings per beam on the edge of the swath. [Kongsberg, 2007]. The number of soundings, 254 per sonar head, is higher than the number of physical beams, 160 per head. The increase of soundings leads to an improved across-track resolution of bathymetric seafloor mapping. The extra soundings are formed with a method, similar to that which is used to calculate conventional zero phase crossing detections (§ 0).

Conventional phase detection looks for the time when the phase difference is zero between two signals (§ 0). But when the signal to noise ratio is sufficient, we can use a shorter part of the phase signal and fit more lines to the phase slope, so that instead of using the zero crossing, we can use  $\frac{1}{4} \pi$ ,  $\frac{1}{2} \pi$ ,  $-\frac{1}{4} \pi$ ,  $-\frac{1}{2} \pi$  etc., as illustrated in Figure 2.10. From the extra points we can calculate the corresponding physical angles with respect to the beam bore site, shown in Figure 2.9. The non-zero phase difference

corresponds to the angle with respect to the centre of the (physical) beam. To add additional lines to the phase slope there has to be enough space within the beam footprint.

[Hughes Clarke, 2009].

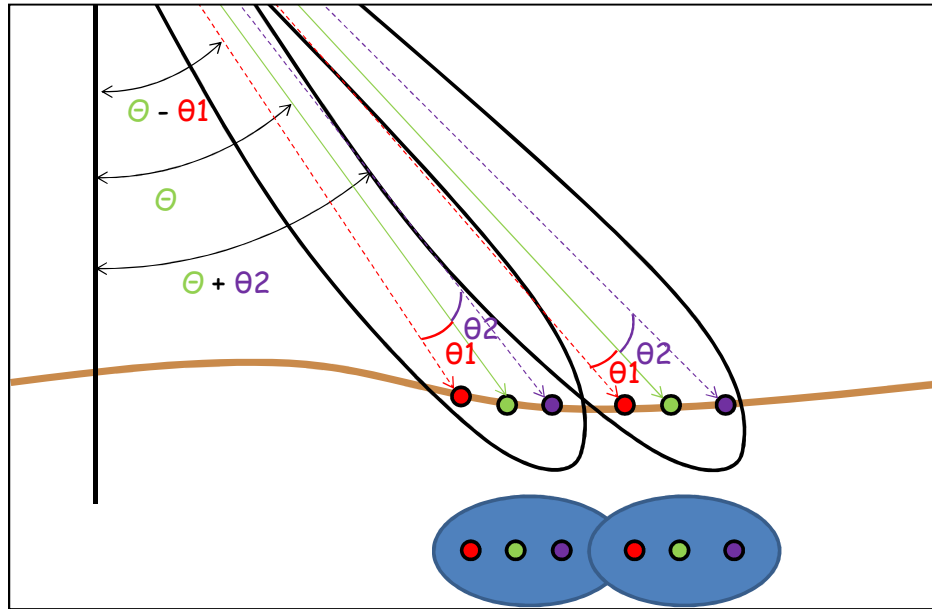


Figure 2.9 – High definition equidistant distribution of soundings.

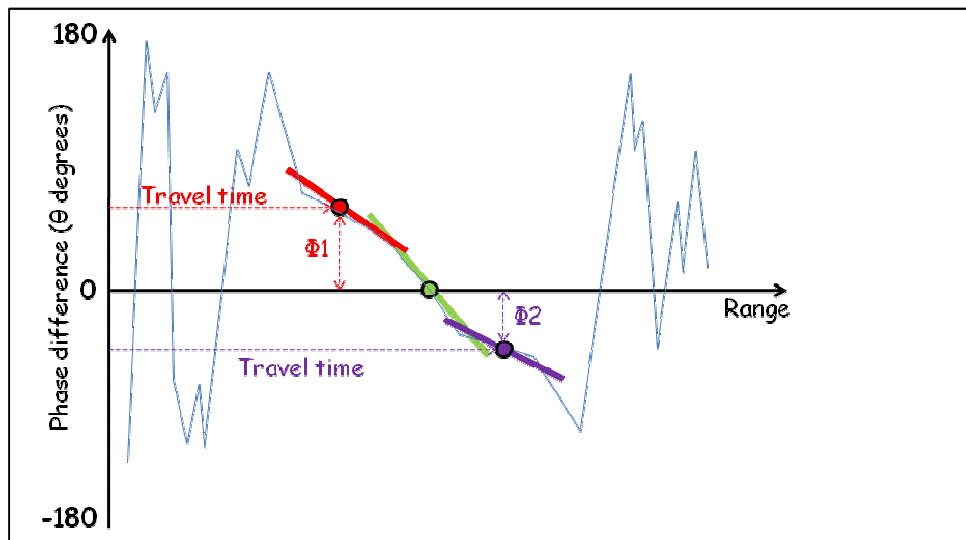


Figure 2.10 – More lines (based on linear or quadratic regression) fitted to a signal with a longer envelope.



## 2.8 Imaging Geometry

Visual inspection of the water column image (that contains a real mid water target) reveals that the image is contaminated with backscatter anomalies due to natural and electronic noise, interference, etc. No current pattern recognition software (other than the human eye) can robustly remove these. Before looking at the images, it is important to understand the imaging geometry, the effect of side-lobes, and angular responses on the water column imagery. For more information about imaging geometry the reader is referred to Hughes Clarke (2006a).

### 2.8.1 Receiver side lobes

All beams away from nadir will pick up sequences of echoes inboard of the bore site and appear in the water column image along that beam's intended boresite angle. For typical multibeam hardware, side-lobe suppression of about 25dB is normally achieved [Hughes Clarke, 2006a].

1 – First arrival. All beams away from nadir will pick up the near specular first arrival, causing an arc of apparent solutions at a common range, which is the minimum slant range (MSR) to the seafloor [Figure 2.11]. The first arrival is so noticeable because vertical incidence backscatter strength of typical seafloors usually is 5 to 20 dB stronger than for oblique echoes [Hughes Clarke, 2006a]. As a result the first arrival is normally

almost as strong as the echo from the main-lobe seafloor intersection [Figure 2.13]. The stronger the echo from the seafloor, the stronger the arc with high intensity at the minimum slant range. So a higher backscatter seafloor will produce a stronger false echo at minimum slant range. If the top of the mast is located at or close to the minimum slant range, it is hard to select the top of the mast confidently because the top of the mast is contaminated by the echo at the MSR.

2 – Inboard receiver side lobes. Inboard side-lobes appear in the water column image above the seafloor beyond the minimum slant range. The strongest (seabed) echo should normally be received from the transmit and receive main-lobe intersection. However, due to (receiver) side lobes a series of echoes will be received both before and after the main echo [Hughes Clarke, 2006a]. In Figure 2.11, Figure 2.12 and Figure 2.13 the main response axis of the first receiver side lobe is pointed out with number 1, the main response axis of the second receiver side lobe is pointed out with number 2 etc. How severe the contamination of the water column signature beyond the minimum slant range is will depend on the level of side-lobe suppression and the nature of the bottom backscatter strength of the seafloor [Hughes Clarke, 2006a]. A mast located beyond the MSR may be confused with these echoes. Whether a mast is discernable will depend on the seabed angular response.

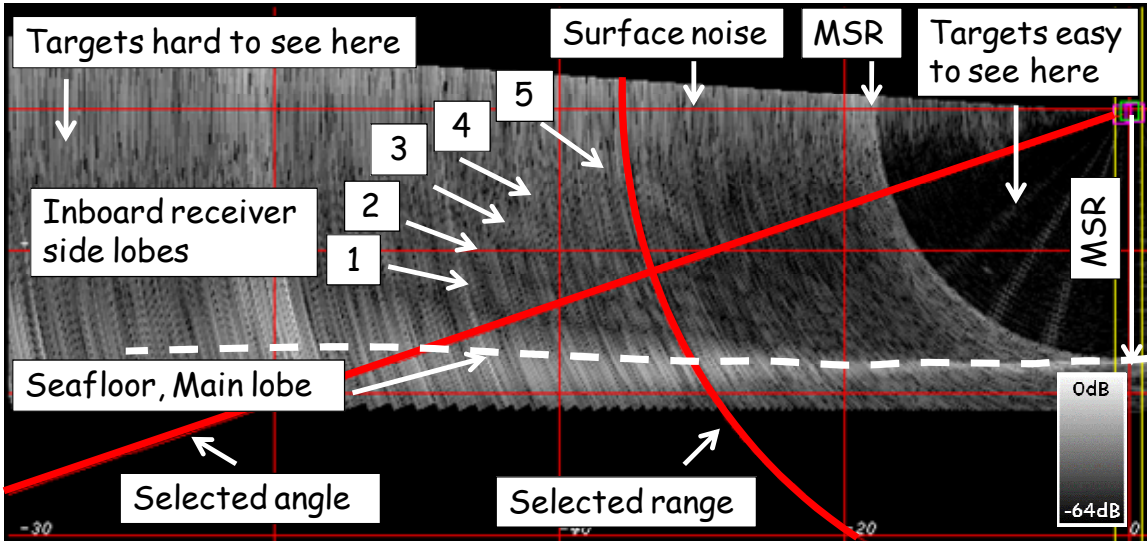


Figure 2.11 – Receiver Side lobes, highlighted selected range and selected angle.

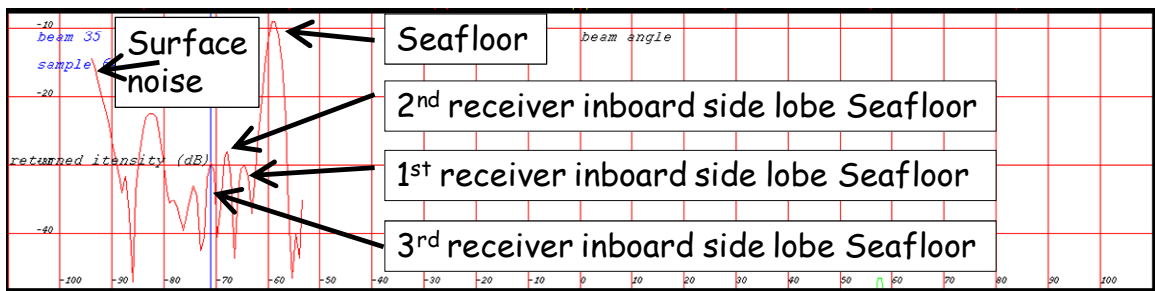


Figure 2.12 – Receiver side lobes appear in the signal plotted in a common range plot.

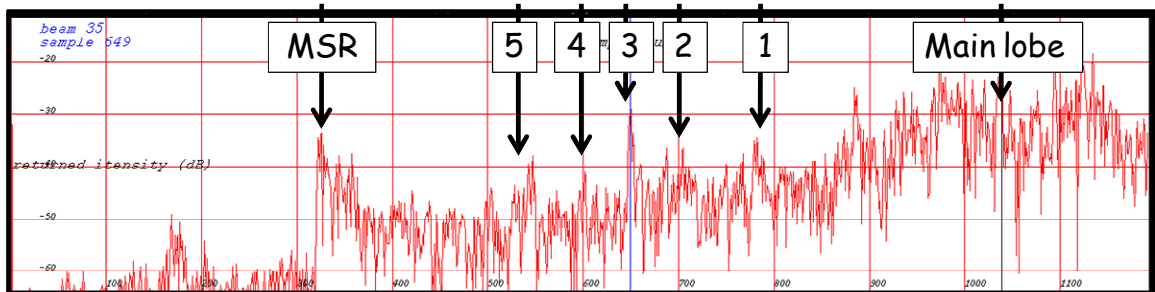


Figure 2.13 – Receiver side lobes appear in the signal plotted in a fixed angle time-series plot.

3 – Specular echoes. An echo off a point or surface, normal to the incident energy, will generate a coherent echo, often termed “specular”. These are usually stronger than incoherent echoes (in which all the scattered contributions are not exactly in phase). The strong echo of the mast will be picked up in all receiver sidelobes, causing an arc of solutions at a common slant range, up to the horizontal. Those echoes are most apparent over high backscatter targets like wrecks but may also appear on weaker reflective objects like fish. Inside the minimum slant range, although there is a wide arc of bright intensities (Figure 2.14,), the peak of the pattern can still be identified (Figure 2.15). The particularly strong sidelobe responses from that point may, however, confuse bottom detection of objects at other angles. If the orientation of the mast is nearly parallel to the expanding wavefront these echoes may be in line with the actual mast like object because it is located at the same slant range but at different elevation angles (Figure 2.16). This makes it hard to confidently pick out the top of the mast.

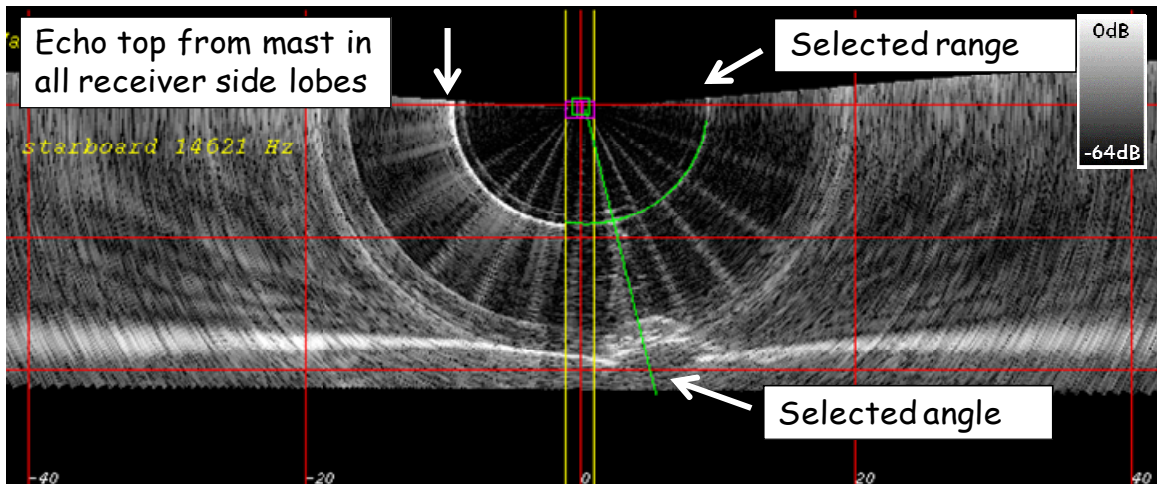


Figure 2.14 – Mast inside the minimum slant range.

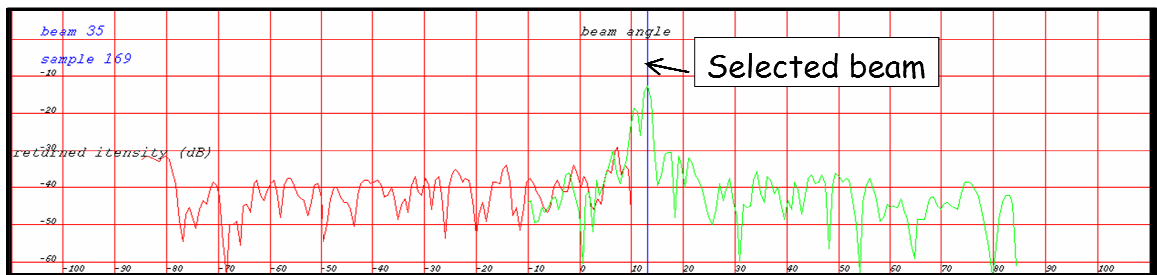


Figure 2.15 – Common range plot of the selected range of the mast inside the minimum slant range.

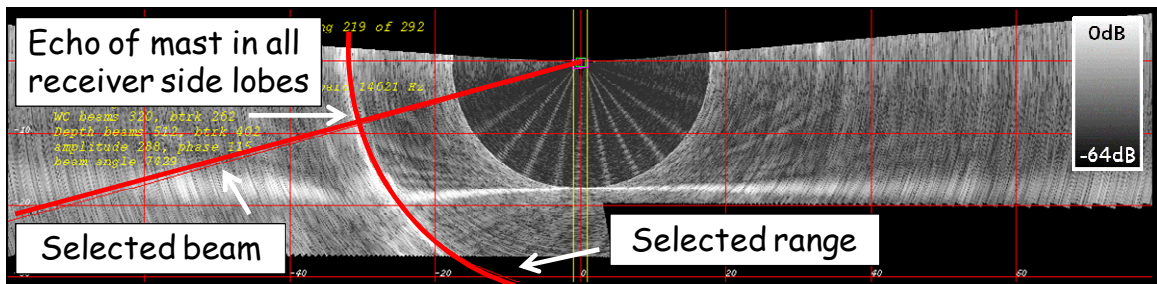


Figure 2.16 – Mast outside the minimum slant range.

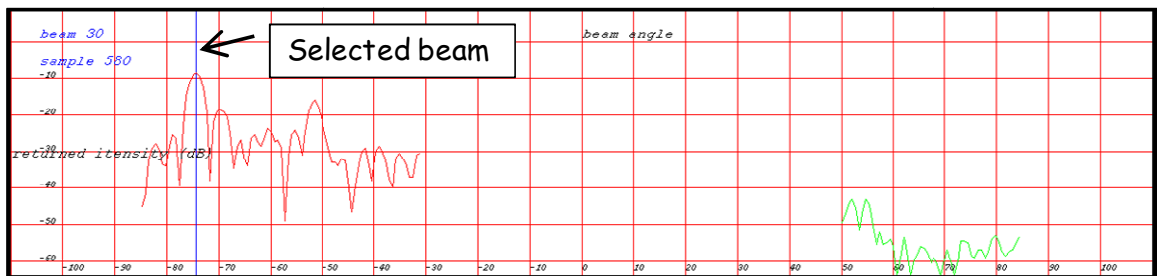


Figure 2.17 – Common range plot of the selected range of the mast outside the minimum slant range.

## 2.8.2 Transmit side lobes

Should there be a specular echo geometry ahead or behind the vessel, or a region of particularly strong scattering that lies within the transmit side lobes, a ghost-like echo will appear in the water column image before the main-lobe reaches the target of interest. As well as the main lobe tracking on the wreck itself, one clearly sees a ghost-like echo indicating the upcoming wreck and the wreck after it has been passed over. The ghost is a result of the wreck lying within the transmit side-lobe footprint (Hughes Clarke, 2006a). In the image of the vertical profile [Figure 2.18], which is made along track, the strong echo of the mast is ensounded by the transmitter side-lobes, before and after passing over the mast. However, those echoes appear always deeper than the echo from the main-lobe, therefore the echo with the least depth represents the echo from the mast received by the main lobe.

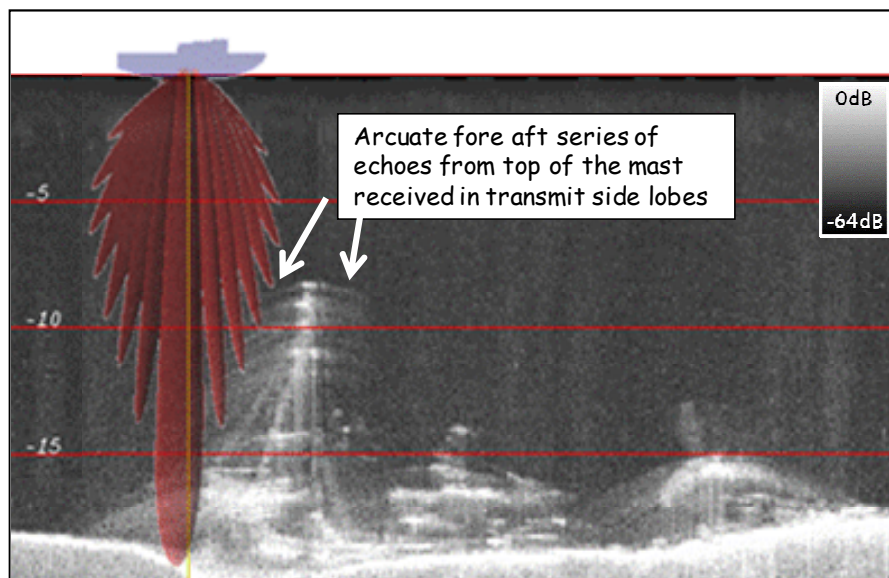


Figure 2.18 – Transmit side lobes.

### 2.8.3 Noise patterns

For some EM3002 models (particularly those where the transducer has been upgraded from a 3000), 5 distinct radial noise patterns (per head) are seen in the water column data, from the transducer until the minimum slant range. The intensity of the noise is so high (< -30dB, Figure 2.20) that they can contaminate the returned echo from the mast. If the top of the mast is located in a noise pattern, it can generally not be used for confident least depth determination and should be rejected. Analysis showed that the frequency of the noise pattern is 50 Hz, which correlates with the frequency of the inputted AC current (50 Hz Europe, 60 Hz America).

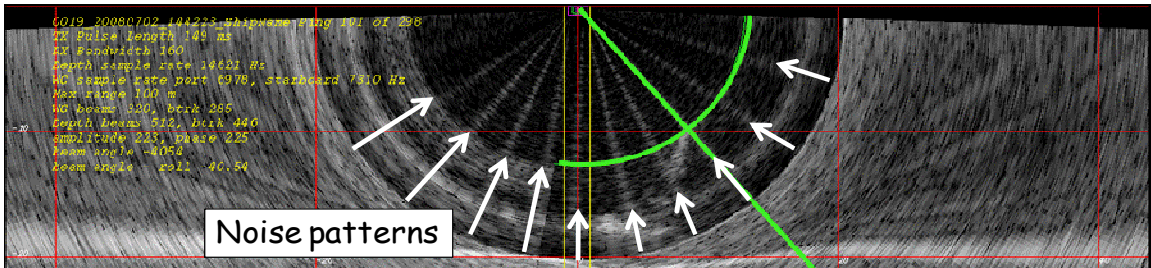


Figure 2.19 – Noise patterns.

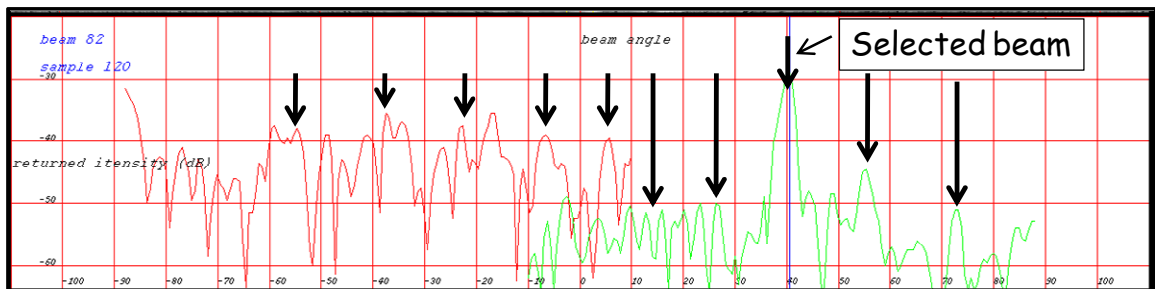
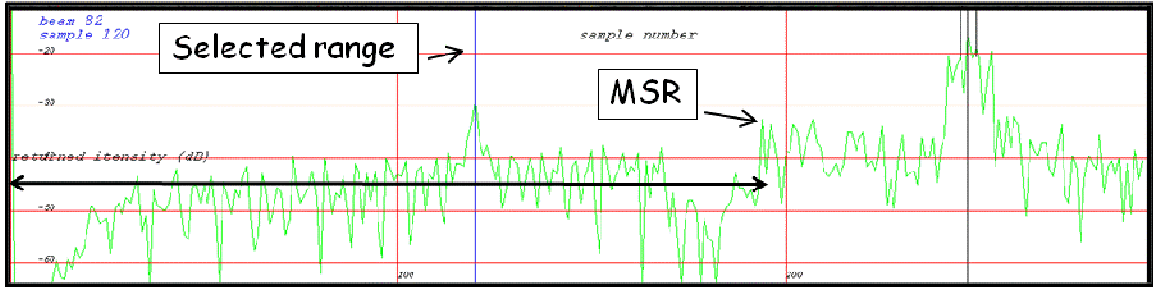


Figure 2.20 – Common range plot where the radial noise patterns become apparent.



**Figure 2.21 – Fixed angle time-series plot where the noise patterns becomes apparent.**

#### 2.8.4 Incomplete Occlusion

In several cases where the beam illuminates the mast, there is still a bottom tracking solution returned on the seafloor, beyond the mast. If energy from the main and/or side lobes makes it past the mast, the energy is able to scatter from the more distant surface, which results in more than one strong echo in a fixed angle time-series. However, since the echo from the seafloor falls within the range gates, it is favored as bottom detection. There is thus a case for tracking multiple solutions per beam. Currently only one detected range is recorded for each beam. At lower grazing angles it is harder to subjectively pick out the mast top through the broader beam widths and the presence of side-lobe contributions.



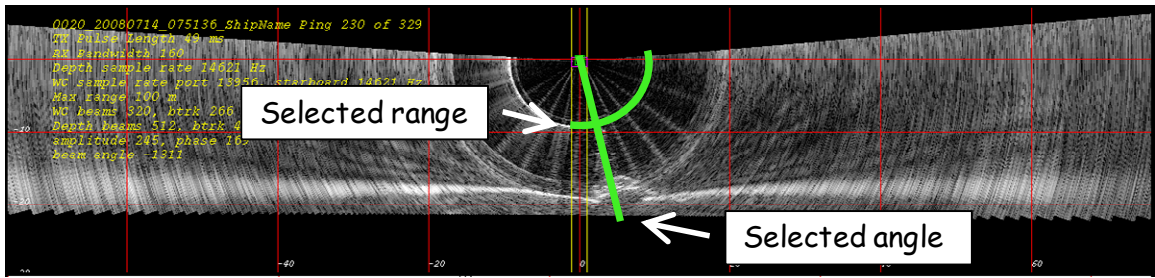


**Figure 2.22 – Mast inside the minimum slant range, in green highlighted the selected angle and selected range.**

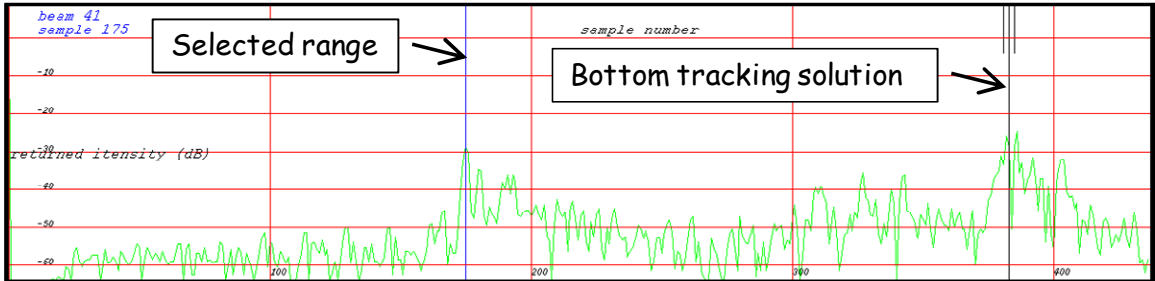


**Figure 2.23 – Incomplete occlusion.**

### 3 ACQUISITION

Part of this thesis was to execute field trials to collect Water Column Imaging (WCI) data for this research. Data were collected with a Dutch Navy survey launch of a wreck on the Dutch Continental Shelf. WCI is a relatively new method and, therefore, there were no data available collected over a wreck with an EM3002 dual head (the system the Dutch Navy would use if WCI would be implemented in their operational procedures). Ideally, the wreck has an object with a high aspect ratio, such as a mast/crane or davit. Kongsberg Maritime's Seafloor Information System (SIS) was used for the multibeam data acquisition. At the time of the survey, SIS was the only acquisition software capable of collecting and storing WCI data with the EM3002 (dual head) multibeam echo sounder. SIS controls the transducer, and enables the operator to alter settings. Data were collected over a wreck with different settings. The experiences from the field trials will be summarized in recommendations on a survey design in chapter 7.

### 3.1 Survey Platform

Data were collected with one of the survey launches of the Dutch Navy. The launch was equipped with a Kongsberg EM3002 dual head multibeam system (§ 2.2). Pictures of the launch and the dual head installation are shown in Figure 3.1. A drawing of the installation geometry of the dual head system is shown in Figure 3.2.



**Figure 3.1 - One of the survey launches of the Dutch Navy (left). Top view of the EM3002 dual head system, with the motion sensor (OCTANS) in the middle (right).**

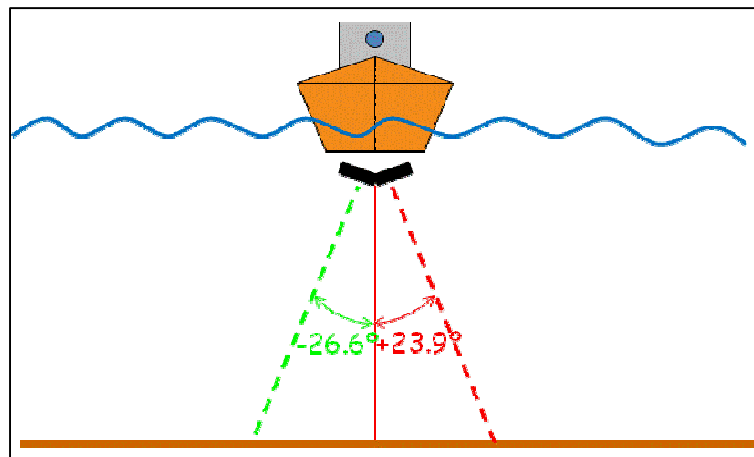


**Figure 3.2 - The heads on this survey launch are mounted at an angle of  $\pm 25$  degrees.**

For positioning, GPS Long Range Kinematic was used. A primary station was set up on the naval base in Den Helder, at a distance of approximately 10 km from the survey site. One of the LRK reference stations along the Dutch coast was used as secondary station (each station has a range of approximately 25 km).

Sound velocity profiles were taken manually. The sound velocity profiles are plotted in Figure 3.3. Even though the survey was conducted in a well mixed area, a sound velocity profile was measured before each consecutive survey. A small stratification can be seen in the upper layer. In addition to the sound velocity profiles, a surface sound speed probe (C-MAX CM2) was installed close to the head of the starboard transducer, and measured the surface sound speed continuously, which was used for beam-forming.

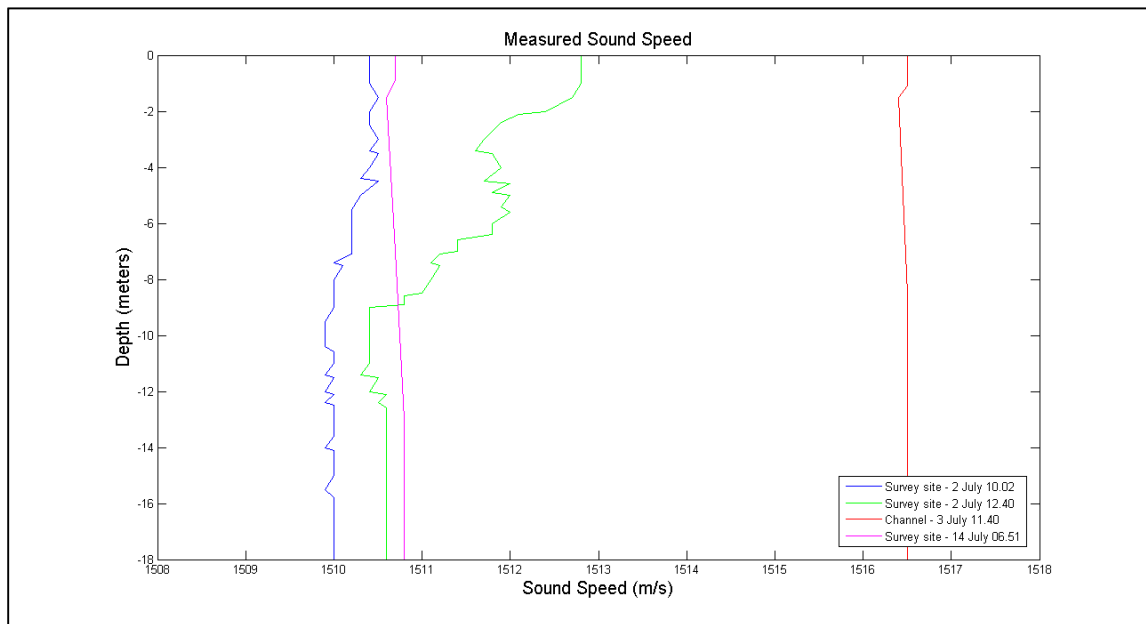


**Figure 3.3 - Sound Velocity Profiles were taken before each survey. In general the North Sea is a well mixed area, a small velocity (< 2 m/s) can be noticed in the top of the water column.**

### 3.2 Object

The Dutch Navy proposed to use the wreck of the fishing vessel HD147 for these trials. The HD147 (Figure 3.4) sank on June 11<sup>th</sup>, 2006. She capsized when the cable of the haul system broke, during an attempt to salvage parts of the wreck of the Hardalion (lying next to the HD147 ). The HD147 is 21.10 metres long, 5.40 metres in wide, and the hull is 2.55 metres high. Least depth measured over the HD147 is 10.82 metres to (Lowest Astronomical Tide (LAT), measured on 11 June 2006 by Rijkswaterstaat, by the survey vessel “Arca” equipped with an EM3002 single head multibeam echo sounder. According to side scan sonar imaging, the masts of the HD147 were still intact, and thus could be used for the WCI trials. The wreck is located ~5 nm (~10 km) west of Den Helder [Figure 3.6].



**Figure 3.4 - The HD147. Reference: “Visserij Jaarboek 2006”.**

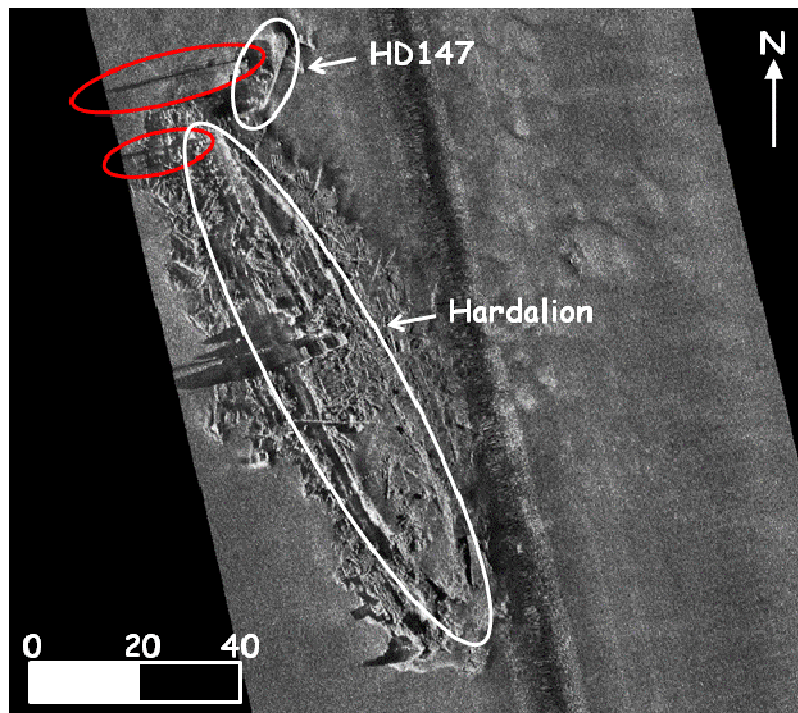


Figure 3.5 - Side scan sonar image of the Hardalion and the HD147. As can be seen from the shadow the HD147 is located at the starboard side of the bow of the Hardalion (white), the masts on the HD147 are still intact (red). As well, a mast-like object can be seen at the bow of the Hardalion (red). [Courtesy of Dutch Navy].

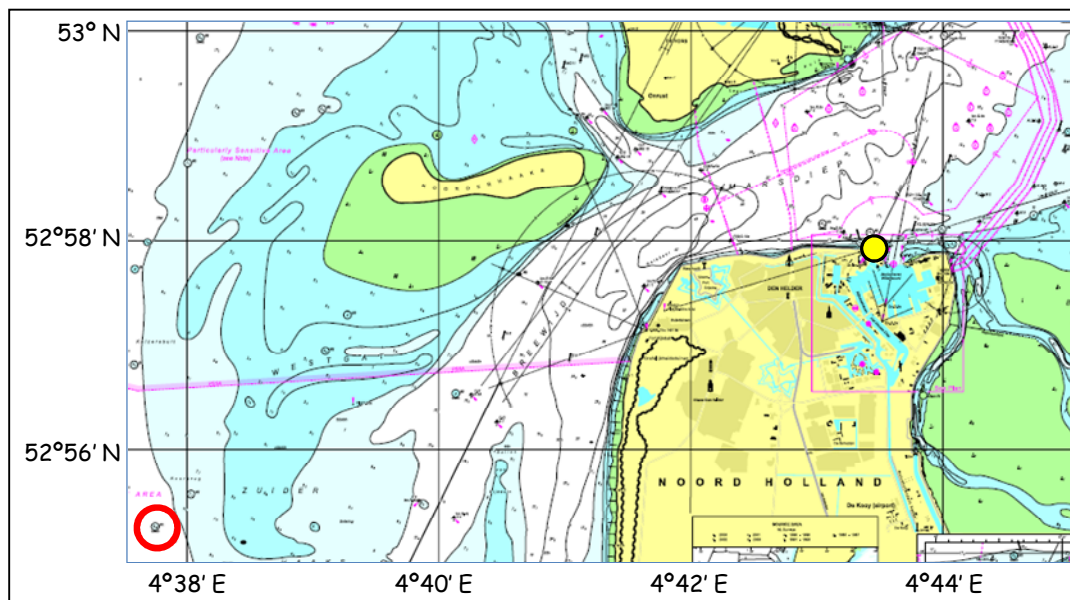


Figure 3.6 - Positions of the surveyed objects. The wrecks of the Hardalion and the HD147 located in the red circle about 5 NM (~10 km) west of Den Helder, the Netherlands. The primary LRK station was located at the position of the yellow dot.

### 3.3 (SIS) Settings

Before the survey started, SIS needed to be installed on the computers of the survey launch. At the time of the survey, only SIS was capable of logging Water Column data with an EM3002 (dual head) echo sounder. The Dutch Navy systems were then using a lower level Kongsberg software package, designed to interface with QINSy Ethernet logging.

#### 3.3.1 Installation parameters

SIS was installed on the survey vessel's desktop computer, and offsets were inserted in the installation parameters according to the ship's reference frame, finally a patch test was performed to calibrate the system (Table 3.1). The results of the ship's reference frame survey can be found in Table 3.2.

	Roll °	Pitch°	Heading°
<b>SB Sonar Head</b>	23.9	3.7	352.5
<b>Port Sonar Head</b>	-26.2	-1.1	358.8

**Table 3.1 - Table with the angular offsets from the patch test, note that the difference in heading between both heads is 6°.**

	Forward (X) (m)	Starboard (Y) (m)	Downward (Z) (m)
<b>Positioning</b>	0.742	0.683	-3.207
<b>SB Sonar Head</b>	-0.183	-0.414	0.159
<b>Port Sonar Head</b>	-0.186	0.452	0.136
<b>Water line</b>			-0.149

**Table 3.2 - Locations of the ships reference frame, measured by the Dutch Navy just before the trials. The OMG convention (used throughout this thesis) for the reference system is, X is positive forward, Y is positive to starboard, and Z is positive downward.**

### 3.3.2 Runtime parameters

In real time, the runtime parameters were adjusted to apply different settings (pulse length, bandwidth, gates, and angular sectors) for each survey. The settings can be divided in two types: settings which remain static and settings which are dynamic throughout the survey. There are many settings which can be changed, only the settings which have a considerable amount of influence on WCI are listed here.

**Static settings:** For all of the data collected during the trials high definition beam forming was used (explained in chapter 2.7); therefore, the beam spacing was set to “Hidens” mode. This results in an equiangular spacing of the physical beams. The ping rate should be set as high as possible (chapter 2). The actual rate depends on the depth and the angular sector.

**Dynamic settings:** The settings that were changed for each consecutive survey are swath angle, pulse length and bandwidth. With the EM3002 dual head system it is possible to set the beam above the horizontal. With a conventional survey, this would not be needed since there is only interest in the bathymetry; not the water column. However, with WCI this gives the advantage that there can be imagery out to, or even beyond the horizontal. When doing so, the outer beams will not detect the bottom and will potentially listen for an infinite period. Therefore, a maximum range is defined in SIS, as shown in Figure 3.7. In this case, the angular coverage should be set to manual as well, otherwise the sector angle will be forced back to a smaller angle to search and detect the bottom. The two way travel time increases with receiver angle; therefore the ping rate will



decrease with a larger angular sector. A new ping is only formed after all signals are returned or the maximum range is reached.

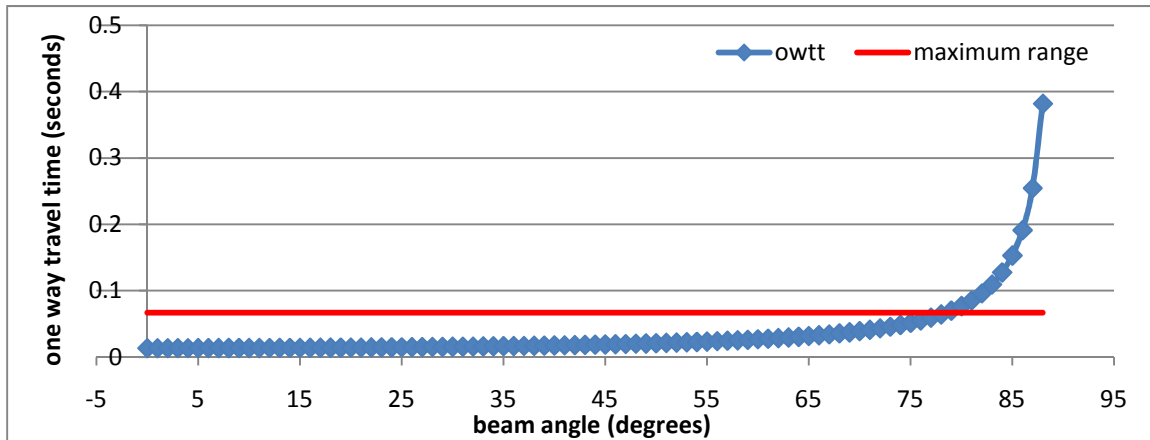


Figure 3.7 - Showing the user defined maximum range (travel time). Calculated to a depth of 20 meters, assuming a constant sound speed of 1500 m/s.

Theoretically, a short pulse length and a high bandwidth would give the best detection (§ 2.4) [Hughes Clarke, 2008]. The pulse length can be user selected (automatic, 50, 100, 150 or 200  $\mu$ s). The bandwidth has to be selected (4 or 8 kHz), since there is no automatic option. 150  $\mu$ s and 8 kHz are normally used. 200  $\mu$ s and 4 kHz can be used to increase range. At a short range 100  $\mu$ s and 8 kHz can give a higher resolution [Nilsen, 2007]. The pulse length also influences the sampling rate of the data samples recorded for the WCI. An overview of each pulse length with the corresponding sampling rate is shown in Table 3.3.

Pulse length ( $\mu$ s)	Sample rate head 293 kHz (Hz)	Sample rate head 307 kHz (Hz)
50	13956	14621
100	13956	14621
150	6978	7310.5
200	4652	4873
automatic	Depends on depth	Depends on depth

Table 3.3 - The sampling frequency depends on the pulse length used during acquisition.

### 3.4 Methodology

The methodology involves two parts; first, a line plan for each survey; and second, the proposed settings for each survey. The proposed method for the wreck of the fishing vessel HD147 were longitudinal lines over the wreck with an offset of 5 metres and cross lines over the wreck with an offset of 5 metres. A visual example can be found in Figure 3.8.

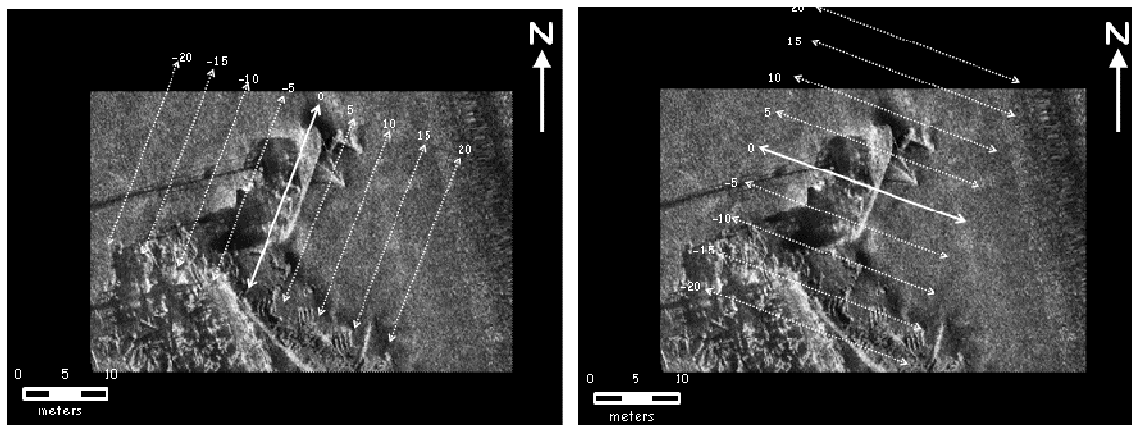


Figure 3.8 - Longitudinal lines over the wreck of the HD147 (left). Cross lines over the wreck of the HD147 (right). Offset between the lines should be ~5 metres. Side scan sonar image on the background [Courtesy of Dutch Navy].

For each survey a different pulse length and bandwidth was used. The trials on the wreck of the HD147 were done in ~20 meters depth (surrounding seafloor). The speed of the survey vessel was kept as slow as possible (~5 knots), to obtain the highest along-track data density possible. Table 3.4 is a summarized log of the survey; with the settings for each survey.

Date	Julian Day	Survey	Object	Lines	Speed (knots)	PL ( $\mu$ s)	BW (kHz)	Angular sector (degrees)	Notes
2-7-2008	JD184	3	HD147	0-22	4-5	auto	8	130	
2-7-2008	JD184	4	HD147	0-25	4-7	auto	8	176	
14-7-2008	JD196	1	HD147	0-23	4-5	50	8	190	

**Table 3.4 - A summarized survey log of all the surveys.**

## 4 SOFTWARE DEVELOPMENT

Part of this research was to modify the existing “water column” toolkit in “Swathed”. Swathed is a UNIX based software package developed at the University of New Brunswick (UNB) for swath sonar research that is active within the Ocean Mapping Group (OMG) (Ocean Mapping Group, 2010). A new toolkit for wreck least depth determination was developed in Swathed, which herein is called the “bar-sweep” toolkit, since it was designed to replace mechanical bar-sweeping for the Dutch Navy. The “bar-sweep” toolkit was designed to locate, determine and calculate the least depth of the mast. Visualizing and analyzing tools were implemented to locate the least depth of the mast, and new algorithms were designed to determine and calculate the least depth of the mast. The “bar-sweep” toolkit is able to process EM3002D water column data, with an angular sector of  $\pm 95$  degrees. Previous visualization examples were an image that only roughly approximates a depth/across-track plane which could not be used for depth determination. Therefore, a significant component of this research was to transform the water column data to true depths in the geographic frame, i.e., the fully translated and ray-traced depth and position of each sample in the water column image can now be calculated.

This section explains how Water Column Imaging (WCI) is implemented and describes the significant developments (new features) and modifications (during this research) in the “bar-sweep” toolkit. More tools (significant for research but not necessary for final depth determination, or developed in Matlab) were developed during this thesis but are not explained here and not implemented in the final toolkit. First, an

explanation of how (dual head) data is represented in Swathed is presented in this chapter; how backscatter data is recorded and processed, the visualization tools introduced, the analyzing tools introduced and finally developed algorithms. Second, an explanation of how WCI data are transformed to depths in the geographic frame is presented in Chapter 6.

#### 4.1 Backscatter Time-series

Multibeam echo sounder systems are primarily bathymetric sonars, i.e., designed to determine the range to the seabed. In addition, most common multibeam systems are capable of recording the returned signal backscatter intensity (commonly referred to as multibeam backscatter) from the seabed, which is used for seafloor classification. However, the multibeam system used herein (i.e., Kongsberg Simrad EM3002) is able to record the backscatter intensity throughout the water column. The multibeam forms receive beams that cover the (user defined) angular sector [Figure 4.1]. The full time-series backscatter are recorded as received by each physical receive beam. Backscatter amplitudes receive corrections during acquisition and are then logged in the water column telegram. The backscatter values are stored in decibels.

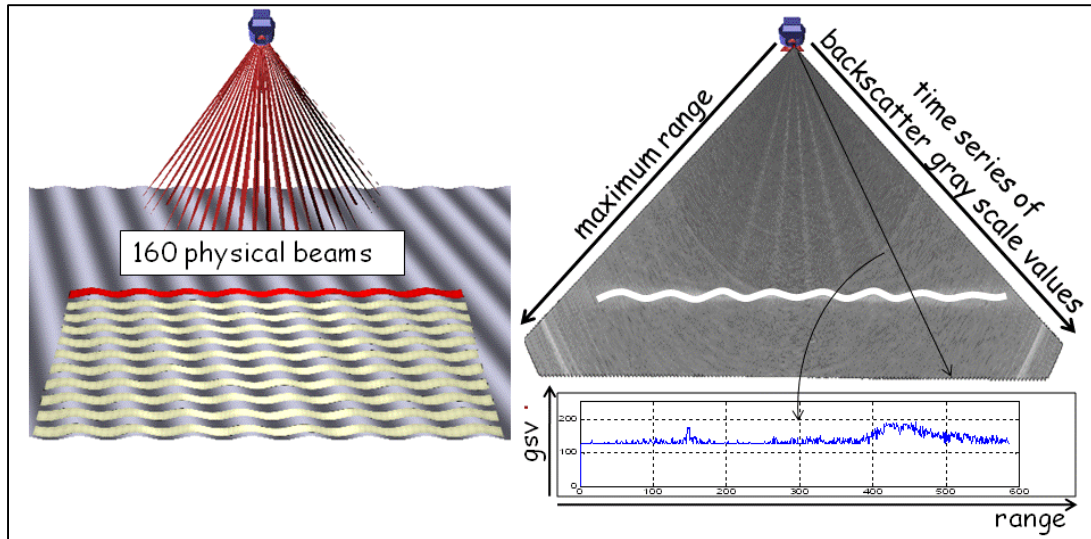


**Figure 4.1 – On the left is a presentation of a single headed multibeam system, on the right is a representation of the backscatter in a polar plot (after Hughes Clarke [2008]).**

Figure 4.2 presents the corresponding backscatter strength values for a single beam forming channel in logarithmic scale. The range is from -64 dB to + 63.5 dB with 0.5 dB resolution. Only if there are sonar calibration problems should amplitudes higher than 0 dB can occur. The backscatter in decibels is calculated by dividing by 2, since the backscatter values are stored in 0.5 dB [Kongsberg, 2010]. The logarithmic values correspond to grey scale in the images (Figure 4.3). Where, without scaling, 0 represents black (low backscatter) and 255 represents white (strong backscatter). However, swathed has the ability for the user to select a dynamic range used for grey scale. In Swathed, the original backscatter intensities are taken from Kongsberg's water column telegram and are mapped in a polar plot according to their receiver vertically referenced beam pointing angle, using an assumed constant sound speed. Logarithmic values are used because the weaker echoes are enhanced rather than peak intensities from the main lobe. Weaker echoes are associated with water column scatterers and side-lobe contributions, which are

discussed in Chapter 5. Linear intensity displays put more emphasis on peak intensities normally associated with just the main lobe bottom interaction. More information about the specific of Kongsberg backscatter algorithms can be found in Oliviera (2007) and Hammerstad (2000).

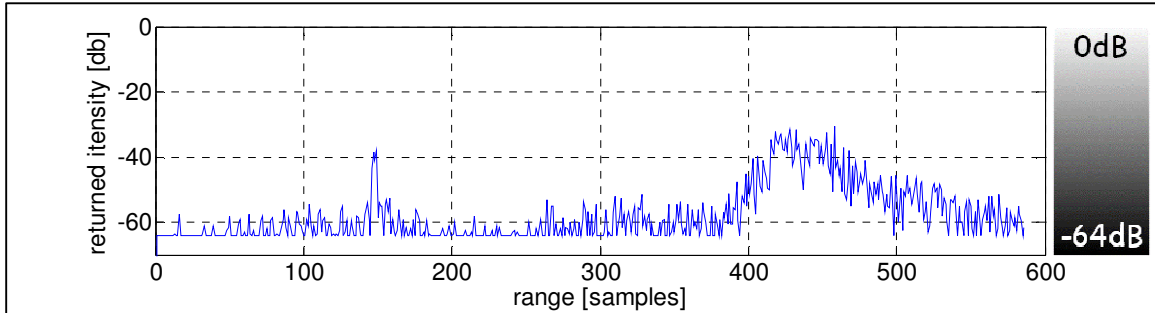


Figure 4.2 – (b) The sample amplitude time-series plotted in decibels.

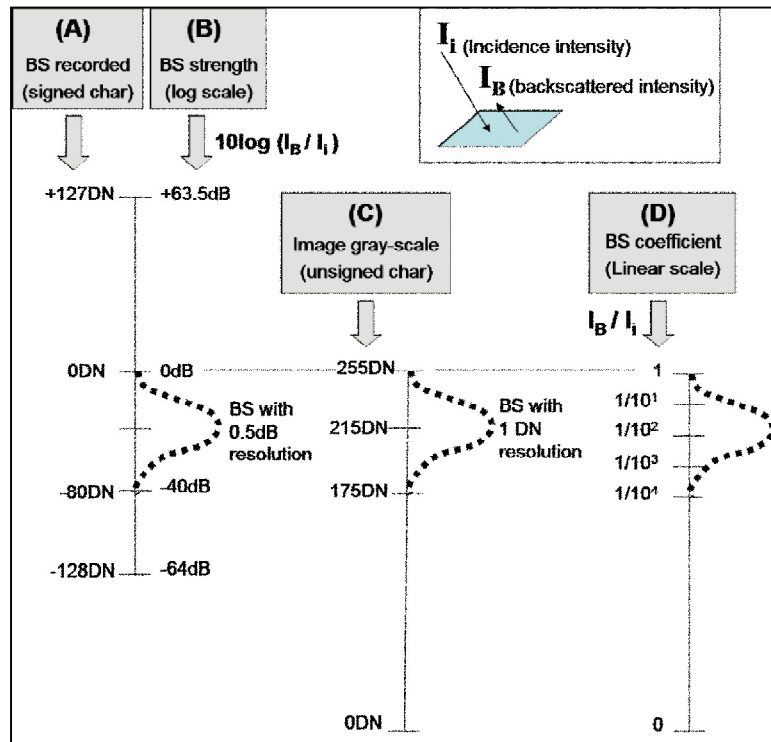


Figure 4.3 -Backscatter is recorded and represented using several scales. (a) Shows the way data are recorded by Kongsberg. (b) Has the corresponding values in log scale. (c) Is the way data are represented in gray-level images. (d) Is the corresponding values in linear scale (from Oliviera, 2007).





#### 4.2.1 Polar plot

WCI data can be represented in two dimensions as a sequence of images, where each image represents one ping (Figure 4.4). Original backscatter intensities are taken from Kongsberg's water column telegram and are mapped in the polar plot according to their vertically referenced beam pointing angle and a fixed sound speed. Time-series of backscatter gray scale values (as in the presented graph) are plotted according to each physical beam pointing angle (160 beams for the EM3002), [Figure 4.1]. Thus the polar presentation makes a simplifying assumption that the beam trace can be represented by a straight line with constant sound speed which is adequate for visualization but does not represent the precise location. Data is imaged up to the horizontal. Where data is overlapped it is possible to either put the data from the port or from the starboard head on top [Figure 4.6].

The polar plot displays common ranges relative to the sonar head. For a single headed system, corrections for transducer offsets and orientation were not necessarily required, and ranges were originally relatively plotted to the origin  $[0, 0]$ , as in Figure 4.5 (left). Depths are visualized relative to the transducer in this case. However, for a dual headed system corrections are required for transducer offsets and orientation to make a true representation, Figure 4.5 (right). Depths are corrected for offsets, heave and draft, and therefore, plotted relative to the waterline, Figure 4.6. Both heads transmit at the same time. When using an angular sector beyond nadir, the heads will overlap around nadir. To ensure full overlap in shallow water, each head partly ensonified this overlapping region. Therefore for analysis purposes, we must be able to look at data from

both heads, as in Figure 4.6 (top) and (bottom). Now two types of resolution become apparent: range resolution and across-track angular resolution.

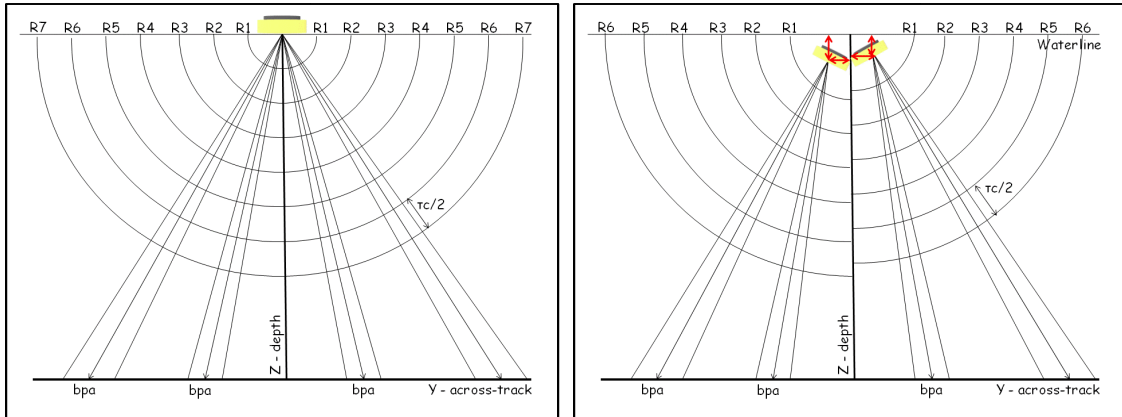


**Figure 4.5 – Backscatter intensities are plotted against each beam pointing angle, according to their sample. R are the ranges relative to each sonar head, which depend on sampling frequency and sound speed.**

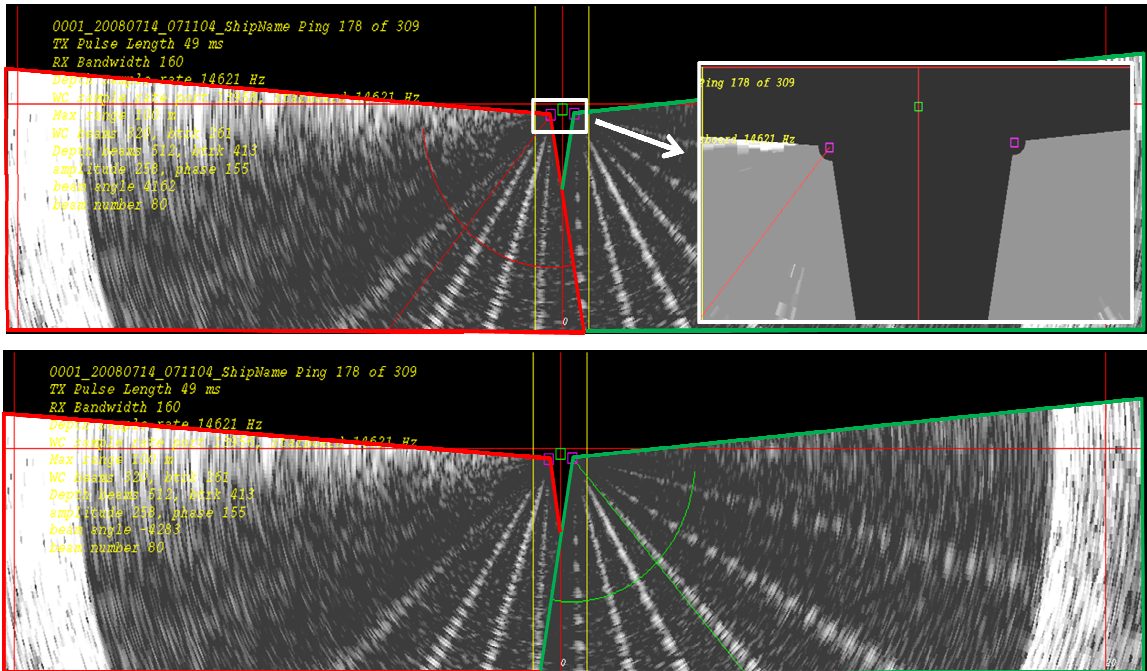


**Figure 4.6 – Polar plot where the port head overlays the starboard head (top), polar plot where the starboard head overlays the port head (bottom). In the zoomed area the transducer offsets become apparent.**

#### 4.2.2 Range resolution

From the polar plots (Figure 4.7) the difference in sampling frequency becomes apparent. The range sampling can be calculated with (4.1). In chapter 2 it was explained that the sampling frequency is controlled by the pulse length. The range sampling calculated for each sampling frequency is listed in Table 4.1. The total number of samples within a beam is a function of the range and sampling frequency (Figure 4.8).

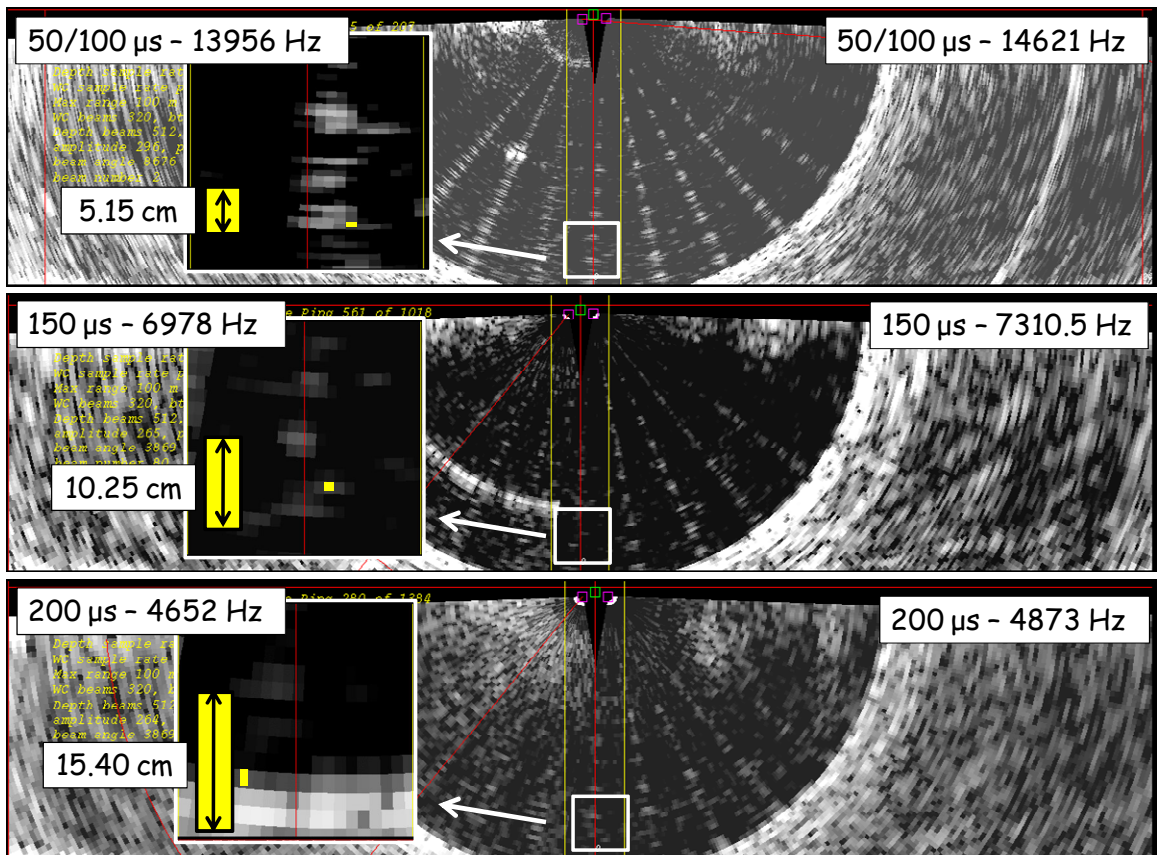


Figure 4.7 - Image resolution with different sampling frequencies, shown in the polar plot frame. In yellow the (scaled) range sampling is represented.

$$\text{distance per sample (m)} = \frac{\text{sound speed (m/s)}}{2 * \text{sampling rate (Hz)}} \quad (4.1)$$

pulse length (us)	Sampling frequency (Hz)	Distance per sample (cm)
50 -100	14621/13956	5.15/5.35
150	7310.5/6978	10.25/11
200	4873/4652	15.40/16.1

Table 4.1 - Correlation between pulse length, sampling frequency and the range sampling. A sound speed of 1500 m/s was assumed to calculate the range sampling; note that sound speed is normally not constant through the water column.

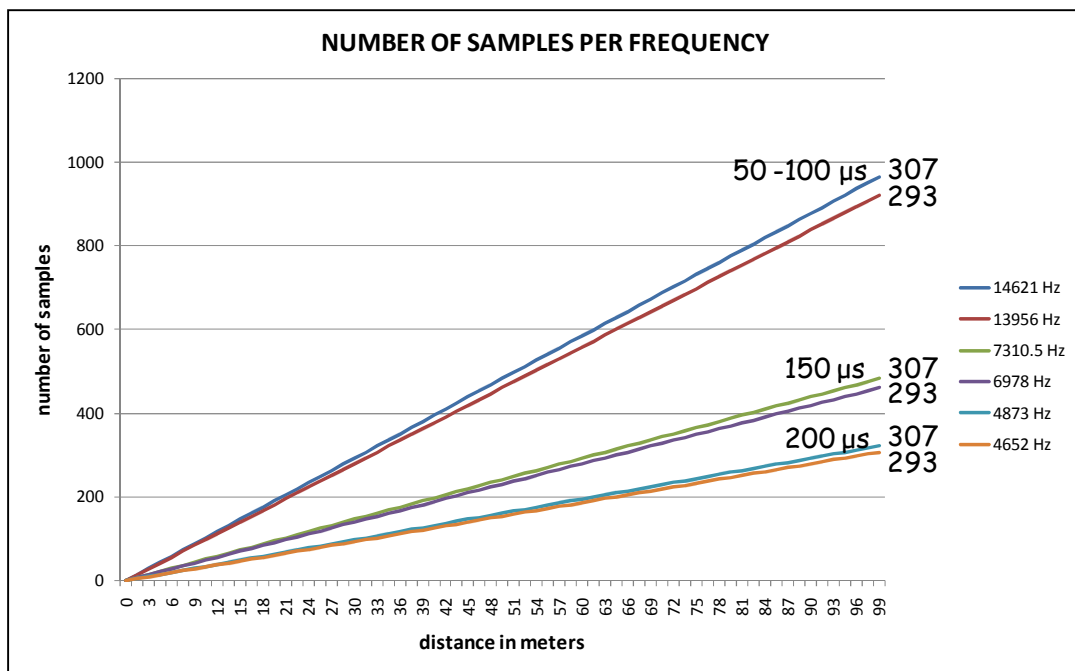


Figure 4.8 – Table showing the number of samples per range (in meters) for each sampling frequency. Assuming a constant sound speed of 1500 meters per second.

### 4.3 Angular resolution

As with the bathymetric data, in which narrowly spaced beams potentially increase resolution of the sampled seabed, narrowly spaced beams increase angular quantization of the water column image. However, as long as the angular beam spacing is smaller or the same as the physical beam width there is no benefit for WCI purposes, i.e. the beam spacing is finer than the physical beam width. With a dual head system is that the angular quantization will be higher compared to a single head system with the same angular sector. Narrow angular sector ( $\pm 65^\circ$ ) is normally used with conventional bathymetric surveys. Wide angular sector (max  $\pm 95^\circ$ ) is used to image the whole water column (Figure 4.9).

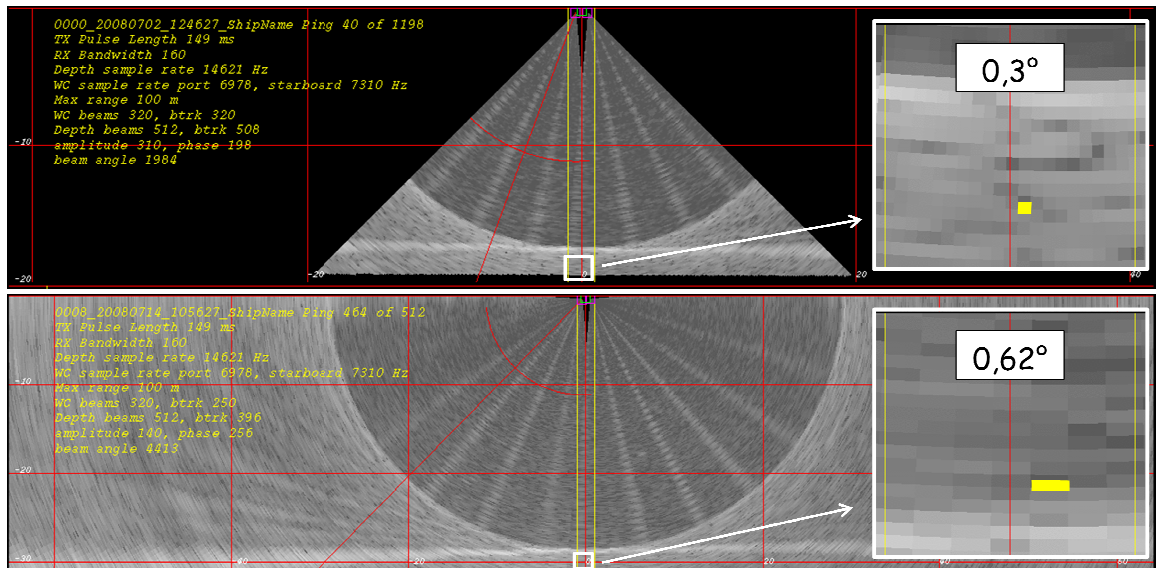
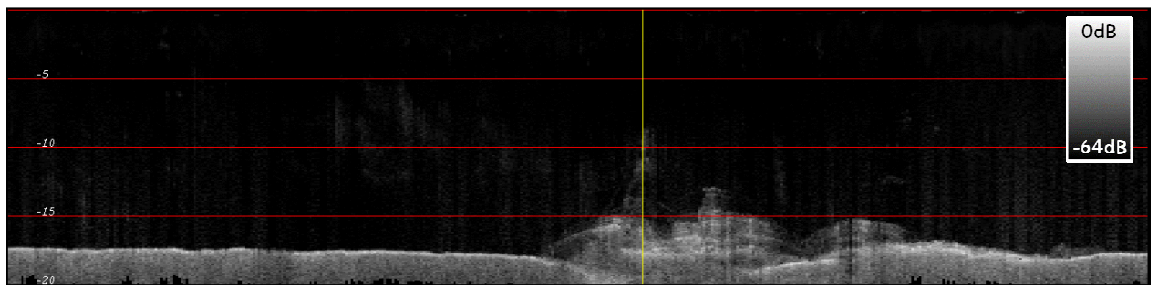


Figure 4.9 - In this figure two different angular sectors are used,  $\pm 65^\circ$  (top),  $\pm 95^\circ$  (bottom).

#### 4.4 Vertical Profile

A single ping polar plot is easy to present, but a survey consists of different sailing lines, and each line consists of hundreds or thousands of pings. It could become an issue to manage all these plots. A more efficient way to handle large volumes of data in a timely manner is to make a vertical profile of all those pings [Figure 4.10]. A cross section can be made, giving rise to a classic single beam echogram; the result is a 2D along-track section of the data [Figure 4.4]. It is important to note that such an image is merely a cross section of all the available data; while informative within the virtual single beam it is incomplete [Buelens, 2006]. This allows one to view the evolution of the central section of the water column very efficiently over long time intervals. The vertical profile is loaded first in the “bar-sweep” tool, this makes it possible to select the data around the wreck and load polar plots of the necessary swaths only.



**Figure 4.10 – Vertical profile with the corridor placed straight below the ship. The yellow line represents the selected swath in the polar plot.**

The vertical profile is build up out of the pixels from the polar plot within the selected corridor (Figure 4.11). The width and the across-track position of this corridor is



given in the polar plot by 2 yellow lines. In the most left example the wreck is located straight below the ship and therefore the echoes of the wreck show up in the near nadir beams which are within the corridor; therefore, those echoes show up in the vertical profile. Should there be water column scatterers of interest inside the minimum slant range, they will usually appear in the near nadir beams at some point. Scatterers beyond the minimum slant range will never appear in the vertical profile. However, it is possible to shift the corridor to port or to starboard, when doing this the resolution will decrease away from nadir. At nadir the resolution is controlled by range resolution, however by moving away from nadir the resolution is more controlled by angular resolution which is worse than the range resolution (in the case of an EM3002D), and decreases away from the ship. Therefore, the more the corridor is moved away from nadir, the poorer the resolution gets, as in Figure 4.11.

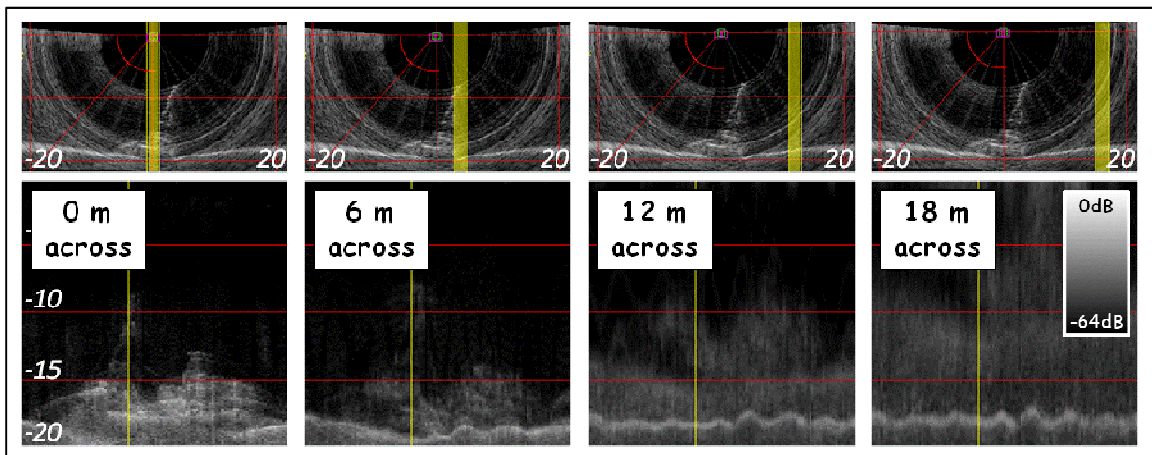


**Figure 4.11 – Representation of the vertical profile moved away from nadir, from the left image towards the right image. Where the yellow box represents the corridor from which the pixels are placed in the vertical profile.**

## 4.5 Analysis tools

For analysis the backscatter was plotted in two graphs: Fixed angle time-series plot and the common-range plot. The selected beam or selected range for which the time series or common range are plotted, are highlighted in the polar plot, both in red when the port head is selected and both in green when the starboard head is selected (Figure 4.12). In the fixed-angle time series plot the backscatter is plotted for the time-series of the selected beam (Figure 4.13). On the x-axis the range in samples is given, and on the y-axis the backscatter as returned intensity in decibels. It is also possible to give the range in travel time (seconds) or as a distance (meters). The blue line represents the selected common range in the polar plot. The black line represents the detected range to the bottom tracking solution, if there is a bottom tracking solution made for the selected beam.

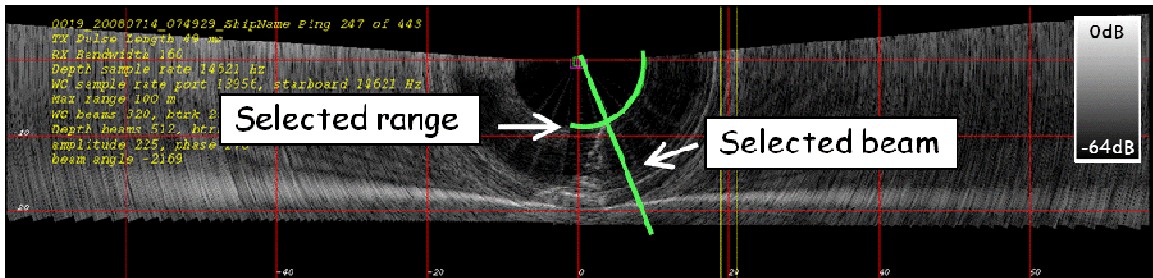


Figure 4.12 – Polar plot with selected beam and selected range highlighted.

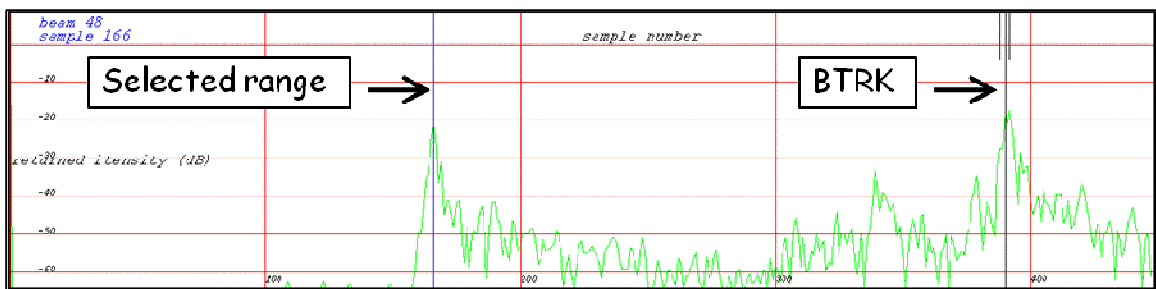


Figure 4.13 – Fixed angle time-series plot.



#### 4.6 Common-range plot

In the common-range plot the backscatter is plotted for the selected common range (Figure 4.14). In red is the backscatter from the port head and in green the backscatter for the starboard head. On the x-axis the beam angle is given, and on the y-axis the backscatter as returned intensity in decibels. The blue line represents the selected beam. Note that the beam angles overlap at nadir. However, the backscatter from the mast will not appear in the same beam angles for each head if the mast is detected in this overlapping region. The mast is measured under an different angle for each head as shown in Figure 4.15. In the port head the object the strongest detection is at  $8^\circ$  but for the starboard head the strongest detection is at  $0^\circ$ .

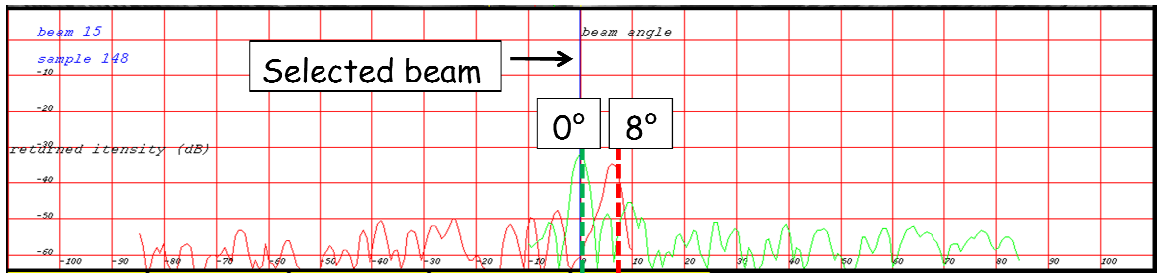


Figure 4.14 - Common-range plot, where the mast is detected in the overlapping region at nadir.

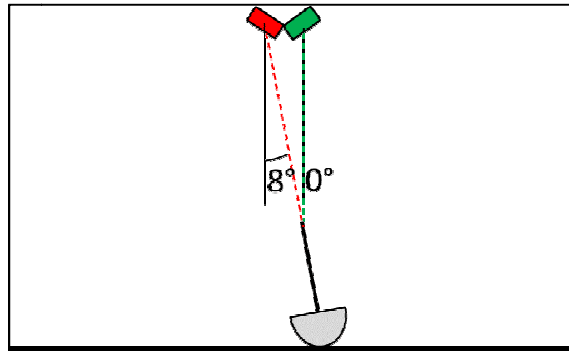


Figure 4.15 – Top of the mast detected in different beam angles for each head.

#### 4.7 Imaging Geometry Quality Factor (IGQF)

To synthesize the results the Imaging Geometry Quality Factor (IGQF) is introduced. The “IGQF” is herein defined as the vertical uncertainty due to the imaging geometry. The “IGQF” describes the vertical component of the uncertainty of the least depth determination inside the MSR, due to the uncertainty caused by the equipment’s angular and range resolution. As the receiver beam width of the main lobe increases with steering angle, the ability to discriminate objects based on angle decreases. The operator cannot discriminate better than the physical resolution of the system. Even though the top of the mast may still be imaged, the angular resolutions decays with steering. The “IGQF” can be calculated as a distance in the depth direction, as explained here below in equation 4.2 till 4.10.

At nadir the quality is controlled by range resolution and is constant. The range resolution depends on the bandwidth of the pulse (a shorter pulse length has a higher bandwidth) and the sound speed (4.2). Where RR is the range resolution in meters, c the sound speed in meters per second and BW the bandwidth in Hertz.

$$RR = \frac{c}{2*BW} \quad (4.2)$$

Away from nadir the vertical component of the uncertainty varies, and depends on beam width (4.3) and range (4.6). The “receiver” beam width for each beam is different and depends on the array length (which, for an EM3002 results in a 1.5 degree beam at nadir) and steering angle (chapter 2). In case of a dual head geometry, the steering angle is the angle reference vertical as stored in the water column datagram minus by the installation angle of the transducer head. The angles ( $\theta_1$  and  $\theta_2$  in Figure 4.16) of each

side of the beam can be calculated using equation 4.4 and 4.5. The range (R) to each sample can be calculated using equation 4.6 and 4.7, where k is the sample number.

$$beam\ width = \frac{1}{\cos(\theta_{steer})} * 1.5 \quad (4.3)$$

$$\theta_1 = \theta_{ref\ vertical} - \frac{beam\ width}{2} \quad (4.4)$$

$$\theta_2 = \theta_{ref\ vertical} + \frac{beam\ width}{2} \quad (4.5)$$

$$R_1 = \frac{c * k}{2 * BW} \quad (4.6)$$

$$R_2 = \frac{c * (k+1)}{2 * BW} \quad (4.7)$$

The depth component for each side of the selected beam and sample, depending on range resolution and “receiver” beam width, can be calculated using equation 4.8 and 4.9 (Z1 and Z2 in Figure 4.16). Finally, the quality or “IGQF” for the selected sample can be calculated using equation 4.10.

$$Z_1 = R_1 * \cos(\theta_1) \quad (4.8)$$

$$Z_2 = R_2 * \cos(\theta_2) \quad (4.9)$$

$$quality = Z_2 - Z_1 \quad (4.10)$$

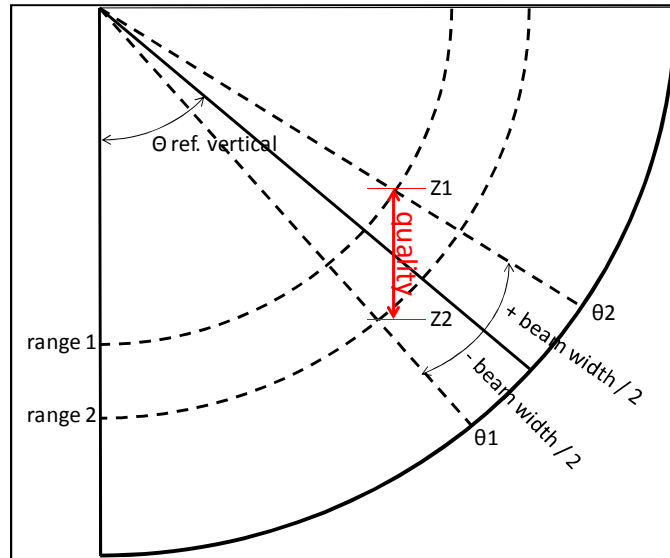


Figure 4.16 - Image describing calculation of the “quality” of each sample.

The result is an “IGQF” for each sample as represented in Figure 4.17. The angular resolution for each beam decays with range and steering angle, therefore, the “IGQF” also decays with range and steering angle.

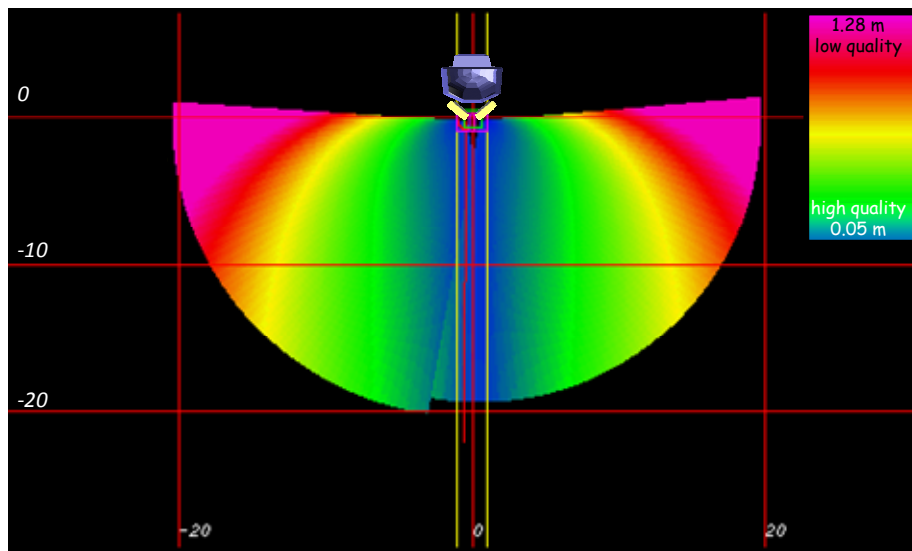
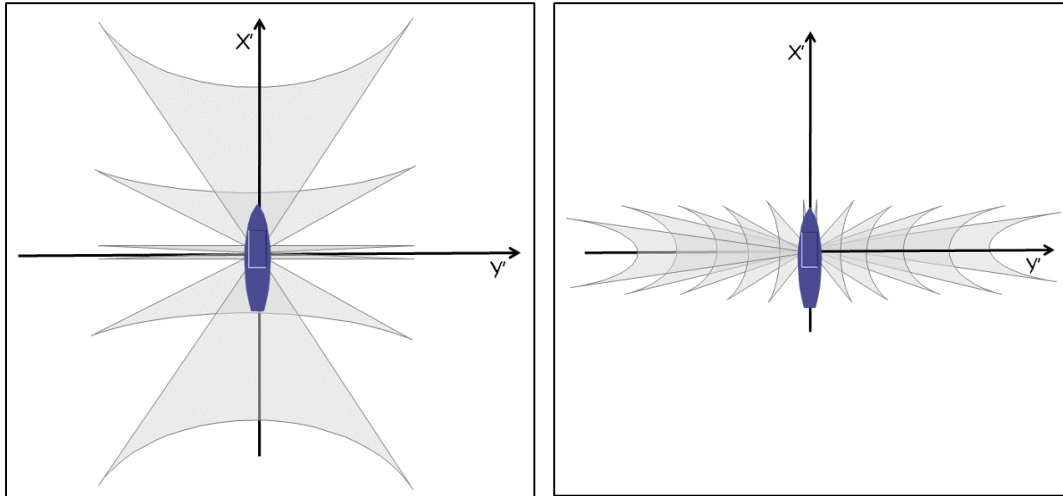


Figure 4.17 – Representation of the calculated Imaging Geometry Quality Factor for an EM3002D with the highest range resolution.

## 5 WATER COLUMN IMAGE GEO-REFERENCING

The current polar display is an image that approximates a vertical plane in the across track direction relatively below the ship rather than a solution in the 3D geographic frame. The polar plot is made up of time-series of intensity plotted along straight lines according to each beam 's pointing angle (from the water column structure) in a vertical flat plane in the across track direction relatively to the receive array. Ranges are calculated assuming a constant sound speed in the water column. The actual ray path is not a straight line but is refracted through the water column depending on the (measured) sound speed profile. The result is not a vertical plane in the across track direction relatively below the receive array but the transmit beam takes on a conic form as we steer, as shown in Figure 5.1 and in Figure 5.2.

After the time/angle which represents the top of the mast is selected in the polar image, the selected pixel needs to be transformed into the 3D geographic frame. Therefore, we need sufficient information to make the transformation from imaging space to geographic space. For the final solution, a depth (tidally reduced and referenced to Chart Datum) with a latitude and longitude in the geographic system, should be the product for referencing it in a nautical chart.



**Figure 5.1 - Due to beam steering the plane takes on a conic form. The more the beam is steered the more obvious the conic shape is. In the left image beam steering for the transmit beam and in the right image beam steering for the receive beams.**

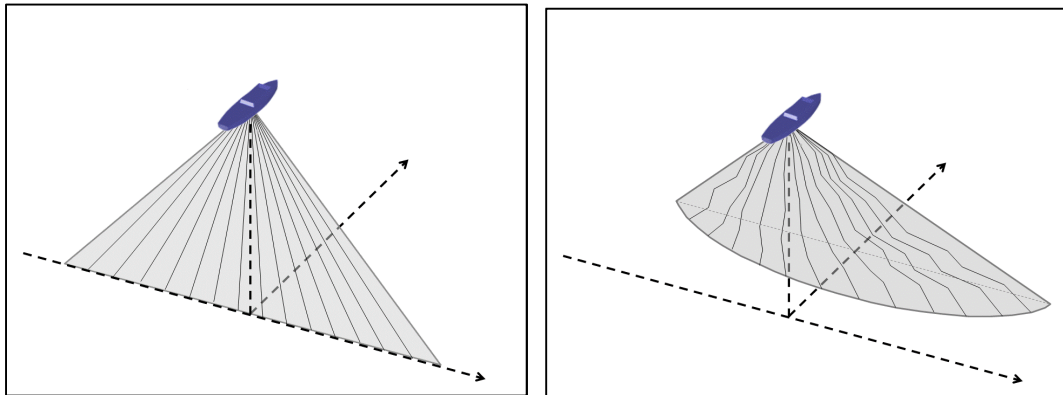


**Figure 5.2 – Left, the water column time-series as a straight line along the beam pointing angle, represented in a flat plane relatively below the ship. Right, representation of the water column time-series along a ray-refracted path, where the beams take on a conical shape.**

## 5.1 Kongsberg Data Structures

Kongsberg multibeam systems record data in a line file (with the suffix .all). The user can choose to store the water column data in the line file or in a separate water column file (with the suffix .wcd). Each line file consists of defined data structures with information. Examples of structures are: depth, raw range and beam angle, water column, attitude, position, sound speed, installation parameters and runtime parameters. A simple polar plot can be produced with information derived only from the water column structure. Additional information from the installation parameter structure (lever arms) and attitude structure is however needed to fully account for sonar offsets and orientation.

To make the transformation from approximate image to exact geographic space, information from the depth structure, or the raw range and beam angle structure and the sound speed profile is also needed. From the depth structure the beam depression angle and azimuth are needed to make a direct ray bending calculation. If beam pointing is required, the raw beam angle from the raw range and beam angle structure is needed for full reprocessing (as explained in Beaudoin, 2004). Attitude data throughout the receive cycle is also required for full reprocessing. To implement this transformation, we therefore need to correlate the beams from the water column structure, firstly to the depth structure and secondly to the raw range and beam angle structure.

In Chapter 2 it was explained that there are three beam spacing methods: equidistant, equiangular and high definition equidistant. In the depth and raw range and beam angle structure 160 solutions are stored when surveying in equidistant or equiangular mode, and 254 solutions are stored when surveying in high definition mode.

In the water column structure 160 solutions are stored independent of the beam spacing method used, because the intensity time-series are only recorded along the physical beams. That means, that when surveying in high definition mode (the mode used for these experiments), the number of solutions in the depth and raw range and beam angle structure is higher than the number of beams in the water column structure and there is indicator that limits the two. This is summarized in Table 5.1.

From this analysis it is concluded that, at this moment, there can be no simple correlation made between the water column structure and the depth or raw range and beam angle structure when surveying in high definition mode. That is to say a beam in the depth or raw range and beam angle structure cannot be matched unambiguously with a beam in the water column structure. It is important to understand that WCI was initially designed for imaging and not designed for rigorous depth measurements.

		Beam spacing method		
		Equidistant	Equiangular	High definition equidistant
Structure	Depth	160	160	254
	Raw range beam angle	160	160	254
	Water column	160	160	160

**Table 5.1 - Number of solutions (per head for an EM3002) for each beam spacing method.**



## 5.2 Re-point water column receiver angles

It was mentioned in chapter 3 that the data for this research was collected in high definition mode only. For data in high definition mode there is no correlation between the water column structure and the depth and raw angle structures. As a result a direct ray-bending calculation from the depression angle and azimuth from the depth structure or a full transformation from the raw angle from the raw range and beam angle structure cannot be made.

In order to make a ray-bending calculation the single angle stored in the water column structure needs to be transformed into the equivalent angle stored in the raw range and beam angle structure. The angle in the water column structure is reported to be the beam pointing angle referenced to the vertical. Such a description is ambiguous as multiple interpretations of such an angle are possible. The EM3002 uses roll stabilized beams. Each receive beam is stabilized for roll by the beam-former, using input in real time from the motion sensor. The roll angles will be different for each unique time of reception for each beam due to the changing vessel motion. The sound speed at the transducer depth is also used in the beam steering. The water column data structure also includes beam angles without a detected range, implying that they were not used for successful bottom detection. This is in contrast to the raw range and beam angle and depth structure which only report beams that have successfully achieved a bottom detection. In the raw range and beam angle structure the beam angles are the original steering angles relative to the transmit array at transmit time and to the receive array at receive time.

After personal communication with Kongsberg Maritime, a solution was proposed to re-calculate the array relative receiver steering angle ( $\theta_{RXsteer}$ ) using the angle ( $\theta_{watercolumn}$ ) stored in the water column structure. The installation roll angle for each head ( $R_{alignment}$ ) and the roll for each beam at receive time ( $R_{orientation}$ ) is subtracted from the physical beam pointing angles in the water column structure, as in (5.1). Note that each measured sample has a unique steering angle at the time of reception, and thus has a unique pointing angle. One example is given in Figure 5.3.

$$\theta_{RXsteer} = \theta_{watercolumn} - R_{alignment} - R_{orientation} \quad (5.1)$$

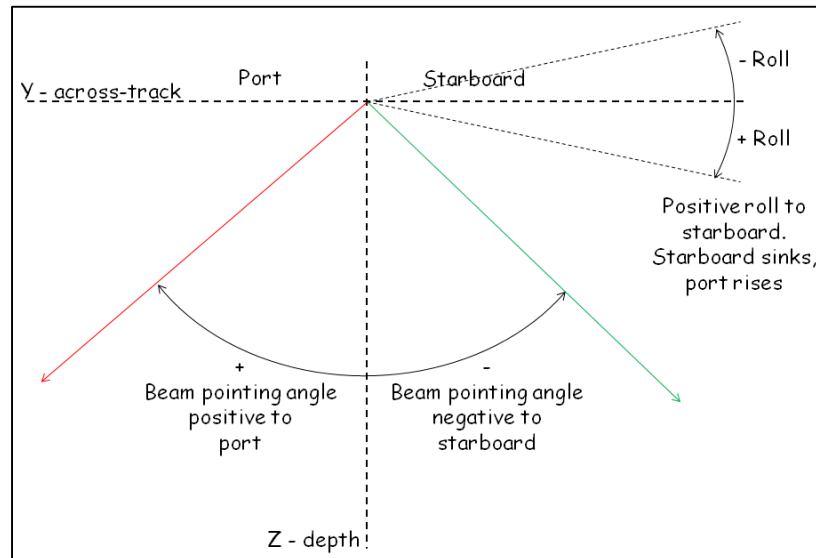


**Figure 5.3 – The water column beam pointing angle has to be uncorrected for the roll, to “un-point” it to the equivalent of a receiver-relative steering angle.**

In Figure 5.4 the adjusted water column angle and the angle from the raw range beam structure are plotted, for a dataset collected in low density mode. This is a special case where the number of solutions between the raw range beam angle structure and the

water column structure are the same (160). There is an offset between the re-pointed angle and the correlating raw angle [Figure 5.5]. In the last paragraph, it was explained that the angle from the water column datagram is corrected with the roll at receive time (for each beam). For this correction the travel time (DR) stored in the water column datagram is used. However, the two way travel time stored in the water column datagram (DR) and in the raw range and beam angle datagram are not the same [Figure 5.6]; therefore, there is an offset in roll [Figure 5.7]. However, the difference in roll (caused by a different travel time) is much smaller than the offset between the re-pointed angle and the raw angle. Thus at best, when surveying in HD mode, the receiver angles can only be approximated.

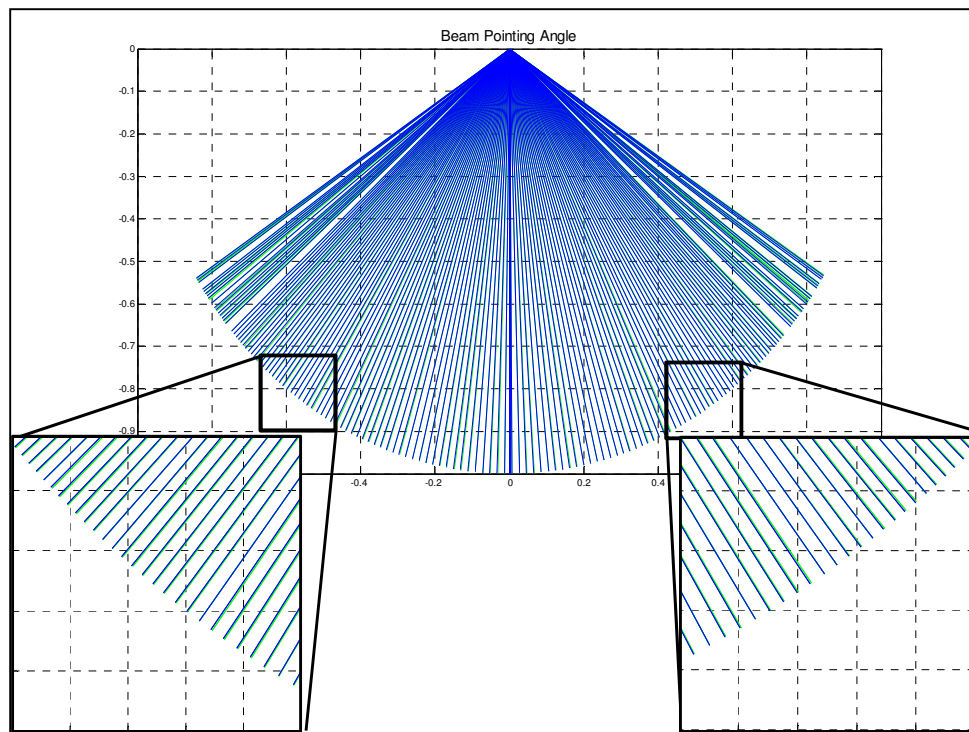


**Figure 5.4 – The beam pointing angles for a single low density (i.e. 160 beams) ping (20937). In blue the beam pointing angle from the raw range and beam angle structure and in green the re-pointed angle from the water column structure.**

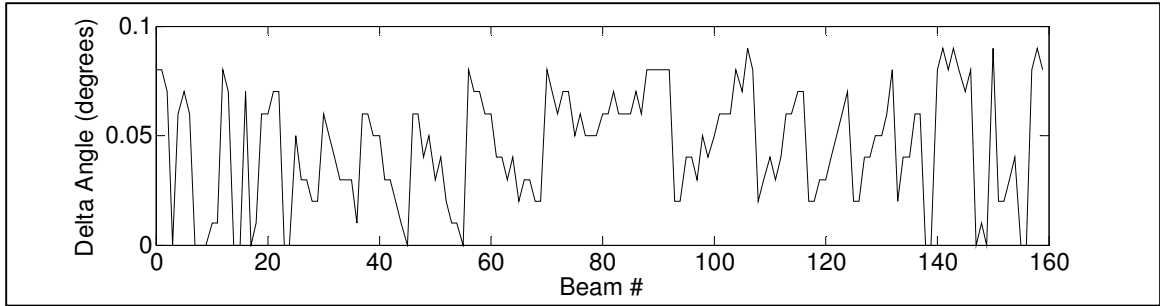


**Figure 5.5 – The difference between the beam pointing angle from the raw range and beam angle structure and the adjusted angle from the water column structure, for a single ping in low density mode (20937).**

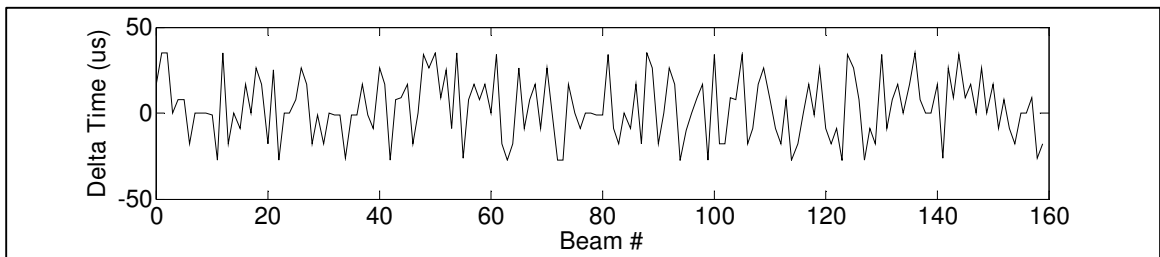


**Figure 5.6 - The difference between the one-way travel time to the bottom detection from the raw range and beam angle structure and the one-way travel time to the detected range from the water column structure, for a single ping in low density mode (20937).**

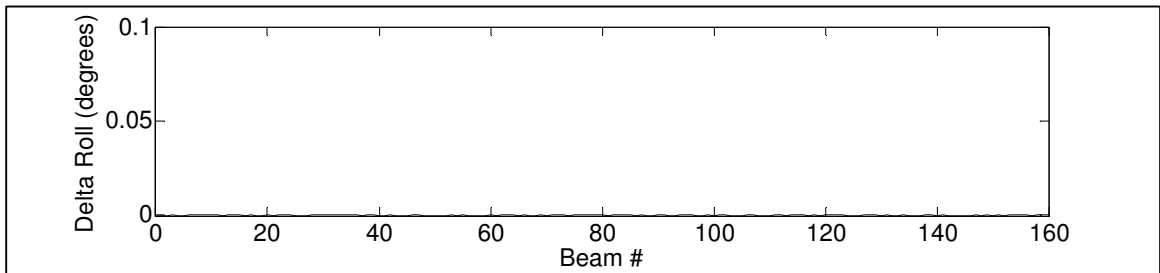


**Figure 5.7 - The difference in roll between the roll calculated at the time of the bottom detection from the raw range and beam angle structure and the roll at the time of detected range from the water column structure, for a single ping in low density mode (20937).**

### 5.3 Depth Calculation

The fundamental measurements made by the sonar, are range (which is known), transmitter steering (which is known) and receiver steering angle (which is approximated). These are used to make a full sounding reduction according to the steps introduced in Beaudoin (2004). For a full review of multibeam depth calculation, the reader is referred to Beaudoin (2004). In this section the significant processing steps for the particular survey platform of the Dutch Navy are discussed, and preliminary results throughout the sounding reduction are shown.

At page 3 and 4 of Beaudoin (2004) a summary of the multibeam sounding reduction is given:

1. The sounding geometry at transmit and receive has to be recreated, in order to determine the beam pointing vector in the primed coordinate system (Figure 6, Beaudoin , 2004).
2. This beam pointing vector is then rotated into the geographic coordinate system.
3. From the geographic launch vector the beam depression and azimuth angle are calculated.
4. Having done this, an acoustic ray-trace provides the depth and horizontal range with the beam azimuth being used to reduce the horizontal measurement into across-track and along-track components.

5. Finally, the lever arms between the reference point and the transducer are rotated using the transmit orientation, and are then added to the depth, across-track and along-track offsets to yield the sounding solution with respect to the reference point. [after Beaudoin, 2004].

Before starting with the multibeam sounding reduction, the sense and orders of coordinate system used throughout this research needs to be defined. Herein the coordinate system used is right-handed with the positive x-axis pointing towards the bow, the positive y-axis pointing towards starboard and the positive z-axis pointing below the vessel. The sign convention for angular measurements follows the right hand rule, i.e., positive roll is to starboard (starboard sinks, port rises), positive pitch is nose-up (bow rises, stern sinks), and positive yaw is clockwise (bow turns to starboard) [Beaudoin, (2004 (1))]. The order of rotations from sonar to geographic reference frame is roll – pitch - heading.

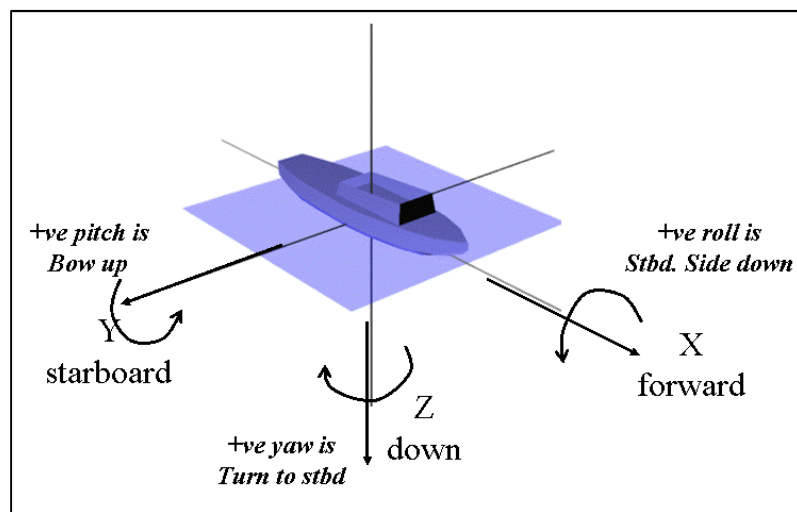


Figure 5.8 – Right handed coordinate system (from Hughes Clarke [2008]).

#### 5.4 Geographic Launch Vector Determination

Throughout the calculation the transmit time from the water column structure is used, which is the same for both heads in the case of a dual headed system. The receive time is computed through the addition of this transmit time and the two-way travel-time to each sample for each receive beam. Note that as the receiver moves over the receiver cycle, each sample along a water column trace potentially uses a different steering angle, but only the final steering angle is recorded (assumed at detection time). Each separate head of the dual head system uses the same mount angles for the transmitter and receiver as they are installed as a single physical unit (assuming perfect orientation within the unit).

Before a ray-trace can be performed the local level referenced beam pointing vector must be calculated. Orientation (roll, pitch and heading) and sonar installation angles need to be accounted for. Therefore, ideal vectors are rotated for alignment and orientation. The ideal vector for transmit is aligned perfectly along the X-axis, the ideal vector for receive is aligned perfectly along the Y-axis. The ideal vectors are rotated for alignment and then for orientation. For a single headed system, the ideal receiver vector would be oriented perfectly with the ship's y-axis, i.e. (0, 1, 0), however, for a dual headed system the receiver vector is always tilted at an angle.

The beam-pointing vector is then computed in the primed coordinate system. After that the beam pointing vector is rotated from the primed coordinate system into the geographical coordinate system (Figure 5.9) and an azimuth and depression angle are derived. Results for a single swath are plotted in Figure 5.10.

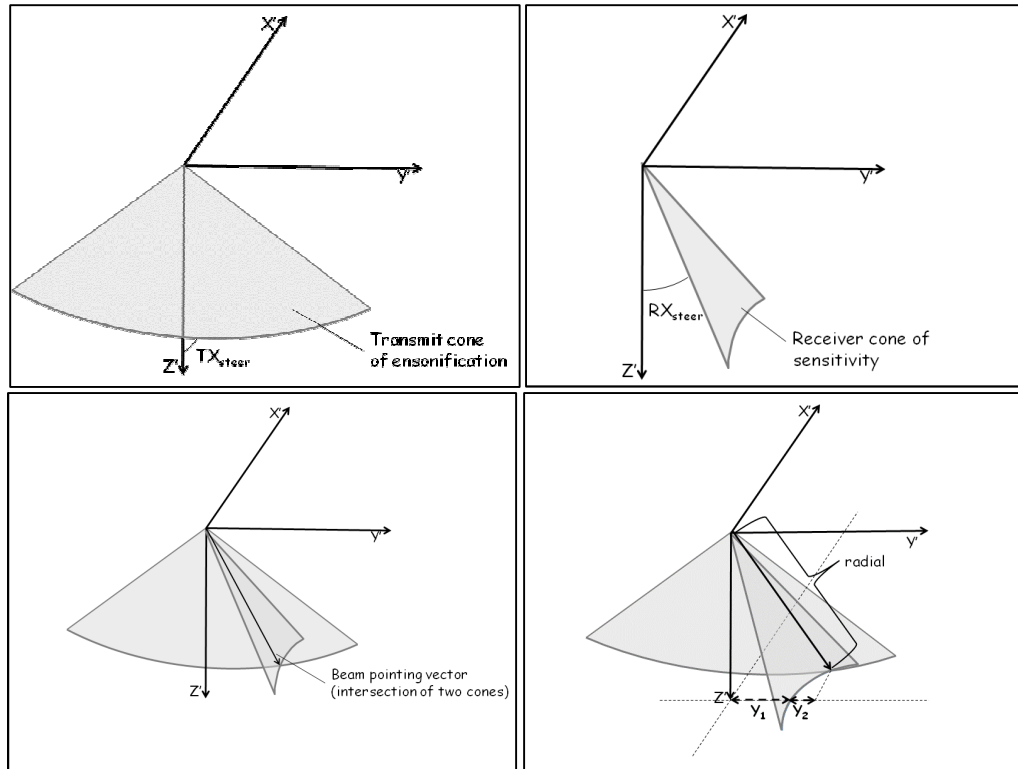


**Figure 5.9 - The beam-pointing vector lies on the intersection of the transmitter cone of ensonification and the receiver cone of sensitivity, shown in (top left) and (top right), respectively with the intersection shown in (bottom left). The image on the bottom right demonstrates the geometry used to derive the beam-pointing vector coordinates. Note that the  $z'$ -axis points downward (after Beaudoin [2004]).**

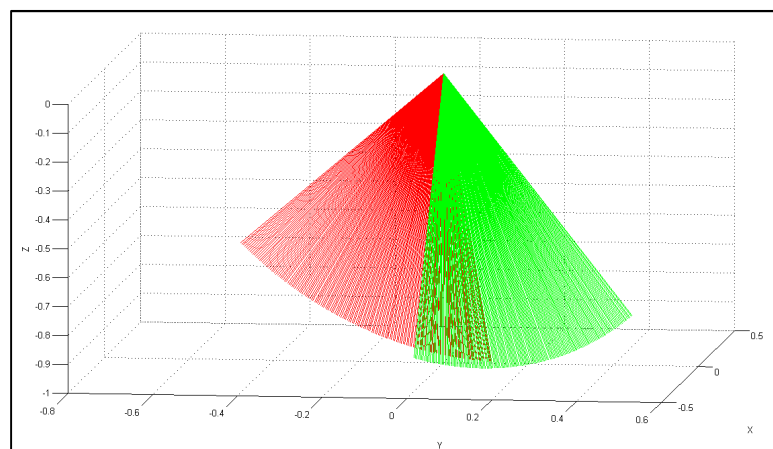


**Figure 5.10 – The beam pointing vectors for all beams in the geographical coordinate system. In red for the port head and in green for the starboard head. Output from the UNB algorithm for the Dutch Navy dual head data.**



## 5.5 Ray-tracing

After the beam depression angle and beam azimuth are computed a ray-trace can be performed. The ray-trace consists of travelling along a ray-path (using initial depression angle) until the two way travel time is exhausted. This results in a horizontal distance a depth, which are then reduced to the vessel reference point (draft, tide (and squat)).

To transform the whole water column image to depths in the geographic frame, the depth and position of each sample at each beam pointing angle is calculated. Therefore the travel time to each sample is used and the unique receiver steering angle at each sample.

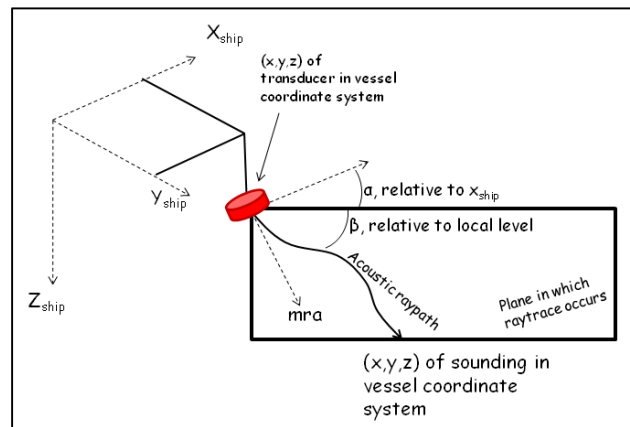


**Figure 5.11 – Representation of ray-tracing in the vessel coordinate system, i.e. relative to the local level [after Beaudoin, 2004].**

## 5.6 Reduction

For the EM3002 dual head additional offsets must be added because the geometric center of the sonar does not coincide with the acoustic center. The transmitter and receiver arrays are offset from the geometric center of the transducer assembly [Figure 5.12]. When the sonar heads are installed at their suggested mount angles, the small lever arms introduce depth and across-track biases of a few centimeters. In both cases, the depth telegrams reported by the transceiver account for these additional offsets. However, the current solution does not account for these additional offsets as numbers were not provided by Kongsberg, and are thus not included in the results.

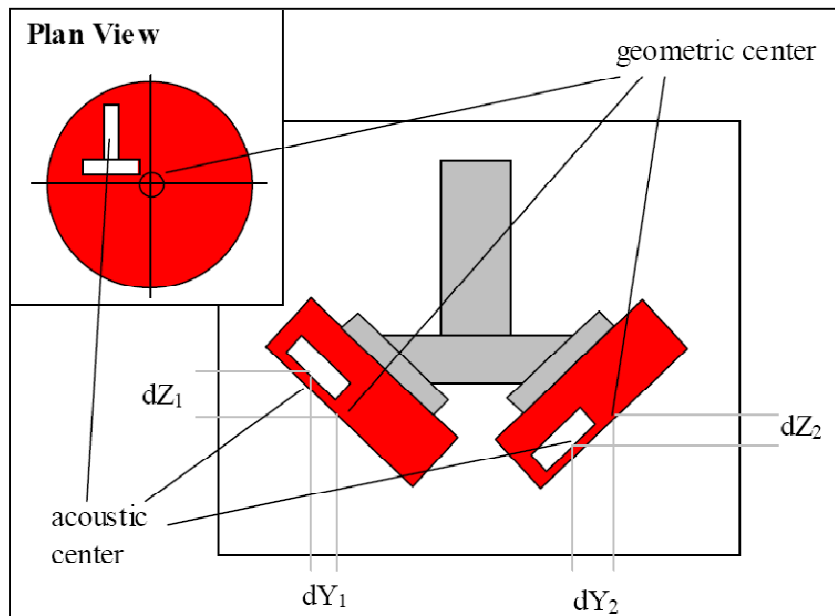


**Figure 5.12 - Internal offsets in typical EM3000D installation. The Mill's Cross is offset from the geometric center of the transducer as shown in the plan view. The centre of the receiver array defines the acoustic centre from which the range measurements are made. When the transducers are mounted in their typical configuration, the acoustic centre of each transducer is offset from the geometric centre of each array. Each transducer thus has an additional depth correction,  $dZ$  and across-track correction,  $dY$  (from Beaudoin [2004 (2)]).**

## 5.7 Results

To verify if the calculation algorithm works, solutions from the algorithm were compared to original bottom tracking solutions as calculated by Kongsberg. The bottom tracking solutions as calculated by Kongsberg however have some discrepancies with the method as described in Beaudoin, 2004. The calculated solutions with the water column algorithm are not able to match the bottom tracking solutions from Kongsberg. Therefore, first, solutions are calculated with the original Ocean Mapping Group (UNB) software, in which the method from Beaudoin (newMergeAtt) is implemented correctly. This method is called the UNB method herein. This method uses information from the raw Kongsberg structures.

For this comparison data from a single head EM3002 in equidistant mode was used. That means that no high definition beam spacing is used and thus only 160 soundings separate the physical beam spacing. The water column algorithm can only calculate solutions for the physical beams, which also results in 160 solutions. Therefore, for the low density there will be 160 bottom tracking solutions and 160 matching equivalent calculated solutions.

First, the results calculated with Beaudoin (UNB) are compared to the solutions from the depth datagram (Kongsberg's solution). In Figure 5.14 the results for the depths are plotted against the along-track direction. The solution from UNB shows some discrepancies in depth and position (as explained in § 5.6). However, the depth offsets are within centimeter level at the nadir beams, to ~4 centimeter at the outer beams. In Figure 5.17 the across-track solution is plotted against the along-track solution. Note the

different scale on each axis. The actual across-track difference is bigger than the along-track difference.

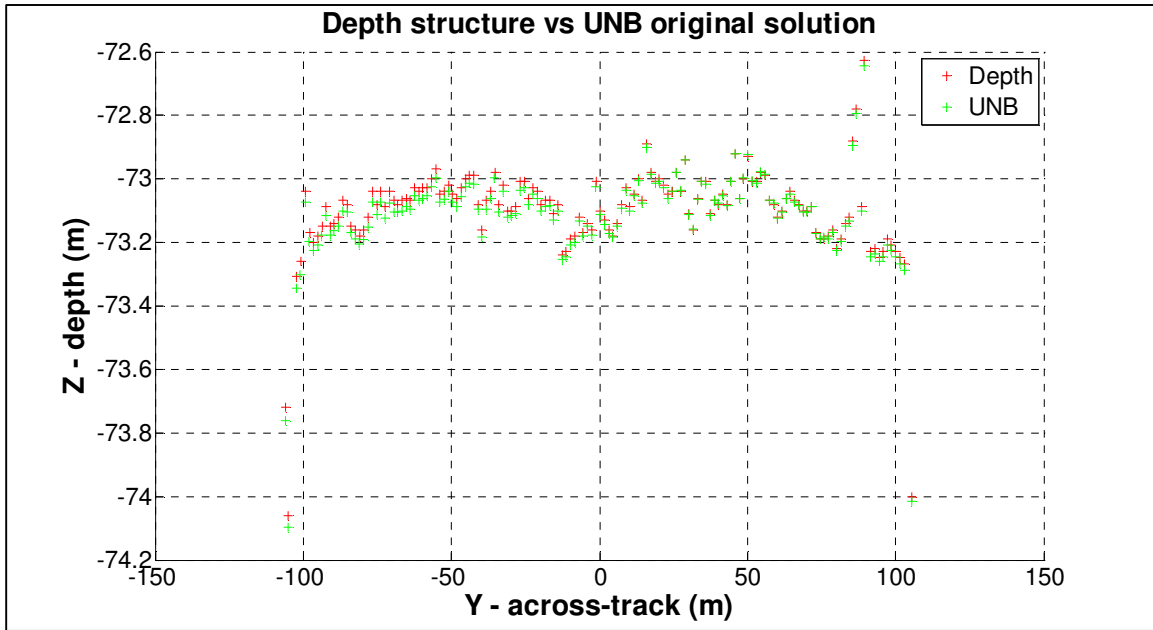


Figure 5.13 – z (depth) and y (across-track) values from the depth structure, versus z (depth) and y (across-track) calculated according to UNB (newmergeAtt).

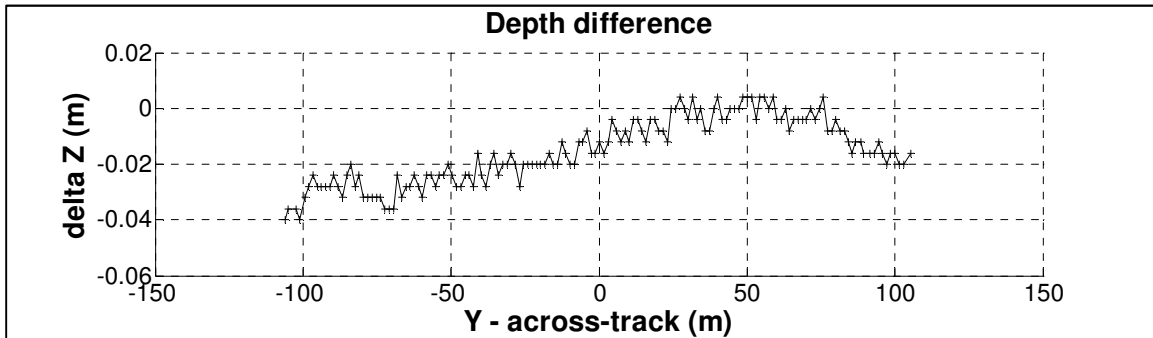


Figure 5.14 – The difference between z (depth) values from the depth structure, depth values calculated according to UNB (newmergeAtt).

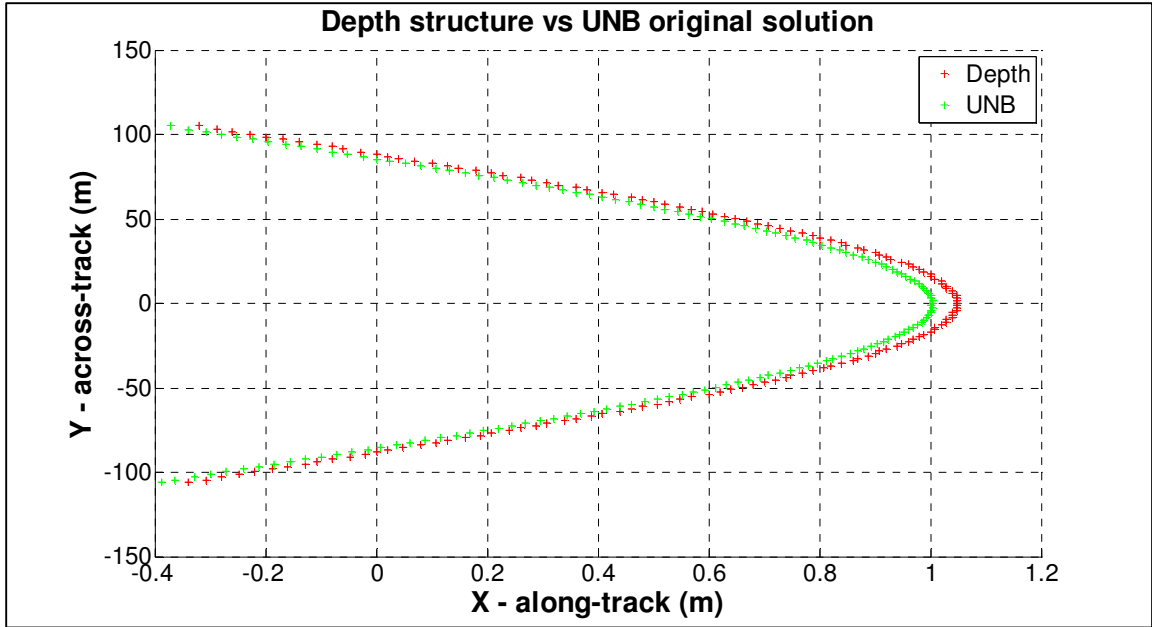


Figure 5.15 - The x (along-track) and y (across-track) values from the depth structure, versus x (along-track) and y (across-track) calculated according to UNB.

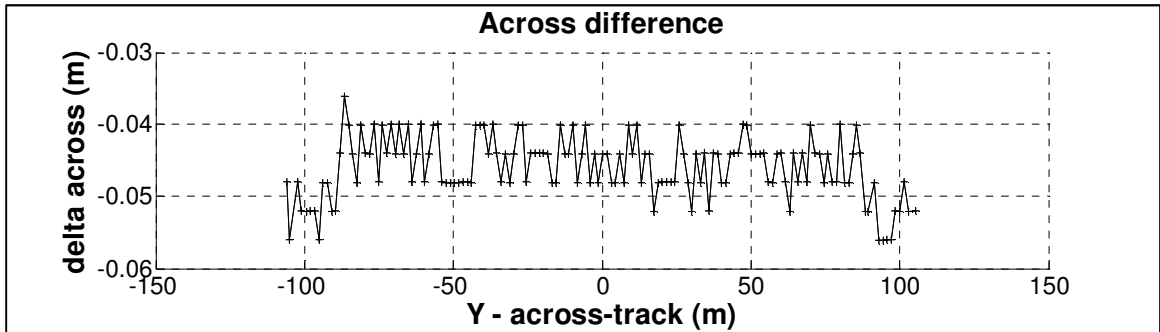


Figure 5.16 – Difference between the across-track values from the depth structure, versus across-track calculated according to UNB.

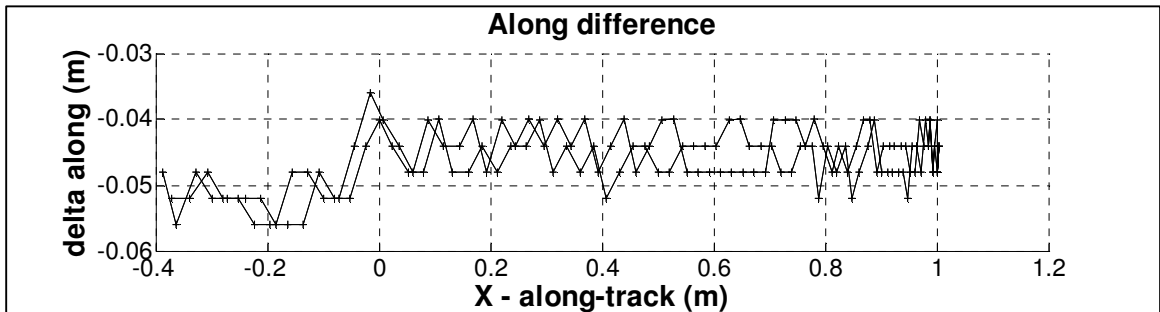


Figure 5.17 – Difference between the along-track values from the depth structure, versus along-track calculated according to UNB. There are two lines, one for the starboard head, and one for the port head.

Second, the solutions from the UNB method are compared to the water column algorithm. To avoid the gross differences due to the water column range not being the same as the bottom detection range, the bottom detection range is used. The two calculations share the same transmit steer and orientation and mount angle only the receiver steering angle differ. If the receiver steering angle is equivalent (see difference plot as in Figure 5.5) the solutions from the water column algorithm should be able to match the solution as calculated by UNB.

In Figure 5.18 the results for the depths are plotted against the along-track direction. There is a difference between both solutions, which is plotted in Figure 5.19. The difference is caused by the re-derivation of the receiver steering from original water column angle. The original water column angle is corrected for roll, this is the roll at receive time of each beam's sample throughout the beam reception cycle. The receive times show a small discrepancy, the corrected water column angle also has a small offset, which causes a difference in depth. It also causes a difference in position [Figure 5.20] from which the along-track difference is plotted in Figure 5.21 and the across-track difference in Figure 5.22. Therefore, the WC solution is not as good as the original UNB method (Beaudoin).

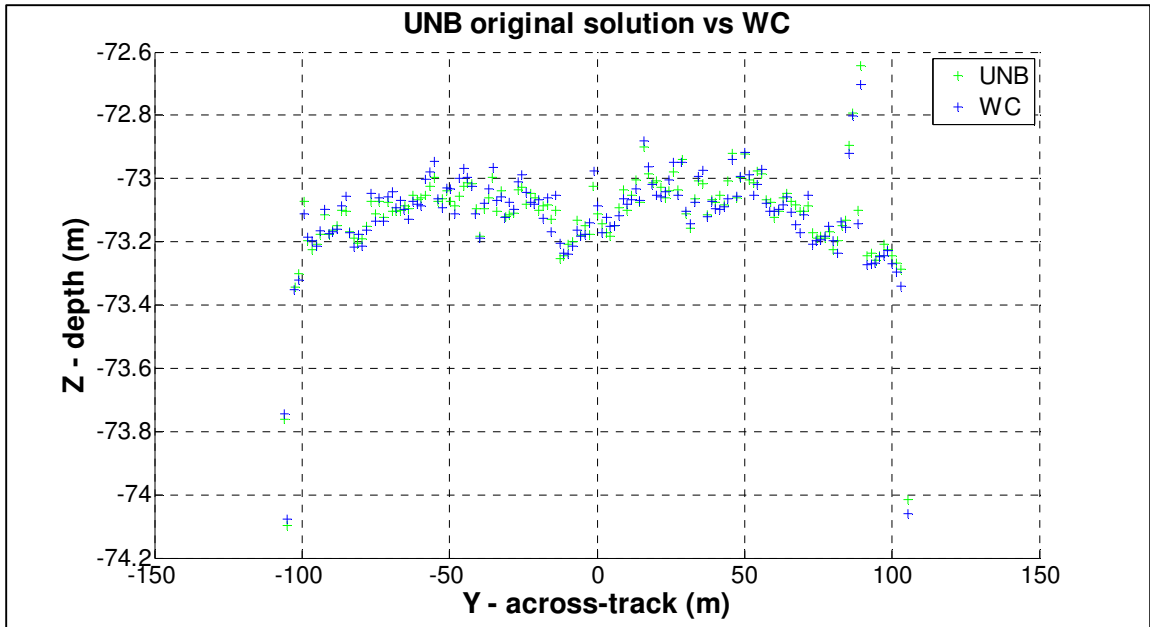


Figure 5.18 – The UNB original solution versus the final output from the Water Column Solution using common two way travel times.

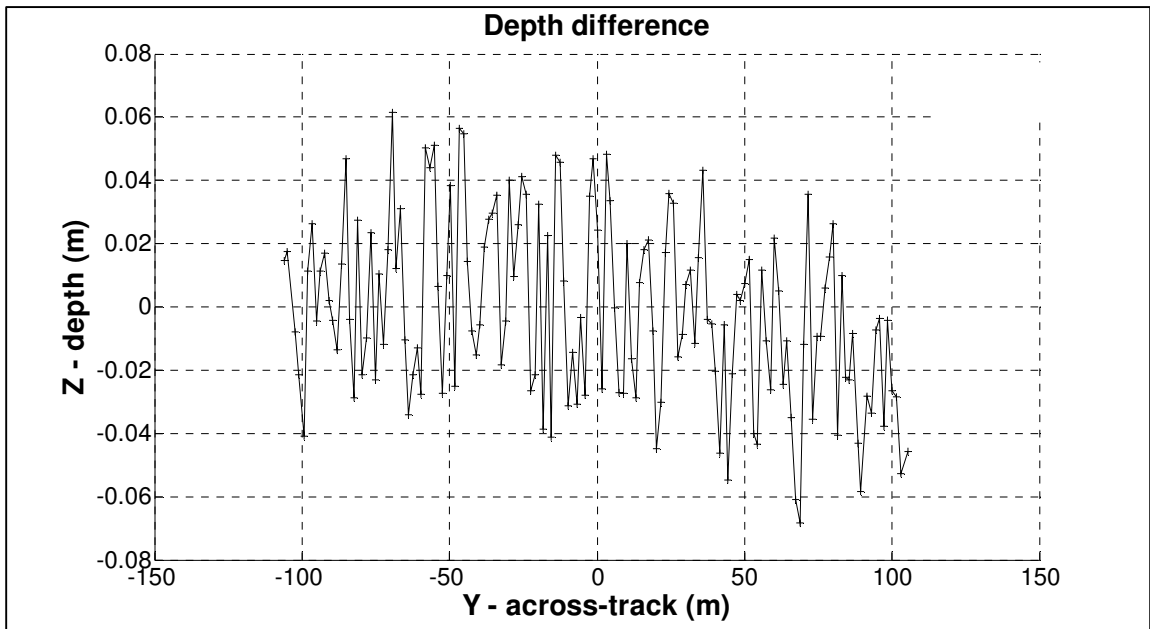


Figure 5.19 - Difference between the UNB original solution and the final output of the Water Column algorithm.

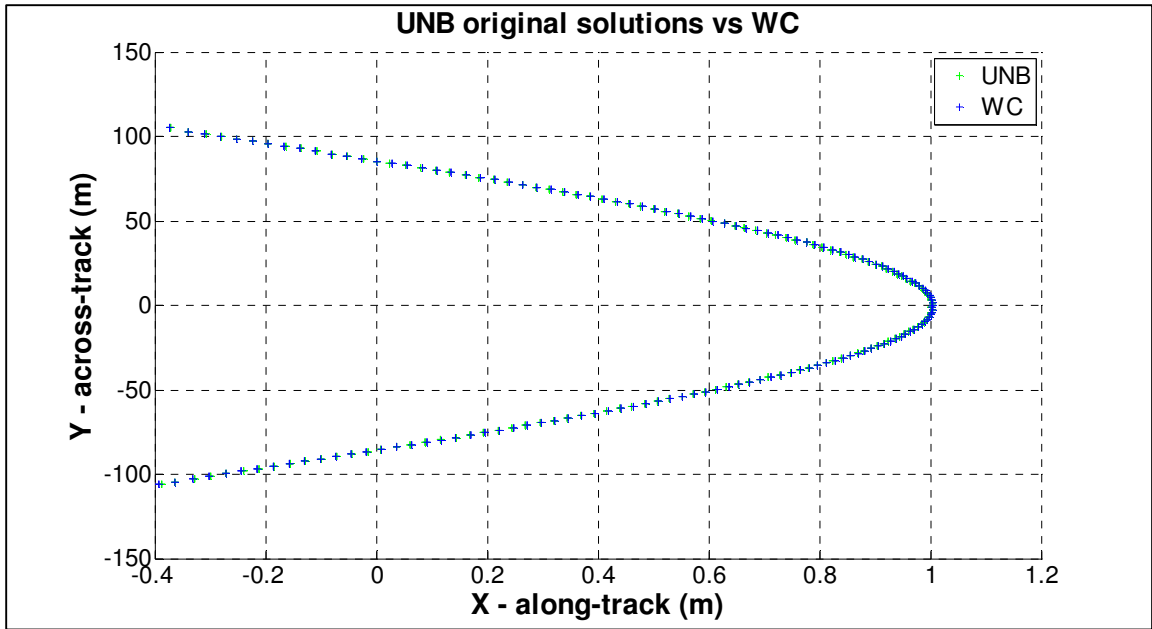


Figure 5.20 – Top-view, along and across track plotted. The x axis scale is stretched.

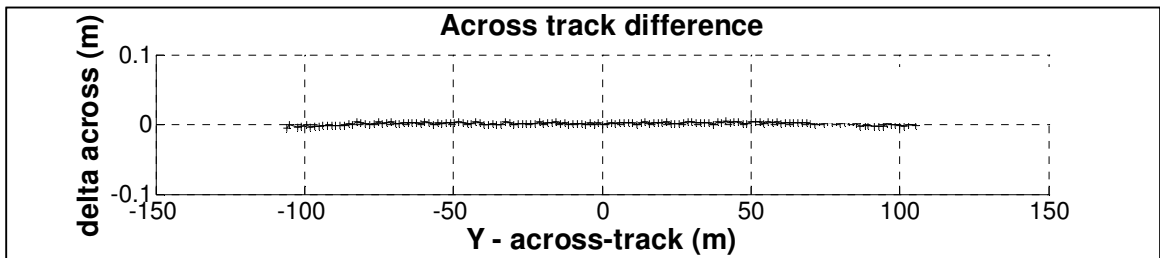


Figure 5.21 – Along track difference.

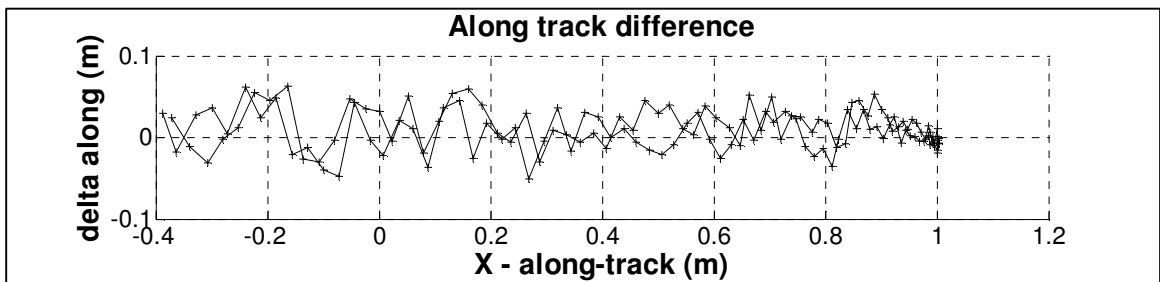


Figure 5.22 – Across track difference. There are two lines, one for the starboard head, and one for the port head.



## 5.8 Output

The output of the ray-trace is the total horizontal and vertical distance traveled during the ray's flight through the water column in a vertical plane lying along the ship's referenced heading (Figure 5.23). The horizontal distance is broken into along-track and across-track components using the beam azimuth as derived during the cone to cone intersection described earlier. The rotated transmitter lever arms are computed, and are added to these components in order to reference the sounding to the origin of the ship's coordinate system at the time of transmit [Beaudoin, 2004].

Now the polar plot, which was an approximation can be represented in a more rigorous geometric fashion. The final (true) depth and across-track distance as outputted by the ray-trace can be presented in a polar plot (Figure 5.24). Each ray-path becomes apparent as shown in Figure 5.25.

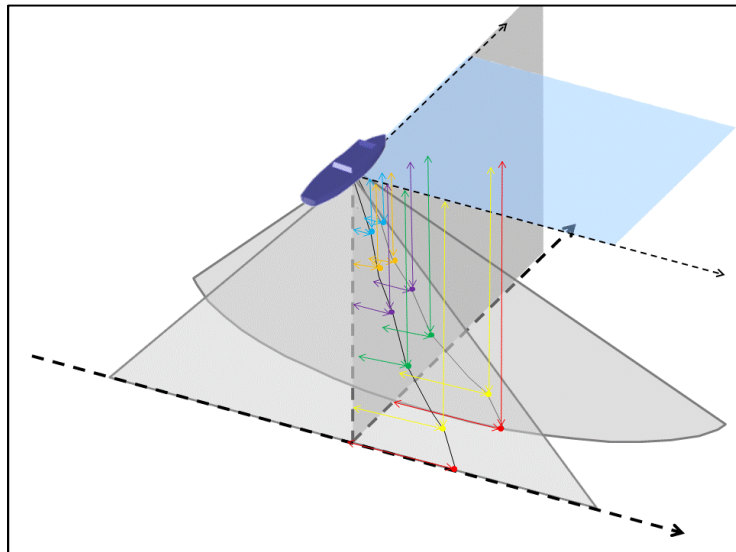


**Figure 5.23 – Representation of a single ray-traced path in a vertical plane relative to the transducer. Note that the depths and the across track distances of each ray-traced sample are the same in the cone and the vertical plane 3D.**

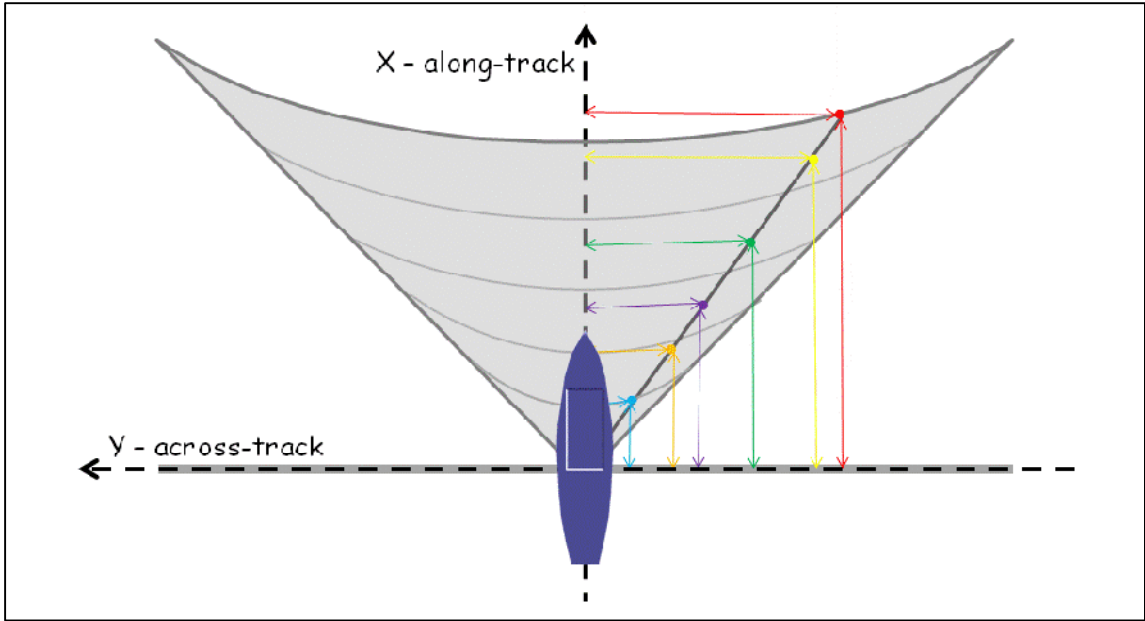


Figure 5.24 - Each ray-traced sample is represented in the 2D vertical plane relative below the ship.

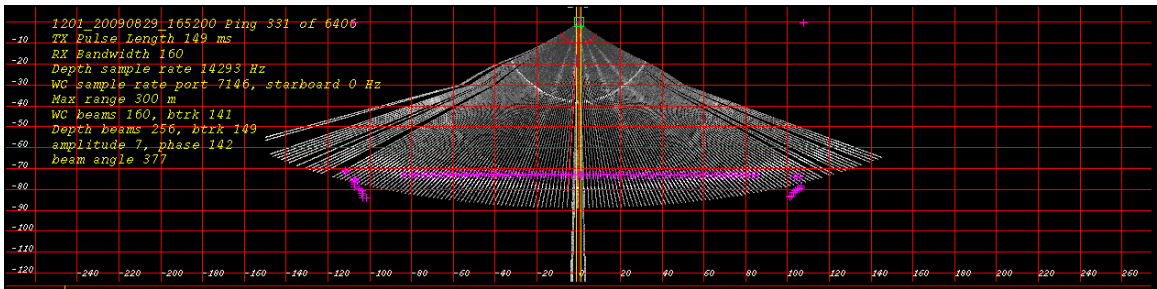


Figure 5.25 – The output of the ray-trace with an exaggerated revised sound velocity profile, to show the horizontal and vertical distance traveled during the ray-tracing. This output is lying in the across-track vertical plane relative (according to heading) below the ship.

## 5.9 Tides

The last step is to transform the selected angle and range to a depth in the geographic frame and reduce the selected point for tide. Therefore a tide file needs to be available. The tide in the tide file is reference to mean sea level (MSL). Specific for the Dutch survey the depth result is corrected to the lowest astronomical tide (LAT), which is used as chart datum (CD), the difference between MSL and LAT is -1.24 meter at the position of the wreck.

## 6 ANALYSIS

Background knowledge about the imaging geometry involved in a water column image as presented in Hughes Clarke, 2006, should allow an operator choose the correct least depth of a mast-like object. Different imaging geometries are better or worse for detection.

In this chapter subjective analysis of data around mast-like objects is undertaken to calculate the least depth of the mast. Data collected over the wreck of the HD147 is used during survey 3 and 4 on Julian day 184 and survey 1 on Julian day 196. Analyzing manually is much more time consuming than the original acquisition time. In this manner the operator rapidly identifies the critical image, and needs to make his/her subjective choice of mast head. By now picking multiple times using multiple passes, an estimate of the uncertainty associated with this method may be achieved, however, all other sources of uncertainty need to be examined as well. Therefore, the water column toolkit is designed to reduce the processing time. The method used can be summarized in the following steps:

1. Select lines passing over the wreck in a digital terrain model (DTM).
2. Select swaths surrounding the wreck in the vertical profile.
3. Analyze swaths surrounding the mast, with use of the polar plot and graphic profiles.

## 6.1 Methodology

### 6.1.1 Select lines

For each survey a DTM was made (Figure 6.1). Preferably only the lines where the wreck was located within the minimum slant range (MSR) were analyzed. Therefore, only the lines close to the wreck were selected.

Note that the lines analyzed here were focused specifically on the wreck. For the more general case of systematic surveying, the operator would identify a hull-like form (or other man-made object) from the regional survey. Those regional lines over the object are unlikely to contain optimal imaging geometry. Also, agencies are currently reluctant to log WCI at all times due to disk space issues. Thus this analysis may not be possible from the regional data. Thus, the operator undertakes “wreck investigation” using tighter line spacing (and possibly slower speeds) and using multiple offsets and azimuths. With the WCI logging enabled those lines provide the basis for this analysis.

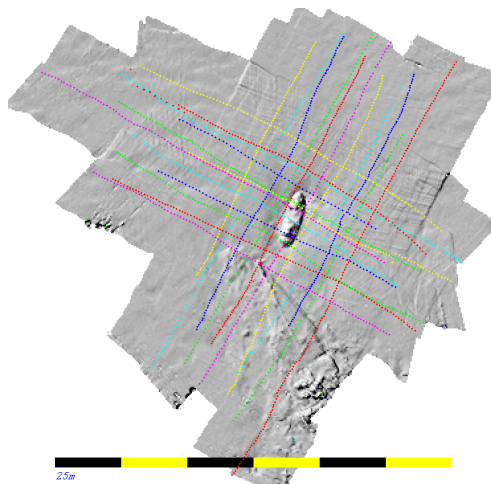


**Figure 6.1- Reducing the processing time by selecting the survey lines close to the wreck. Preferably the wreck should be located within the MSR.**

### 6.1.2 Select swaths

Swaths surrounding the wreck were selected in the vertical profile (Figure 6.2). The processing time to image and view each swath is computationally intensive; therefore, the swaths around the wreck, can be selected from the along-track vertical profile to bring the processing time down. If the echo of the wreck is located within the corridor it will show up in the vertical profile. However, care has to be taken since echoes outside the corridor will not show up in the vertical profile.

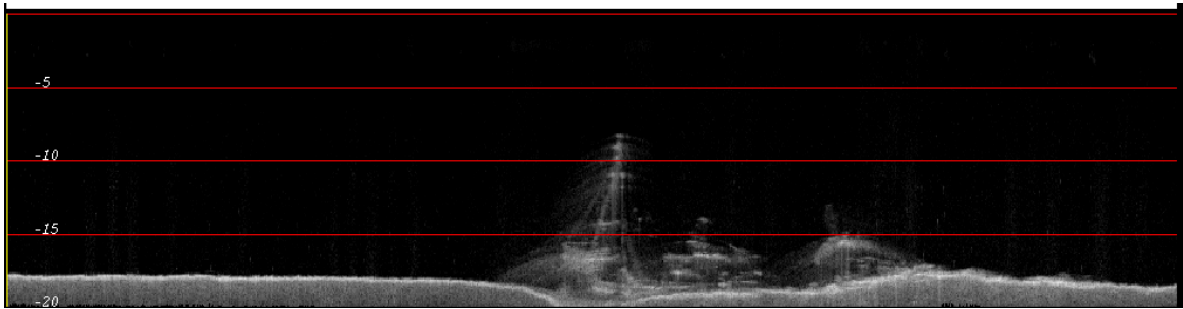


**Figure 6.2 - Reducing the processing time by selecting swaths. When located within the MSR the wreck usually shows up in the vertical profile as shown in this image.**

### 6.1.3 Analyze

The selected swaths are loaded in the polar plot. It is adequate to search for the top of the mast in the polar plot and the vertical profile imagery, even though they are not properly placed in time and space. For each line there is ideally one swath which shows the top of the mast; however, due to transmit side lobes, scattered energy from the same point will be seen as well in the swath(s) before and after. Therefore, more consecutive swaths showing the top of the mast have to be analyzed. With an understanding of the imaging geometry, it is possible to select the top of the mast manually. In the next section is summarized how to select the top of the mast with use of the graphic profiles (common-range plot and fixed angle time-series plot, explained in chapter 4) the steps involved for each polar plot include:

1. Find the beam angle to the top of the mast
2. Find the range to the top of the mast
3. Calculate the least depth.
4. Use the swath with the least depth (which involves repeating step 1 to 3 for consecutive swaths).

1 – Find the beam angle to the top of the mast: In Figure 6.3 and Figure 6.4 the echo from the top of a mast is shown. The top of the mast is picked up in the (receiver) side lobes of the beams around the mast, and will be placed at each beam bore site. Therefore, (weaker) echoes appear in the water column images shallower and deeper than the real top of the mast. Run through each common range in the common-range plot, starting at the transducer or above the suspected location of “the mast” and increasing the range, from the horizontal (waterline) to the vertical (nadir), till an echo of the mast is detected. The backscatter of a mast ( $> -30$  dB for this specific dataset) is stronger than the backscatter of each type of noise ( $< -30$  dB). However, this is not the same in each situation and it is recommended to do more research on the noise levels in different situations and at different depths.

When running through a common range, from above the suspected location of the mast, towards the vertical, there are more consecutive echoes above the threshold. The first echo above the threshold is A. Even though this echo probably has the least depth, it represents a weaker side lobe echo from the mast and not the “real top of the mast”. The next beams return a stronger echo (B and C). The top of the mast is represented by the beam with the strongest echo, which is C. This beam is used to calculate the least depth of the mast.



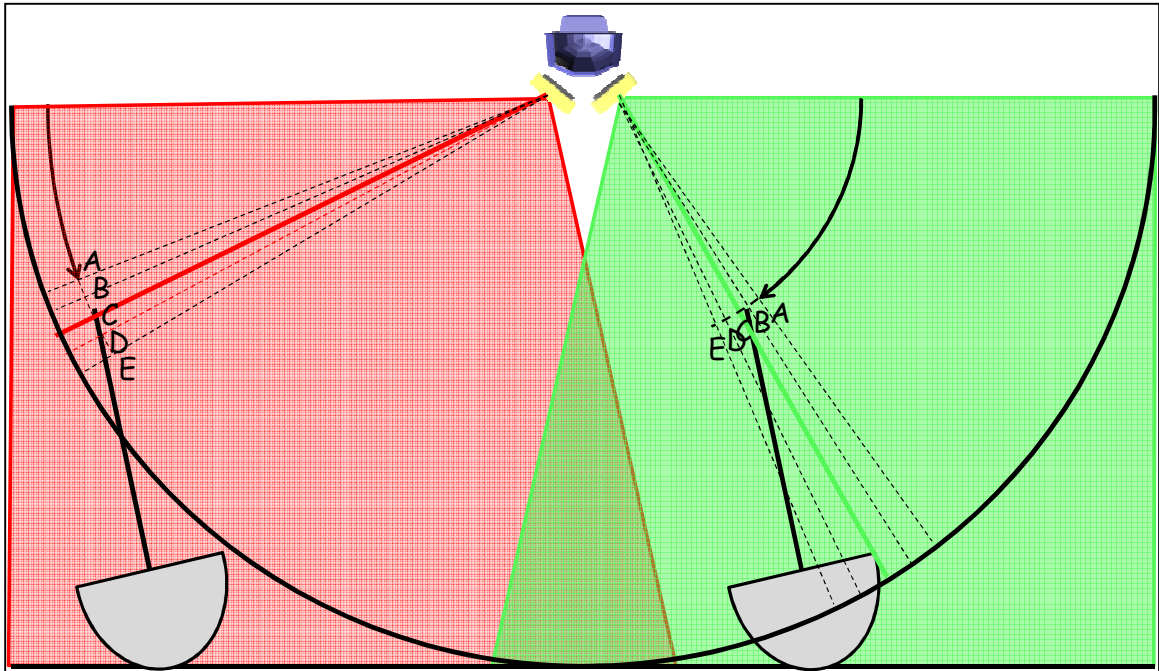


Figure 6.3 – Synthetic polar plot image, representing the top of the mast. Due to receiver side lobes the top of the mast is projected onto beams which don't have the mast on their maximum response axis.

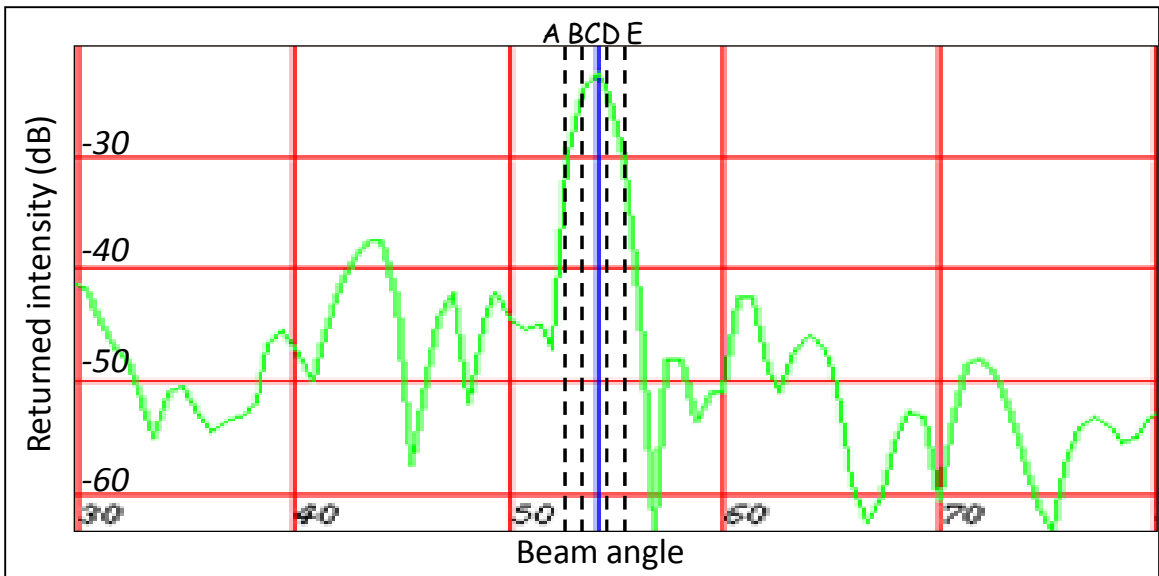
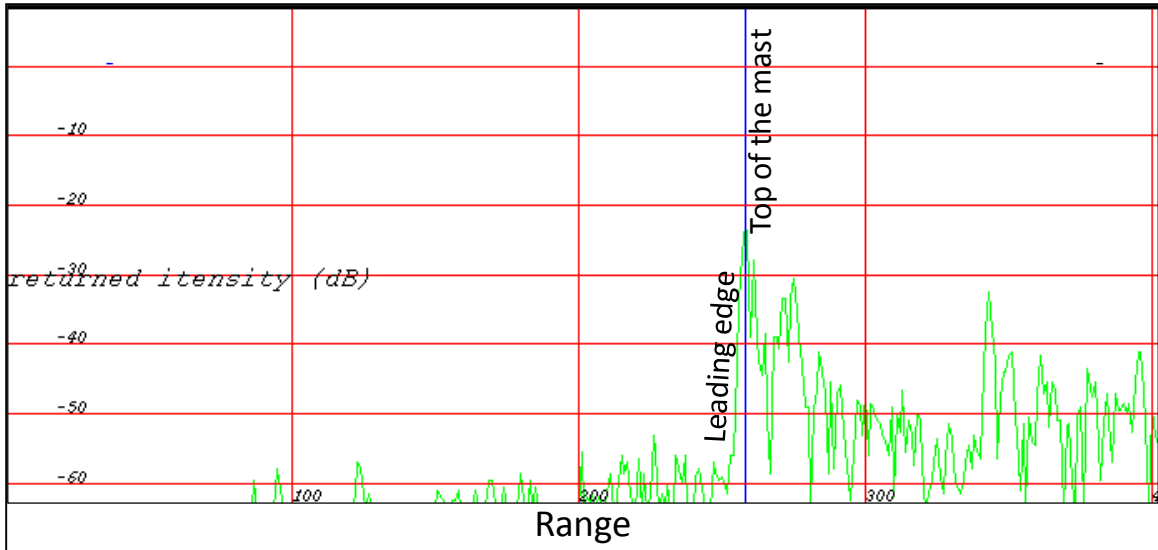


Figure 6.4 – Common-range plot, representing the top of the mast.

2 - Now the backscatter time-series along the selected beam (C) can be viewed in the fixed angle time-series plot to confirm that the correct range is selected. Note that the top of the mast is not necessarily represented by the strongest backscatter, but will lie on the leading edge.



**Figure 6.5 – Fixed angle time-series plot, representing the top of the mast.**

3 – Calculate least depth: Once the beam (implying receiver angle) and range are selected, the selected point can be placed correctly in the geographic frame as explained in chapter 6. Therefore, there is no need to ray-trace the whole image which is time expensive.

4 - As explained before, the top of the mast may also be seen in the swaths before and after the main echo, due to transmit side lobes. The echo in the main lobe is the swath with the least depth, because the range to the mast in the transmit side lobes is

longer (Figure 6.6). Therefore, the swath with the least depth to the top of the mast is selected, and used as least depth of the top of the mast for the selected line.

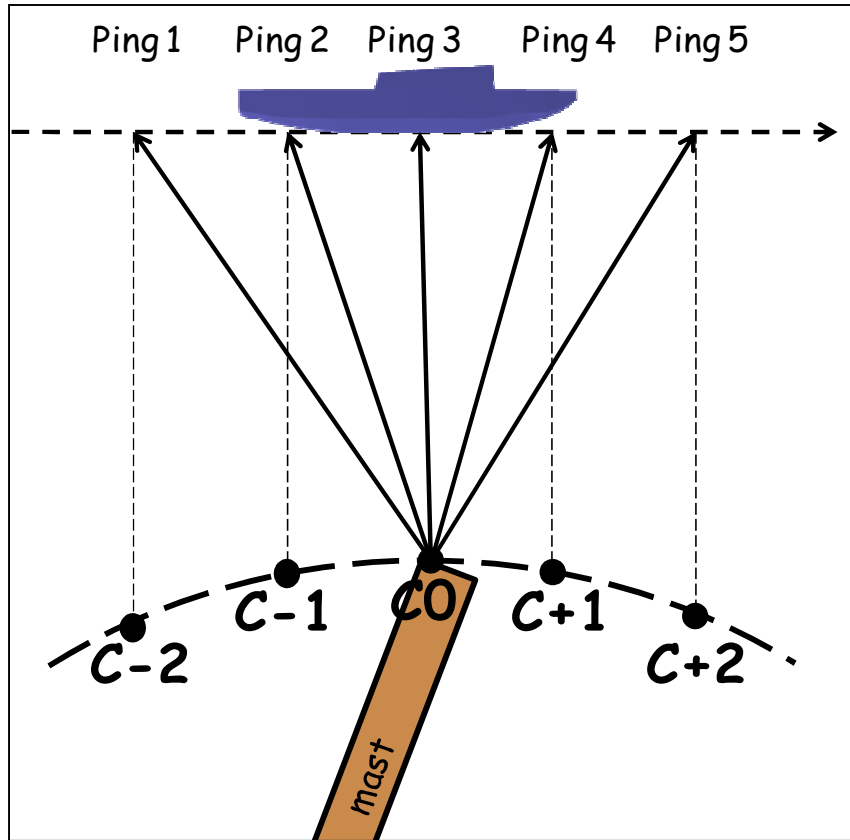


Figure 6.6 – Top of the mast picked up by transmit side lobes.

## 6.2 Imaging Geometry Quality Factor (IGQF)

As explained in Chapter 4, the quality of the operator's choice is potentially better at nadir, and decays with steering angle in a manner quantified in Figure 4.17. Therefore to synthesize the results the Imaging Geometry Quality Factor is introduced for each solution. If the mast is illuminated close to nadir, the IGQF is high (defined as  $< 0.20$  meter); if the mast is illuminated in the middle of the water column the Quality Factor is moderate (defined as between 0.20 meter and 0.35 meter), if the mast is illuminated more towards the outer swaths (close to the MSR) the Quality Factor is low (defined as  $> 0.35$  meter) (Figure 6.7). Outside the MSR the quality is bad, and no selection is made (as explained in section 2.8.1).

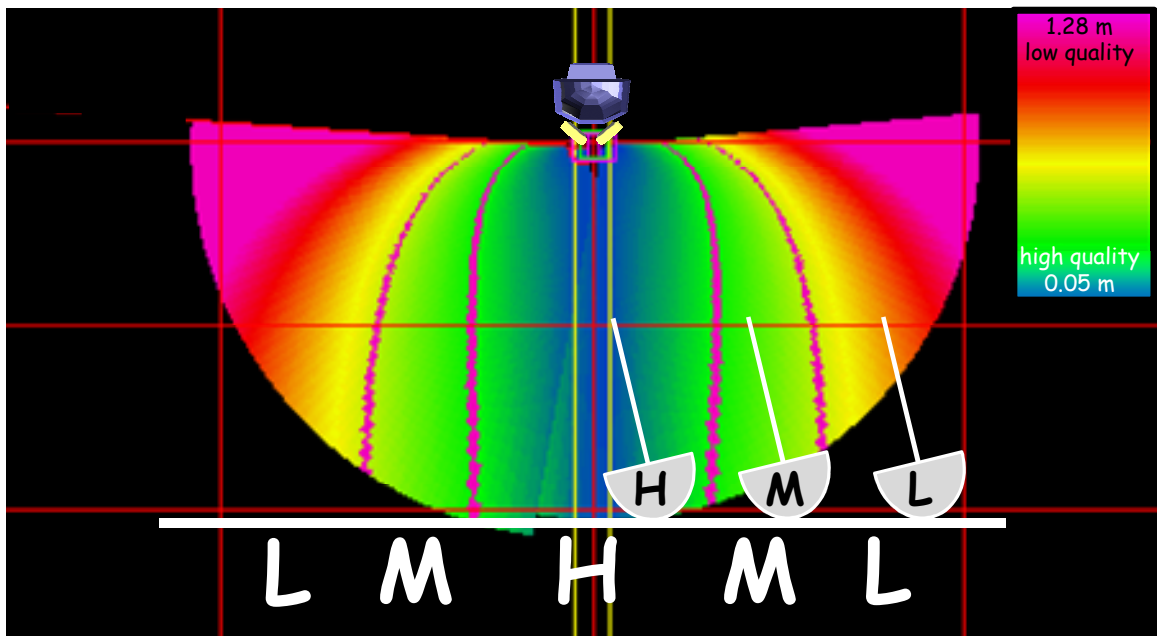
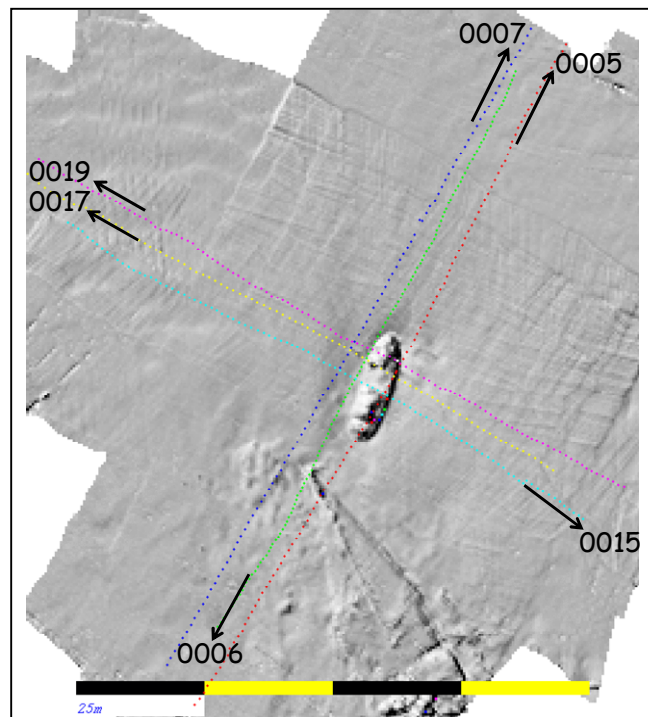


Figure 6.7 - The IGQF introduced for each line.

### 6.3 Julian Day 184, survey 3

The following lines with the mast within the MSR are now analyzed. The direction of each line is shown with a black arrow towards the line number in Figure 6.8.

Throughout this particular survey an angular sector of +/- 65 degrees was used, the pulse length was set to automatic and the bandwidth was set to 8 kHz. From the analysis, it becomes clear that the wreck is lying on its port side, and the mast is therefore pointing to port (Figure 6.10 (b)). The orientation of the mast might influence the illumination of the mast and therefore the strength of the backscatter. Therefore, it is important to survey the wreck from multiple different directions.



**Figure 6.8 – DTM of the data collected in survey 3 on Julian Day 184, with the survey lines plotted used for this analysis. The orientation of the line is given by an arrow towards the line number.**

### 6.3.1 Line 0005

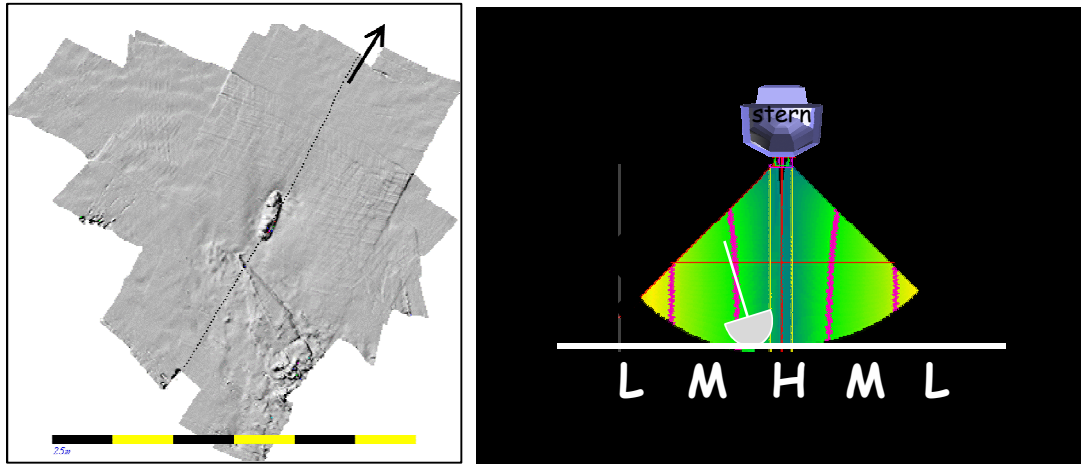


**Figure 6.9 – DTM with position and orientation (left), image with IGQF (right) for line number 0005 on Julian day 184, survey 3 (left).**

In this first case the survey line lies along the long axis of the wreck, it is sailed from stern to bow over the centre of the wreck. The viewer is looking at the starboard side of the wreck in the vertical profile (Figure 6.10 (a)). In this case the swaths around the wreck or even the mast can easily be selected. Once consecutive swaths around the wreck are selected in the vertical profile, the user needs to find the single swath where the top of the mast with the least depth appears. First the number of swaths can be narrowed down by analyzing only the swaths where the top of the mast is viewed best. Therefore the backscatter of the mast is viewed in the common-range plot (Figure 6.10 (d)), and the swath with the best detection is used for selecting the least depth. In this case the top of the mast with the least depth returned the highest backscatter. Finally the beam with the highest intensity is selected in the common-range plot and viewed in the fixed angle time-series plot (Figure 6.10(e)). In this case the range with the highest backscatter correlates

with the top of the mast. In the polar plot it can be seen that the top of the mast is exactly in line with the digitizer noise (Figure 6.10(c)) which also appears in the fixed angle time-series plot (Figure 6.10(e)). However, the backscatter from the mast is sufficiently stronger than the digitizer noise (Figure 6.10(e)) so that it can be unambiguously identified. From the fixed angle time-series plot it also becomes apparent that sufficient energy makes it past the mast, and a bottom tracking solution is locked onto the seafloor. There is a case for multiple solutions in the selected beam.

The depth is measured at 7.41 m (reduced to LAT for all solutions), at the latitude  $52.938756^{\circ}$  N and longitude  $4.578362^{\circ}$  E.

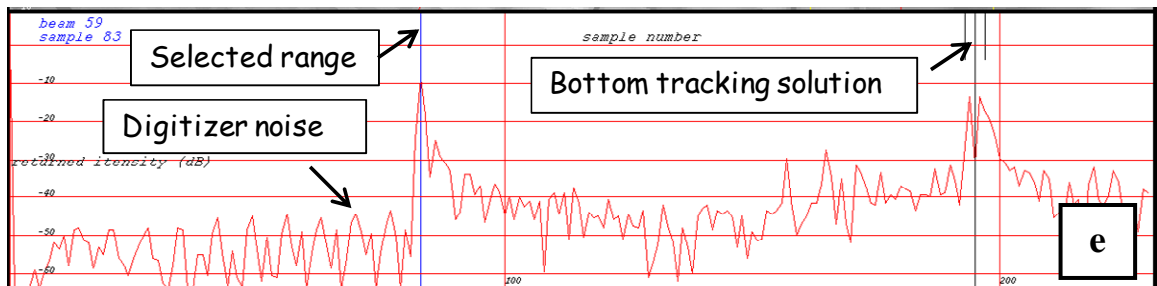
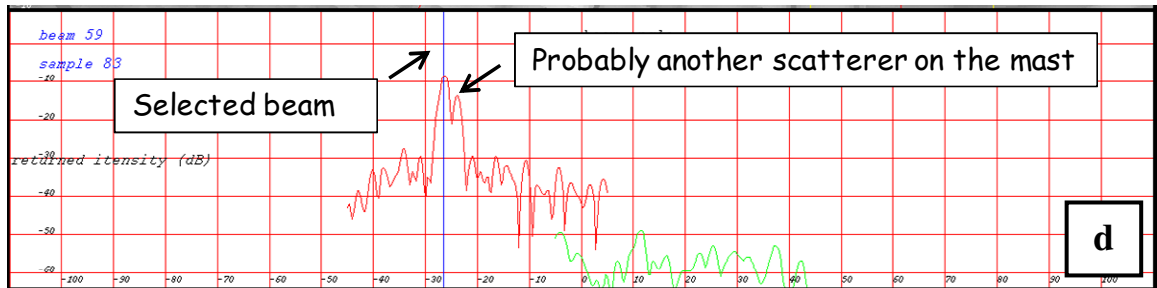
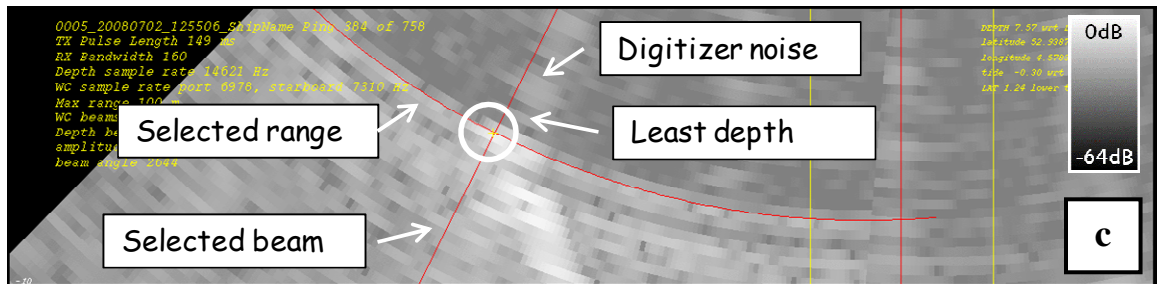
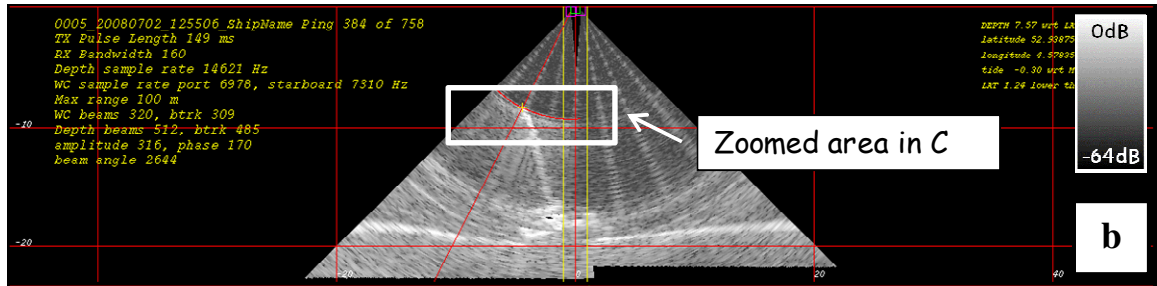
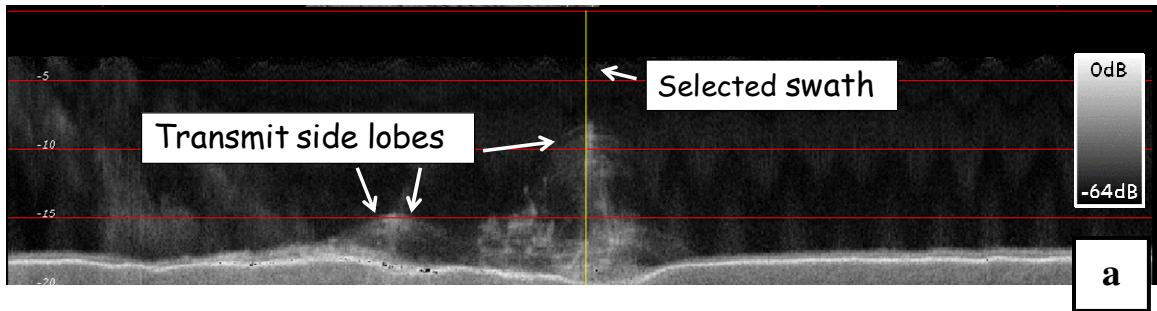
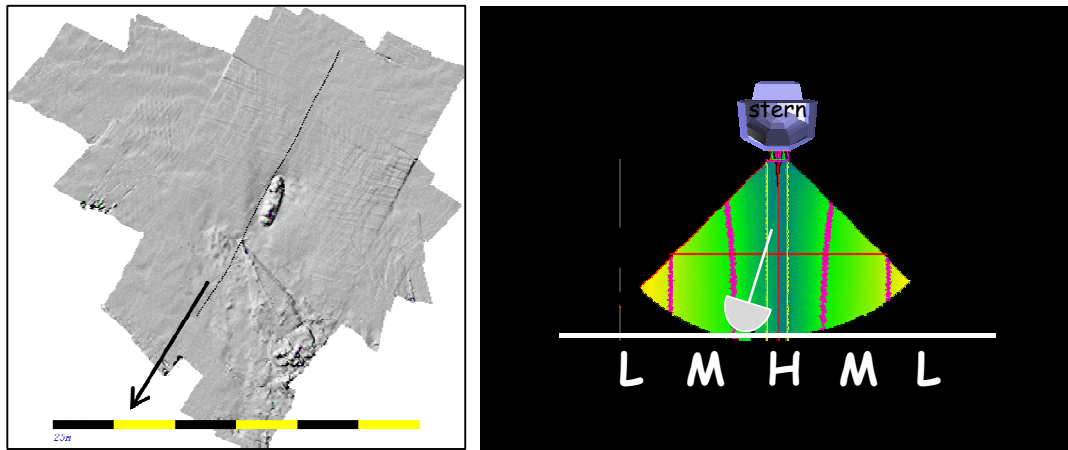


Figure 6.10 – Julian Day 184, survey 3, line 0005 - (a) vertical profile, (b) polar plot with real data, (c) polar plot zoom, (d) common-range plot, (e) fixed angle time-series plot.



### 6.3.2 Line 0006



**Figure 6.11 - DTM with position and orientation (left), image with IGQF (right) for line number 0006, Julian day 184, survey 3.**

This survey line also lies along the long axis of the wreck, and is sailed from bow to stern, close to the centre of the wreck. The viewer looks at the port side of the wreck in the vertical profile (Figure 6.12 (a)). Even the rigging of the mast becomes apparent in this plot; therefore, the swaths around the mast can easily be selected. Because the mast is located in the beams at nadir, and there is an overlap used between both heads at nadir, the mast appears in data of both heads. But the detection is stronger in the port head (Figure 6.12 (d)); therefore, the port head is selected, which means that the port head is plotted on top of the starboard head in the polar plot and the data for the port head is used for analysis (Figure 6.12 (c)). From the common-range plot the digital noise patterns become apparent, clearly for the starboard head. However, for the port head they are weaker than the specular echo from the mast at the selected common range (Figure 6.12 (d)). First the range with the highest backscatter is selected in the common-range plot, which is the least depth of the mast in this case (Figure 6.12 (d)). From the fixed angle

time-series plot it becomes apparent that there are other bottom tracking solutions on the mast but they are not located at the absolute top of the mast (Figure 6.12 (e)).

The reduced depth is measured at 7.38 m, at the position latitude  $52.938760^\circ$  N and longitude  $4.578318^\circ$  E.

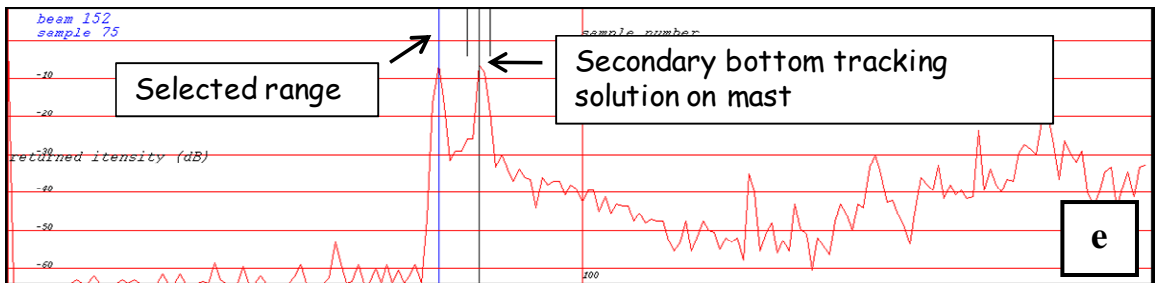
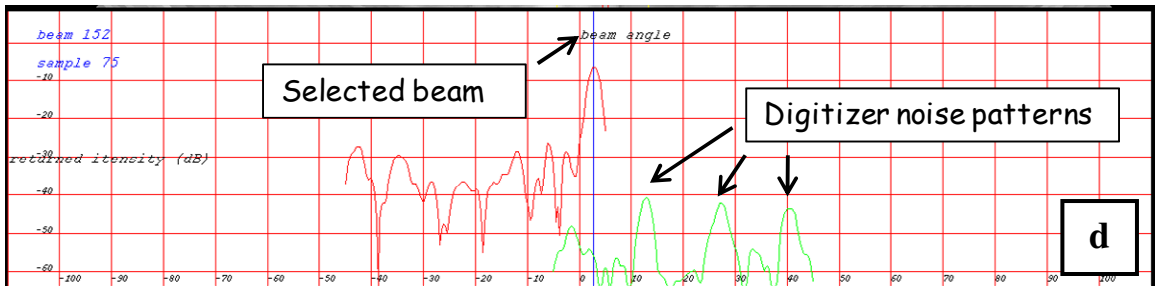
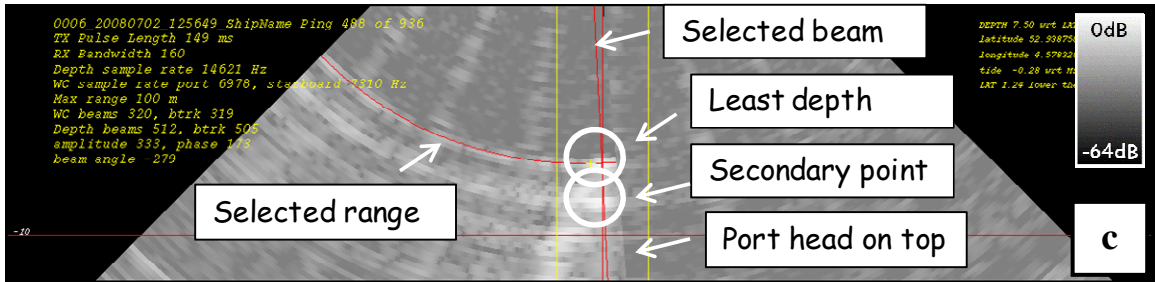
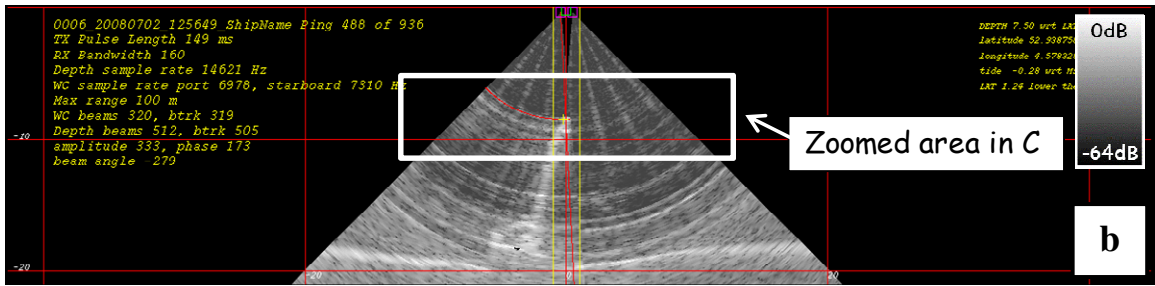
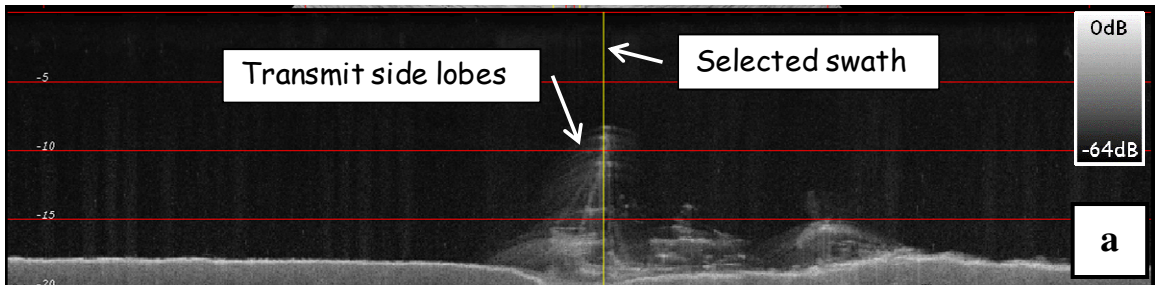
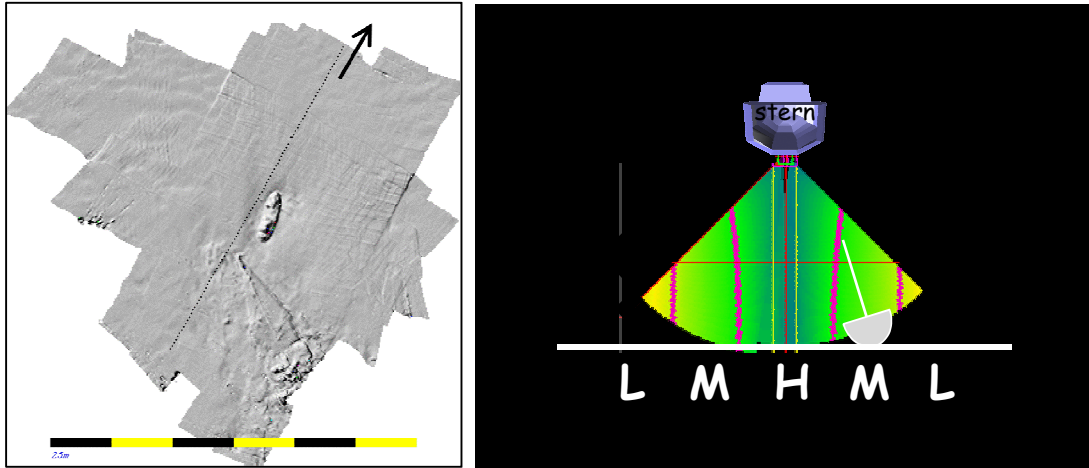


Figure 6.12 – Julian Day 184, survey 3, line 0006 - (a) vertical profile, (b) polar plot with real data, (c) polar plot zoom, (d) common-range plot, (e) fixed angle time-series plot.

### 6.3.3 Line 0007



**Figure 6.13 - DTM with position and orientation (left), image with IGQF (right) for line number 0007, Julian day 184, survey 3.**

This survey line lies along, but offset from, the long axis of the wreck, and is sailed from stern to bow, on the port side of the wreck. The top of the mast is not contaminated by digitizer noise, or strong specular echoes (Figure 6.14 (c)). The top of the mast returns backscatter with the same intensity over different ranges, and therefore it is hard to choose the part of the mast with the least depth. In this case the point with the strongest backscatter is chosen to be the top of the mast (Figure 6.14 (d) (e)). From the fixed angle time-series plot it becomes apparent that, in this case, enough energy makes it past the mast, and there is a bottom tracking solution on the seafloor. Thus there is a case for multiple solutions for this given beam (Figure 6.14 (e)).

The reduced depth is measured at 7.27 m, at latitude 52.938766° N and longitude 4.578346° E.

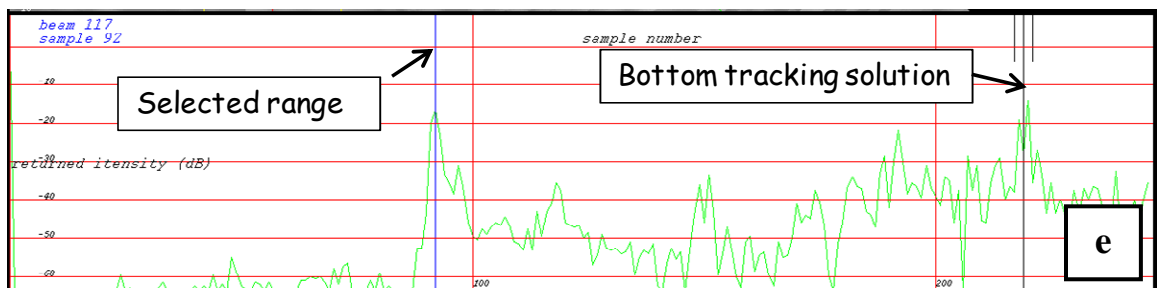
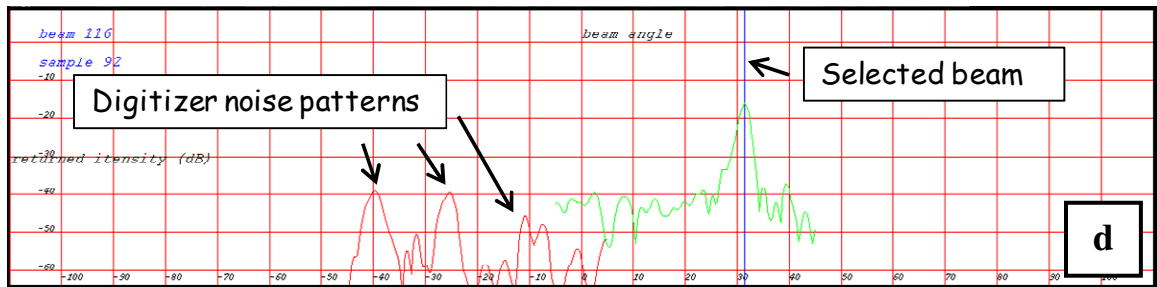
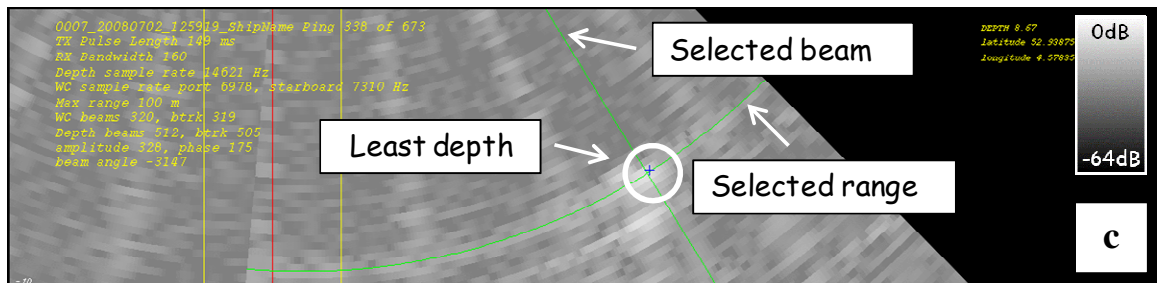
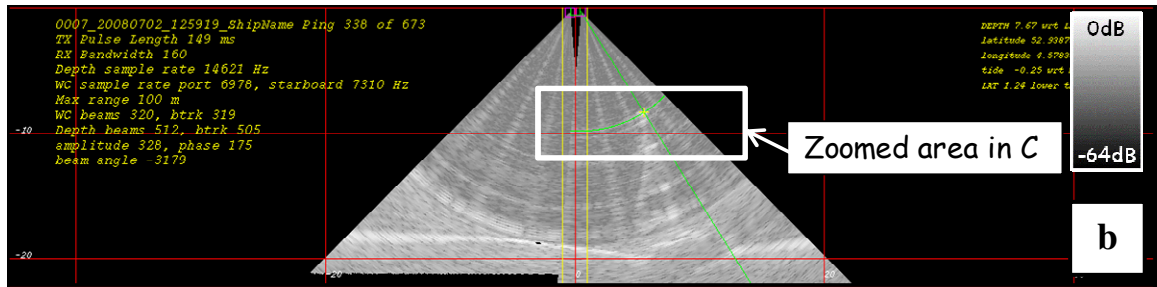
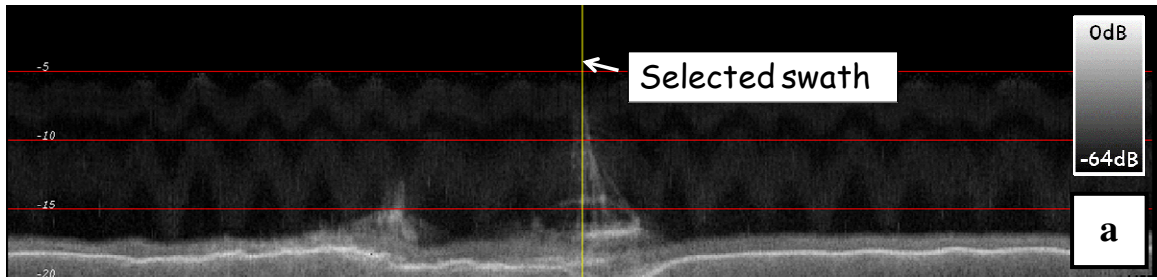
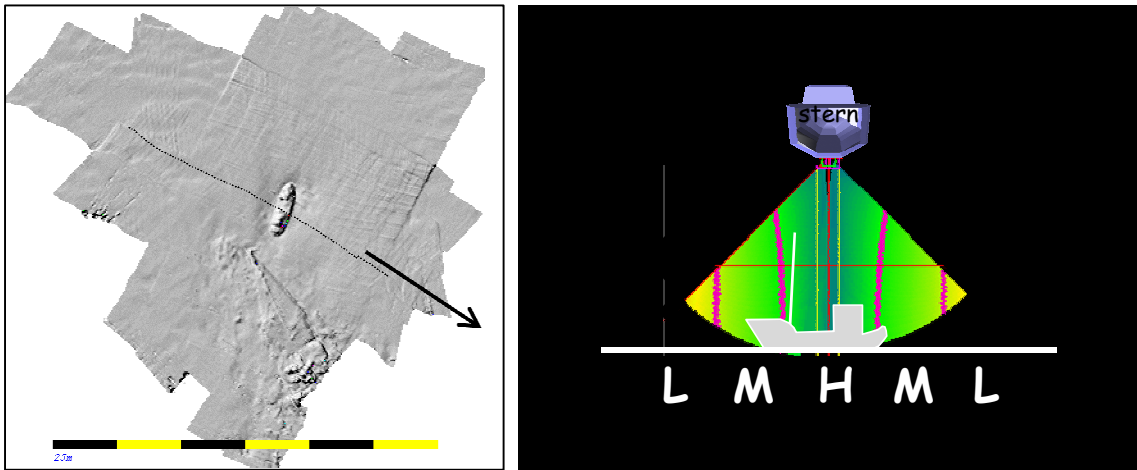


Figure 6.14 – Julian day 184, survey 3, line 0007 - (a) vertical profile, (b) polar plot with real data, (c) polar plot zoom, (d) common-range plot, (e) fixed angle time-series plot.

### 6.3.4 Line 0015



**Figure 6.15 - DTM with position and orientation (left), image with IGQF (right) for line number 0015, Julian day 184, survey 3.**

In this case the survey line lies orthogonal to the long axis of the wreck, and was sailed from port to starboard over the centre of the wreck (Figure 6.15). Because the wreck appears in the near nadir beams, it shows up in the vertical profile, the viewer looks at the stern of the wreck (Figure 6.16 (a)). From the vertical profile it becomes clear that the wreck is lying over its starboard side. The range with the strongest backscatter off the top of the mast is selected in the polar plot (Figure 6.16 (b)(c)). The top of the mast is not contaminated by digitizer noise or strong specular echoes (Figure 6.16 (d)). The least depth of the mast is represented by the highest backscatter at the top of the mast. However, when the beam with the strongest backscatter at the least depth is selected it becomes apparent that there are more strong echoes from the mast at the same beam (Figure 6.16 (e)). The 2<sup>nd</sup> echo may possibly be caused by features on the mast, like rigging or a pulley block. The reduced depth is measured at 7.40 m, at the latitude 52.938744° N and longitude 4.578339° E.

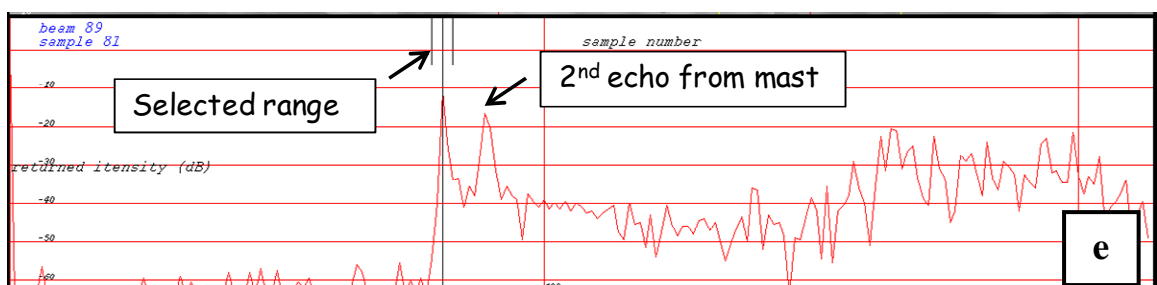
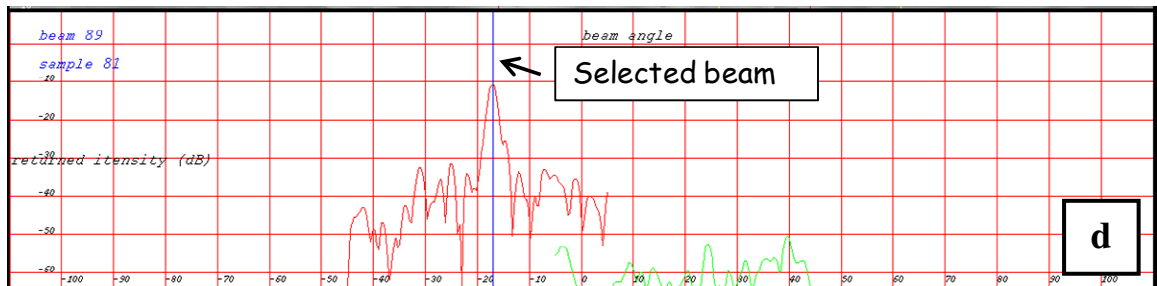
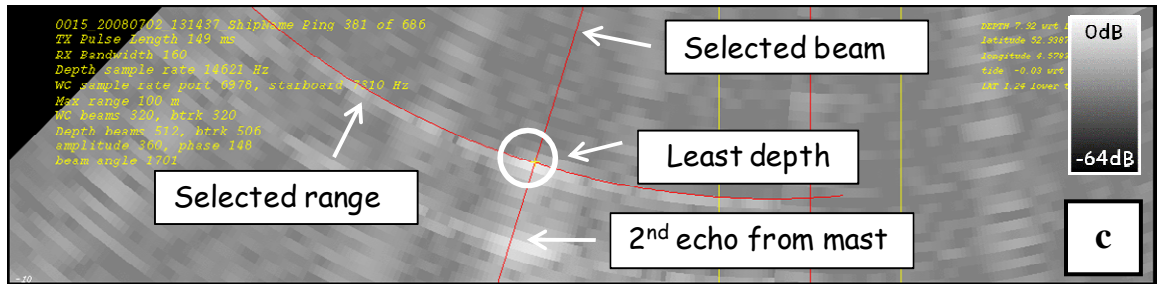
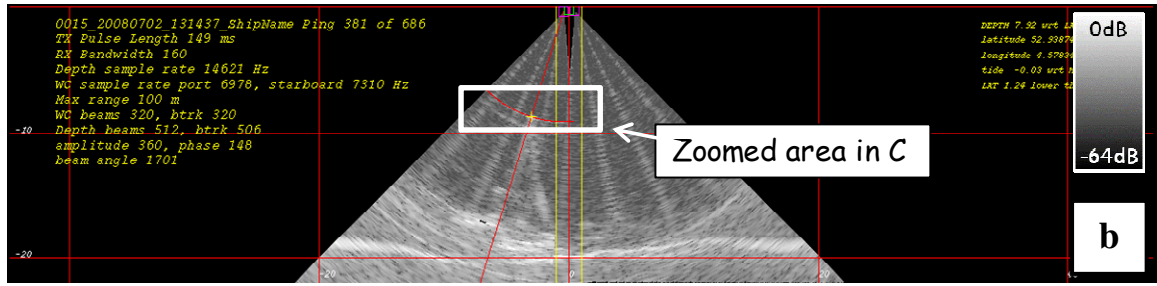
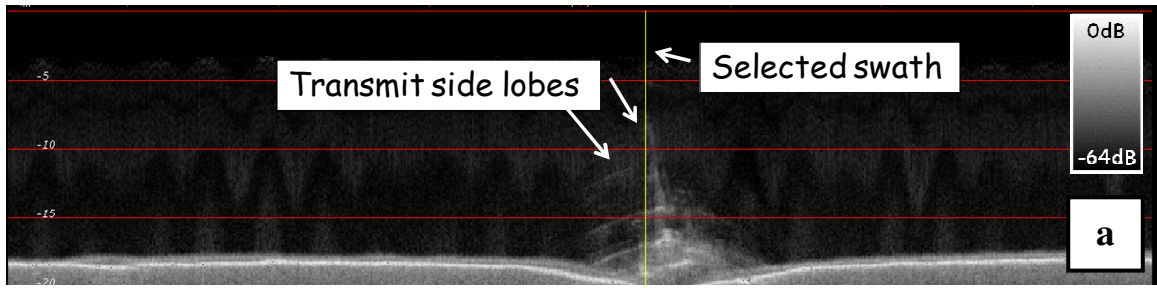


Figure 6.16 – Julian day 184, survey 3, line 0015 - (a) vertical profile, (b) polar plot with real data, (c) polar plot zoom, (d) common-range plot, (e) fixed angle time-series plot.



### 6.3.5 Line 0017

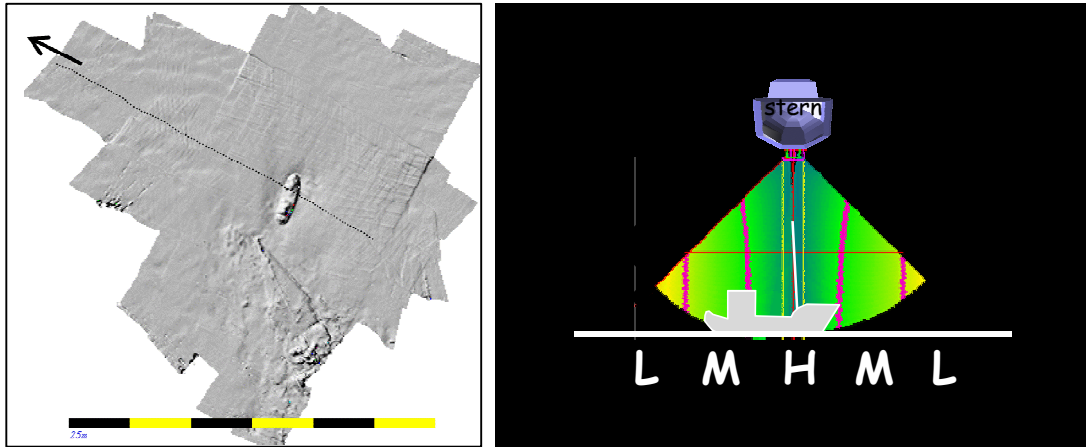


Figure 6.17 - DTM with position and orientation (left), image with IGQF (right) for line number 0017, Julian day 184, survey 3.

This survey line lies orthogonal to the long axis of the wreck, it is sailed from starboard to port over the centre of the wreck (Figure 6.17). Therefore, the viewer looks at the bow of the wreck in the vertical profile (Figure 6.18 (a)). The mast is located in the nadir beams and best viewed using the starboard head, which is therefore used for the least depth selection (Figure 6.18 (b)(c)). When the mast is located at nadir it returns a strong echo from the top of the mast (Figure 6.18 (d)). Also in this case sufficient energy makes it past the mast, maybe because the echo is scattered from the highly reflective hull behind, which causes a real time bottom track solution on the seafloor (Figure 6.18 (e)). There is thus again a case for multiple solutions for this given beam.

The reduced depth is measured at 7.47 m, at the latitude  $52.938759^{\circ}$  N and longitude  $4.578342^{\circ}$  E.



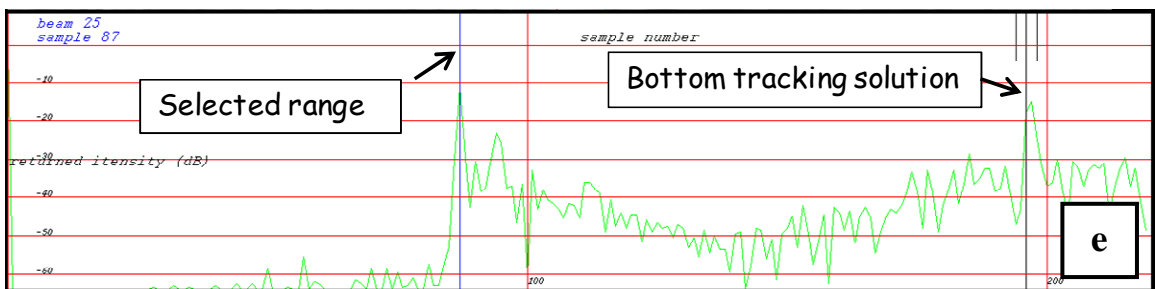
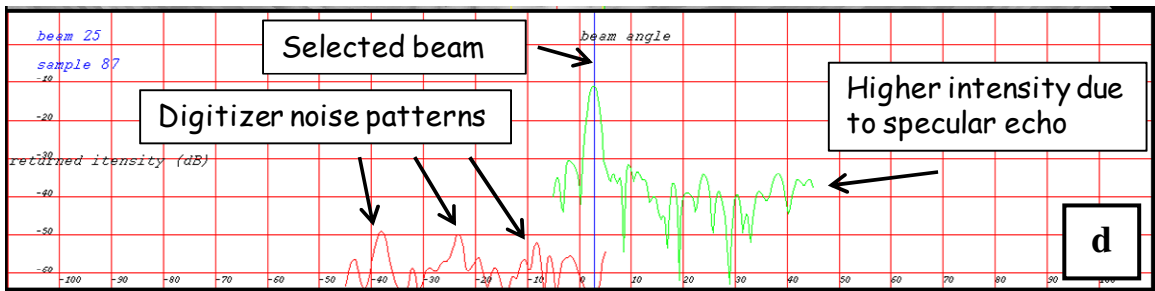
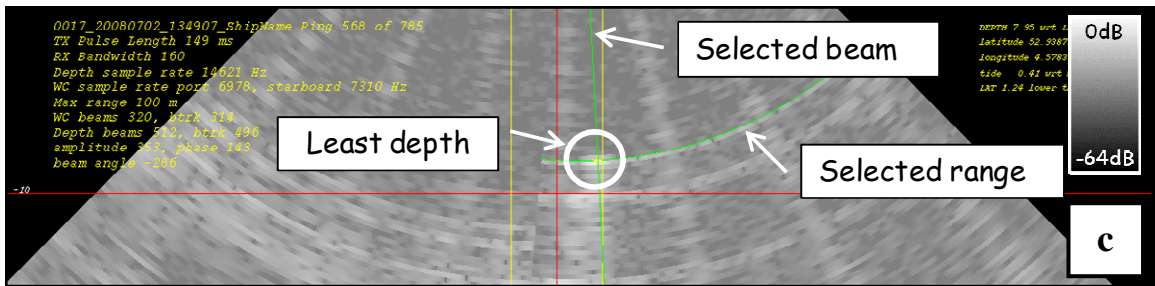
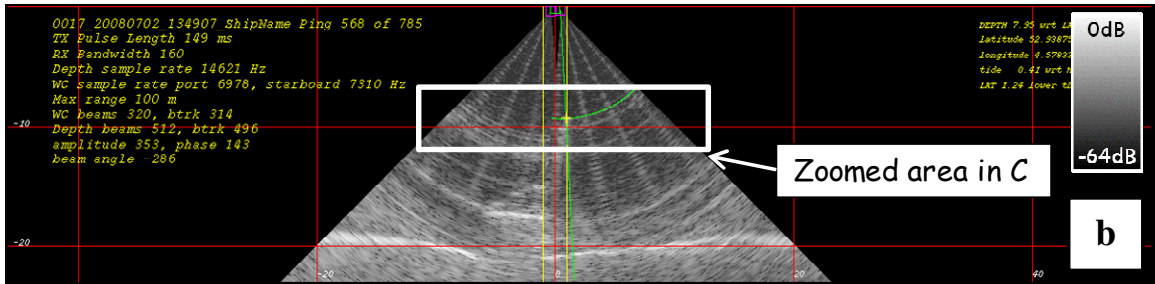
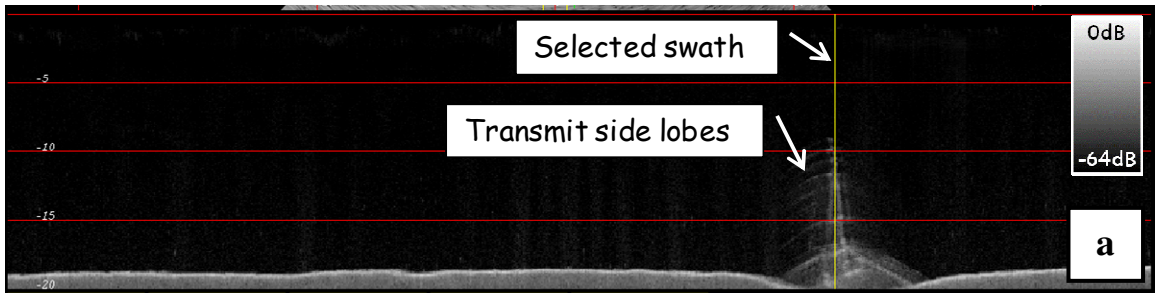


Figure 6.18 – Julian day 184, survey 3, line 0017 - (a) vertical profile, (b) polar plot with real data, (c) polar plot zoom, (d) common-range plot, (e) fixed angle time-series plot.

### 6.3.6 Line 0019

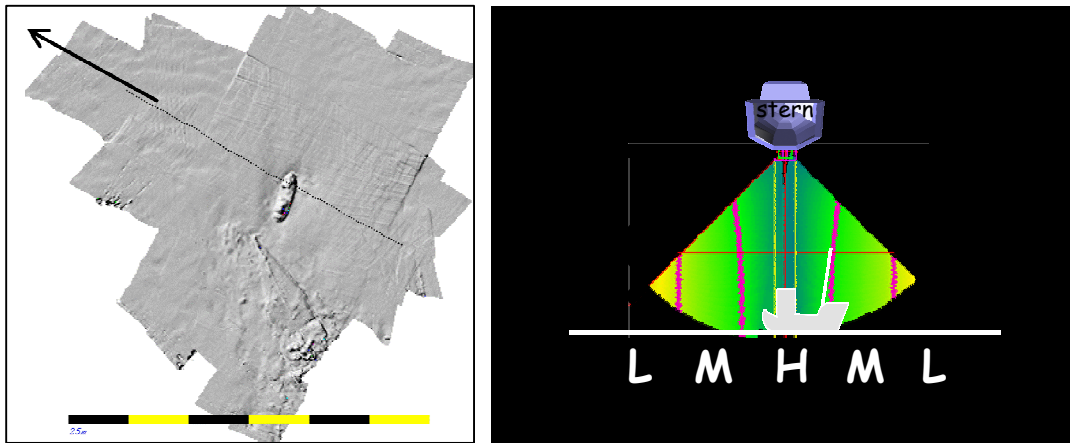


Figure 6.19 - DTM with position and orientation (left), image with IGQF (right) for line number 0019, Julian day 184, survey 3.

This survey line lies orthogonal to the long axis of the wreck, and is sailed from port to starboard over the bow of the wreck (Figure 6.19). Therefore, the viewer looks at the bow of the wreck in the vertical profile (Figure 6.20 (a)). The mast is clearly visible in the vertical profile, and therefore the swaths around the mast can confidently be chosen. The least depth of the mast is again the point with the highest backscatter at the top of the mast (Figure 6.20 (d)). The digitizer noise patterns become very clear from the common-range plot, but do not contaminate the top of the mast. Once the beam with the highest backscatter is selected, it becomes apparent that also for this beam enough energy makes it past the mast, and there is a bottom tracking solution on the seafloor (Figure 6.20 (e)). Thus for this particular beam there is once again a case for multiple solutions within a single beam.

The reduced depth is measured at 7.45 m, at the latitude  $52.938759^{\circ}$  N and longitude  $4.578348^{\circ}$  E.

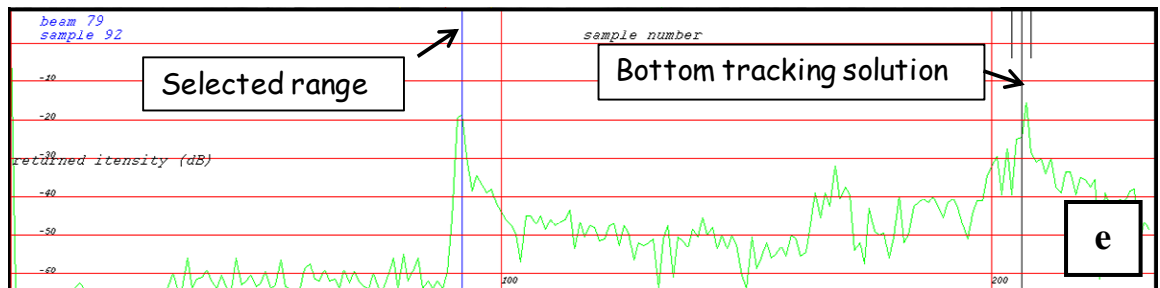
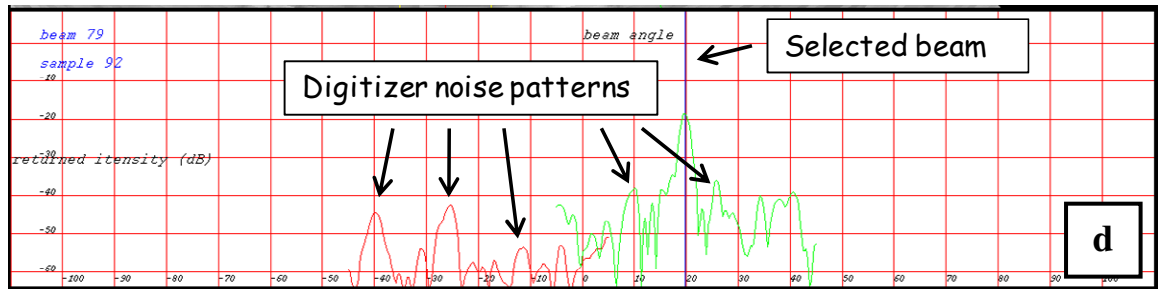
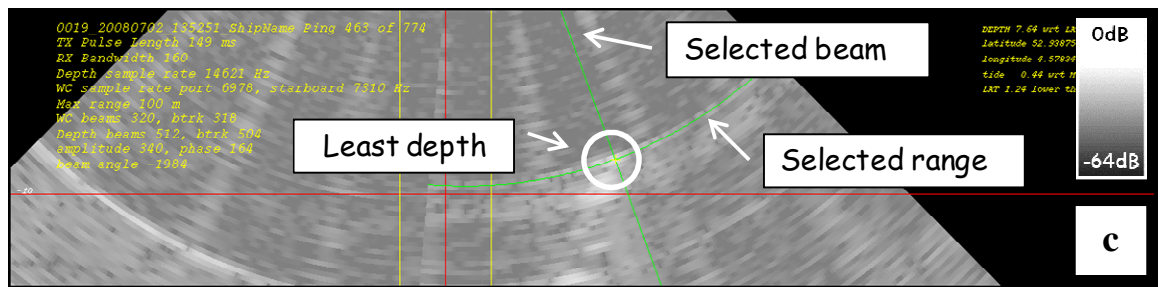
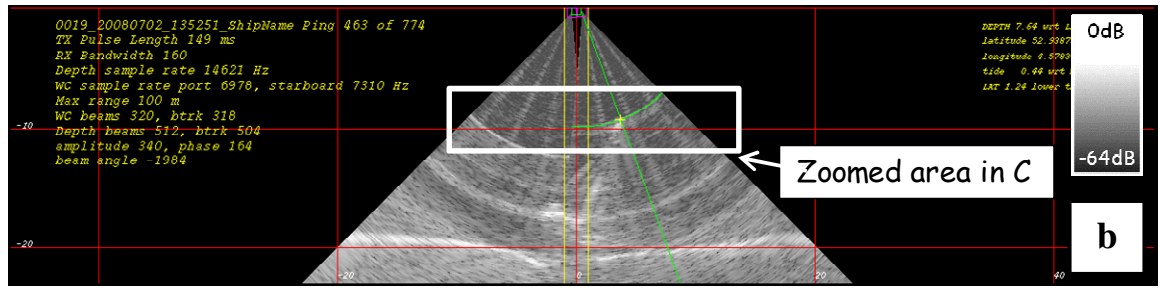
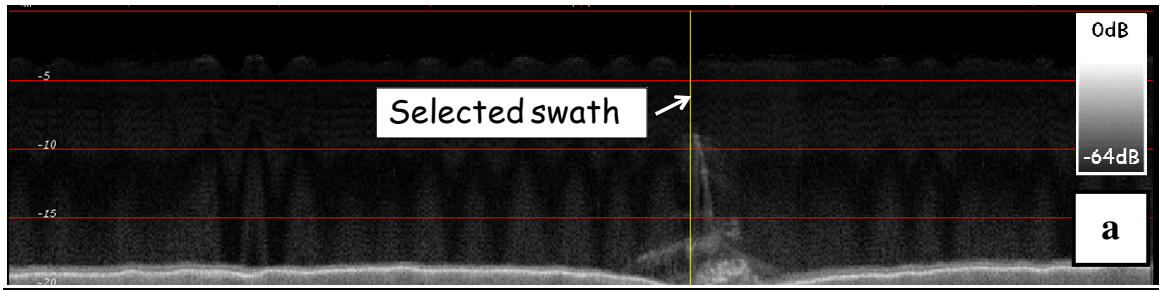


Figure 6.20 – Julian day 184, survey 3, line 0019 - (a) vertical profile, (b) polar plot with real data, (c) polar plot zoom, (d) common-range plot, (e) fixed angle time-series plot.

### 6.3.7 Results

In this particular survey a small angular sector is used (+/- 45°); therefore, it is necessary to sail directly over the wreck to image the top of the mast. Having done so, high quality imaging is expected (dominated by range resolution). In Table 6.1 the depth and position results for this particular survey are given (Julian day 183 survey 3). Where the depth is the depth referenced to RP and the reduced depth, is the depth reduced for tide to LAT. Positions are recalculated from latitude and longitude to easting and northing. The difference between highest and lowest depth is 0.20 m, and the standard deviation is 0.07 m. The pulse length used was set to automatic for this survey, from analysis it was noted that a pulse length of 150  $\mu$ s was used. Therefore, the range resolution was ~10 cm. That means that the least depth point is chosen within 2 times the range resolution. The horizontal deviations are within special order; however, the magnitude of the standard deviation shows that the accuracy of the positions has the potential to be improved.

julian day	survey	line	ping	reduced depth	easting	northing	quality
184	3	5	383	7.41	606070.63	5866623.66	M - 0.19
184	3	6	488	7.38	606067.66	5866624.04	H - 0.11
184	3	7	338	7.27	606069.53	5866624.75	M - 0.21
184	3	15	382	7.4	606069.11	5866622.29	H - 0.16
184	3	17	567	7.47	606069.27	5866623.97	H - 0.11
184	3	19	461	7.45	606069.68	5866623.98	H - 0.17
<b>mean</b>				7.40	606069.31	5866623.78	
<b>standard deviation</b>				0.07	0.97	0.81	

**Table 6.1 – Depth and position results of survey 3 on Julian day 184.**

#### 6.4 Julian Day 184, survey 4

The following lines with the mast within the MSR are now analyzed. The direction of each line is shown with a black arrow towards the line number in Figure 6.21. Note that the top of the mast was detected from different directions. In this survey there were more lines sailed close to the wreck than the previous survey, where the mast is located inside the MSR, which is more suitable for analysis. Throughout this particular survey an angular sector of  $\pm 88^\circ$  degrees was used, the pulse length was set to automatic and the bandwidth was set to 8 kHz. The biggest difference with the previous survey is the wider angular sector, as result of which almost the whole water column is imaged up to the horizontal. Therefore, solutions may have a lower quality. Note the much higher presence of bathymetric outliers. This is because of the sonar's desire to reduce the swath and forcing it to attempt bottom detection at unreasonably low grazing angles.

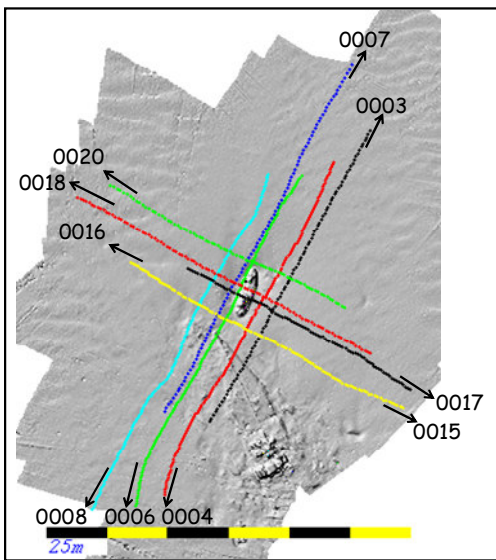


**Figure 6.21 - Digital terrain model of the data collected in survey four on Julian Day 184.**

#### 6.4.1 Line 0003

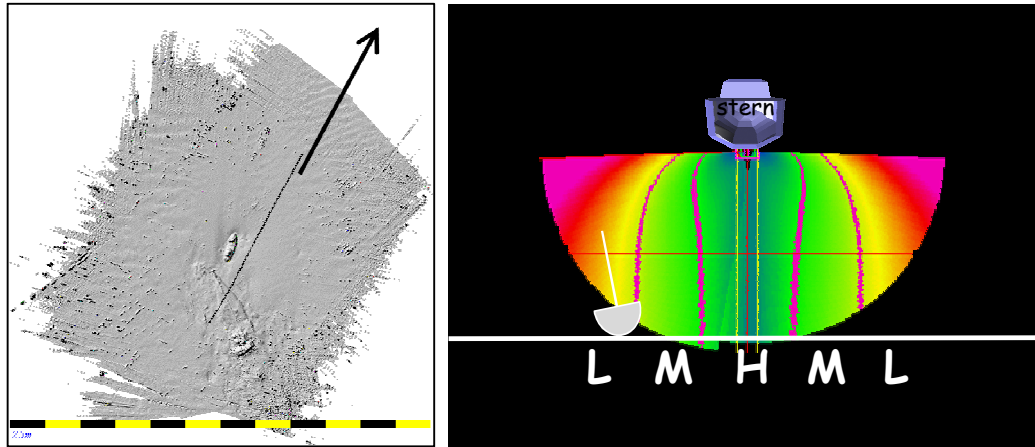


Figure 6.22 - Map with position and orientation (left), image with IGQF (right) for Julian day 184, survey 4, line number 0003.

This survey line lies along the long axis of the wreck, the survey line is sailed from stern to port, on the starboard of the wreck (Figure 6.22). The hull is beyond the MSR. The mast is picked up in receiver side lobes which causes an arc of higher returned intensity along the same common range of the top of the mast (Figure 6.23 (c)). However by running through different common ranges on the mast, the range and beam with strongest backscatter from the top of the mast can still confidently be selected (Figure 6.23 (d)). Because the selected beam has a larger steering angle, which means a larger beam width, enough energy makes it past the mast and back to return a bottom tracking solution on the seafloor (Figure 6.23 (e)).

The reduced depth is measured at 7.63 m, at the latitude  $52.938760^{\circ}$  N and longitude  $4.578370^{\circ}$  E.



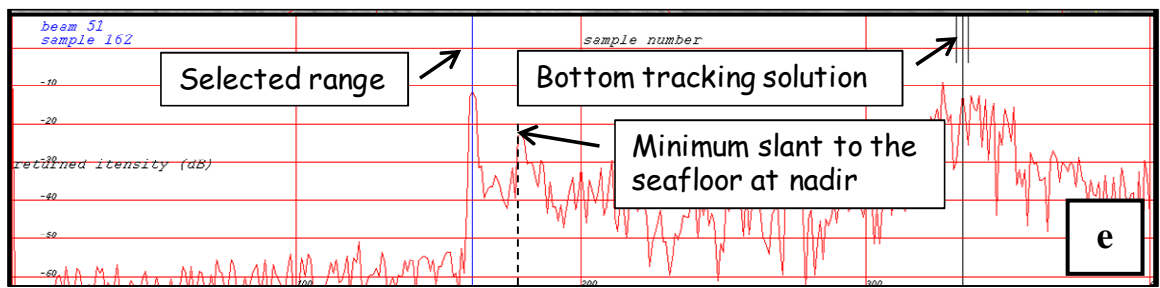
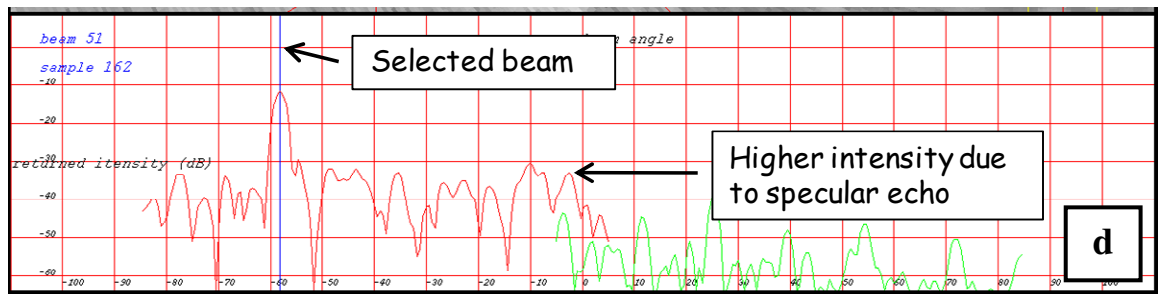
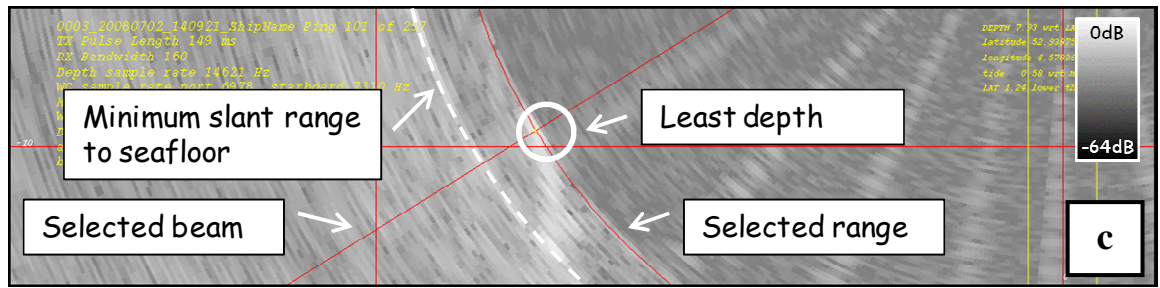
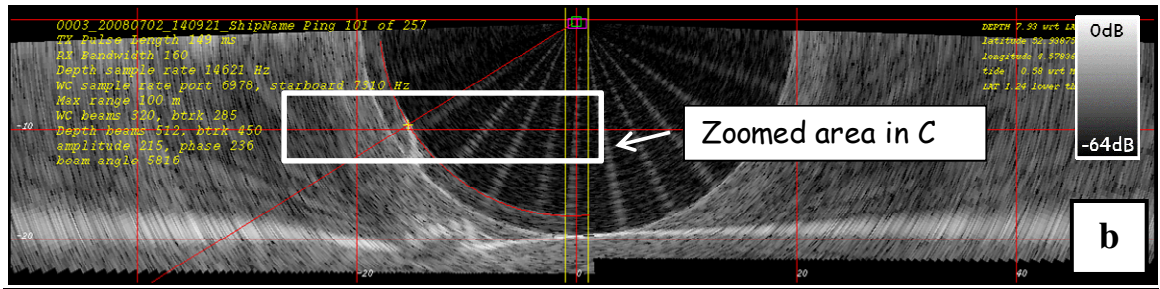
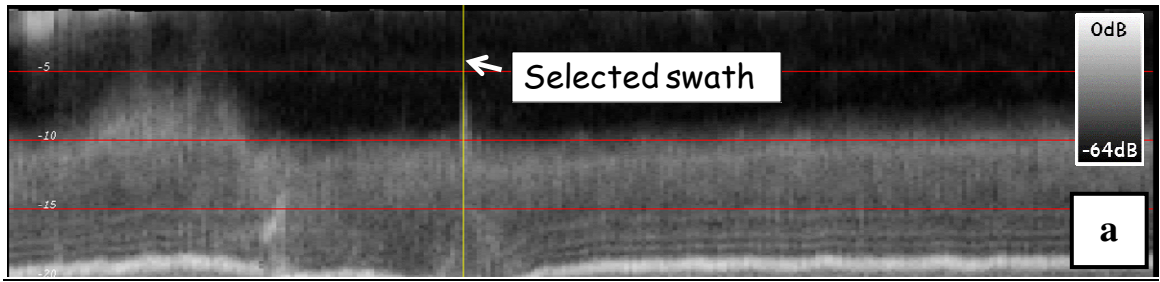
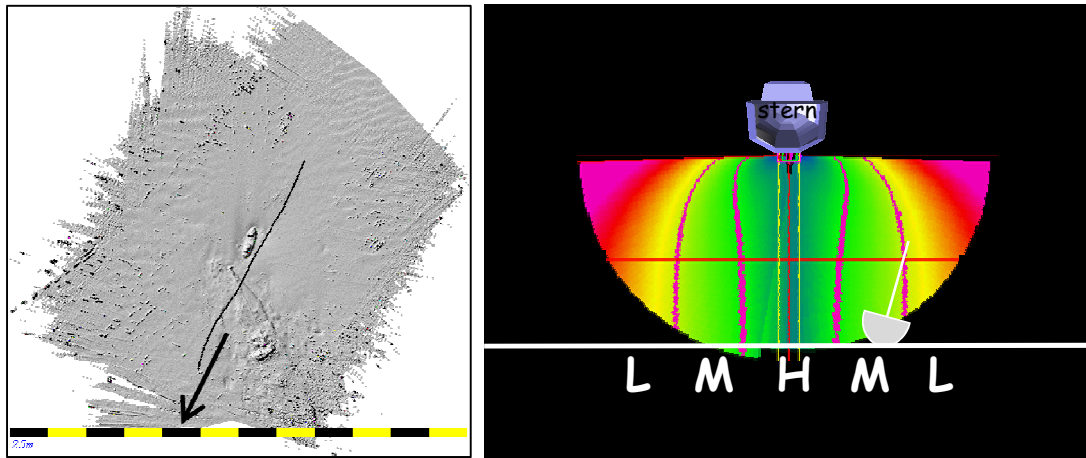


Figure 6.23 – Julian Day 184, survey 4, line 0003 - (a) vertical profile, (b) polar plot with real data, (c) polar plot zoom, (d) common-range plot, (e) fixed angle time-series plot.

#### 6.4.2 Line 0004



**Figure 6.24 - Map with position and orientation (left), image with IGQF (right) for Julian day 184, survey 4, line number 0004.**

This survey line lies along the long axis of the wreck, it is sailed from bow to stern, on the starboard side of the wreck (Figure 6.24). The hull is at MSR, and the mast is located in the low IGQF zone (Figure 6.25 (b)). Because the mast is tilted away from the sonar the mast causes more closely spaced strong echoes off the mast (Figure 6.25 (b)(c)). However, the top of the mast can confidently be chosen as the strongest backscatter (Figure 6.25 (d)). In the fixed angle time-series plot of the selected beam, more strong echoes of the hull become apparent (Figure 6.25 (c)(e)). Again enough energy makes it past the mast to return a bottom tracking solution from the seafloor. Due to the strong backscatter from the side lobe echoes off the hull, it would be dangerous to pick out multiple solutions for this selected beam (Figure 6.25 (e)). The reduced depth is measured at 7.53 m, at the latitude  $52.938756^{\circ}$  N and longitude  $4.578340^{\circ}$  E.



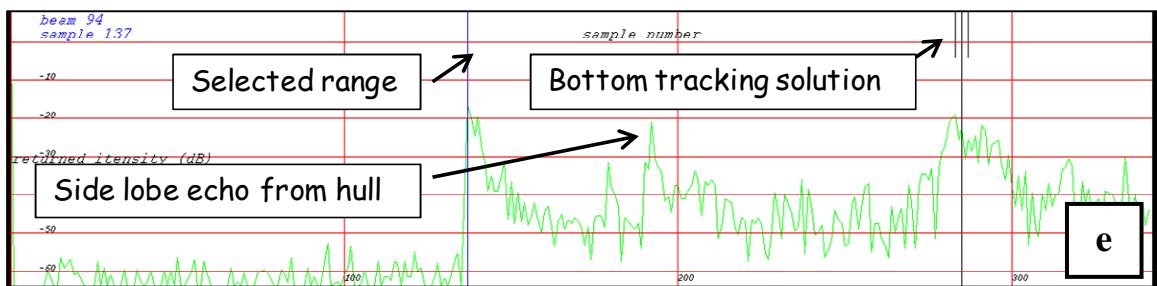
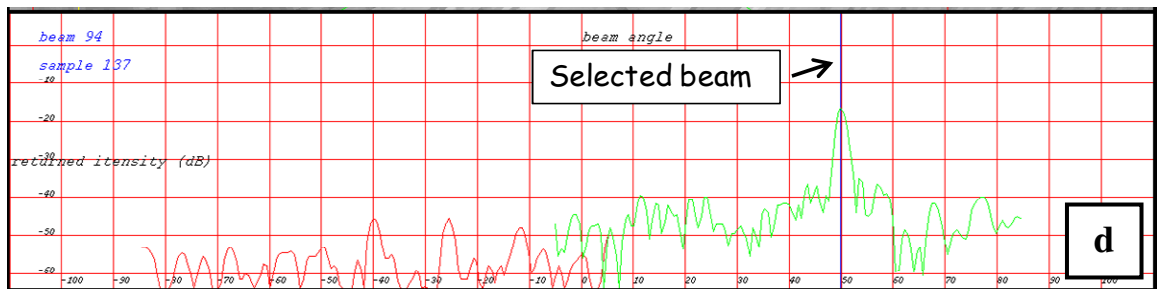
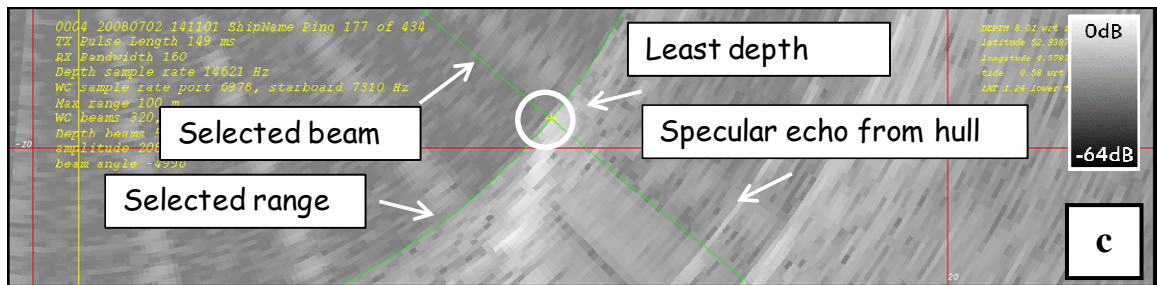
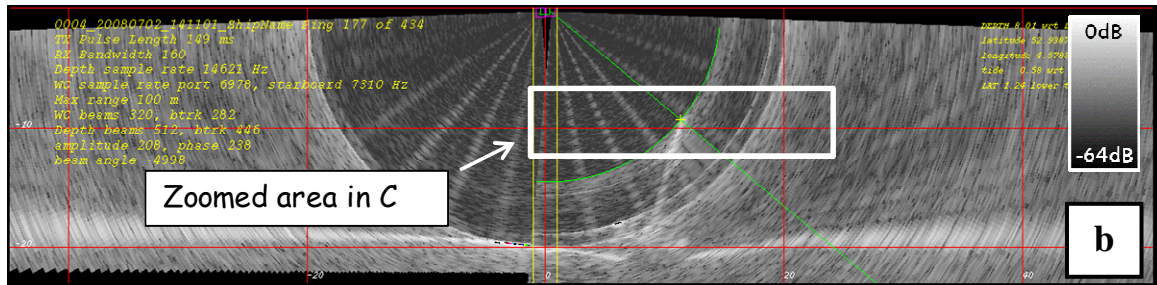
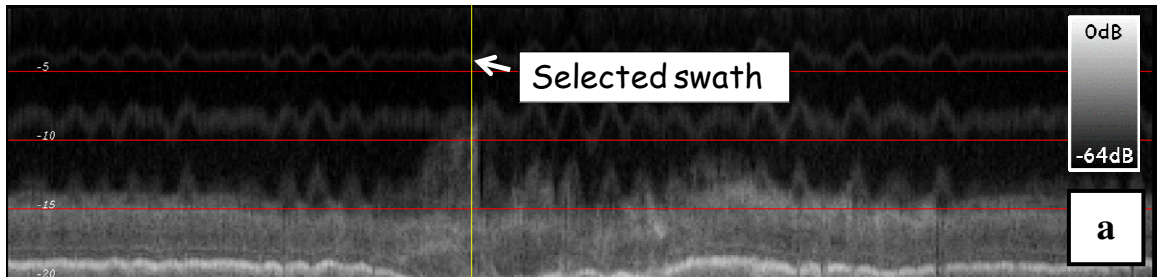


Figure 6.25 – Julian day 184, survey 4, line 0004 - (a) vertical profile, (b) polar plot with real data, (c) polar plot zoom, (d) common-range plot, (e) fixed angle time-series plot.

### 6.4.3 Line 0006

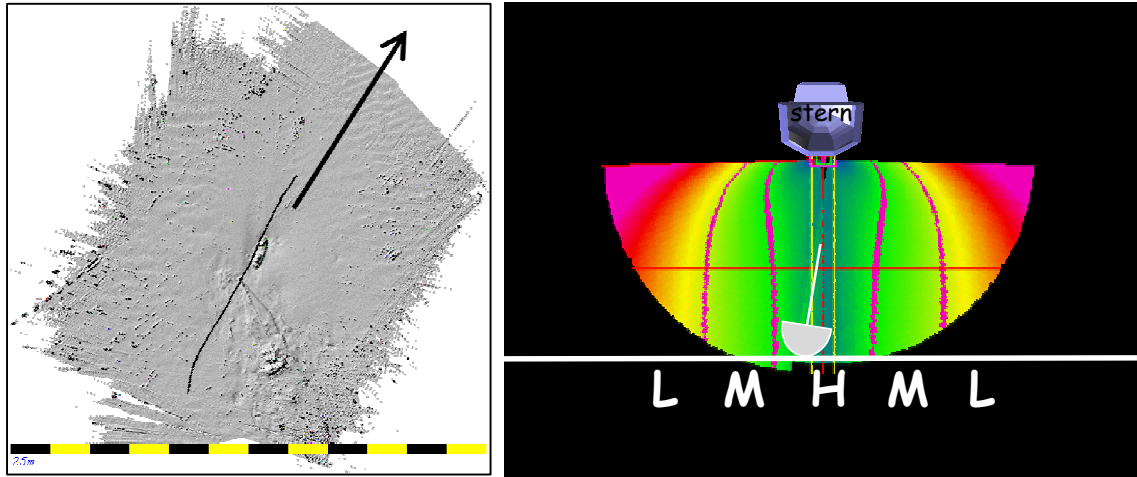


Figure 6.26 - Map with position and orientation (left), image with IGQF (right) for Julian day 184, survey 4, line number 0006.

This survey line lies along the long axis of the wreck and is sailed from the stern towards the bow of the wreck, over the centre of the wreck (Figure 6.26, Figure 6.27 (b)). Because the wreck appears in the near nadir beams, the wreck shows up clearly in the vertical profile, the viewer looks at the starboard side of the wreck (Figure 6.27 (a)). From the vertical profile the swaths around the mast can easily be distinguished. The top of the mast does not return a strong specular echo, but lower on the mast more specular echoes are visible, possibly created by rigging and pulley blocks (Figure 6.27 (b)(e)). The top of the mast is the shortest range with a high returned backscatter (Figure 6.27 (c)(d)). The fixed angle time-series plot of the selected beam shows that the top of the mast is represented by the first high amplitude of backscatter; however, the side lobe echoes of the lower sections of the mast also return a strong signal. An example where the human selection of the shallowest rather than the strongest is important, automation would be

difficult. Enough energy makes it past the mast to create a bottom tracking solution on the seafloor; therefore, there may be a case for multiple solutions for this beam.

The reduced depth is measured at 7.46 m, at latitude  $52.938753^\circ$  N and longitude  $4.578325^\circ$  E.

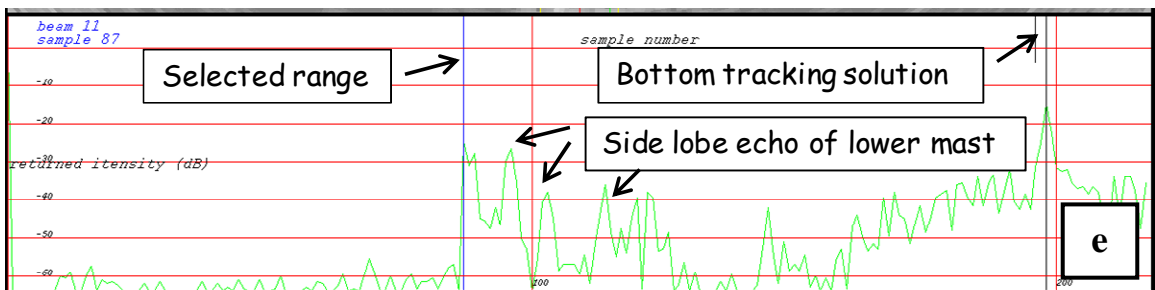
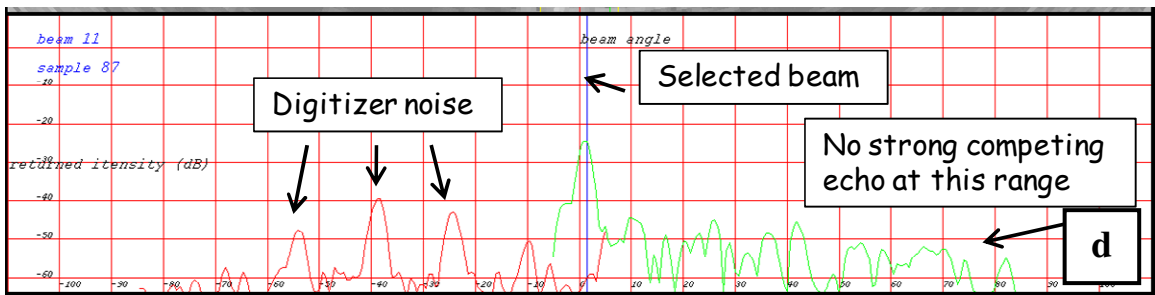
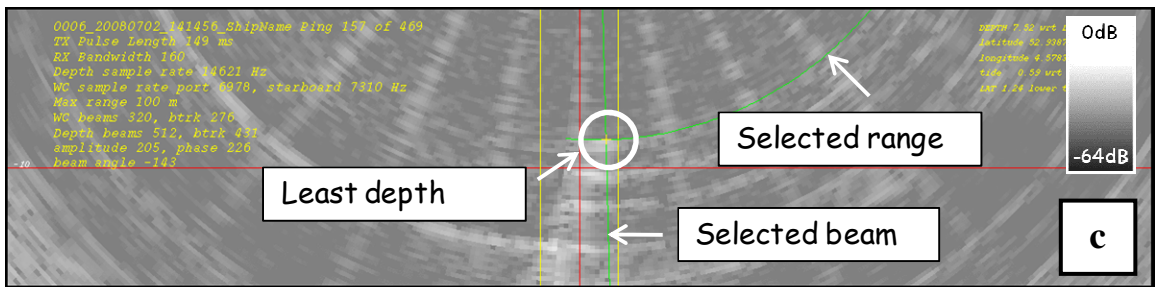
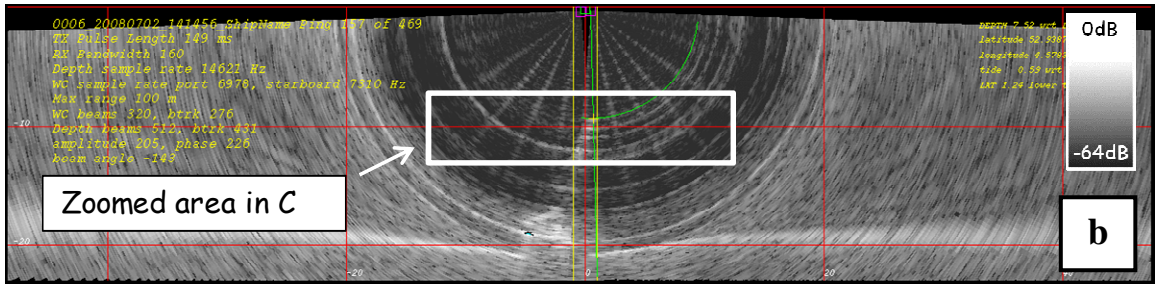
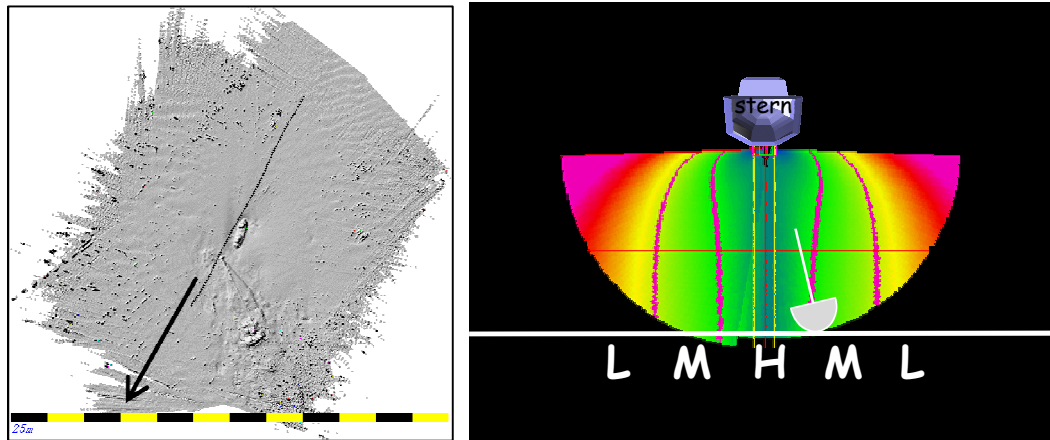


Figure 6.27 – Julian day 184, survey 4, line 0006 - (a) vertical profile, (b) polar plot with real data, (c) polar plot zoom, (d) common-range plot, (e) fixed angle time-series plot.

#### 6.4.4 Line 0007



**Figure 6.28 - Map with position and orientation (left), image with IGQF (right) for Julian day 184, survey 4, line number 0007**

In this case the survey line lies along the long axis of the wreck, and is sailed from bow to stern almost directly over the wreck (Figure 6.28). In the polar plot the mast and even the rigging is imaged, where side lobe echoes are received off the hull of the wreck (Figure 6.29 (b)(c)). The mast is not contaminated by digitizer noise, or a strong competing echo at the same range and can therefore easily be distinguished (Figure 6.29 (d)). From the fixed angle time-series plot of the selected beam the range to the mast becomes apparent. The side lobe echoes of the hull actually return a higher backscatter than the top of the mast or the seafloor beyond. However, because it is located at a greater range, it does not cause confusion. Enough energy makes it past the mast, to create a bottom tracking solution on the hull of the wreck before the signal arrives at the seafloor, maybe because the hull of the wreck lies within the receiver side lobes and has a stronger return (Figure 6.29 (e)). The reduced depth is measured at 7.54 m, at latitude 52.938760° N and longitude 4.578351° E.



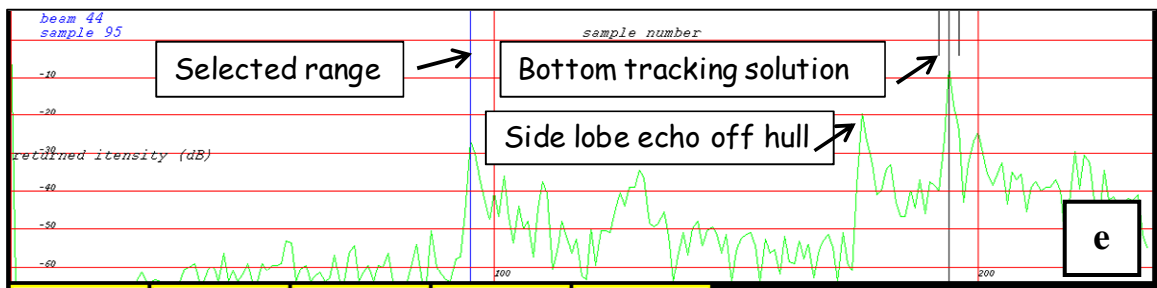
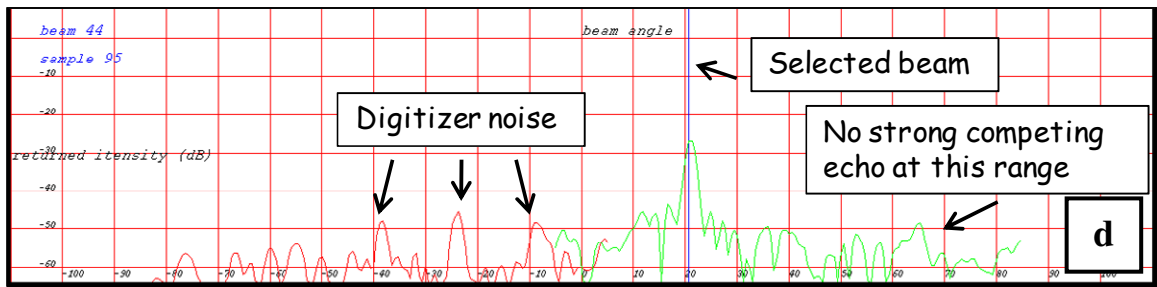
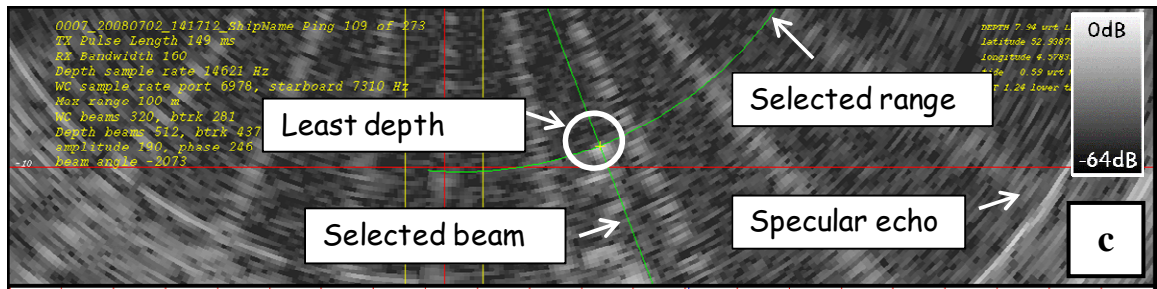
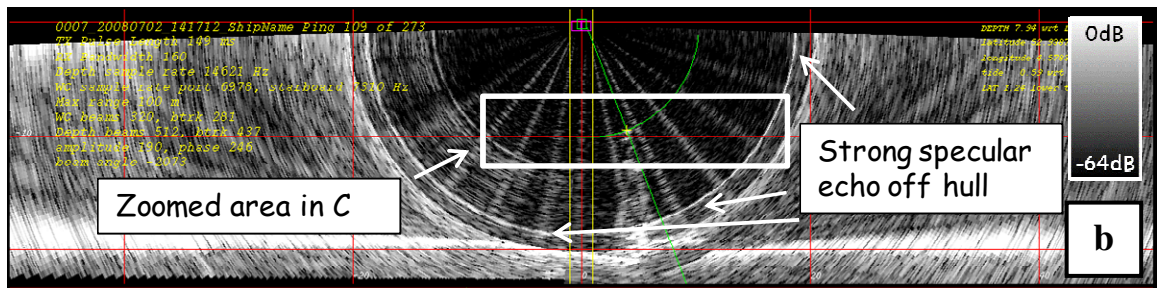
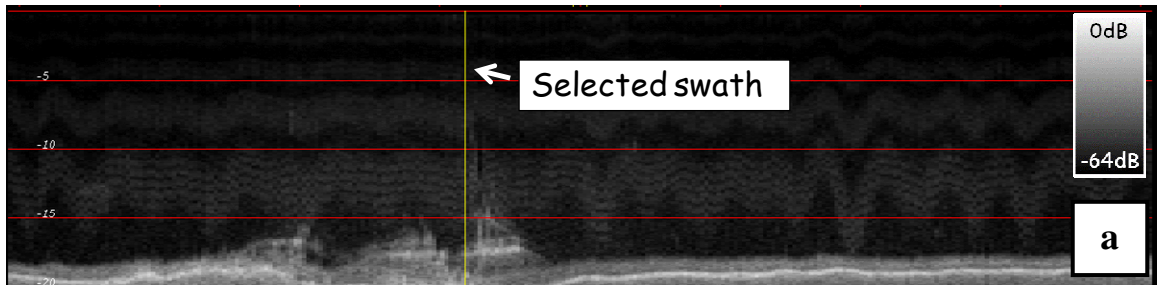
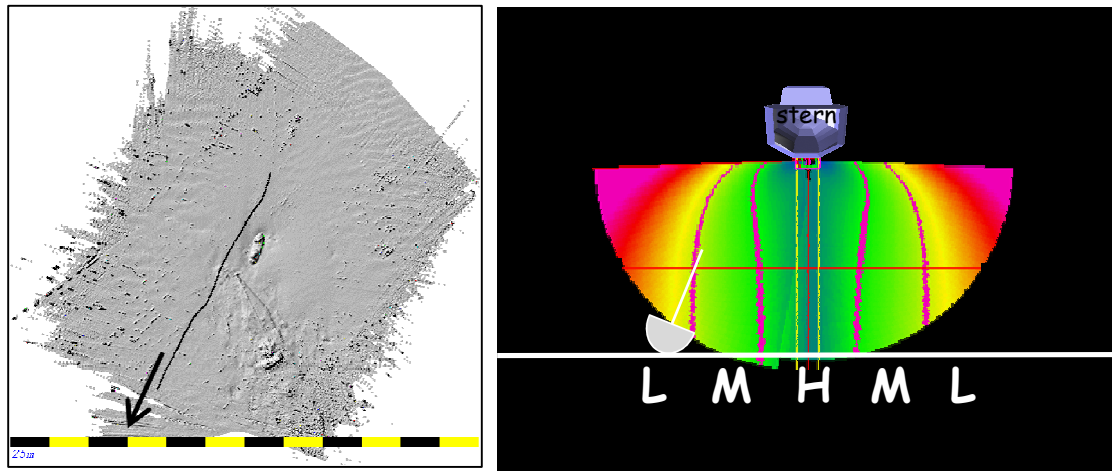


Figure 6.29 – Julian day 184, survey 4, line 0007 - (a) vertical profile, (b) polar plot with real data, (c) polar plot zoom, (d) common-range plot, (e) fixed angle time-series plot.

#### 6.4.5 Line 0008



**Figure 6.30 - Map with position and orientation (left), image with IGQF (right) for Julian day 184, survey 4, line number 0008.**

This line lies along the long axis of the wreck, and is sailed from stern to bow with the wreck on the port side of the line (Figure 6.30). The hull of the wreck is located outside the MSR and the mast is located inside the MSR (Figure 6.31 (b)). The mast is oriented towards the sonar, and therefore the specular echoes on the mast are not in line with the orientation of the mast. This makes it easier to confidently pick out the top of the mast (Figure 6.31 (c)(d)). However the lower sector mast causes a lot of side lobe echoes in the same beam which show up in the fixed angle time-series plot of the selected beam ((Figure 6.31 (e)). The range to the top of the mast is represented by the first high amplitude backscatter. Enough energy makes it past the mast to return a bottom tracking solution of the seafloor (Figure 6.31 (e)). The reduced depth is measured at 7.54 m, at latitude 52.938758° N and longitude 4.578319° E .

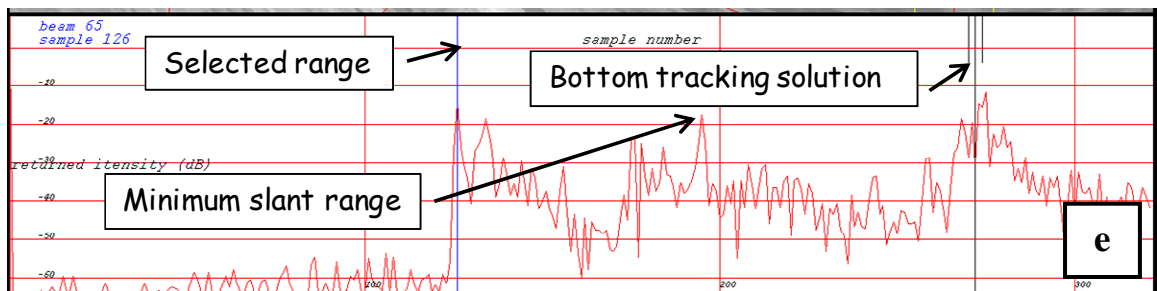
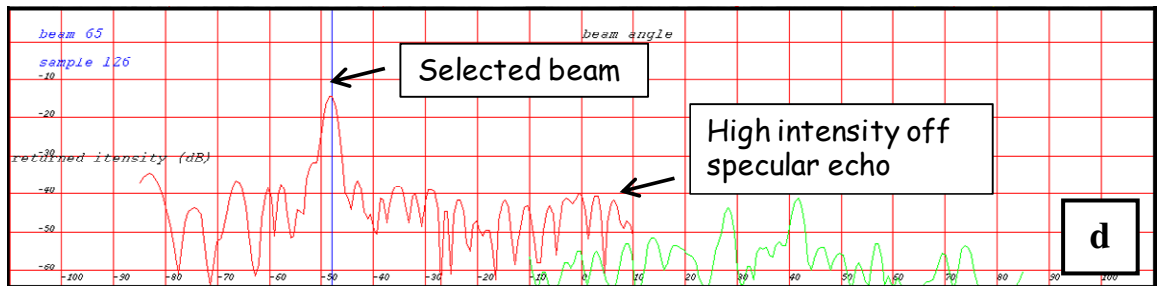
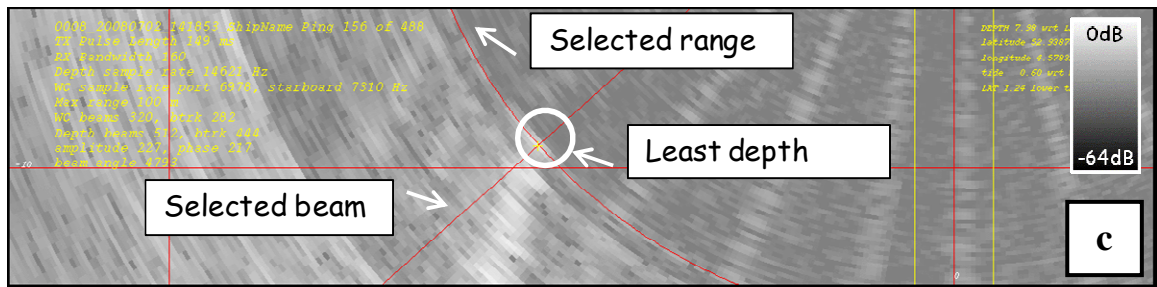
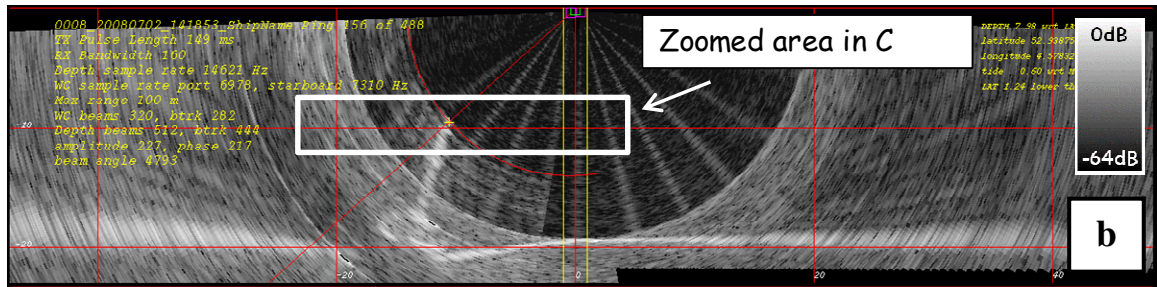
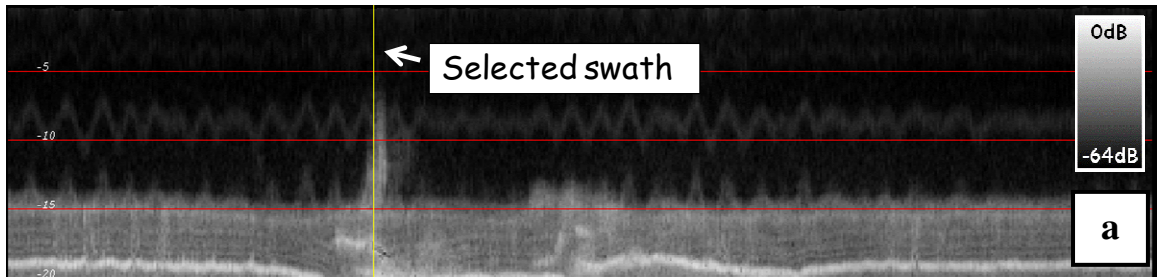
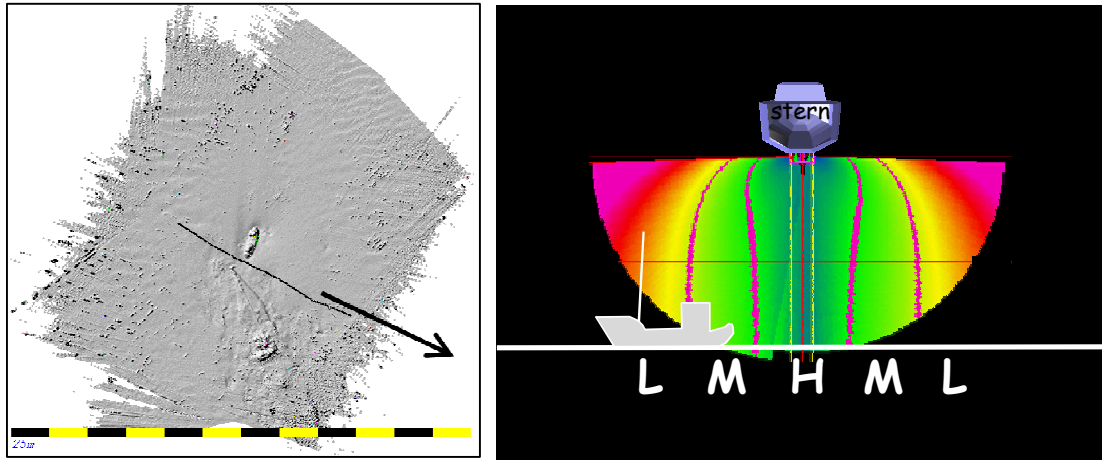


Figure 6.31 – Julian day 184, survey 4, line 0008 - (a) vertical profile, (b) polar plot with real data, (c) polar plot zoom, (d) common-range plot, (e) fixed angle time-series plot.



#### 6.4.6 Line 0015



**Figure 6.32 - Map with position and orientation (left), image with IGQF (right) for Julian day 184, survey 4, line number 0015.**

In this case the survey line lies orthogonal to the long axis of the wreck, it is sailed from port to starboard, behind the stern of the wreck (Figure 6.32). The top of the mast is located just inside the MSR and nearly vertical, and the hull of the wreck mainly outside the MSR (Figure 6.33 (b)). The top of the mast generates a lot of echoes which can be confused with side-lobe echoes off the nadir seafloor (Figure 6.33 (c)). The stronger echo; however, from the top of the mast can be distinguished and selected (Figure 6.33 (d)). Enough energy makes it past the mast to return clear and stronger bottom tracking solution of the seafloor; however, it might be difficult to select more solutions for this given beam, due to the noise at and beyond the MSR. Note as the beam elevation is large, the depth estimate is mainly dependent on the angle and thus the IGQF is low (0.56 meter). The reduced depth is measured at 7.73 m, at latitude 52.938741° N and longitude 4.578344° E.

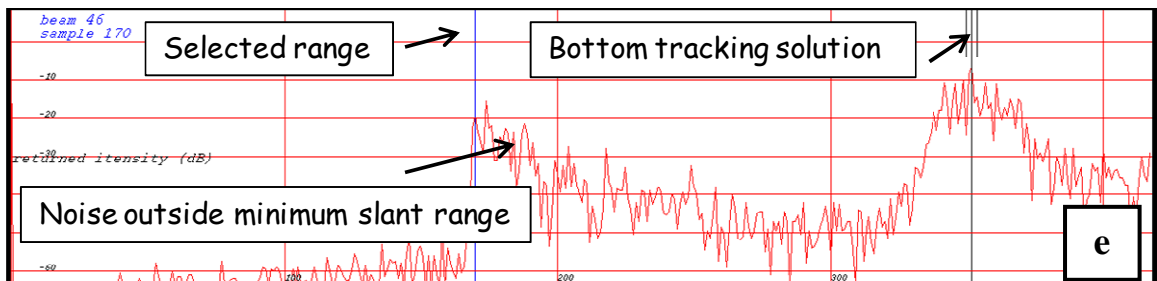
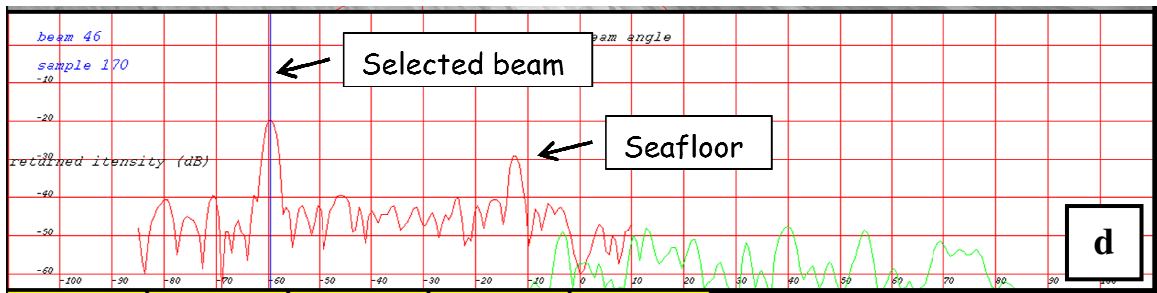
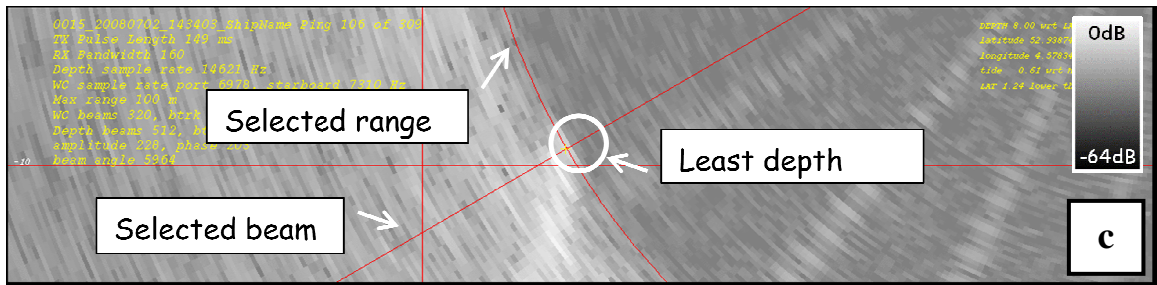
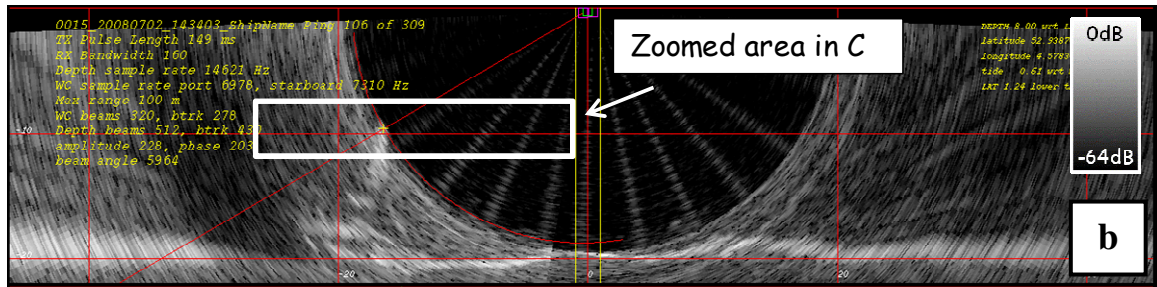
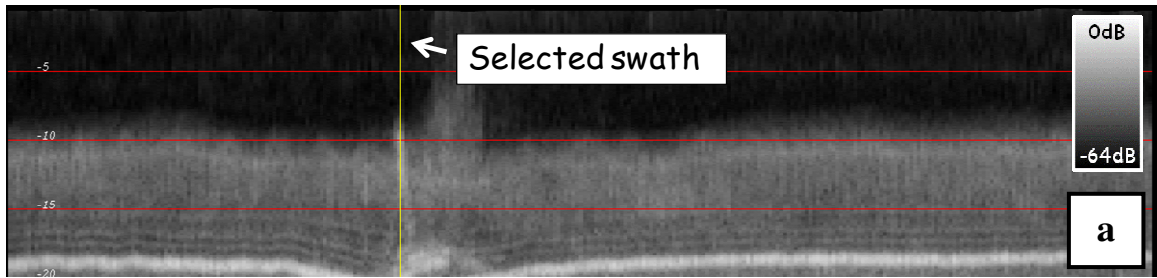
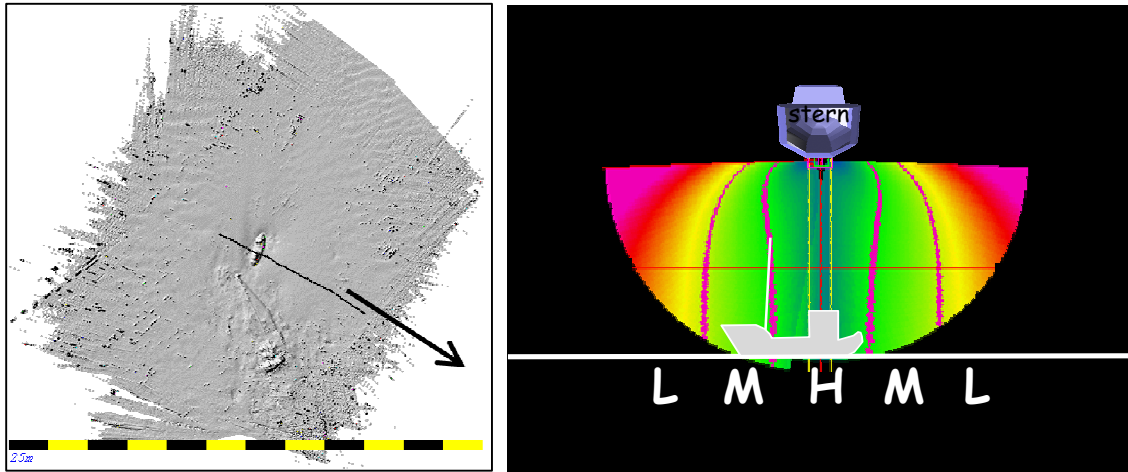


Figure 6.33 – Julian day 184, survey 4, line 0015 - (a) vertical profile, (b) polar plot with real data, (c) polar plot zoom, (d) common-range plot, (e) fixed angle time-series plot.

#### 6.4.7 Line 0017



**Figure 6.34 - Map with position and orientation (left), image with IGQF (right) for Julian day 184, survey 4, line number 0017.**

In this case the survey line lies orthogonal to the long axis of the wreck and is sailed from port to starboard over the centre of the wreck (Figure 6.34). From the polar plot it becomes clear that the mast is contaminated by digitizer noise, and that there are stronger echoes lower on the mast (Figure 6.35 (c)). In this particular case the top of the mast is not the point with the strongest backscatter (Figure 6.35 (d)). In the fixed angle time-series plot of the selected beam, the digitizer noise, and the noise from beyond the mast become apparent; however, the least depth range can clearly be distinguished (Figure 6.35 (e)). For once, there is a bottom tracking solution locked onto the top of the mast. The reduced depth is measured at 7.52 m, at latitude 52.938746° N and longitude 4.578340° E.

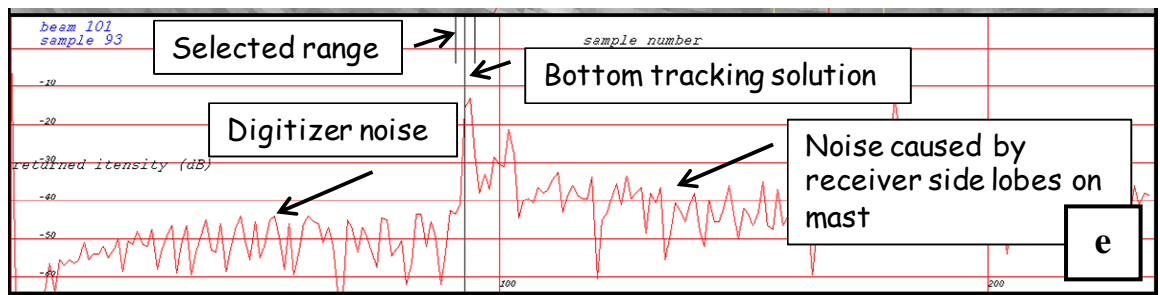
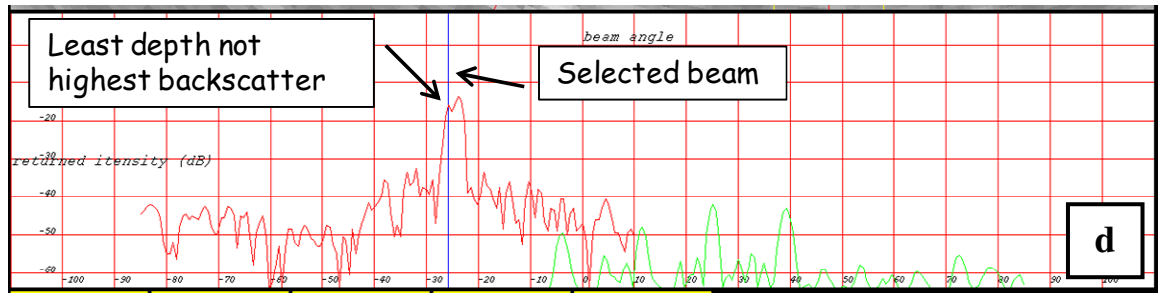
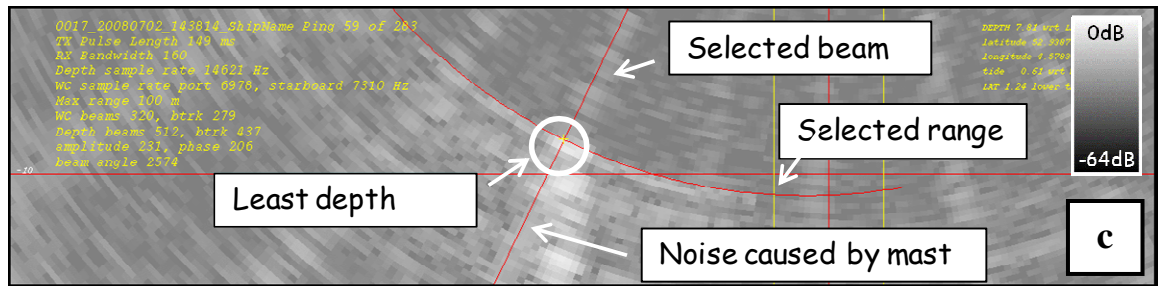
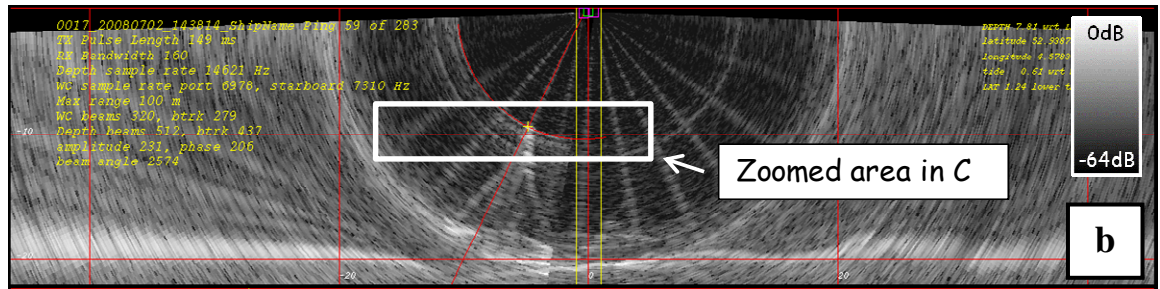
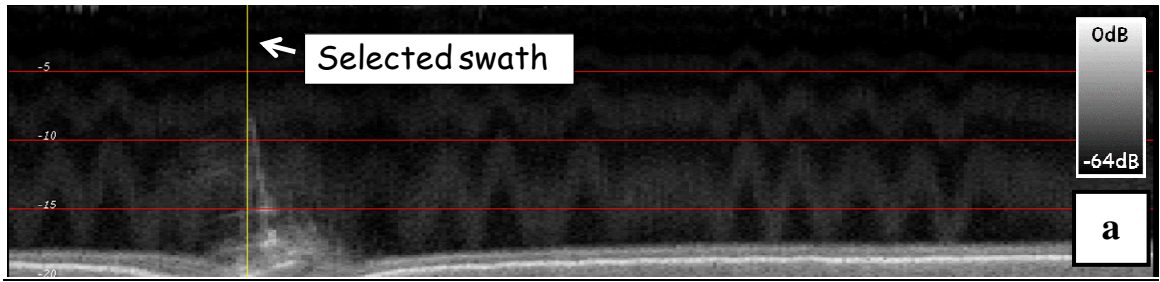


Figure 6.35 – Julian day 184, survey 4, line 0017 - (a) vertical profile, (b) polar plot with real data, (c) polar plot zoom, (d) common-range plot, (e) fixed angle time-series plot.

#### 6.4.8 Line 0018

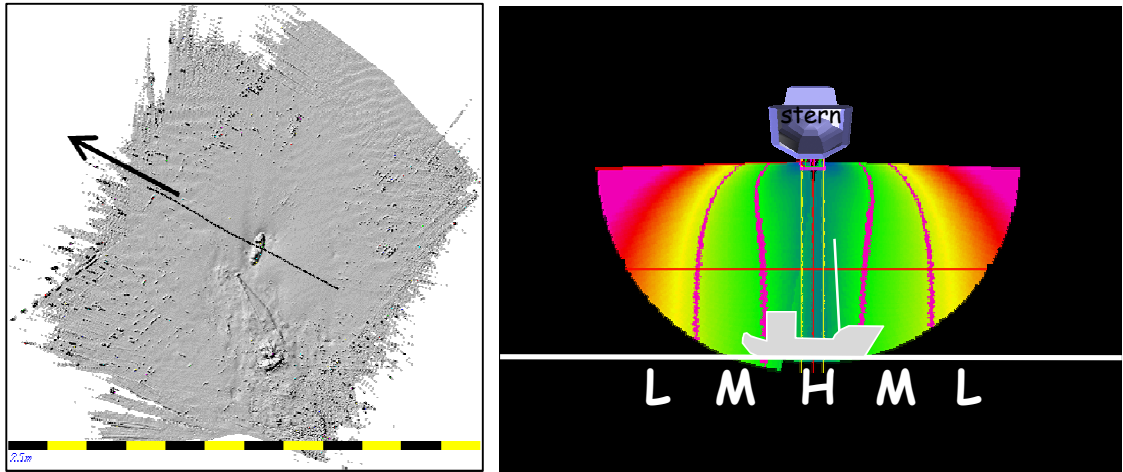


Figure 6.36 - Map with position and orientation (left), image with IGQF (right) for Julian day 184, survey 4, line number 0018

In this case the survey line lies orthogonal to the long axis of the wreck, and is sailed from starboard to port over the centre of the wreck (Figure 6.36). Therefore, the viewer looks at the bow of the wreck in the vertical profile (Figure 6.37 (a)). The mast of the wreck is located close to nadir and is corrupted by digitizer noise (Figure 6.37 (b)(c)). However, the least depth point can still be distinguished in the common-range plot (Figure 6.37 (d)). In the fixed angle time-series plot of the selected beam, the digitizer noise and the noise after the mast becomes apparent again, just as in the previous line (Figure 6.37 (e)). In this case the bottom tracking solution is located at the top of the mast at the same angle and range as the selected depth.

The reduced depth is measured at 7.49 m, at latitude  $52.938761^{\circ}$  N and longitude  $4.578331^{\circ}$  E.



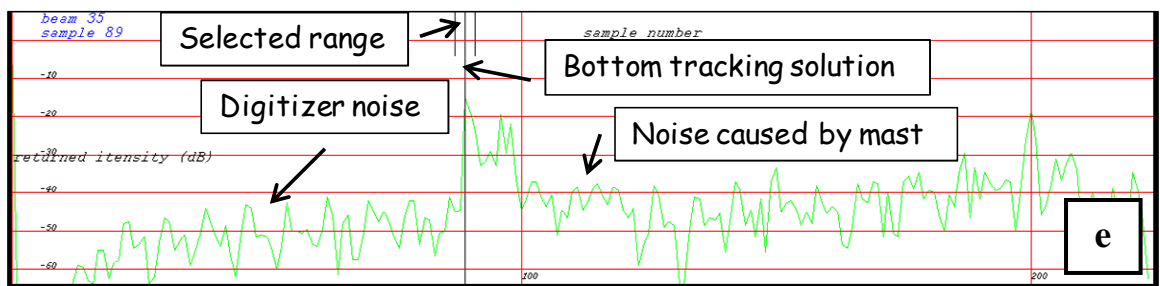
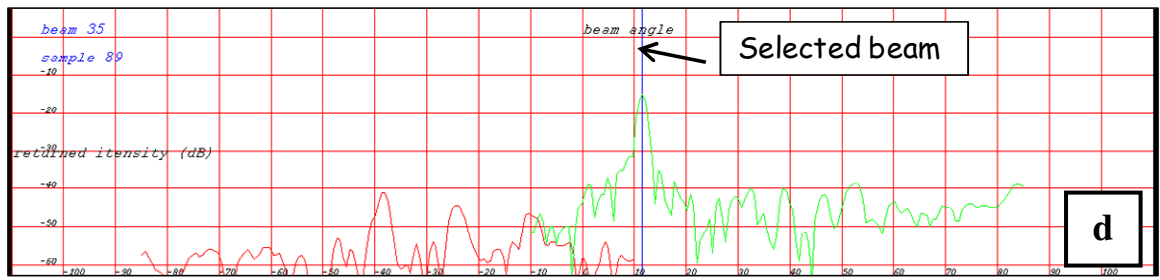
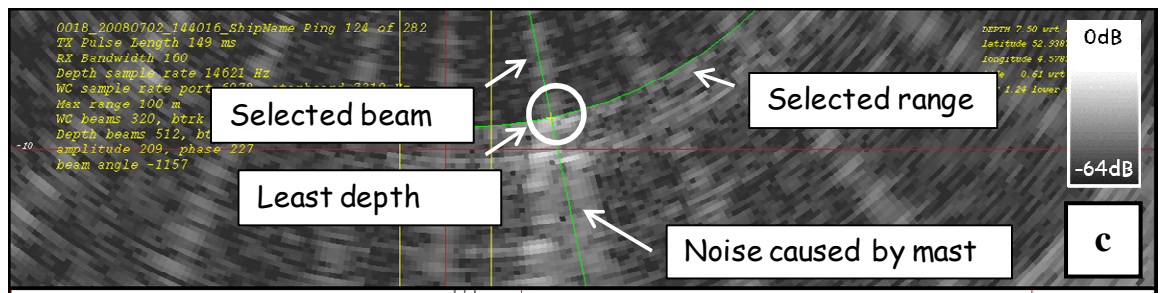
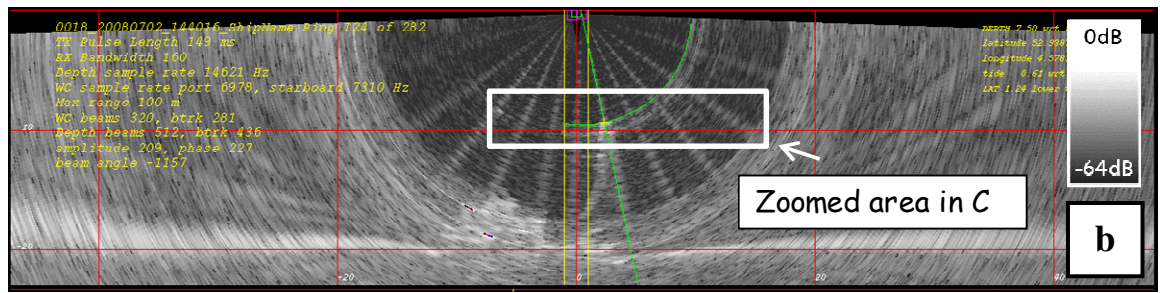
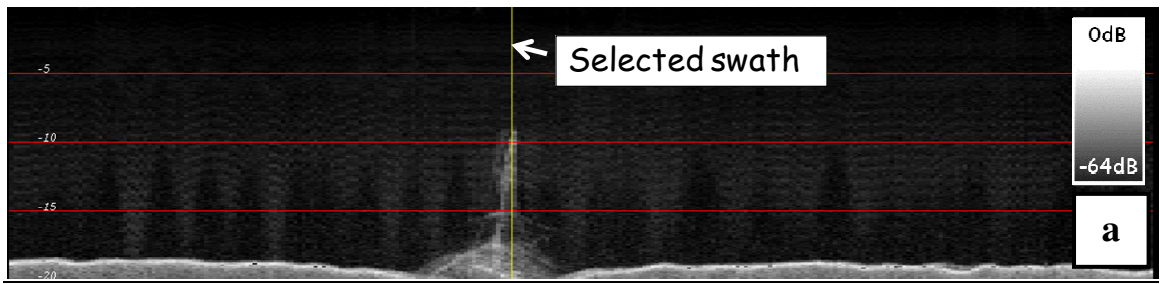
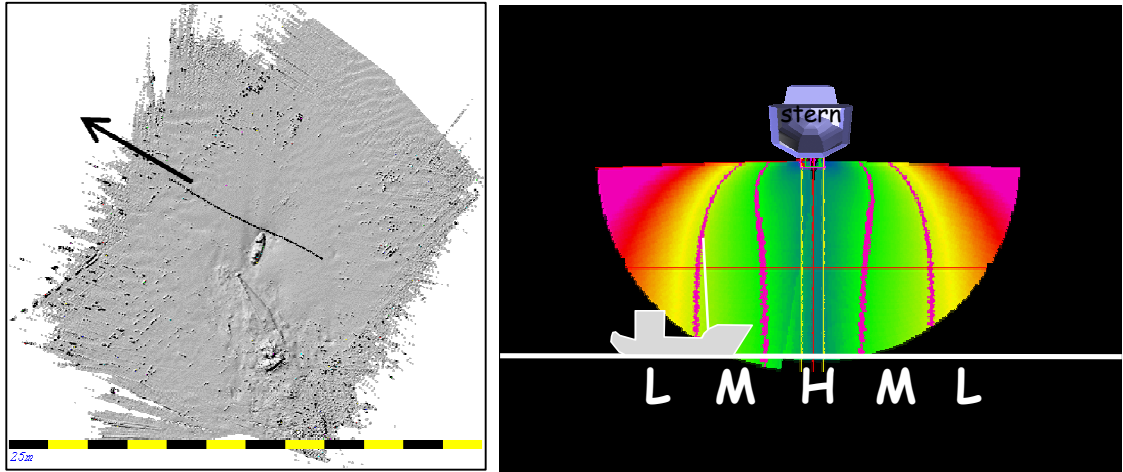


Figure 6.37 – Julian day 184, survey 5, line 0018 - (a) vertical profile, (b) polar plot with real data, (c) polar plot zoom, (d) common-range plot, (e) fixed angle time-series plot.

#### 6.4.9 Line 0020



**Figure 6.38 - Map with position and orientation (left), image with IGQF (right) for Julian day 184, survey 4, line number 0020.**

In this case the survey line lies orthogonal to the long axis of the wreck, and is sailed from port to starboard behind the stern of the wreck (Figure 6.38). The wreck is located outside the MSR and the top of the mast is located inside the MSR tilted away from the sonar (Figure 6.39 (b)). Pronounced receiver side-lobe echoes are formed on the mast which becomes apparent in the common-range plot (Figure 6.39 (d)); however, the main-lobe echo from the mast remains still significantly stronger. From the fixed angle time-series plot of the selected beam the range to the top of the mast is the first high amplitude backscatter. Interesting in this case is that there is an exponentially decaying noise from beyond the mast, which decreases over time (Figure 6.39 (e)). The selected beam lies in line with the hull of the wreck outside the MSR and enough energy makes it past the mast and returns a bottom tracking solution on the hull of the wreck. The reduced depth is measured at 7.51 m, at latitude 52.938774° N and longitude 4.578328° E .

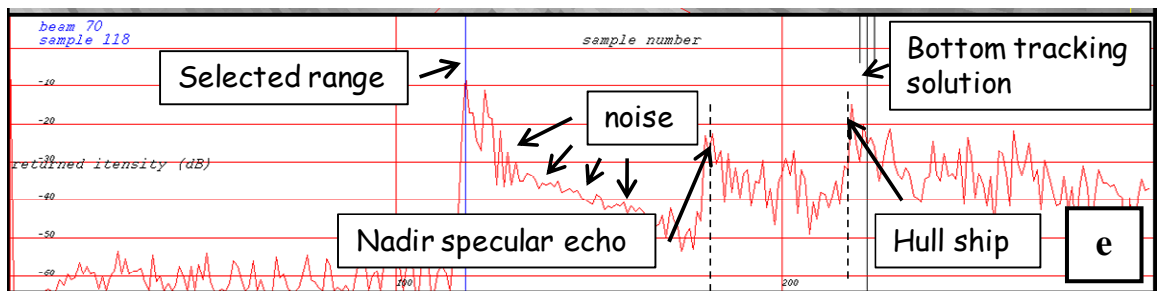
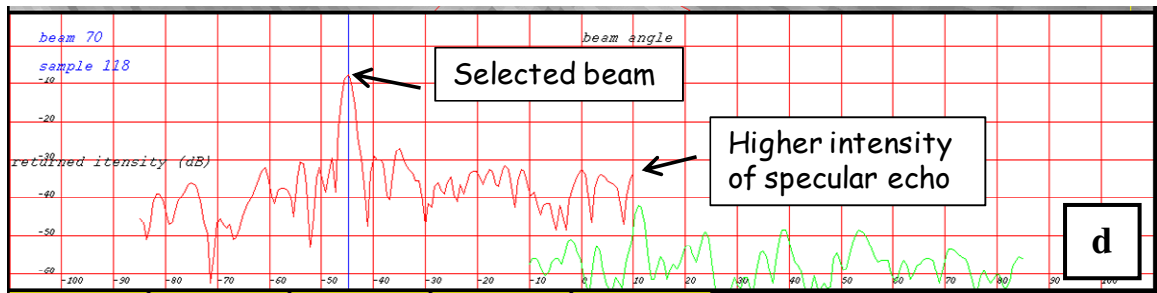
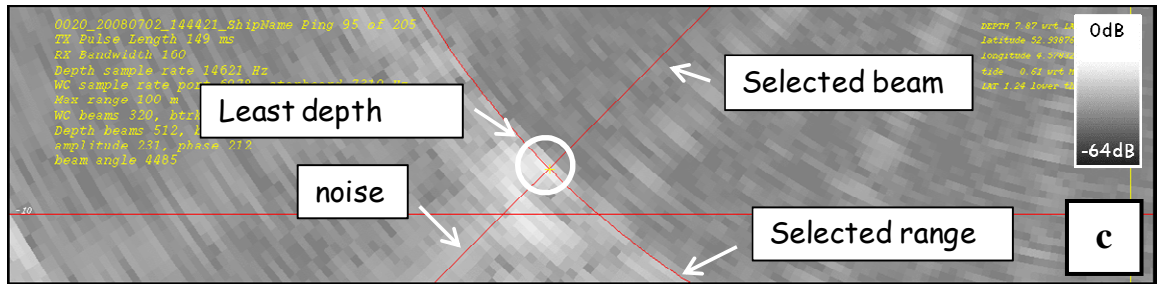
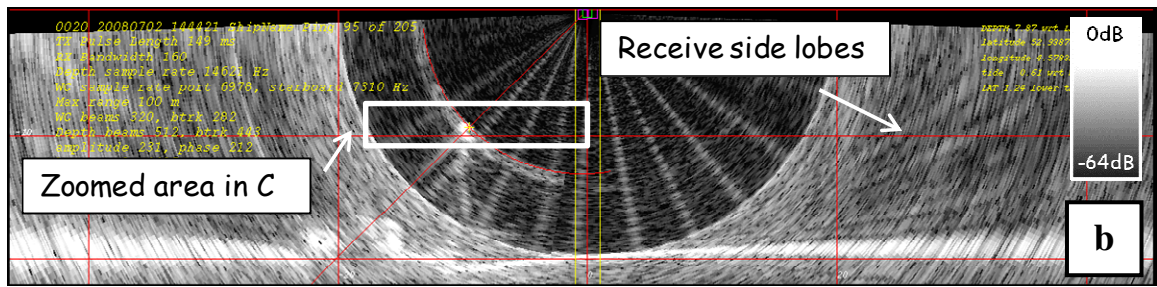
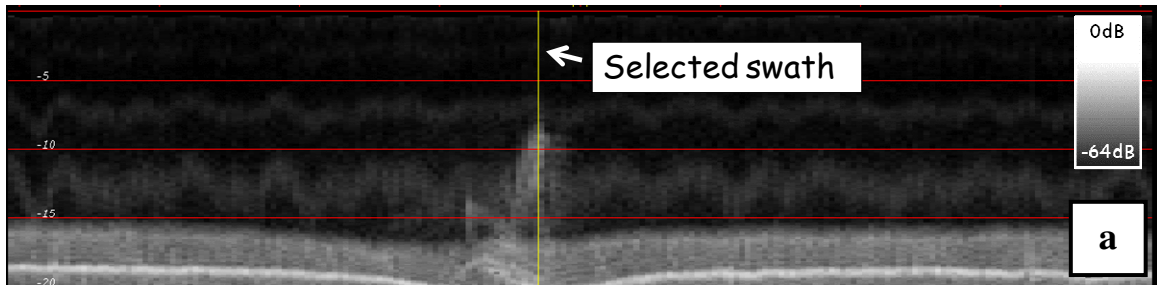


Figure 6.39 – Julian day 184, survey 4, line 0020 - (a) vertical profile, (b) polar plot with real data, (c) polar plot zoom, (d) common-range plot, (e) fixed angle time-series plot.



#### 6.4.10 Results

The difference between the previous survey (JD184 #3) and this survey (JD184 #4), is that a bigger angular sector is used. Therefore, there is extra possible search space within the MSR. However, even though echoes beyond the MSR were logged, only the swaths where the mast was located within the MSR were analyzed. Table 6.2 the depth and position results for this survey are given, where the depth is the depth referenced to RP, and the reduced depth is the depth reduced for tide to LAT. Positions are recalculated from latitude and longitude to easting and northing. The difference between the minimum and maximum depth is 0.27 metre, and the standard deviation is 0.08 metre. The pulse length used was set to automatic for this survey, but from analysis it was concluded that a pulse length of 150 ms was used, which results in a range resolution of ~10 cm. That means that the least depth point is chosen within 3 times the range resolution.

julian day	survey	line	ping	reduced depth	easting	northing	quality
184	4	3	102	7.63	606071.15	5866624.12	L – 0.53
184	4	4	176	7.53	606069.15	5866623.63	L – 0.39
184	4	6	156	7.46	606068.15	5866623.28	H – 0.11
184	4	7	109	7.54	606069.88	5866624.09	H – 0.19
184	4	8	156	7.54	606067.73	5866623.82	M – 0.35
184	4	15	106	7.73	606069.45	5866621.97	L – 0.56
184	4	17	59	7.52	606069.17	5866622.52	M – 0.20
184	4	18	124	7.49	606068.53	5866624.17	H – 0.15
184	4	20	95	7.51	606068.30	5866625.62	M – 0.33
<b>average</b>				7.55	606069.06	5866623.69	
<b>standard deviation</b>				0.08	1.04	1.05	

**Table 6.2 – Depth and position results of Julian Day 184 survey 4.**

## 6.5 Julian Day 196, survey 1

In this last case, the angular sector was set to  $\pm 95^\circ$ . That means that the angular sector was even wider than that of the previous survey, and recorded the whole water column up to the water line. The following lines with the mast within the MSR were analyzed. The direction of each line is shown with a black arrow towards the line number in Figure 6.40. Note that the top of the mast was detected from different directions. Throughout this particular survey the pulse length was set to  $0.05 \mu\text{s}$  and the bandwidth was set to 8 kHz.

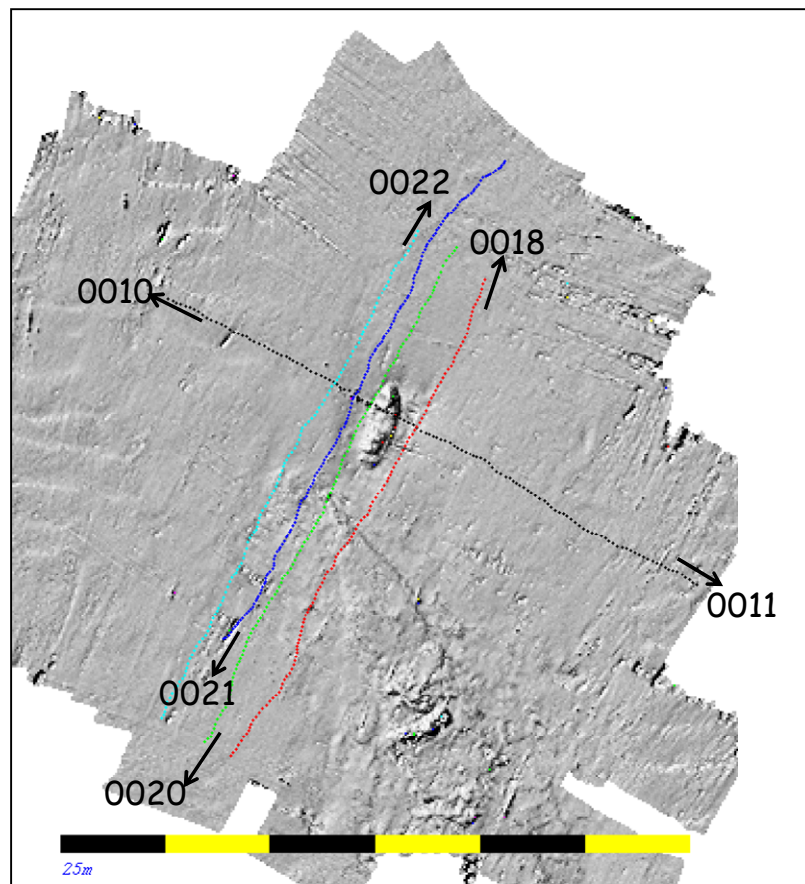
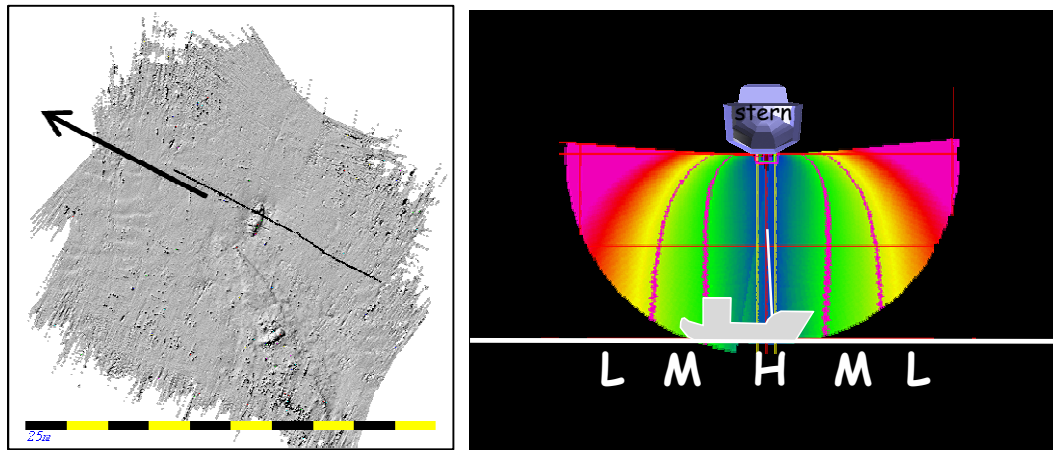


Figure 6.40 - Digital terrain model of the data collected in survey 1 on Julian Day 196.

### 6.5.1 Line 0010



**Figure 6.41 - Map with position and orientation (left), image with IGQF (right) for Julian day 196, survey 1, line number 0010**

In this case the survey line lies orthogonal to the long axis of the wreck, and is sailed from starboard to port directly over the wreck (Figure 6.41). The viewer is looking at the bow of the wreck in the vertical profile (Figure 6.42 (a)). Because the top of the mast is located at nadir, echoes are received on both heads due to the overlap (Figure 6.42 (d)). The echo in the starboard head is strongest and therefore this head is used for analysis. Why the top of the mast is not measured in the same beam angle for both heads in the common-range plot is explained in §4.3.2. In the fixed angle time-series plot of the selected beam the top of the mast is represented as the high amplitude backscatter with the closest range. But there are more echoes from lower on the mast. Enough energy makes it past the mast to return a bottom tracking solution from the hull of the wreck. The reduced depth is measured at 7.32 m at latitude 52.938767° N and longitude 4.578341° E.

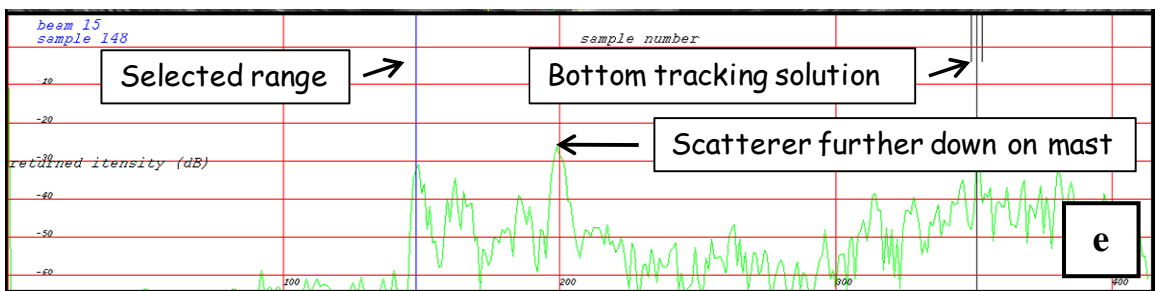
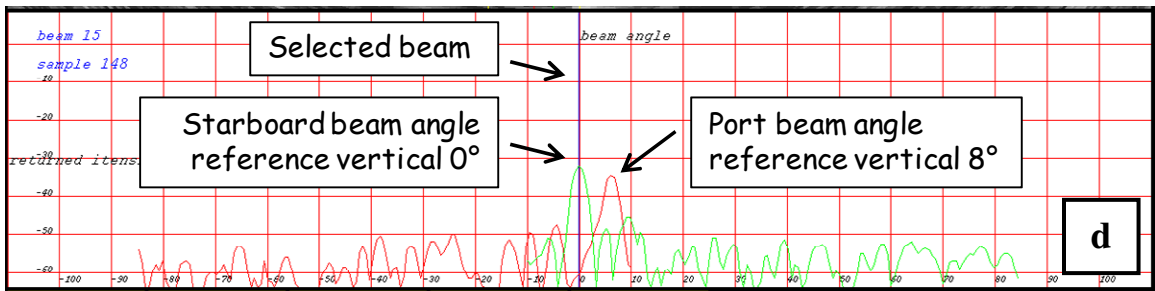
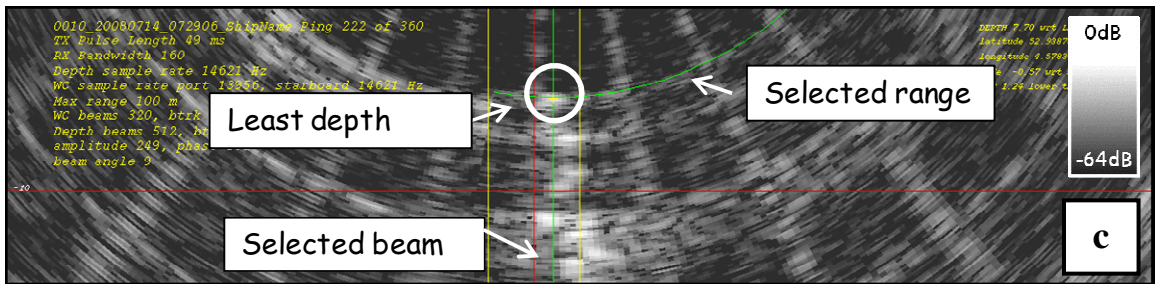
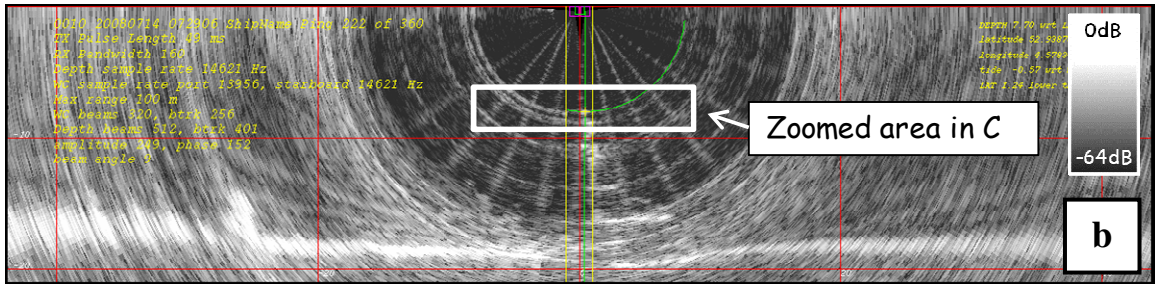
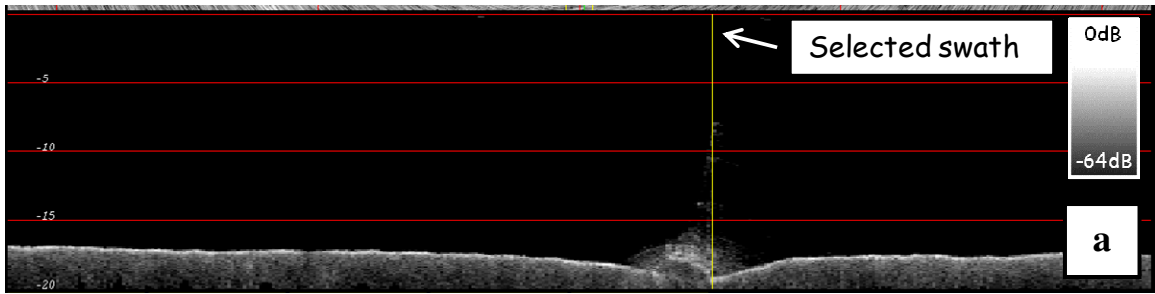
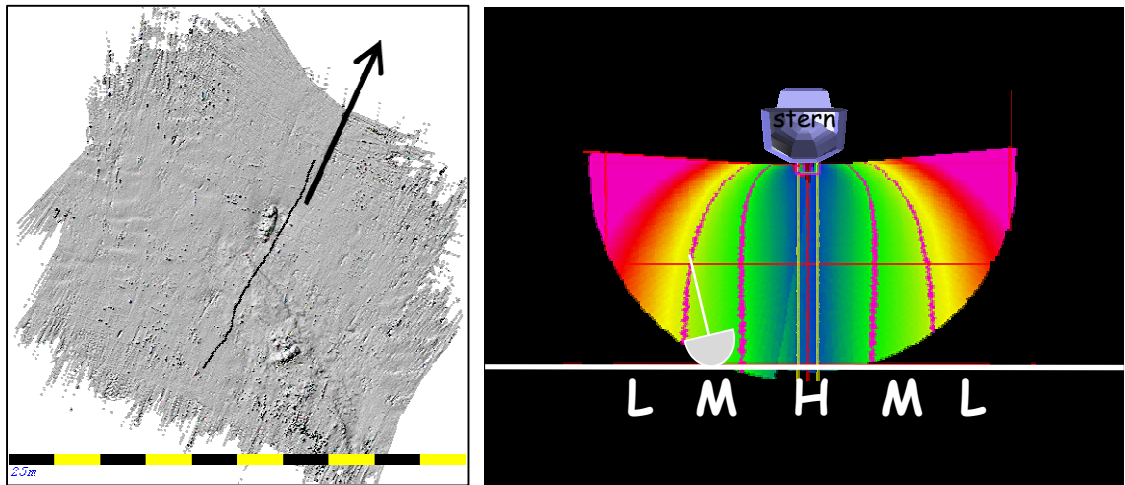


Figure 6.42 – Julian day 196, survey 1, line 0010 - (a) vertical profile, (b) polar plot with real data, (c) polar plot zoom, (d) common-range plot, (e) fixed angle time-series plot.

### 6.5.2 Line 0018



**Figure 6.43 - Map with position and orientation (left), image with IGQF (right) for Julian day 196, survey 1, line number 0018**

In this case the survey line lies along the long axis of the wreck, and is sailed from stern to bow on the starboard side of the wreck (Figure 6.43). The top of the mast is lying off the alignment of one band of the digitizer noise. Because a lot of echoes closely spaced in time are produced along the length of the mast (the orientation of the mast is almost orthogonal to the direction of the receive beams) it is tricky to pick the angle of the shallowest point (Figure 6.44 (b), Figure 6.44 (d)). Enough energy makes it past the mast to create a bottom tracking solution on the seafloor (Figure 6.44 (e)).

The reduced depth is measured at 7.40 m, at latitude 52.938760° N and longitude 4.578367° E.



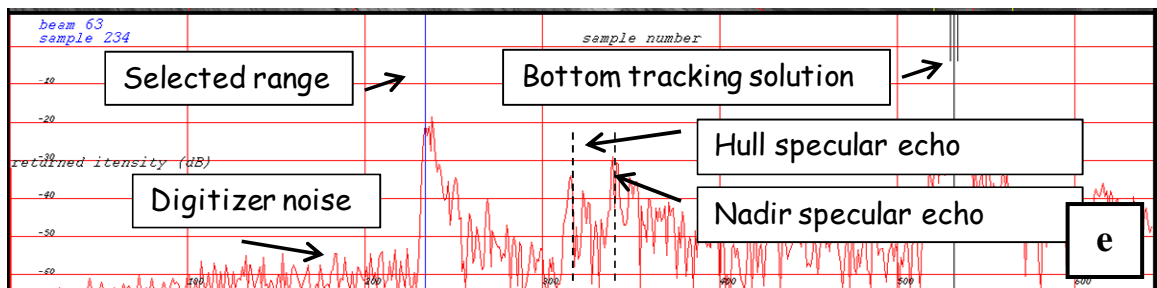
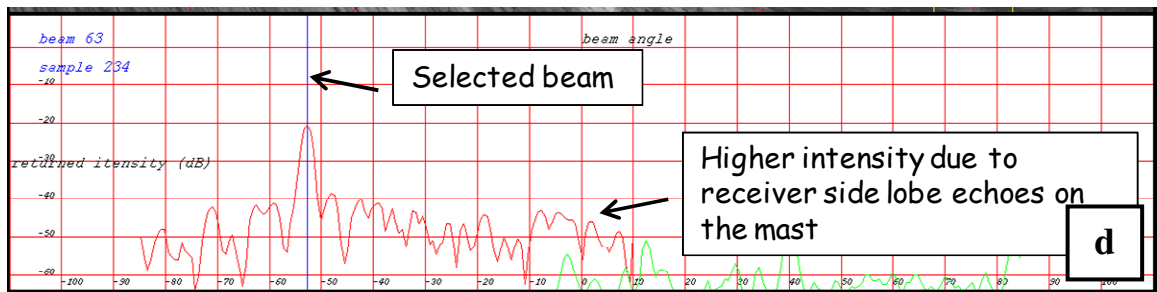
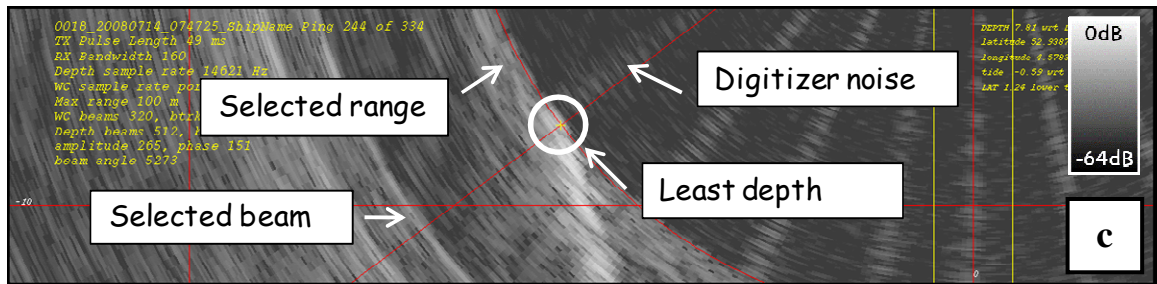
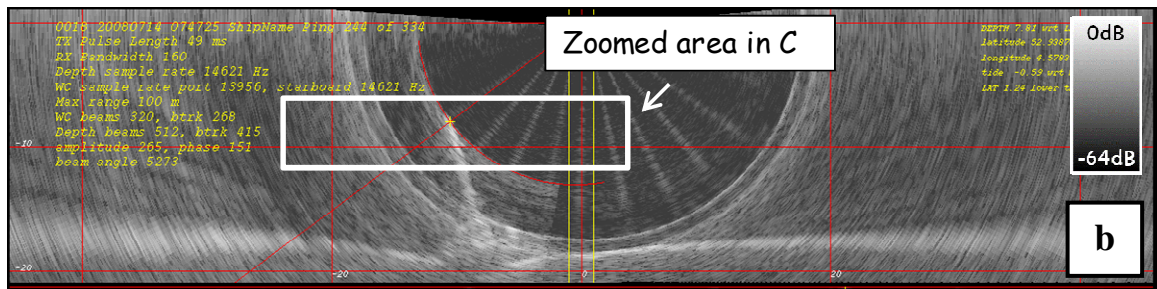
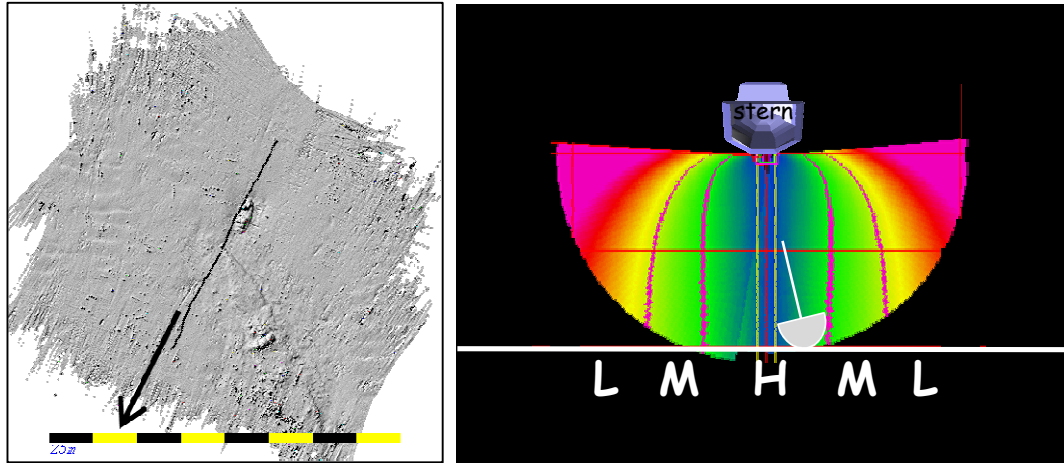


Figure 6.44 – Julian day 196, survey 1, line 0018 - (a) vertical profile, (b) polar plot with real data, (c) polar plot zoom, (d) common-range plot, (e) fixed angle time-series plot.

### 6.5.3 Line 0020



**Figure 6.45 - Map with position and orientation (left), image with IGQF (right) for Julian day 196, survey 1, line number 0020**

In this case the survey line lies along the long axis of the wreck, and is sailed from bow to stern almost directly over the wreck (Figure 6.45). The mast is located close to nadir tilted towards the sonar. Note the specular echo caused by the mast (the second echo from the top), which is picked up much stronger in the port head (Figure 6.46 (b)). The top of the mast can confidently be distinguished from the common-range plot (Figure 6.46 (d)). The fixed angle time-series plot of the selected beam shows clearly the minimum range to the echo of the top of the mast, but there is also an echo lower on the mast where the bottom tracking solutions lock onto (Figure 6.46 (e)).

The reduced depth is measured at 7.37 m, at latitude 52.938755° N and longitude 4.578346° E.

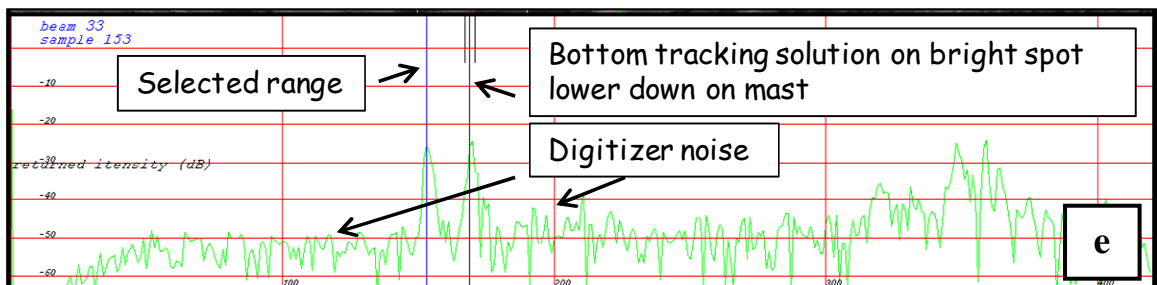
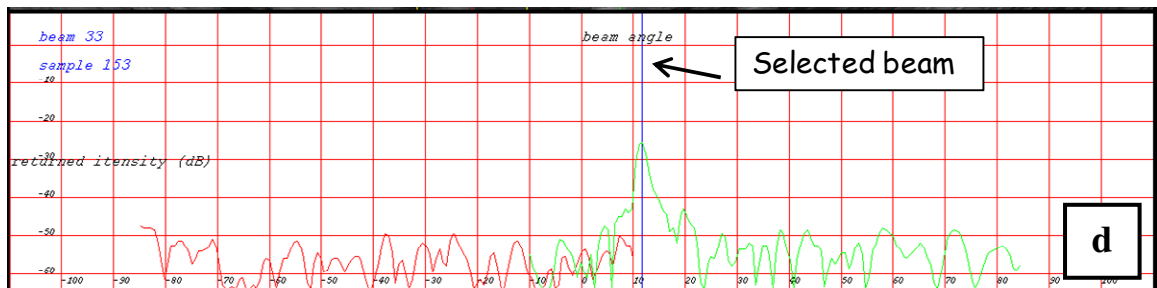
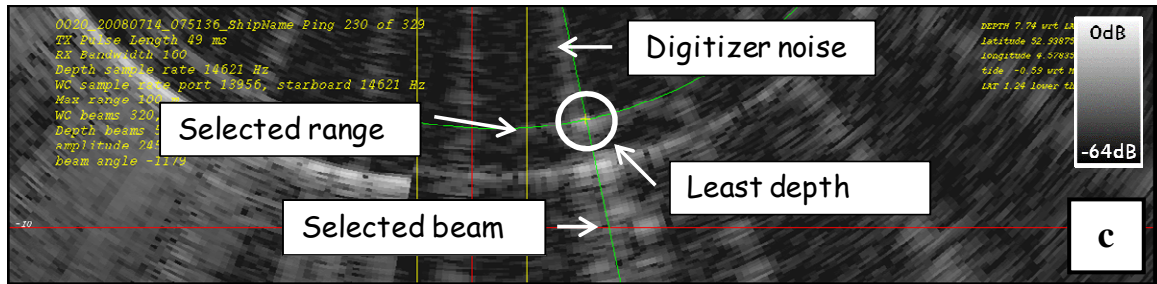
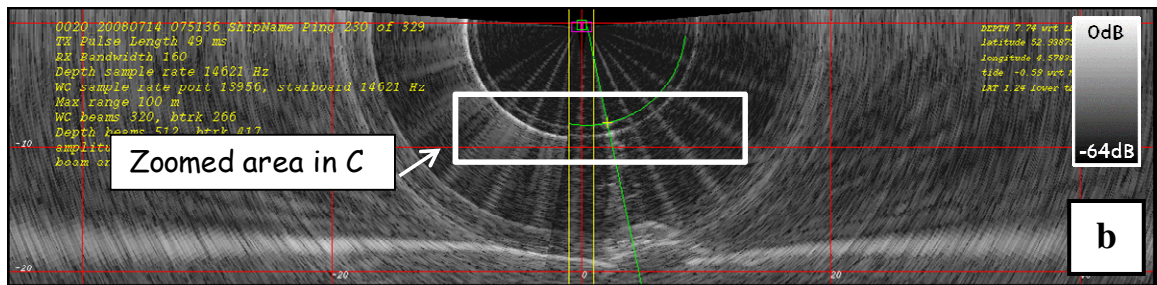
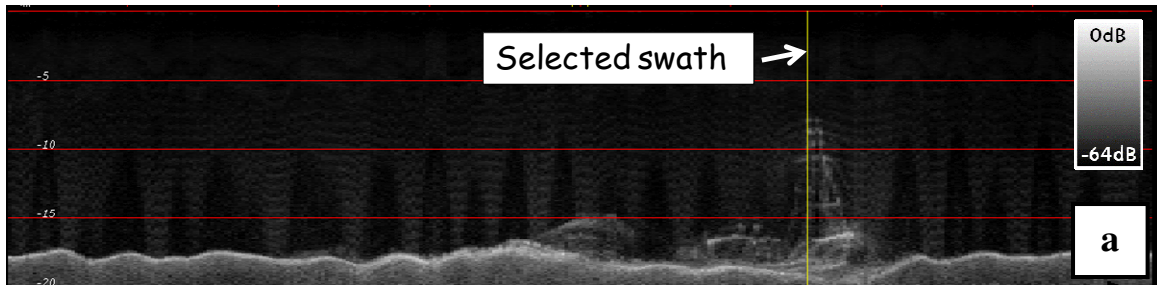
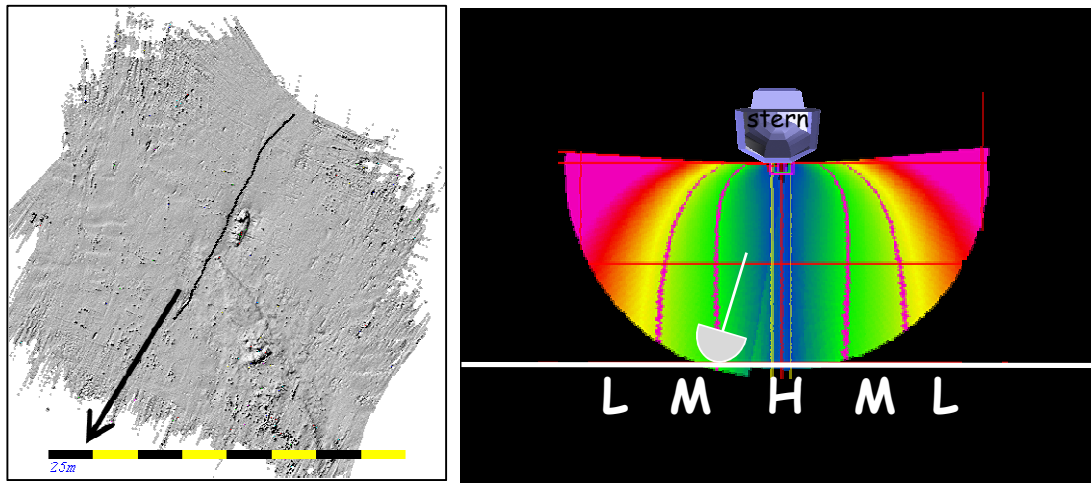


Figure 6.46 – Julian day 196, survey 1, line 0020 - (a) vertical profile, (b) polar plot with real data, (c) polar plot zoom, (d) common-range plot, (e) fixed angle time-series plot.



#### 6.5.4 Line 0021



**Figure 6.47 - Map with position and orientation (left), image with IGQF (right) for Julian day 196, survey 1, line number 0021**

This survey line lies along the long axis of the wreck, and is sailed from bow to stern on the port side of the wreck (Figure 6.47). There are many specular echoes coming from the mast, and the top of the mast is contaminated by digitizer noise (Figure 6.48 (b)(c)). However, the top of the mast returns a stronger echo than the side-lobe echoes or the digitizer noise and therefore can be distinguished (Figure 6.48 (d)). In the fixed angle time-series plot of the selected beam digitizer noise becomes apparent, as well echoes lower from the mast which may be caused by a pulley block or rigging on the mast (Figure 6.48 (e)). Because energy makes it past the mast, a bottom tracking solution is locked onto the hull of the wreck. The reduced depth is measured at 7.43 m, at the latitude 52.938759° N and longitude 4.578317° E.

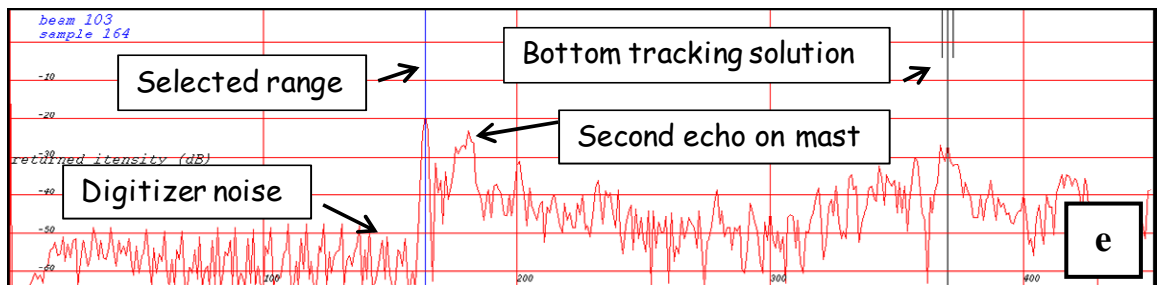
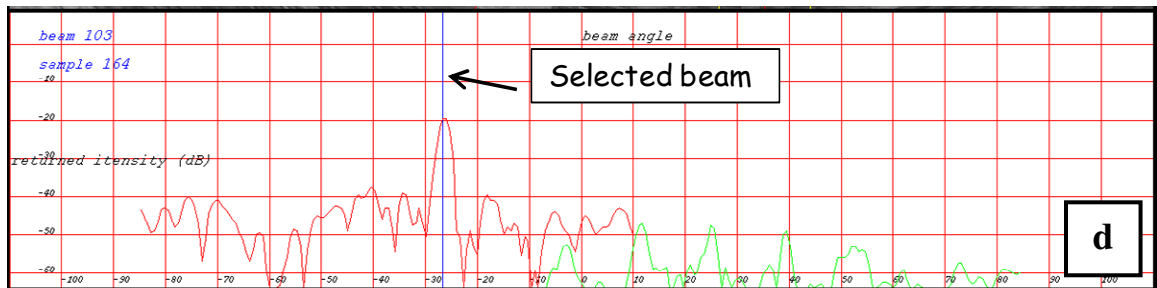
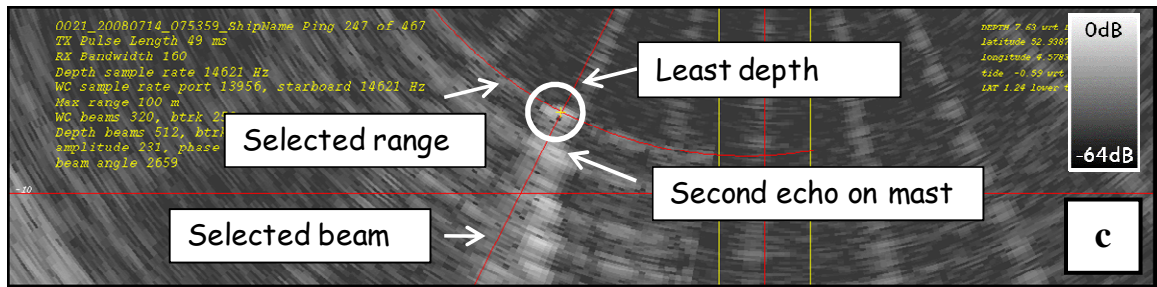
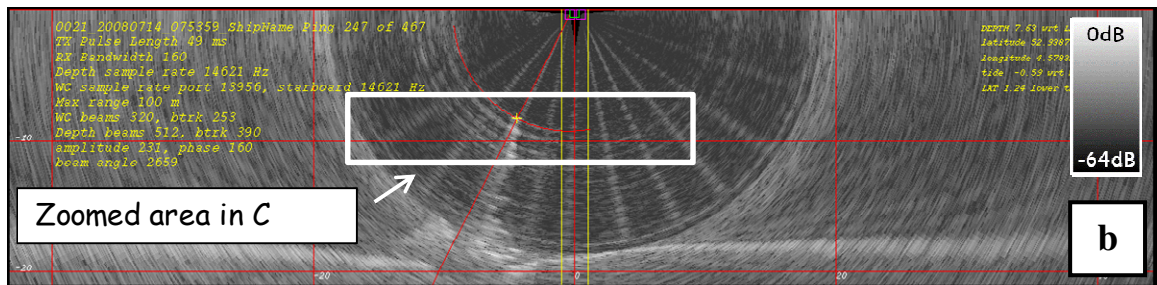
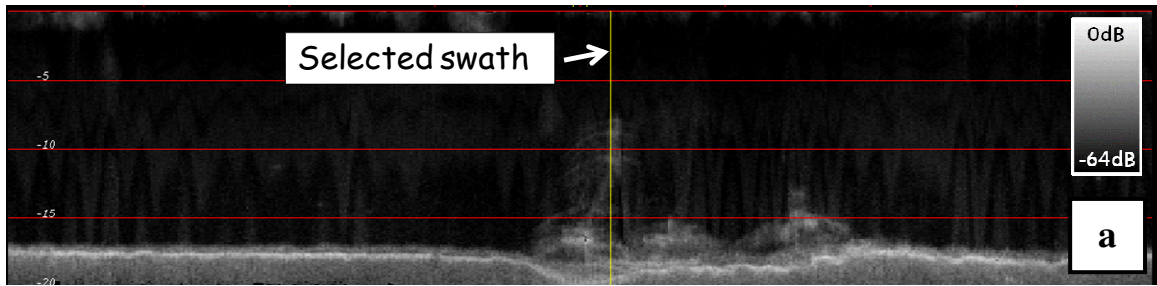
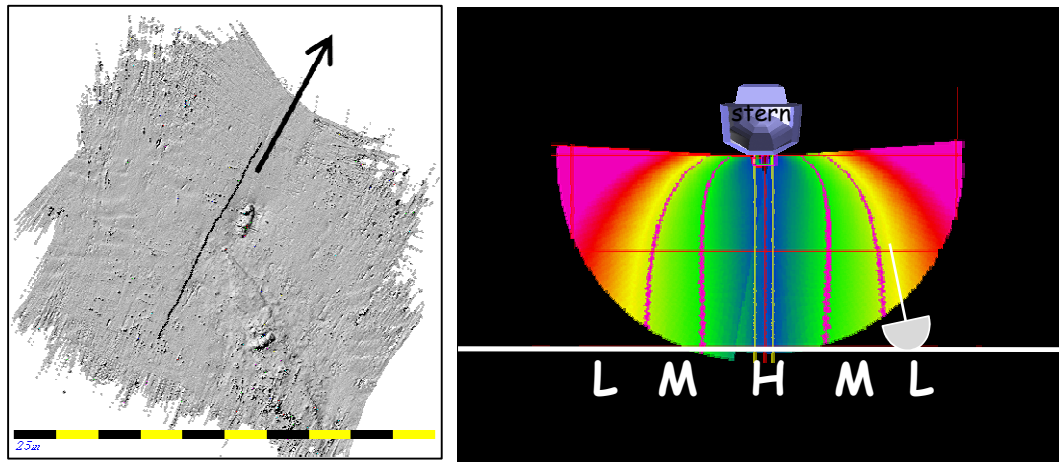


Figure 6.48 – Julian day 196, survey 1, line 0021 - (a) vertical profile, (b) polar plot with real data, (c) polar plot zoom, (d) common-range plot, (e) fixed angle time-series plot.

### 6.5.5 Line 0022



**Figure 6.49 - Map with position and orientation (left), image with IGQF (right) for Julian day 196, survey 1, line number 0022**

This survey line lies along the long axis of the wreck, and is sailed from stern to bow on the port side of the wreck (Figure 6.49). Where the hull of the wreck is lying outside the MSR, the top of the mast is lying inside the MSR due to its orientation to port tilted towards the sonar (Figure 6.50 (b)(c)). The strongest echo from the top of the mast can be selected with help of the common-range profile (Figure 6.50 (d)), where the top of the mast is represented by the strongest backscatter at that range. The selected beam is viewed in the fixed angle time-series plot (Figure 6.50 (e)), where the least depth point has the strongest backscatter at the least range. As almost always, enough energy makes it past the mast to have a bottom tracking solution on the seafloor. The reduced depth is measured at 7.52 m, at latitude 52.938765° N and longitude 4.578348° E.

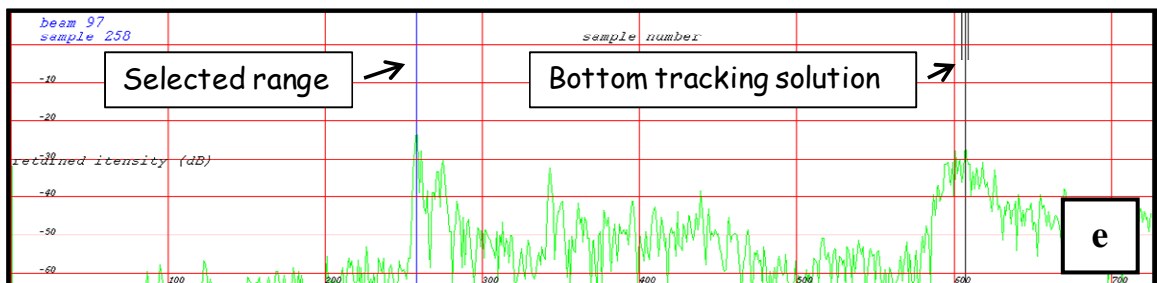
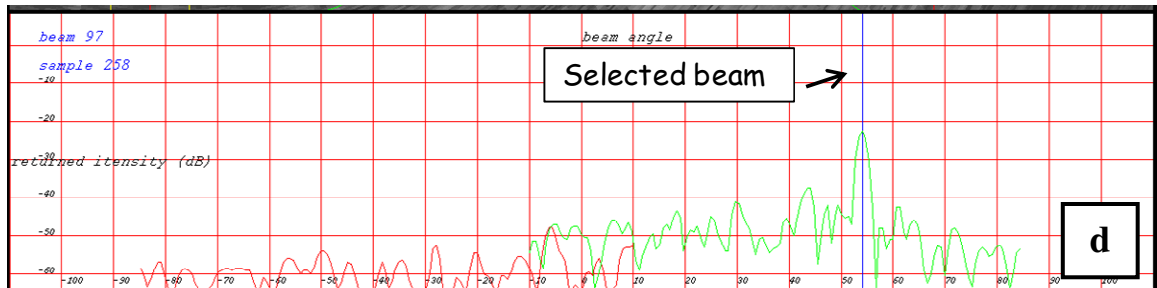
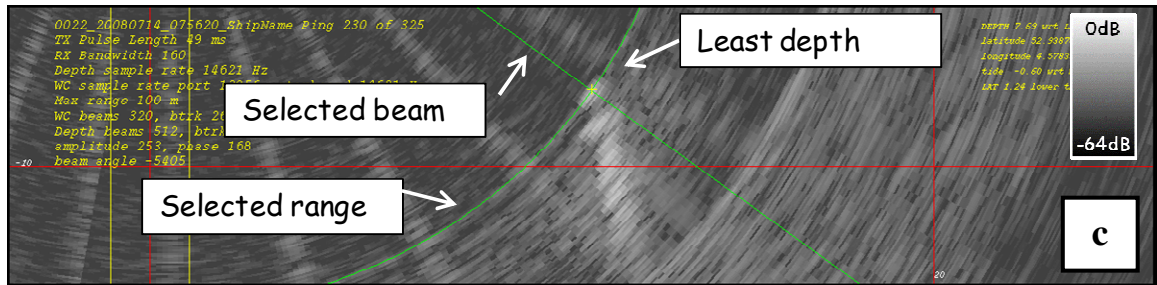
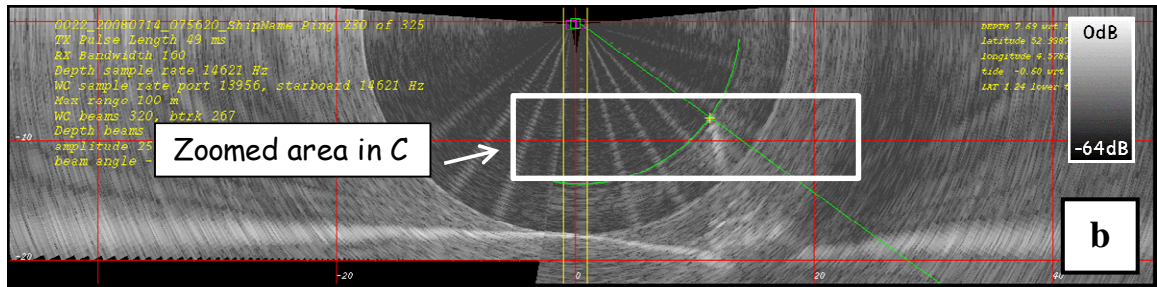
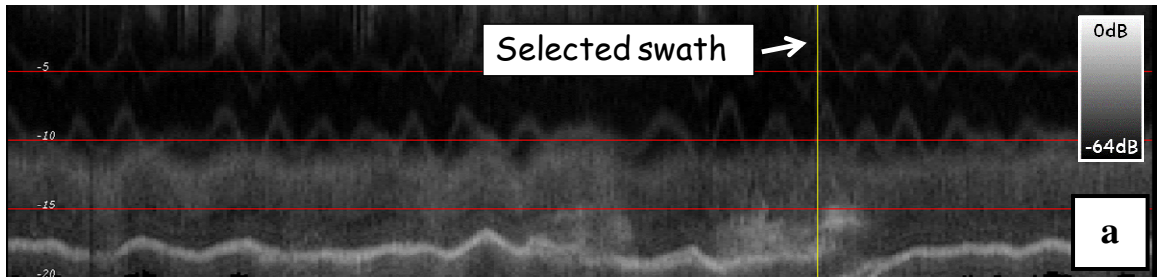


Figure 6.50 – Julian Day 196, survey 1, line 0022 - (a) vertical profile, (b) polar plot with real data, (c) polar plot zoom, (d) common-range plot, (e) fixed angle time-series plot.

### 6.5.6 Results

This survey used the biggest angular sector. In Table 6.3 the depth and position results for this particular survey are given. Positions are recalculated from latitude and longitude to easting and northing. The difference between the minimum and maximum selected depth is 0.15 metre. The standard deviation is 0.07 metre. The pulse length used was set to 50  $\mu$ s for this survey which corresponds with a range resolution of ~5 cm. That means that the least depth point is chosen 3 times the range resolution.

julian day	survey	line	ping		reduced depth	Easting	northing	quality
196	1	10	222		7.32	606069.19	5866624.86	H – 0.05
196	1	18	244		7.4	606070.95	5866624.12	M – 0.34
196	1	20	230		7.37	606069.55	5866623.53	H – 0.09
196	1	21	246		7.43	606067.59	5866623.93	H – 0.14
196	1	22	230		7.52	606069.66	5866624.64	L – 0.35
<b>average</b>					7.41	606069.39	5866624.22	
<b>standard deviation</b>					0.07	1.21	0.54	

**Table 6.3 – Depth and position results of survey 1 on Julian day 196.**

## 6.6 Results

After the analysis the results were compared to the Special Order standard from the International Hydrographic Organization (IHO, 2008), both for the vertical and for the horizontal. In total 20 solutions were calculated over the three surveys. Even though from a statistical point of view the populations are small, it is not (practical) realistic to have greater populations. Next to the uncertainty caused by the equipment and the tide, a source of uncertainty is the choice of selection by the operator.

### 6.6.1 Vertical

The solutions are reduced for tide and heave to Chart Datum, therefore, they might be prone to (unknown) uncertainty caused by vessel loading, squat and heave errors. However, the results give a representation of how consistent the results are, and can be compared to the maximum allowable vertical uncertainty (TVU) as described by the IHO. The TVU is calculated by (IHO, 2008):

$$\sqrt{a^2 + (b * d)^2} \tag{6.1}$$

Where a is the portion of uncertainty which does not vary with depth, and is 0.25 metres for the special order. Where b is the coefficient which represents the portion of uncertainty which varies with depth, and is 0.0075 for the special order. Where d

represents the depth, and the minimum reduced depth for the mast is used herein, which will return the smallest allowable total vertical uncertainty. The difference between the maximum measured depth and minimum measured depth is 46 centimetres; however, this is between the different surveys.

### **Selected by survey**

From Table 6.4 and Figure 6.51 one can see that the standard deviation for the first survey (JD184 #3) is 0.07 metres and is smaller than for the second survey (JD184 #4) 0.082 metres, and for the third survey ( JD196 #1) 0.075 metres. Because JD184 #3 uses a small angular sector, and JD 196 #1 uses a big angular sector, the width of the angular sector seems not to influence the results. JD184 #3 and JD184 #4 use a longer pulse length than JD196 #1 and thus the pulse length seems not to influence the results as well. The tidal difference is larger in JD184 #3 (1 m) than in JD184 #4 and JD196 #1 (~0.1 m); therefore, it is more likely to have a greater uncertainty caused by tides in JD184 #3; however, from the results one can see that JD184 #3 has the smallest standard deviation.

### **Selected by Quality Factor**

The Quality Factor can be calculated for each solution, which is the accuracy for each estimate. So for estimates with a high quality the accuracy is better than for estimates with a low quality. The standard deviation for measurements with a High IGQF is 0.068 metres, for measurements with a Moderate IGQF is 0.094 metres and for measurements with a Low IGQF 0.098 metres (Table 6.5). Regardless of the utilized angular sector and/or pulse length, or tidal influence, measurements with a High IGQF seem to be more accurate and shallower (Figure 6.52). Measurements with a Low IGQF, and thus a larger

incidence angle, have a larger standard deviation, and are located deeper. Measurements with a Moderate IGQF are located in between the two. From Table 6.4 and Table 6.5 one can see that the standard deviation is within the required total vertical uncertainty, this would mean that the IHO special order is met for the vertical in all surveys.



TOTAL VERTICAL UNCERTAINTY					
		JD184_3	JD184_4	JD196_1	
# passes		6	9	5	
angular sector		65	85	95	(+/-°)
pulse length (μs)		0.15	0.15	0.05	μs
tidal difference (m)		~1	<0.1	~0.1	metres
minimum depth of the mast		7.27	7.46	7.32	metres
standard deviation		0.070	0.082	0.075	metres
TVU 95% confidence level		0.138	0.160	0.146	metres
maximum allowable TVU		0.256	0.256	0.256	metres

Table 6.4 – The standard deviation, special order TVU at 95% confidence level and the maximum allowable TVU selected by survey.

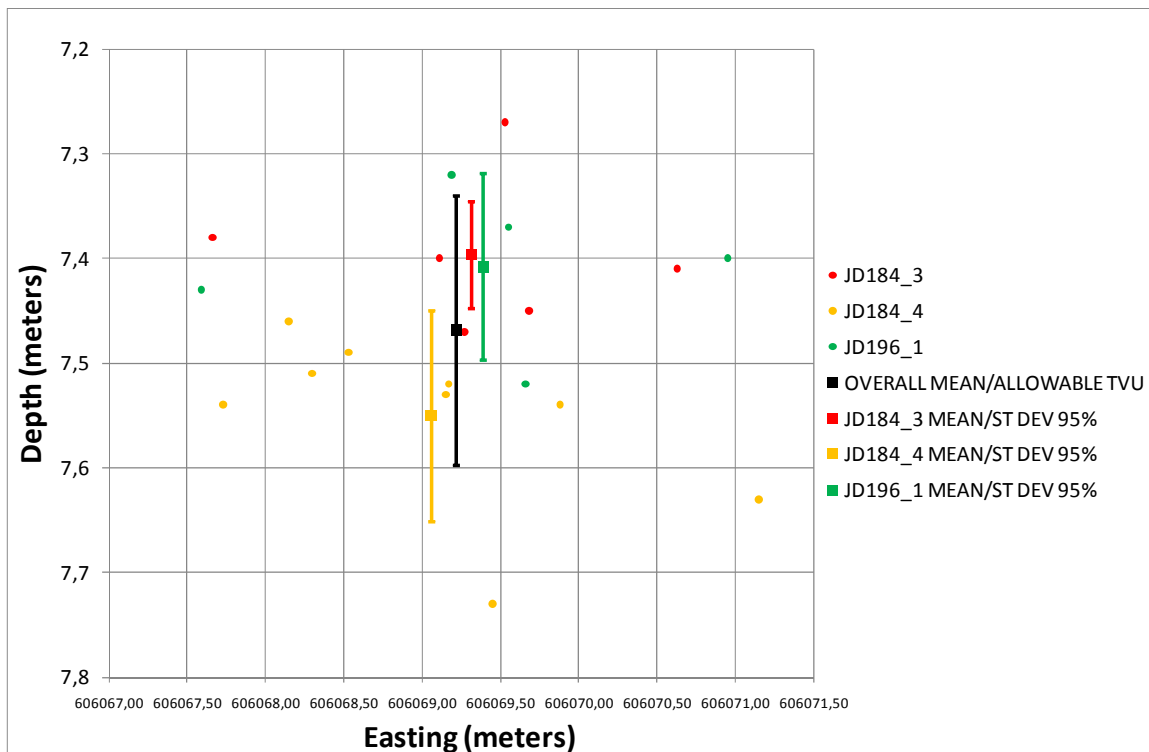


Figure 6.51 – Depth results selected by survey (i.e. by angular sector and pulse length).

TOTAL VERTICAL UNCERTAINTY				
	High	Moderate	Low	
# passes	9	7	4	
minimum depth of the mast	7.32	7.27	7.52	metres
standard deviation	0.068	0.094	0.098	metres
TVU 95% confidence level	0.134	0.184	0.193	metres
maximum allowable TVU	0.256	0.256	0.256	metres

Table 6.5 - The standard deviation, special order TVU at 95% confidence level and the maximum allowable TVU selected by Quality Factor.

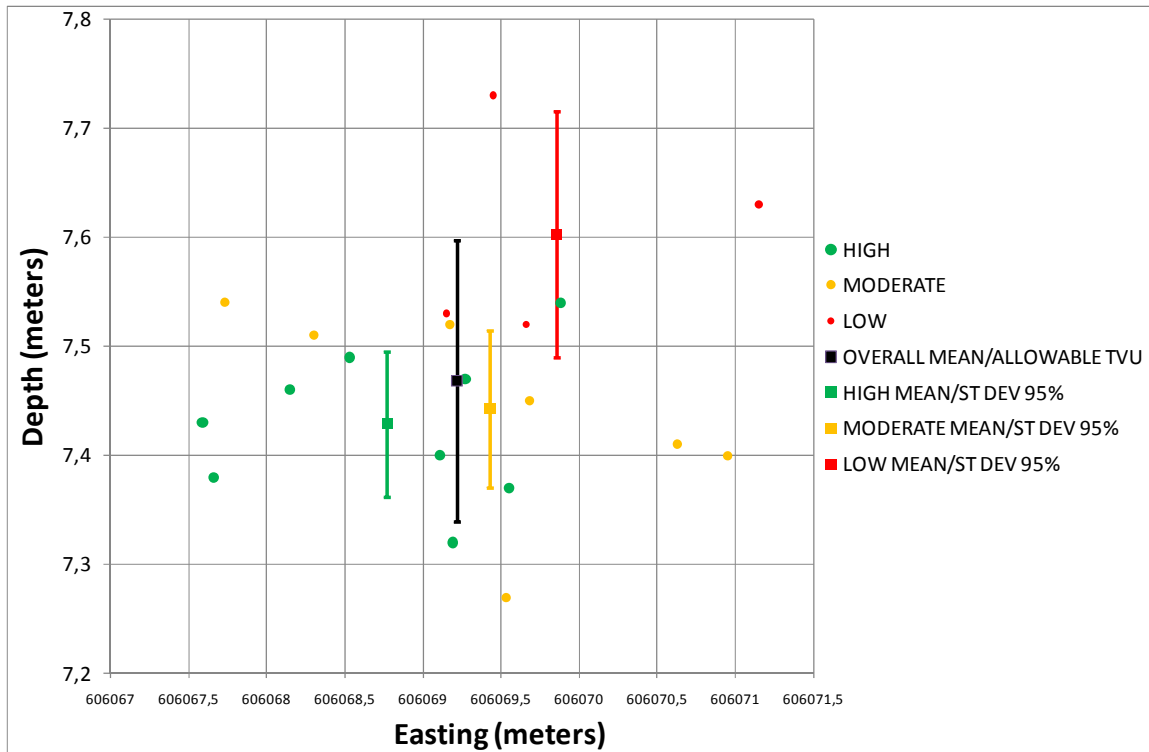


Figure 6.52 – Depth results selected by Quality Factor.

## 6.6.2 Horizontal

Positions were recalculated from latitude and longitude to UTM (Universal transverse Mercator) (with PC trans 4.2.6. free software from the Hydrographic Service of the Dutch Navy). The horizontal uncertainty exceeds the maximum allowable horizontal THU of the IHO special order, which is 2 metres. The horizontal uncertainty is, however, not influenced by survey or by quality factor. For positioning Long Range Kinematic (LRK) was used. During the trials not always centimeter level accuracy positioning was received. Therefore, the positioning results may be prone to error, which may explain the uncertainty in the position of the results. Another reason may be: In most examples the mast is illuminated in more swaths due to the transmit side lobes. The shallowest measurement is theoretically in the main lobe, and used as the "real" depth of the mast. Because of the ping period and the speed there is a distance up to 1 meter between pings (angular sector of  $\pm 95^\circ$ ). So considering that the pings are not at the same position for each line, the choice of the ping could cause horizontal uncertainty.

TOTAL HORIZONTAL UNCERTAINTY									
			JD184_3		JD184_4		JD196_1		
			easting	northing	easting	northing	easting	northing	
<b>standard deviation</b>			0.969	0.815	1.041	1.050	1.205	0.538	metres
<b>THU 95% confidence level</b>			2.373	1.996	2.550	2.572	2.953	1.317	metres
<b>maximum allowable THU</b>			2	2	2	2	2	2	metres

Table 6.6 - The standard deviation, special order THU at 95% confidence level and the maximum allowable THU selected by survey.

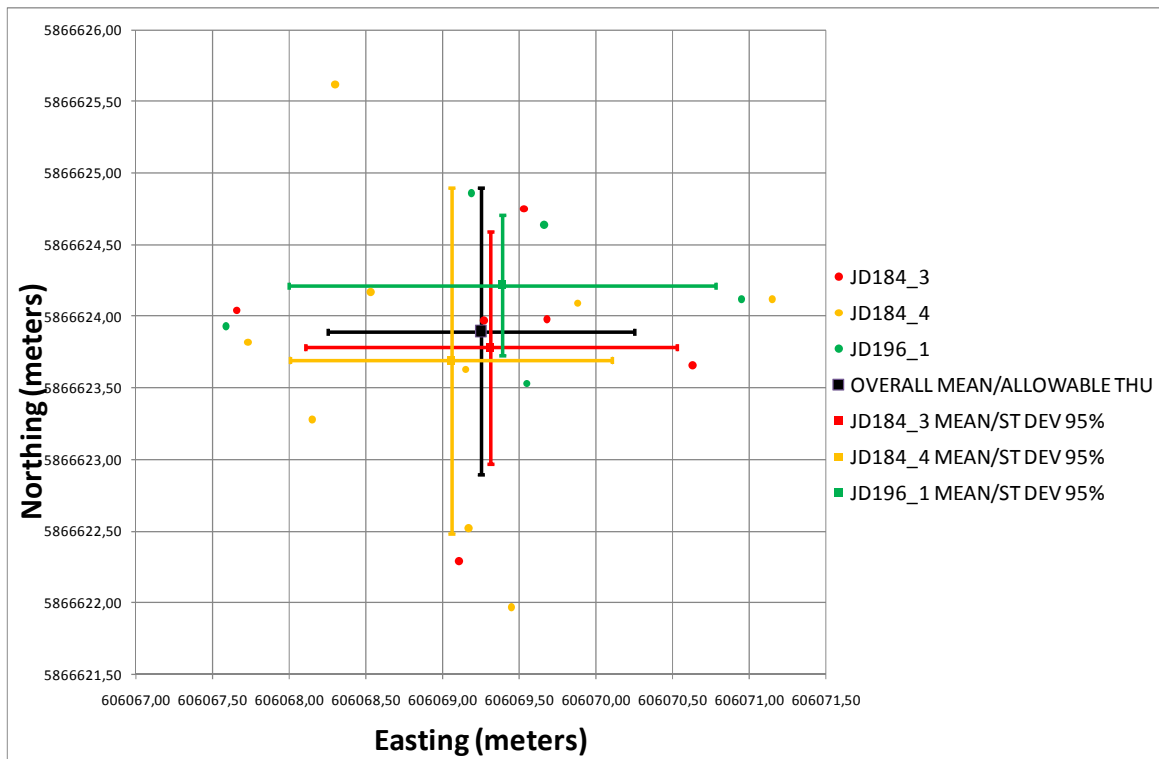


Figure 6.53 – Graph of the final positions in Northing and Easting selected by survey.

TOTAL HORIZONTAL UNCERTAINTY									
			High		Moderate		Low		
			easting	northing	easting	northing	easting	northing	
standard deviation			0.825	0.713	1.159	0.958	0.890	1.156	metres
THU 95% confidence level			2.022	1.748	2.839	2.348	2.180	2.832	metres
maximum allowable THU			2	2	2	2	2	2	metres

Table 6.7 - The standard deviation, special order THU at 95% confidence level and the maximum allowable THU selected by Quality Factor.

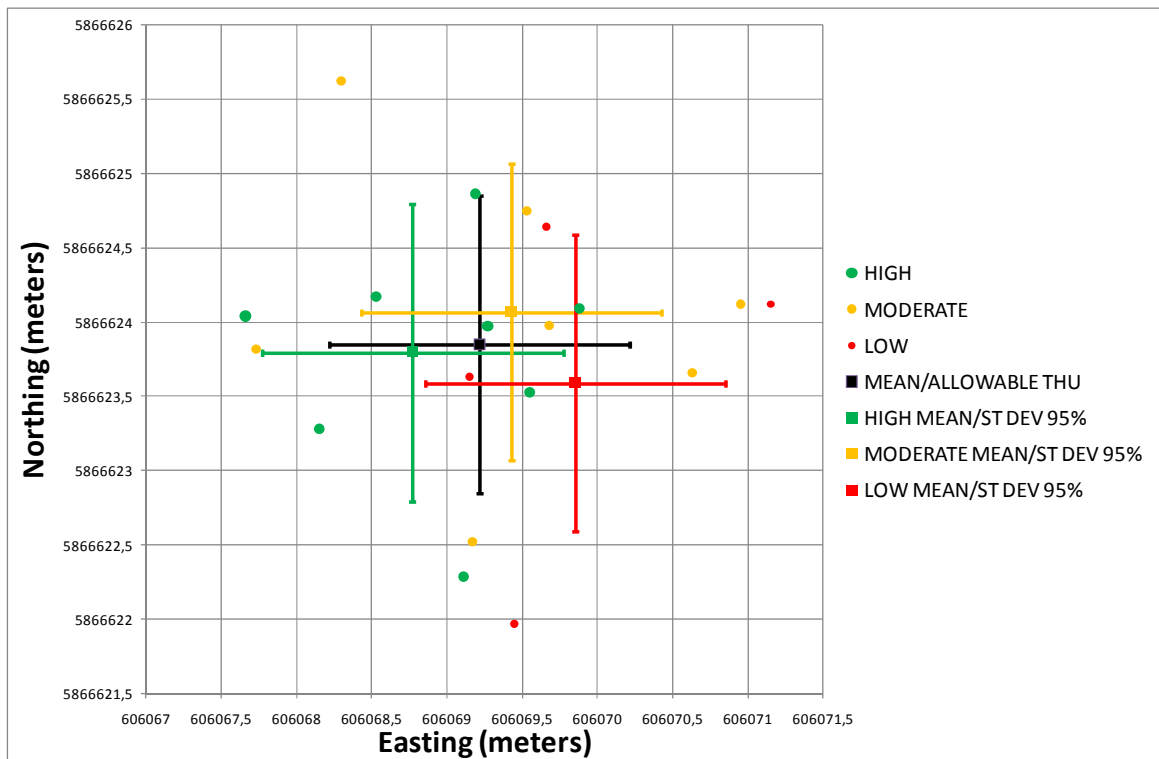
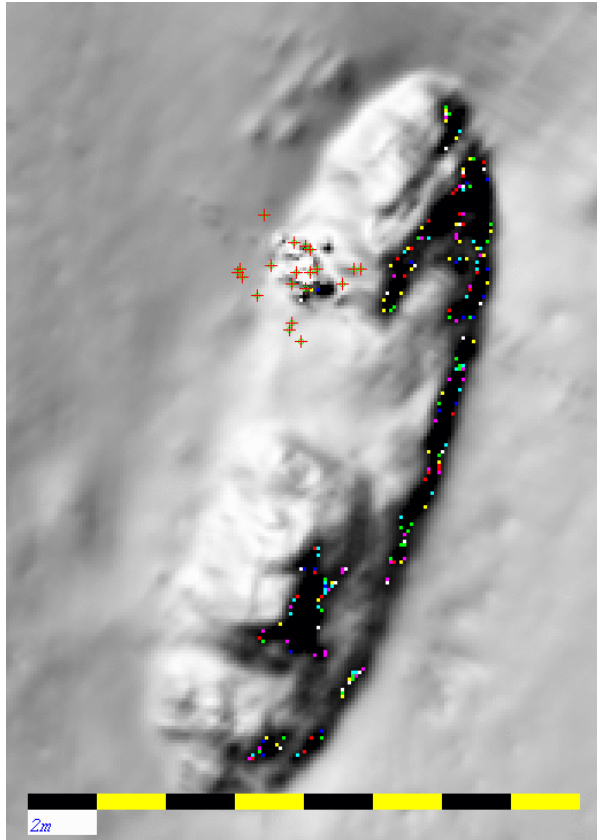


Figure 6.54 - Graph of the final positions in Northing and Easting selected by Quality Factor.



**Figure 6.55 – The positions of the final solutions plotted on top of a DTM of the wreck.**

## 7 CONCLUSIONS AND RECOMMENDATIONS

### 7.1 Conclusions

The Dutch Navy requires information and recommendations on acquiring and calculating the least depth of a mast-like object above a wreck with Water Column Imaging (WCI). Multibeam WCI is a method which has the capability to record backscatter in the water column. Raw backscatter is recorded throughout full time-series for each physical receive beam.

Data has been acquired with the Dutch Navy over a wreck on the Dutch continental shelf in ~20 meters of water (these depths are of most interest for navigational hydrography). The Dutch Navy uses Kongsberg EM3002 dual head multi-beams which are capable of logging water column imaging data. A particular advantage of the EM3002 dual head is that it can image out to the horizontal.

Feature detection is primarily controlled by range resolution, beam widths (angular resolution), side-lobe suppression and noise levels. Any small and strong scattering target on the wreck will generate a scattered intensity field that reflects the side-lobe patterns of the transmit–receive product. Inside the minimum slant range the echo can be contaminated by digitizer noise. Outside the minimum slant range it is harder to subjectively pick out the mast top through the broader beam widths and the presence of side-lobe contributions from the inboard seafloor. Therefore, the top of the mast is best viewed within the minimum slant range. To subjectively choose a point in the image, the hydrographer needs to obtain background knowledge about those anomalies. It is

demonstrated that a trained hydrographer can visually infer the true shallowest point on a mast within the minimum slant range. 20 solutions were obtained in this manner and they agree to be better than IHO Special Order vertical accuracy requirements.

The advantage of WCI is that a trained hydrographer can infer the true shallowest point on a mast more confidently from the water column image than from the real time bottom detections. The water column image can be used as a quality control for the bottom detection data. With the context of the water column image the hydrographer is able to make decisions about apparently spurious, solitary and discontinuous series of soundings in the vicinity of suspected wrecks, which provides the confidence that the shallowest sounding has been ascertained over a wreck.

The aim of this research is to use WCI directly for wreck least depth determination. Therefore the selected pixel in WCI is transformed to depths in the geographic frame, which gives a greater ability to estimate the minimum clearance over wrecks, possibly to the extent of eliminating the requirement to bar-sweep the wreck.

A tool has been developed in Swathed to implement a method which could replace bar-sweeping. Digital terrain models and vertical profiles are used to select the data around the object thereby minimizing the processing time. The most likely echo candidate in the imaging space can be determined through operator selection. The problem is that the features are ambiguous (otherwise bottom detection would have succeeded in the first instance). Object detection algorithms are often too simplistic (e.g. strongest echo), ad-hoc methods that break down in more complicated situations such as among the many scattering targets in the rigging. Therefore, the least depth is determined



on a subjective basis but using knowledge of the imagery geometry and sonar characteristics. By analyzing backscatter at common ranges and along fixed angle time-series, it is possible to select the top of the mast. A big part of this research was the adoption and implementation of an algorithm in the bar-sweep tool, with which it is possible to transform the whole image, or a selected point to properly referenced depths in the geographic frame with the current information from the water column datagram.

The initial results show that the least depth is measured at 7.27 meter with reference to Chart Datum (which is Lowest Astronomical Tide). This compares to a diver estimate of 7.62 meter to LAT. The standard deviations between depth results are within the specifications of the IHO Special Order. The accuracy depends in part on user selection of optimal imaging geometry; however, it is shown in the examples herein that, with background knowledge, it is possible to use WCI to select the least depth of a wreck well within the IHO Special Order. With care and training reliable least depth determination of anthropogenic targets may be achieved with WCI without resorting to laborious mechanical bar-sweeping or diver methods.

## 7.2 Recommendations

The Dutch Navy should make the upgrade from EM3000 to EM3002 because these systems are capable of logging water column data.

Water column backscatter is only recorded along the physical beams. When surveying in high definition mode, which is the normal and recommended mode of operation of these sonars, the beams in the water column datagram (160 solutions) can currently not be correlated to the beams in the depth datagram and the raw range and beam angle datagram (254 solutions). If additional information were added to the current water column data structure, a depth calculation could be made without assumptions when surveying in high definition mode. A direct ray-trace could be performed from the angles in the depth datagram or a full sounding reduction from the angles in the raw range and beam angle datagram.

For the case where the targets subtend solid angles smaller than the beam width, there is the possibility for multiple solutions per beam (like Lidar). Thus a modified bottom detection algorithm might be considered which allowed for this.

More trials on other wrecks should be performed. The solutions should preferably be compared with solutions determined by conventional methods like a mechanical bar-sweep or divers. Recommended is to use Long Range Kinematic (LRK) or Real Time Kinematic (RTK) for positioning and vertical reduction. Which gives the opportunity to

reduce the solutions to Chart Datum, and not be prone to (unknown) uncertainty caused by vessel loading, squat and heave.

The Dutch Navy is advised to adopt an operational procedure for practical implementation of WCI. A proposed design for surveys of wreck-like objects is formulated here:

- One has to take into account:
  - Sound speed profiles at the location of the wreck.
  - **Survey speed: < 5 knots.** The survey speed should be kept as slow as possible over the wreck, to maintain the highest along-track density.
  
- Settings have to be adjusted correctly before the survey is started:
  - Static settings which have a considerable amount of influence for a survey with WCI on a wreck:
    - **Beam spacing: Hidens mode**, which results in high definition equiangular beam spacing for the conventional beams (254), and equiangular beam spacing for the physical “water column” beams (160).
    - **Ping rate: 40 Hz.** Should be set as high as possible, if the ping rate is set too low, it will decrease the along-track density. The actual ping rate depends on the angular sector and on the depth.
  - Dynamic settings for depths in water of < 40 meters (IHO Special Order) were concluded and can be summarized as:

- **Angular sector: +/- 95 degrees**, which means the angular sector images out to the horizontal.
  - **Pulse length: 0.05 microseconds**. The shortest pulse length, which uses the highest sampling rate and delivers the best range resolution in the water column image.
  - **Bandwidth: 8 kHz**. The bandwidth controls the range of frequencies used by the receiver, to match the choice of pulse length.
  - **Maximum range:** Depending on the depth. Two times the depth would be sufficient, when not looking outside the MSR. Outside two times the depth range the echo will decay and not be useful for mast detection.
  
- To ensure safety of navigation for the survey vessel, data is first collected in the outer beams outside the minimum slant range to ensure that there is enough water over the wreck and to determine the position and orientation of the wreck and its mast. There is also the possibility there is no mast or there are more masts on a single wreck. Lines are sailed along the location of the wreck moving towards the wreck with each line, until the wreck, and preferably the mast, is visualized just inside the minimum slant range (Figure 7.1).

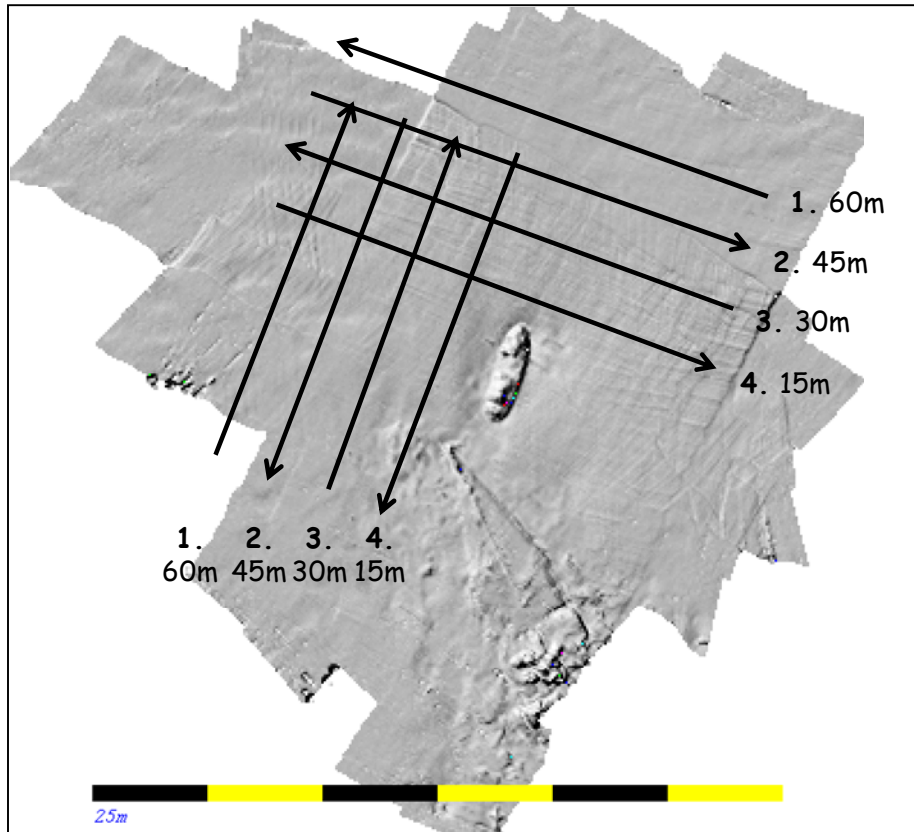


**Figure 7.1 – Survey lines towards the wreck, to reveal the position and orientation of the wreck, and ensure safety of navigation for the survey vessel.**

- Once the exact position and orientation of the wreck and the mast, or number of masts, are determined, and it is safe to pass directly over or close to the wreck, data inside the minimum slant range can be acquired (Figure 7.2). The aim is to collect data within that range from different directions. The lines can be positioned depending on currents, waves and wind. In this example the line spacing is based on a depth of 20 meters. With a depth of 20 meters the minimum slant range is 20 meters, to keep the wreck inside the minimum slant range the lines are sailed no further than 20 meters alongside the wreck.

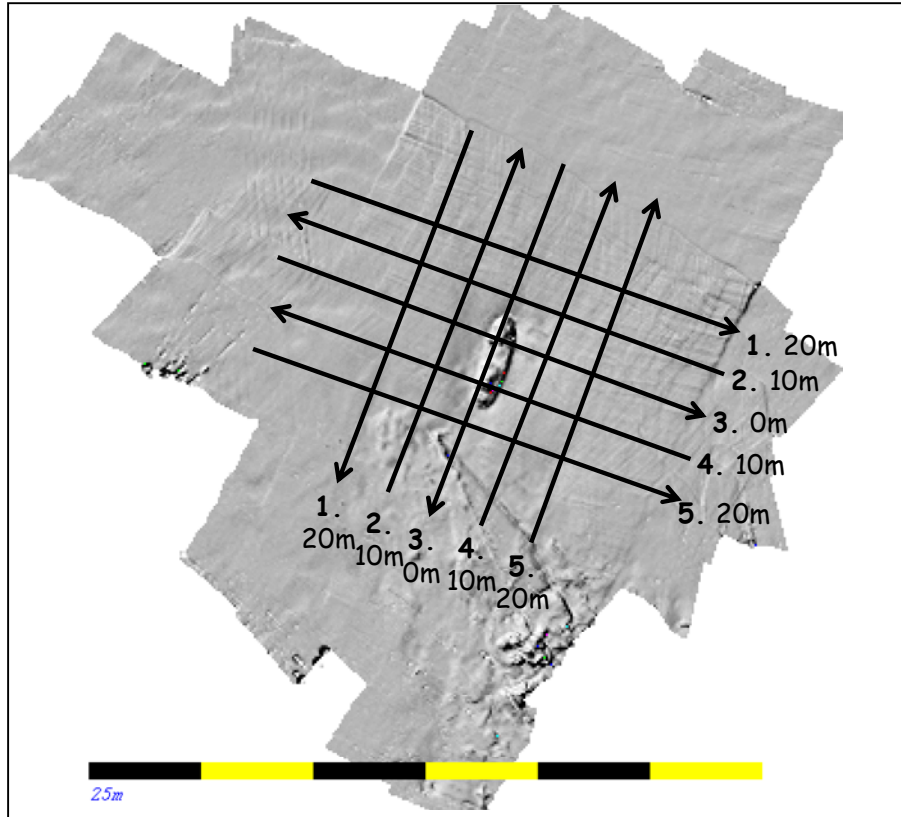


**Figure 7.2 – Survey lines to detect the least depth of the wreck with WCI. Preferably the wreck is measured within minimum slant range, the minimum slant range is the same as the depth. Therefore, in this case, the line spacing is based on a depth of ~20 meters. It is important to survey the wreck from different directions.**

The time for a single survey depends on the number of lines, the size of the wreck, the number of masts, and on the survey vessel. For example because larger ships like the Snellius or the Luymes would take more time to turn than one of the smaller launches. Considering that direct turns should be avoided, not to cause heave artifacts. But even then a survey with sufficient (minimum 10, up to 20) lines could possibly be acquired within significantly less time (~1 hour) than what was needed for a mechanical bar-sweep (up to 6 hours).

## BIBLIOGRAPHY

- Beaudoin, J., Hughes Clarke, J., and Bartlett, J. (2004). "*Application of Surface Sound Speed Measurements in Post-Processing for Multi-Sector Multibeam Echosounders*": International Hydrographic Review, v.5, no.3, p.26-31.
- Beaudoin, J., and Hughes Clarke, J.E.( 2004). "*Retracing (and re-raytracing) Amundsen's Journey through the Northwest Passage*": proceedings of the Canadian Hydrographic Conference 2004, Ottawa, CDROM.
- Buelens, B., Williams, R., Sale, A., and Paulyet, R. (2006). "*Computational challenges in processing and analyzing of full-watercolumn multibeam echo sounder data*". Proceedings of the Eighth European Conference on Underwater Acoustics, 8th ECUA.
- Hammerstad, E. (1995). "*Advanced Multibeam Echosounder Technology*". Sea Technology 36, pp 76-69, 1995.
- Hammerstad, E. (2005). "*Meeting the Challenges of the IHO and LINZ Special Order Object Detection Requirements*". US Hydro 2005.
- Hammerstad, E. (2000). "*Backscattering and seabed image reflectivity.*"  
[http://www.km.kongsberg.com/ks/web/nokbg0397.nsf/AllWeb/226C1AFA658B1343C1256D4E002EC764/\\$file/EM\\_technical\\_note\\_web\\_BackscatteringSeabedImageReflectivity.pdf?OpenElement](http://www.km.kongsberg.com/ks/web/nokbg0397.nsf/AllWeb/226C1AFA658B1343C1256D4E002EC764/$file/EM_technical_note_web_BackscatteringSeabedImageReflectivity.pdf?OpenElement) [on-line] 18-02-2010.
- Hughes Clarke, J.E., Fabre, D., Martinolich, R., Broadus, M., Milner, P., Sargent, E., (2009). "*Assessing target detection capability using single and dual swath sonars with high definition beam forming*". *Femme 2009*, Lisbon, Portugal.

- Hughes Clarke, J.E., Beaudoin, J. (2008). “*GGE 3353 - Imaging and Mapping II : Submarine Acoustic Imaging Methods*”. Course Lectures University of New Brunswick – Department of Geodesy and Geomatics Engineering.
- Hughes Clarke, J.E. (2006a). “*Applications of Multibeam Water Column Imaging for Hydrographic Survey*”: The Hydrographic Journal, April Issue.
- Hughes Clarke, J.E., Brucker, S. and Czotter, K. (2006b). “*Improved Definition of Wreck Superstructure using Multibeam Water Column Imaging*”: Lighthouse, Journal of the Canadian Hydrographic Association, Edition No. 68.
- Hughes Clarke, J.E., Lamplugh, M. and Czotter, K. (2006c). “*Multibeam Water Column Imaging: Improved Wreck Least-Depth Determination*”: Proceedings, Canadian Hydrographic Conference 2006.
- IHO, International Hydrographic Bureau, Monaco (2005) “*Manual on Hydrography (1<sup>st</sup> edition)*”  
[http://www.iho.shom.fr/PUBLICATIONS/IHO\\_Download.htm#M-13](http://www.iho.shom.fr/PUBLICATIONS/IHO_Download.htm#M-13), [on-line] 21-05-2009.
- IHO, International Hydrographic Bureau, Monaco (2008) “*IHO Standards for Hydrographic Surveys (5<sup>th</sup> edition)*”  
[http://www.iho.shom.fr/PUBLICATIONS/IHO\\_Download.htm#S-44](http://www.iho.shom.fr/PUBLICATIONS/IHO_Download.htm#S-44), [on-line] 21-05-2009.
- Kongsberg Maritime (2010). “*Instruction Manual: EM Series Datagram Formats*”.  
January 2010
- Kongsberg Maritime (2009). “*Datasheet – EM 3002 Multibeam echo sounder*”.
- Kongsberg Maritime (2007). “*Operator Manual SIS – Seafloor Information System*”.



- Kuus, P. (2008). “*Bottom tracking issues and recognition thereof using shoals-3000 green laser beam in dense fields of zosteria marina and laminaria sp.*”.
- Lurton, X. (2002), “*An Introduction to Underwater Acoustics, Principles and Applications*”. Springer-Praxis, London.
- Ministry of Transport, Public Works and Water Management (2009). “*Organization of the Ministry*”.
- [http://www.verkeerenwaterstaat.nl/english/topics/organization/organization\\_of\\_the\\_ministry/090\\_organization\\_elements/060\\_dg\\_public\\_works\\_and\\_water\\_management/](http://www.verkeerenwaterstaat.nl/english/topics/organization/organization_of_the_ministry/090_organization_elements/060_dg_public_works_and_water_management/) [on-line] 25-05-2009.
- Netherlands Hydrographic Service (2009). “*Hydrographic Service of the Royal Netherlands Navy*”. [http://www.hydro.nl/pgs/en/index\\_en.htm](http://www.hydro.nl/pgs/en/index_en.htm) [on-line] 25-05-2009.
- Nilsen, K. E. (2007). “*Signal processing in EM3002*”. Femme 2007, Lisbon.
- Presentation of Kongsberg Maritime, Horten, Norway.
- Ocean Mapping Group (2010). “*Swath Sonar Analysis Software*”.
- [http://www.omg.unb.ca/omg/research/swath\\_sonar\\_analysis\\_software.html](http://www.omg.unb.ca/omg/research/swath_sonar_analysis_software.html) [on-line] 01-06-2010.
- Oliveira Jr., A. M. (2007). “*Maximizing the Coverage and Utility of Multibeam Backscatter for Seafloor Classification*”. Ocean Mapping Group, University of New Brunswick, Fredericton, Canada.
- Pohner, F. (2004). “*High Resolution Focused Multibeam Echo Sounders: EM3002 and EM710*”. Presentation of Kongsberg Maritime, Horten, Norway.

Quality Positioning Services BV (2006). “*Total Integrated Hydrographic Solutions*”.

<http://www.qps.nl/default.asp?view=1&parent=&showsub=1> [on-line] 25-05-

2009.

## **CURRICULUM VITAE**

**Candidate's full name:** Auke van der Werf

**Universities attended:** University of New Brunswick  
Fredericton, NB, Canada  
September 2007 – June 2010  
M.Sc.E. Geodesy and Geomatics Engineering

Maritime Instituut Willem Barentz,  
West-Terschelling, the Netherlands,  
September 2002 – June 2007,  
B.Sc. (Hydrography);